Molecular interactions of AMIGO family members in the Nogo receptor complex

By

Rachael Hannah Bennett

A thesis submitted to the University of Birmingham for the degree of DOCTOR OF PHILOSOPHY

School of Clinical and Experimental Medicine

College of Medical and Dental Sciences

University of Birmingham

UNIVERSITY OF BIRMINGHAM

Abstract

The capacity for regeneration in the central nervous system is limited, with little functional recovery following injury or disease. Upon injury, the CNS responds by releasing myelin associated inhibitory factors (MAIFs), including Nogo, MAG and OMgp, which act to suppress axonal regrowth by binding to the Nogo receptor (NgR) complex. The complex consists of the Nogo receptor (NgR), p75 neurotrophin receptor ($p75^{NTR}$)/ (or an alternative protein, TROY) and LINGO-1, a leucine rich repeat (LRR) and Ig domain containing protein. Signalling through the complex leads to activation of RhoA, resulting in actin depolymerisation and growth cone collapse. However, the specific mechanisms by which the complex exhibits its effects remain unclear, particularly as more recent data suggest that specific members of the AMIGO family of proteins may be critical mediators of the inhibitory signaling pathway. Mammalian expression and subcellular fractionation and co-immunoprecipitation experiments established binding between both NgR and $p75^{NTR}$ with AMIGO-1, -2 and -3 and have shown the AMIGO proteins are expressed in the cell membrane as are NgR and $p75^{NTR}$. Interestingly LINGO-1 was also shown to be expressed intracellularly. Furthermore, injection of soluble LINGO-1, AMIGO-1 and AMIGO-3 in surface plasmon resonance (SPR) approaches confirmed direct and specific interaction with surface bound NgR. Finally, to gain a more in depth molecular understanding of the AMIGO proteins and their role in the NgR complex, the structure of the human AMIGO-1 ectodomain, including LRR and Ig domains was determined to 1.9Å resolution. The protein formed a dimer in solution and crystal form and comparisons with structurally similar LRR and Ig domain containing proteins, combined with electrostatic properties and localisation of glycosylation

sites, was used to ascertain likely ligand binding sites on the surface of the protein and AMIGO family in general.

Collectively these results indicate that the AMIGO proteins may form a component of the axon growth inhibitory complex, and are potentially novel therapeutic targets for CNS injury.

Dedication

I dedicate this thesis to my Dad, Alan, who although was present at the start of my PhD journey, did not live to see me complete it. His work ethic has always driven me to strive to be the best I can, and he was, and remains, an inspiration to me always.

Also to my children Isla and Matthew, whom I hope I can make proud.

Acknowledgments

There are a number of people I would like to thank for the hard work and time they put in to helping me complete my thesis. Firstly, I would like to thank my supervisors Professor Ben Willcox and Dr Michael Douglas, who expertly guided me through my postgraduate education. Their enthusiasm for the subject kept me engaged with my research and made my time studying enjoyable. Secondly, I would like to thank Fiyaz Mohammed, without whom I would not have been able to collect and analyse my data. Fiyaz is the best teacher and mentor I could ever have hoped for, and I am extremely grateful for all the hours he has spent helping me. My appreciation also extends to the members of the Willcox group, who were always on hand to provide advice on practical matters in the lab, and the University of Birmingham Protein Expression Facility (PEF).

Finally, I would like to thank my Husband, Mum and Sister, who looked after my children while I was writing this thesis. I am forever grateful to them for everything they do for me.

Abbreviations

Å = Angstrom

μg = Microgram

μl = Microlitre

μM = Micromolar

μm = Micrometer

Ala = Alanine

Arg = Arginine

Asn = Asparagine

Asp = Aspartic acid

BBB = Blood brain barrier

BSA = Bovine serum albumin

CNS = Central nervous system

Cys = Cysteine

dH2O = Distilled water

DMEM = Dulbecco's modified eagles medium

DMSO = Dimethyl sulfoxide

DNA = Deoxyribose nucleic acid

dNTPs = Deoxyribonucleotide triphosphate

DTT = Dithiothreitol

ECL = Enhanced Chemiluminescence

EDTA = Ethylenediaminetetraacetic acid

FCS = Fetal calf serum

FPLC = Fast protein liquid chromatography

g = Gram

Glu = Glutamic acid

Gln = Glutamine

Gly = Glycine

hAMIGO-1 = Human AMIGO-1

HEPES = 4-(2-hydroxyethyl)-1-piperazineethanesulfonic acid

His = Histidine

Ile = Isoleucine

Kb = Kilobase

kDa = kilo Daltons

L = Litre

LB = Lysogeny broth

Leu = Leucine

LRR = Leucine rich repeat

Lys = Lysine

mAMIGO-1 = Mouse AMIGO-1

Met = Methionine

mg = Milligram

min = Minutte

ml = Millilitre

mM = Millimolar

Mr = Molecular mass

NaCl = Sodium Chloride

ng = Nanogram

nm = Nanomolar

OD = Optical density

PBS = Phosphate buffered saline

PCR = Polymerase Chain Reaction

PEI = Poly(ethylenimine)

Phe = Phenylalanine

Pro = Proline

RI = Ribonuclease Inhibitor

Rpm = Revolutions per minute

SCI= Spinal cord injury

SDS = Sodium dodecyl sulfate

SDS – PAGE = Sodium dodecyl sulphate polyacrylamide gel electrophoresis

Sec = Seconds

Ser = Serine

SOB = Super optimal broth

SOC = Super optimal broth with catabolite repression

TBE = Tris/Borate/EDTA

TBS-T = TRIS buffered saline Tween 20

Thr = Threonine

TRIS = tris (hydroxymethly) aminomethane

Trp = Tryptophan

Tyr = Tyrosine

Val = Valine

W/v = Weight/Volume

Contents

List of Figures

Chapter 5. Analysis of the hAMIGO-1 LRR domain structure

Chapter 6 Molecular and structural studies of NgR complex interactions

Chapter 1

Introduction

Introduction

1.1 Spinal cord injury

Every year between 250,000 and 500,000 people around the world are affected by spinal cord injury (SCI) [1], which is mostly the result of trauma but can also be caused by tumours, inflammation or degenerative disease. The consequences vary widely from person to person and may include loss of motor, sensory, or autonomic function (such as breathing and bladder control). SCI also brings with it the risk of developing secondary conditions such as pressure sores and urinary tract infections [2], which can have further debilitating effects. Clinically, with most spinal cord injuries, the secondary damage, caused by inflammation after injury, contributes significantly to the final impact of the neural damage and in turn the extent of the long term disability [3].

SCI can be segregated into 4 phases, these are; (i) acute, from 2 – 48 hours after injury, (ii) sub-acute, from 2 days to 2 weeks post injury, (iii) intermediate, which occurs between 2 weeks and 6 months after SCI and (iv) a chronic phase which begins at around 6 months after injury and persists thereafter [4].

The acute phase is characterised by haemorrhage, oedema and inflammation [5] into the lesion site which can contribute to further axonal injury and cell death. This stage is associated with an increase in the permeability of the blood brain barrier (BBB), caused by the direct mechanical disruption at the site of the SCI and the local effects of upregulated inflammatory mediators. The acute phase after SCI is likely to be the best time to administer neuroprotective interventions for two reasons, first the BBB is disrupted during this phase, which allows increased perfusion of therapeutic agents into the central nervous system (CNS) at this time

point than if they were to be given once the BBB had returned to normal. Lastly, at this stage tissue scaring is not established yet.

The subacute phase is characterised by the removal of cell debris by macrophages, which also enables the removal of growth inhibitory components found in the myelin debris. The phagocytic response, and therefore removal of some inhibitory factors, is greater following injury in the peripheral nervous system (PNS) than that seen in the central nervous system (CNS), and this could account for some of the differences in their respective regenerative abilities. During this phase astrocytes in the lesion start to proliferate and will form the bulk of the glial scar [4] which forms a physical barrier against regeneration. During the intermediate phase the astrocytic glial scar continues to grow, with the result that axons are no longer able to transverse the lesion core, completing the injury response which now enters the chronic stage.

1.1.2. A definition of 'regeneration'?

It is important to clarify what the term regeneration means when discussing it as part of this body of work. According to the Oxford English Dictionary, regeneration refers to the growth of new animal or plant tissue. In the nervous system neuroregeneration refers to the regrowth and/or repair of nervous tissues and cells including neurons, axons, myelin and glia, and in this body of work it refers more specifically to the regrowth of severed axons.

1.2 Processes limiting axonal regeneration in the damaged CNS.

The ability of the central nervous system (CNS) to regenerate after injury is poor with damage to the brain or spinal cord being considered irreversible. Failure of axons to regenerate in the CNS is the main reason spinal cord injuries result in a permanent loss of sensation and paralysis. This contrasts to the regenerative capacity of the PNS which is generally able to regenerate successfully after injury. The putative biochemical and cellular mechanisms underlying these differences are complex, and are a subject of substantial interest, as a better understanding of them could lead to new therapeutic opportunities.

In contrast to the human CNS, many lower vertebrate species are capable of CNS regeneration, leading many to question whether the ability to regenerate was a trait that was present in our metazoan ancestors, which has been lost during evolution, or whether it was not present in our ancestors and arose during evolution. That is, is it an ancestral trait or an evolutionary one? [6]. There are many arguments for each of these theories but as yet we can only speculate on why these differences occur.

In the human CNS, the brain and spinal cord are protected from trauma by encasement in bony structures, the skull and vertebrae, and are protected from peripheral infection and chemical influences by the BBB which maintains the stability of the internal environment of the brain and spinal cord. However, the actual response to injury in the nervous system is muted when compared to the rest of the body, and also when compared to responses mediated by invertebrates. The limited ability to repair neural tissue after injury suggests that selection has not acted to the same extent on the processes that occur after injury as it has on those that protect the nervous system from such trauma [7] i.e. we have evolved only to prevent injury. Evolutionarily, any ancestors who suffered CNS trauma likely died, due to

lack of supportive medical interventions, and therefore natural selection would not have been able to act, so adaptive responses to injury would have been impeded. Even if survivable the chance of reproduction after injury is unlikely. Additionally, damage to the CNS as the result of diseases that were not commonly experienced by ancestors, due to their shorter and less sedentary lives, means that these diseases are unlikely to have shaped the evolution of regeneration. Indeed it has been suggested that the injured CNS does not favour a strategy of regeneration but rather one of minimising further damage and it seems likely that evolutionarily, pressure to prevent damage would have outweighed the potential benefits of axonal regeneration [7]. In contrast, damage to the peripheral nerves may have been associated with injuries that were survivable and hence these nerves have adapted to be able to regenerate after injury.

The inflammatory reaction after injury has been shown to contribute to progressive tissue damage. The infiltration of inflammatory cells such as neutrophils, macrophages and lymphocytes in the minutes and hours post injury causes the accumulation of soluble inflammatory mediators such as chemokines and cytokines at the injury site. This response in part removes damaged cells and pathogens from the injury site, but in doing so also damages the surrounding healthy tissue [7]. This is also true in the PNS; however, damage to surrounding tissue here is not as detrimental because the damaged tissue can be repaired over time. Furthermore, the removal of cellular debris from the CNS may take weeks, compared to days in the PNS, therefore prolonging the effects of the inhibitors of regeneration which may partially explain why CNS regeneration is limited. The differences between the CNS and PNS neurons' ability to regenerate can be ascribed to differences in intrinsic factors of the neurons [8] , however, it is well established that myelin breakdown products are largely responsible

for failure of CNS axons to regenerate [9] and CNS neurons can regenerate when given a permissive environment to be able to do so.

1.2.1 The environment in the CNS prevents regeneration

Using certain experimental protocols, CNS axons can be induced to grow through the area of post-injury scarred tissue, demonstrating that the inability of axons to regenerate cannot be primarily attributed to intrinsic neuronal factors [10]. It has been shown that adult CNS neurons can re-grow after injury if they are given access to a permissive environment [11, 12], which suggests that failure of adult CNS neurons to regenerate is not an intrinsic deficit of the neuron but a characteristic feature of the damaged environment [13]. Identifying the specific inhibitory factors of the external environment in the CNS after neuronal injury is key. Upon damage in the CNS, a number of events occur, immediately and over the course of days and weeks which contribute to an inhibitory environment. A physical barrier to regeneration is composed in the form of a glial scar which is established over a few weeks. The main cell types involved are astrocytes, oligodendrocyte precursors, and microglia which arrive to the injury site at different times as the scar evolves. The first cells to the injury site are macrophages and microglia from the bloodstream and surrounding tissue, respectively, which are seen within a few hours of injury[14]. After 3-5 days, oligodendrocytes are recruited, followed by astrocytes which fill the cavity [14]. A framework of interwoven astrocytes is formed which are bound together by tight junctions and in which there is little extracellular space [14]. The astrocytes within the glial scar also upregulate the production of several extracellular matrix-associated inhibitors of regeneration [15] including chondroitin sulphate proteoglycans (CSPGs), which are important in the development and maintenance of the normal CNS, and

are also the main inhibitory molecules to axon regeneration in the glial scar [16]. Two receptors have been identified as being important in mediating CSPG inhibition, these are Protein Tyrosine Phosphatase, PTPσ and LAR, to which CSPGs bind with high affinity to mediate their suppression of axon elongation [17]. Furthermore, by use of the bacterial enzyme Chondroitinase ABC the function of CSPGs has been inferred as promoting axon regeneration in the CNS [18, 19]. In contrast, myelin associated inhibitory proteins are released immediately following damage to the CNS and collectively inhibit regeneration before the glial scar is formed (Figure 1.1).

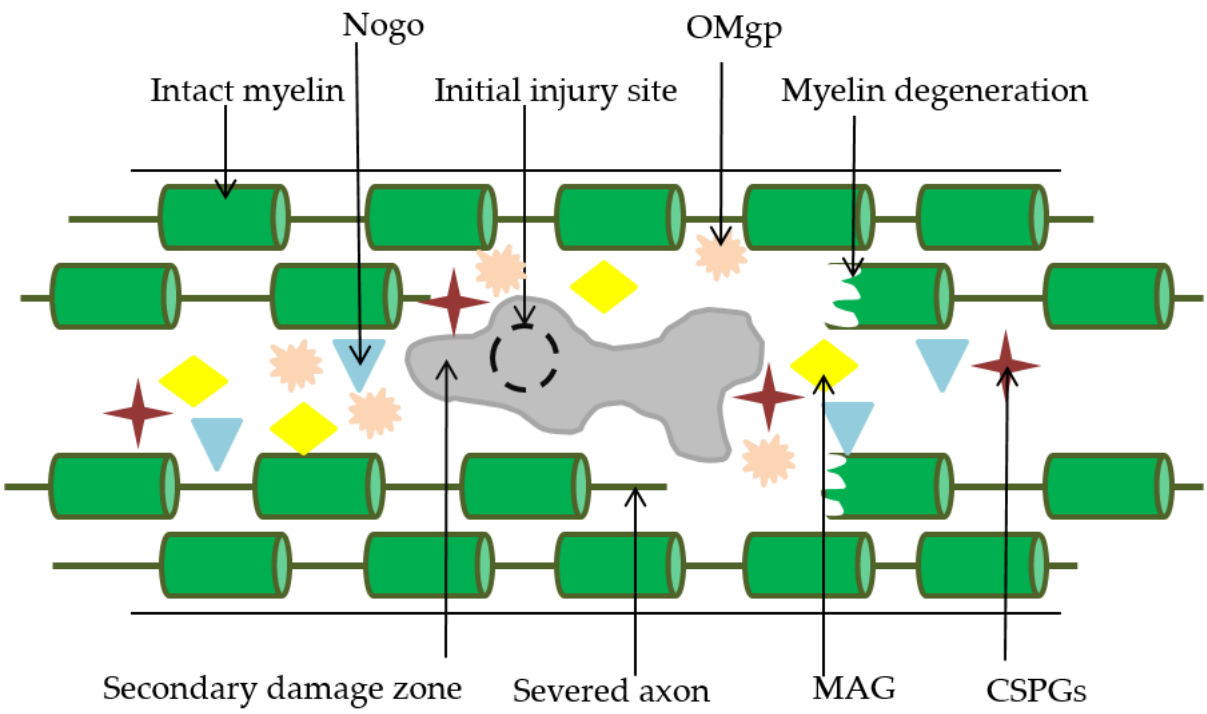

Figure 1.1. Spinal Cord Injury Response.
Upon injury to the CNS, myelin associated inhibitory factors (MAIF's) including Nogo, Myelin Associated Glycoprotein (MAG), Oligodendrocyte myelin glycoprotein (OMgp) and Chondroitin sulphate proteoglycans (CSPGs) are released creating an environment inhibitory to regeneration.

1.3 Myelin Associated Inhibitory Factors

Several growth inhibitory proteins present in the CNS play a crucial role in preventing axonal regeneration in the injured adult mammalian CNS. These include Nogo, myelin associated glycoprotein (MAG) and oligodendrocyte myelin glycoprotein (OMgp), which account for a significant fraction of the inhibitory activity from CNS myelin (Figure 1.2). However, removal of some or all of these myelin associated inhibitors in knockout mice results in poor or inconsistent regeneration [20, 21]. Indeed, MAG knockout mice only display a limited enhancement of axon regeneration in the CNS [22], likewise a blocking antibody to Nogo resulted in a low level of axon regeneration [23] suggesting that other myelin derived molecules may also be involved. Presumably in these situations, other myelin-derived molecules are still present, acting to prevent axons from regenerating [15]. There may also be a relative lack of regeneration-promoting trophic factors in the CNS as compared to the PNS, but this issue does not detract from the different profile of inhibitory molecules in the CNS and PNS.

Nogo proteins were first discovered as a high molecular weight (250kDa) species extracted from spinal cord myelin which was shown to inhibit neurite outgrowth [24]. Nogo is a member of the Reticulon (RTN) family of proteins, which are membrane-associated proteins present in all eukaryotic organisms [25] and are products of the Reticulon 4 (RTN4) gene. There are 3 Nogo isoforms named Nogo-A, -B and –C which are generated by alternative splicing, resulting in multiple isoforms [26] sharing a 188-amino acid reticulon homology domain (RHD) at their C- terminus [27]. Nogo- A is the longest isoform of the Nogo proteins and is highly expressed in oligodendrocytes but is not expressed in Schwann cells [28]. Importantly, Nogo-A expression levels are increased after spinal cord injury, suggesting their

importance in recovery after injury [29]. In addition, the monoclonal antibody, IN-1 was raised against a 250kDa myelin extract corresponding to Nogo-A, and this antibody was shown to neutralise neurite outgrowth inhibition [30], further illustrating that the Nogo-A protein is a major factor in neurite outgrowth inhibition. The topology of the Nogo protein is unusual (Figure 1.2), with the conserved C-terminal containing two hydrophobic domains separated by a 66-residue hydrophilic segment [31, 32]. It is predicted that the N- and C- termini of the protein are cytosolic while the short 66- amino acid loop protrudes into the extracellular space. Nogo-A possesses two inhibitory domains, the Nogo-66 domain and the amino-Nogo domain. The Nogo-66 domain can also interact with the paired immunoglobulin-like receptor B (PirB) on the surface of neurons [33] to mediate at least part of its inhibitory activity in certain neuronal types [33, 34]. The amino-Nogo domain has also been detected on the surface of oligodendrocytes and is thought to act *via* an independent mechanism to disrupt neuronal integrin function [34, 35]. This demonstrates that Nogo-66 is able to limit axon regeneration *in vivo* [36]. The method by which Nogo-A is responsible for the inhibition of axonal regeneration is through high affinity binding of the Nogo-66 loop to the Nogo receptor, NgR [37]. The NgR acts as a point of convergence for several myelin associated inhibitors which act upon NgR to inhibit neurite regeneration through the RhoA pathway.

MAG is a sialic acid binding- SIGLEC (sialic acid- dependent immunoglobulin- like family member lectin) protein [38] and is a transmembrane protein with 5 Ig-like domains [39] (Figure 1.2) expressed in both the CNS, by oligodendrocytes, and the PNS, by Schwann cells [40]. MAG binds to gangliosides GD1a and GT1b on neuronal cell bodies and axons [41] and has roles in axon stability, controlling axon cytoarchitecture and regulating axon outgrowth [41]. Interestingly, embryonic neuronal expression of MAG suggests that outgrowth is

actively promoted by MAG but switches to inhibition around birth [42] [43]. The function of MAG appears to be complex, inhibiting specific axon growth pathways and it has been found to be a ligand for the Nogo receptor (NgR), which it binds with high affinity.

OMgp is a 120kDa leucine rich repeat (LRR) containing glycoprotein [44] and is GPI anchored to the surface of oligodendrocytes and myelin adjacent to axons. OMgp is expressed in both the developing and adult CNS and is a relatively small component of myelin again found to be inhibitory to axon regrowth [45]. It has been suggested that OMgp is involved in the formation and maintenance of myelin sheaths [44]. *In vitro* experiments showed MAG, OMgp and Nogo are all members of the myelin associated inhibitory family that bind NgR, with OMgp and Nogo exhibiting more pronounced outgrowth inhibition than MAG [45].

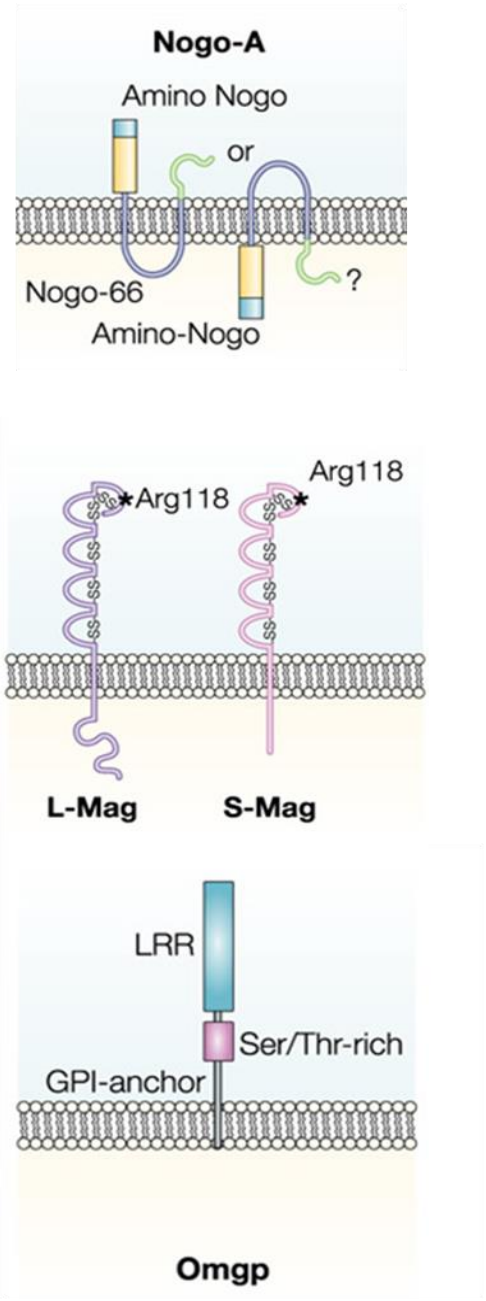

Figure 1.2. Illustrations of myelin associated inhibitory proteins

There are three isoforms of Nogo- A, B and C, however only Nogo-A is enriched in oligodendrocytes. Nogo- A contains two inhibitory domains; Nogo-66, which is common among all isoforms and amino-Nogo which is unique to Nogo-A. Myelin associated glycoprotein (MAG) contains multiple Ig domains and exists as two isoforms; large (L) and small (S) which differ only in their cytoplasmic sequences. Oligodendrocyte myelin glycoprotein (OMgp) is a GPI-linked LRR domain containing protein expressed on the surface of oligodendrocytes.

Diagram adapted from [15]

1.4 The Nogo receptor

The Nogo receptor (NgR) is a GPI-anchored protein and is one of a family of three receptors (NgR-1, -2 and -3) which display high level of sequence identity. The NgR protein is predicted to contain 473 amino acids [28]. The protein ectodomain contains 8 leucine rich repeats flanked by cysteine rich C- (LRRCT) and N- (LRRNT) terminal domains (Figure 1.3) [46]. The leucine rich repeats conform to the motif xLxxLxxLxLxxN/CxLxxLPxxFx where X can be any amino acid and L can also be occupied by V, I and F. Nogo Receptor (NgR) proteins are expressed throughout the CNS in a distribution complementary to Nogo-A. The other myelin associated inhibitory factors MAG and OMgp also mediate their inhibitory actions through the Nogo receptor [37], which is surprising, as these inhibitory proteins do not share any sequence similarities with Nogo-A. However, the co-ordinated distribution between Nogo-A and NgR contrasts to that of MAG and OMgp, which are expressed in many tissues where there is little or no NgR expression [29] indicating that these inhibitory proteins may also engage other receptors. This suggestion is supported by research showing that deletion of NgR does not completely abolish the inhibitory effects of Nogo, MAG and OMgp [33] as limited regeneration, largely in rubrospinal tracts after spinal cord injury was seen. The data suggested that NgR is important for mediating some of the inhibitory effects of the myelin inhibitors, but that further redundancy may exist. The roles of NgR-2 and NgR-3 are unknown, with the only common ligands being MAG which binds to NgR-1 and NgR-2 [47] CSPG which binds NgR-1 and NgR-3 [48] and amyloid beta precursor protein (APP) which binds all 3 family members [49].

Ligand binding to NgR causes activation of RhoA, a small GTP binding protein, leading to actin depolymerisation and growth cone collapse which ultimately leads to inhibition of axon regeneration. Neurones cultured from NgR knockout mice, which interestingly are viable, do not bind Nogo-66 and do not undergo growth cone collapse in the presence of myelin inhibitors. Furthermore, these mice show improved recovery of motor function after spinal cord transection compared to wild type mice [50]. Additionally, blocking the binding of ligands to NgR has also been shown to improve neurite outgrowth, for example by blocking interactions using either an NgR antibody or using a soluble NgR antagonist peptide which competes with the neuronal receptor for binding to myelin derived inhibitors. Both methods have been shown to promote axonal regeneration by preventing the signal for inhibition being transduced into the neuron [51] [31].

Binding studies between Nogo-66 and NgR, involving domain deletions throughout the NgR ectodomain have identified which domains facilitate binding. These studies demonstrate that both the LRRCT and LRRNT of NgR are necessary for binding to occur and that deletion of any two LRR domains also abrogates binding [32]. The crystal structure of NgR suggests that there is a conserved putative ligand binding site within the concave face of the LRR domain [46]. Two hydrophobic regions were identified on the LRR concave surface as being possible areas of binding. The same study also postulated that the promiscuous ligand interactions of the protein involving binding to the structurally unrelated ligands MAG, OMgp and Nogo, is due to the broad region of exposed residues in the concave face which allows for binding to a range of different ligands [46, 52].

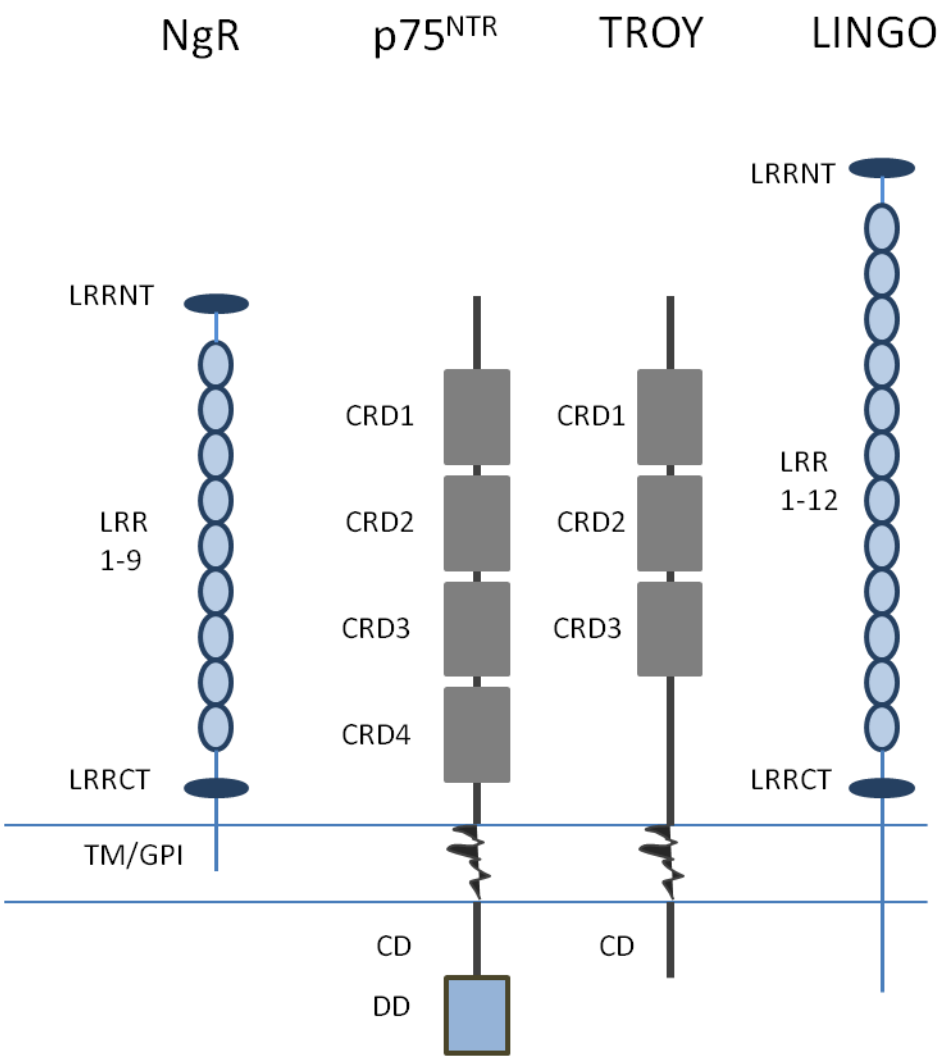

Figure 1.3 Domain organisations of the members of the NgR complex, including NgR, p75^{NTR}, TROY and LINGO-1.

NgR contains 9 leucine rich repeats (LRR) in its extracellular domain flanked by leucine rich N- and C terminal capping domains (LRRCT and LRRNT) and is GPI linked in the transmembrane region. p75^{NTR} extracellular domain contains four cysteine rich domains (CRD), and intracellularly there are chopper (CD) and death domains (DD). TROY is similar to p75^{NTR} and contains three cysteine rich domains (CRD) in its extracellular portion. LINGO-1 is a LRR domain containing protein, having 12 LRRs flanked by cysteine rich LRRCT and LRRNT domains.

1.5 The Nogo Receptor complex

Since NgR is GPI anchored and the entire protein is extracellular with the exception of a short stalk region, a co-receptor is needed to transmit any signals received into the cell. Wang et al. [53] discovered that $p75^{NTR}$, a 399-amino acid type 1 transmembrane protein and a member of the tumour necrosis factor receptor family (TNFR), specifically interacts with NgR [53]. NgR/$P75^{NTR}$ binding was demonstrated using cell surface binding assays where an alkaline phosphatase fusion protein containing the extracellular domain of $p75^{NTR}$ was able to specifically bind to NgR expressed on the surface of CHO cells. Controls using the AP protein alone and control CHO cells not expressing NgR showed no binding. In addition, $p75^{NTR}$ was shown to be necessary in mediating all myelin associated inhibitory factor signalling through NgR, as neurons from $p75^{NTR}$ -/- mice did not show neurite outgrowth inhibition in the presence of MAG, Nogo and OMgp [53].

Since its discovery almost 30 years ago, $p75^{NTR}$ has been implicated in a wide number of cellular processes, although its exact physiological role has remained undefined as many of the associated processes are apparently contradictory. For example, $p75^{NTR}$ has been shown to transduce signals from neurotrophins to promote nerve growth, while conversely transducing signals from myelin derived growth inhibitory factors to trigger growth cone collapse [54]. $P75^{NTR}$ is widely expressed in the developing nervous system but expression is switched off in most adult cells, however, some cells retain expression at low levels, for example basal forebrain cholinergic neurons, sensory neurons and spinal cord motor neurons [55]. Adult tissues re-express $p75^{NTR}$ in many cell types after injury or cellular stress, including peripheral nerve crush [55]. A significant increase in expression is seen after spinal cord injury, highlighting the role of $p75^{NTR}$ in mediating the inhibitory effects of myelin.

Whilst NgR and $p75^{NTR}$ have been shown to immunoprecipitate with each other in a number of experimental models, the formation of the complex between NgR and $p75^{NTR}$ was shown to be enhanced in the presence of soluble MAG protein, which suggests that the complex is formed in response to inhibitory myelin breakdown products [53]. Within the Nogo receptor complex, $p75^{NTR}$ allows activation of RhoA through the recruitment of the Rho inhibitor Rho-GDI. Upon the association of myelin associated inhibitory factors to the NgR-$p75^{NTR}$ complex, Rho-GDI binds the $p75^{NTR}$ death domain which causes the release of RhoA-GDP from Rho-GDI. RhoA then becomes active by exchanging GDP for GTP and the activated RhoA causes growth cone collapse and inhibition of axonal growth via phosphorylation of various substrates including LIMK (Lin-11, Isl-1, and Mec-3 kinase), MLC (myosin light chain) and CRMPK (collapsin response mediator protein-2 kinase) (Figure 1.4) [56-58]. Growth cones are thus able to combine a number of molecular signals in order to make a decision to extend or retract.

The intracellular domain of $p75^{NTR}$ is critical in transmitting inhibitory signals into the cells; truncated $p75^{NTR}$ lacking an intracellular domain expressed in complex with NgR has been shown to allow neurite outgrowth in the presence of myelin inhibitory molecules [53]. Interestingly, blocking the association between the extracellular regions of $p75^{NTR}$ and NgR reduced the effects of the myelin breakdown products MAG, OMgp and Nogo-66 [53], confirming that the extracellular domain is also crucial. The crystal structure of the ectodomain of NgR showed that the concave surface of the LRR domain contains the aromatic residues Tyr, Phe and His, with this surface involved in high affinity ligand binding [32]. In addition, a large acidic patch on the NgR concave face has been identified as being in contact with a basic LRRCT subdomain of a second NgR molecule. This suggests that this area may

be responsible for ligand-independent receptor-receptor binding which has previously been identified at the cell surface [32, 59]. Furthermore, an area, at the C-terminal end of the NgR ectodomain was identified as a further region where $p75^{NTR}$ may associate [46].

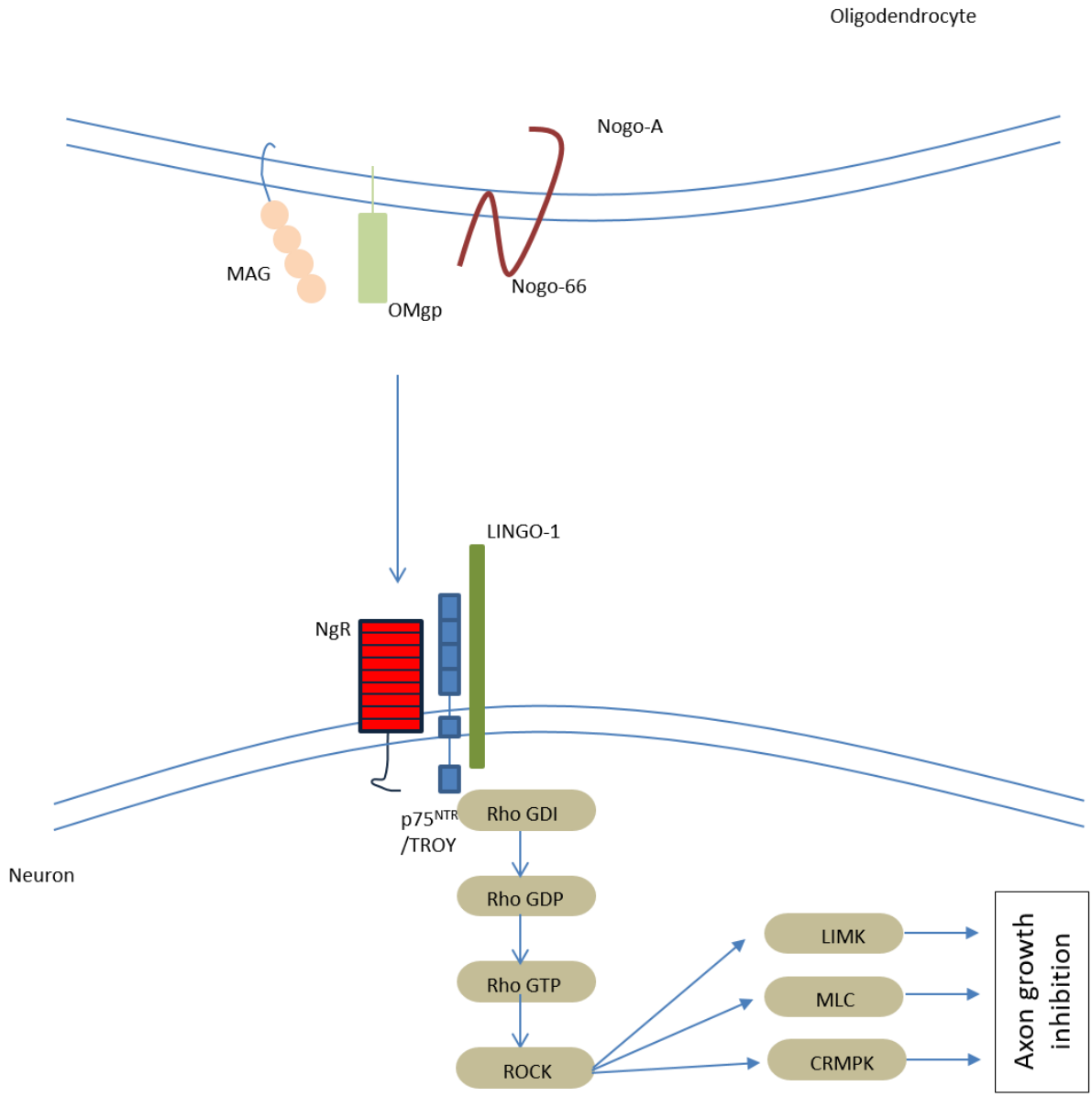

Figure 1.4. Signalling cascade of myelin associated inhibitors acting on the NgR complex.

Myelin associated inhibitors bind to NgR, co-receptors $p75^{NTR}$ and LINGO-1 to mediate the inhibitory signals which prevent axon regeneration by activating Rho and ROCK which in turn leads to the phosphorylation of several substrates LIMK; Lin-11, Isl-1, and Mec-3 kinase, MLC; myosin light chain and CRMPK; collapsin response mediator protein-2 kinase, resulting in axon growth inhibition. TROY may replace $p75^{NTR}$ in some neurons.

It was therefore hypothesised that depletion of p75^{NTR} should help to reduce the impact of myelin associated inhibitory proteins and enhance regeneration in the CNS after injury. Blocking the effects of p75^{NTR} *in vitro* with neutralizing antibodies prevented death of neurons after axotomy. However, p75^{NTR} knockout mice exhibited little enhanced neuroregeneration after spinal cord injury [60] indicating that other proteins may be able to substitute for p75^{NTR} *in vivo*. Further evidence supporting the notion of a substitute protein is derived from the tissue distributions of NgR and p75^{NTR}. Expression of p75^{NTR} does not correspond fully to the distribution of NgR, which is expressed throughout the CNS [61] whereas expression of p75^{NTR} in the adult CNS is very low and only increases after injury [55]. In some neurons the expression of p75^{NTR} remains low even after injury[62]. The absence of p75^{NTR} from neuronal cell types that respond to myelin inhibition led many to question how inhibitory signals are transduced in neurons lacking p75^{NTR} [63], and it is possible that NgR can partner with other receptors.

Subsequent studies have shown that, in neurons that lack p75^{NTR}, TROY can serve to functionally substitute in the NgR complex to activate RhoA and induce growth cone collapse causing inhibition of axonal regeneration [64, 65]. TROY has been shown to be widely expressed in the adult brain [64-66] and binding between TROY and NgR and LINGO-1 (Leucine rich repeat and Ig domain-containing Nogo receptor interacting protein) has been demonstrated *in vitro* indicating that the proteins can form a functional receptor complex that can mediate the effects of myelin associated inhibitors [64, 65]. Furthermore, it was demonstrated that TROY has a higher affinity for NgR than p75^{NTR} [64]. The importance of TROY has been highlighted in experiments demonstrating greater outgrowth of neurons from mice deficient in TROY in the presence of myelin associated inhibitors [64]. TROY is a TNF

receptor family member [64] selectively expressed in the adult CNS [66]. Structurally related to $p75^{NTR}$, it is a single pass type I transmembrane protein 416 aa in size. TROY mRNA is strongly expressed in the brain, with lower levels being seen in the heart, lungs and liver [66]. Within the CNS, TROY is more widely expressed in postnatal and adult neurons than $p75^{NTR}$ [67].

As described previously, NgR has two structurally related homologues, NgR2 and NgR3. It has been shown that MAG binds NgR2 selectively and with a greater affinity than NgR, to mediate axon inhibitory effects [47]. Furthermore, it has been suggested that NgR2 can mediate its effects independently of $p75^{NTR}$ however; no co-receptors for NgR2 have been identified [47]. It is possible that, TROY could act as a co-receptor for NgR2 to mediate the effects of MAG or perhaps that there are more, as yet unidentified, co-receptors for NgR. Indeed, in a subset of neurons where $p75^{NTR}$ is not expressed but TROY is, it has been demonstrated that $TROY^{-/-}$ mutant neurons showed no significant difference in neurite length than wild-type neurons when assessed using MAG as an inhibitor. This suggests that, in this case, TROY does not functionally substitute $p75^{NTR}$ and indicates that other receptors are involved in axon inhibition.

1.6 LINGO-1

Co-expression of $p75^{NTR}$ with NgR in reconstituted non-neuronal systems fails to demonstrate activation of RhoA in response to myelin breakdown products [68] suggesting that although $p75^{NTR}$ is necessary for the negative regulation of neurite outgrowth, it is not sufficient, therefore other components must be involved in order to activate RhoA. LINGO-1 has been shown to be the third component of the Nogo receptor complex with $p75^{NTR}$ [68], as co-expression of NgR, $p75^{NTR}$ and LINGO-1 in non-neuronal cells conferred responsiveness to OMgp allowing activation of RhoA [68].

LINGO-1 (Leucine rich repeat and Ig domain-containing Nogo receptor interacting protein) is a central nervous system-specific single transmembrane spanning glycoprotein [69], also described as LERN1 [70]. LINGO-1 has been shown to bind both NgR and $p75^{NTR}$ *in vitro* and as part of the tertiary complex that enables activation of RhoA, an intracellular regulator of the cytoskeleton which mediates the effects of signals of myelin inhibition [68]. The activation of RhoA correlates with the inhibition of axon growth whereas inactivation of RhoA correlates with axonal outgrowth and extension [71]. This demonstrates that LINGO-1 is a key component of the Nogo receptor complex.

LINGO-1 has been shown to be exclusively expressed in the neurons and oligodendrocytes of the central nervous system [68, 70] in a non-uniform distribution, with highest expression in the cortex of the brain and lowest levels in the spinal cord [68]. LINGO-1 expression is exclusively CNS-specific with no expression observed in non- neuronal tissues by northern blot analysis [68]. During development, LINGO-1 mRNA levels were shown to peak at postnatal day 1 and decline thereafter into adulthood where they remain at background levels, until after axonal injury when an increase in expression is observed [68], indicating the

potential importance of the protein after injury. LINGO-1 knockout mice have more myelinated axon fibres in their spinal cords than wild type mice, however there are no differences in the peripheral (sciatic) nerves, suggesting that the myelination effects are CNS-specific [72].

The functional importance of LINGO-1 within the NgR/p75^{NTR} complex has been demonstrated by blocking experiments using soluble LINGO-Fc, administered after spinal cord injury in rats, resulting in significantly improved functional recovery due to increased axonal sprouting and reduced RhoA activation [73]. In subsequent *in vitro* experiments, soluble LINGO-1-Fc was also shown to reverse the inhibitory effects of OMgp on neurite outgrowth [68]. Blocking the effects of LINGO-1 by use of a monoclonal antibody, mAb 1A7 has similar effects to those observed using soluble LINGO-1-Fc proteins [74]. Clinically, LINGO-1 is an attractive target for drug trials for the treatment of CNS diseases, such as the demyelinating disease multiple sclerosis (MS), with antibodies being preferred for their potency and selectivity. Consistent with LINGO-1 being a therapeutic target in this context, over-expression of LINGO-1 *in vivo* can decrease myelination, possibly due to the extracellular domain of LINGO-1 being able to self- associate in trans [75], providing an inhibitory signal for myelination [76]. However, problems can arise with the use of antibodies against CNS diseases because of their poor penetration into the CNS after systemic administration as only approximately 0.1% of the administered drug reaches the target [77] due to the selectivity of the BBB. Anti-LINGO-1 antibody, Li81, has been shown to enter the CNS after systemic administration sufficiently, at 0.1%-0.4% of blood levels [78], to promote remyelination in rats [77]. As yet, there is very little convincing *in vivo* evidence for the functional effects of LINGO-1 blockade on CNS injury, with one published phase 2 trail [79], and 1 published phase 1 trial

[80] [81]. Furthermore, it has been shown that the expression of LINGO-1 in dorsal root ganglion neuronal cells (DRGN) does not rise until 14 days post injury [68] supporting the notion that other co-receptors for NgR/p75^{NTR} may mediate axon growth inhibition before that.

Human LINGO-1 is a 614 aa protein and it has three paralogs; LINGO-2, LINGO-3 and LINGO-4 [82]. It is highly conserved, with human and mouse LINGO-1 being 99.5% identical [68]. LINGO-1 is a leucine rich repeat (LRR) containing protein, which contains 12 LRRs, each 23-25 residues in length. The LRRs are flanked by cysteine rich N- and C- terminal capping domains (Figure 1.3), each of which contain two disulphide bridges, followed by an Ig domain at the C- terminal end, followed by a single pass transmembrane domain and a short cytoplasmic tail [77]. Structurally the LINGO-1 ectodomain folds into a two module structure composed of the LRR and Ig domain connected by a flexible linker region, the LRR domain forming a horseshoe shape typical of other LRR domain containing proteins [83]. The Ig domain is composed primarily of β sheets with one α helix and is positioned at a near 90^{o} angle to the LRR domain [69]. LINGO-1 has been shown to exist in a number of forms, under physiological conditions, including dimers and higher order oligomers. Determination of the crystal structure of LINGO-1 ectodomain illustrated that the protein forms a tetramer, where the four monomers interact in a circular ring-like fashion, forming a closed structure [69]. The monomers link together head-to-tail and back-to-back, meaning that the convex faces of the monomers form the protein-protein interfaces and the concave faces are solvent exposed [69]. However, the protein has also been identified in monomeric, dimeric and tetrameric states in solution [77] but, in the presence of ligand, no tetrameric form was observed, indicating that

the ligand prevented formation of the tetramer [77]. Indeed, the tetrameric form observed may have been influenced by crystallisation conditions.

By measuring the lengths of processes formed by oligodendrocyte precursor cells (OPCs) transfected with LINGO-1 missing either its ectodomain, cytoplasmic domain or LRR domain it has been demonstrated that the inhibitory actions of LINGO-1 in the NgR/p75^{NTR} complex are abrogated upon deletion of the entire ectodomain or the cytoplasmic domain of LINGO-1, but surprisingly not by the deletion of either the LRR domain [84]. This indicates that the LRR domain does not contribute to the inhibitory potential, which is surprising considering that LRR domains are typically involved in protein-protein interactions. Furthermore, it has been suggested that the Ig domain of the protein is sufficient for its activity [68, 77, 84], and those sites identified as being potential binding sites in the Ig domain are solvent exposed [77].

1.7. Leucine rich repeats

LINGO-1 is part of a broader family of proteins containing leucine rich repeats. Leucine rich repeats (LRRs) are present in over 60,000 proteins from viruses, bacteria, archae and eukaryotes [85] and include cell adhesion molecules, receptors and enzymes, with evidence suggesting that they mediate diverse protein-protein and protein-ligand interactions [86] in a variety of processes such as DNA repair, signal transduction, cell adhesion and apoptosis. LRR motifs were first identified in the protein leucine rich α_2 glycoprotein (LRG) [87], so named because 66 of the 312 amino acids were leucine residues [87],[88]. Leucine rich repeats are, as expected, distinguished by a consensus sequence containing many hydrophobic

leucine residues, and can vary in length, typically between 20 and 29 amino acids but most commonly 24 residues [89]. These repeats contain 11 conserved residues with the sequence LxxLxLxxN/CxL where x denotes any amino acid and the leucine residues can be substituted for other hydrophobic residues: isoleucine, valine or phenylalanine (Figure 1.5). This ability to substitute Leucine, coupled with the fact that, apart from the 11 conserved residues, the other parts of the repeats may vary quite considerably between LRR proteins, means that LRR motifs are often overlooked when examining protein sequences [89].

X ray data analysis of the ribonuclease inhibitor (RI) protein, which is composed entirely of LRRs, was the first to reveal the structure of the repeats. The primary structure of this protein shows 15 leucine rich repeats that alternate between 29 and 28 residues long, named type A and type B repeats respectively [90]. Individual leucine rich repeats each consist of a β strand and an α helix and in proteins with multiple repeats these are arranged in such a way so that all the β strands and the α helices are parallel to a common axis, which results in a non-globular horseshoe-shaped molecule with curved parallel β sheets lining the concave face and the α helices located at the convex surface [89, 91, 92]. Proteins with fewer repeats tend to be less curved in shape, i.e. more banana-like, and those with a larger number of repeats form a more horseshoe-like structure (Figure 1.5). However, the length of the individual LRRs also influences the shape of the domain and the longer the individual repeats are, the more curved the domain. For example, when comparing the structures of the RI (Figure 1.5a), which contains 15 LRRs of 28-29 residues in length [93], and NgR (1.5d), which contains 9 LRRs of 24-25 residues each [32], the differences in curvature of the LRR domains are quite noticeable, with the former being much more curved than the later. Other LRR domain containing proteins of interest are decorin (Figure 1.5b), which contains 12 LRRs of varying length (from

21-30 residues) [94], and LINGO-1 (Figure 1.5c) which contains 12 LRRS 23-24 residues long [69].

The hydrophobic residues of the LRRs are normally packed in the core of the protein providing stability to allow for protein-protein interactions that most commonly occur at the concave face of the protein. The core LRR domain is commonly flanked at either end by cysteine-rich capping domains, which serve to protect the most N- and C- terminal leucine rich repeats [92]. These LRRCT and LRRNT flanking domains tend to be cysteine-rich and are distinct in structure from the central LRRs. The consensus residues, mostly leucine or other hydrophobic amino acids, are normally buried at the core of the structure, while residues at the variable positions are mostly solvent exposed [95] .

All LRRs contain a highly conserved and a variable region, suggesting the existence of leucine rich repeat subfamilies which contain the same conserved regions. With only one type of repeat being observed per protein it has been suggested that each type has evolved individually [92]. Subfamilies include the RI-like and the more common 'typical' subfamilies which include repeats containing 28-29 and 24 residues respectively, and which also differ in the variable region of the repeat [91]. Other subfamilies include one represented by the yeast SDS22+ protein, which contains 22 residue repeats that have less regular structures, and the cysteine-containing LRR subfamily that is represented by the protein Skp2 and contains LRRs of between 23 and 27 residues in length [91, 92]. Also, there are bacterial- and plant-specific LRR subfamilies, which contain 20-22 and 23-25 residues respectively, and the leucine rich repeat transmembrane (LRRTM) subfamily, which have not been fully characterised.

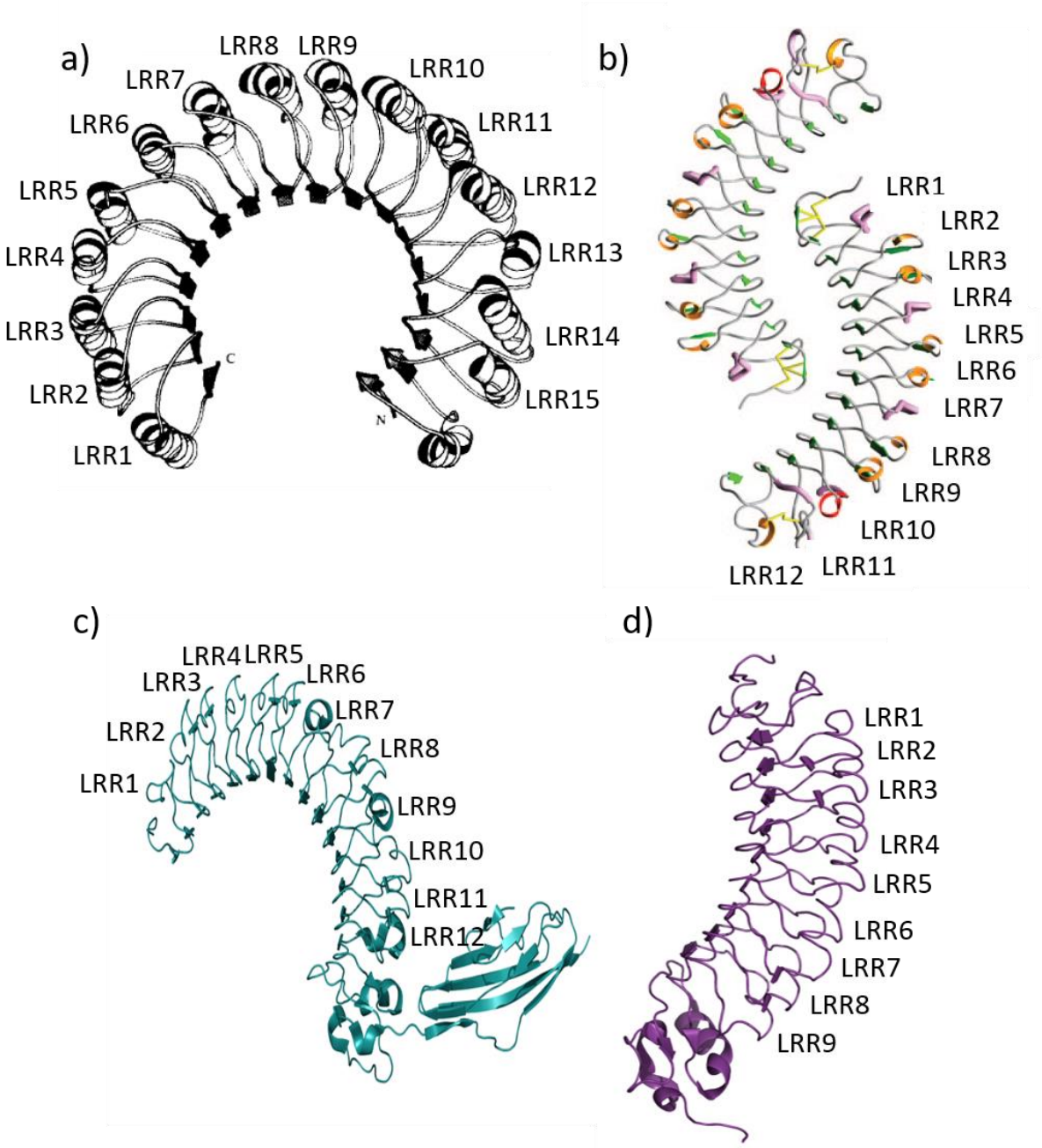

Figure 1.5. Leucine rich repeat domains

a) The structure of the ribonuclease inhibitor which contains 15LRRs (PDB code 1DFJ) [93]. b) The Decorin dimer, each monomer contains 12 LRRs (PDB code 1XCD) [94]. c) The crystal structure of LINGO-1 which contains 12 LRRS (PDB code 2ID5, 4OQT) [69, 77] d) The crystal structure of the NgR which contains 9 LRRs (PDB code 1P8T) [32]. Proteins with a larger number of LRR domains tend to be more horseshoe shaped whilst those with fewer LRRs the more banana shaped.

1.8. The AMIGO family of proteins.

LINGO-1 is part of a group of CNS enriched, LRR domain containing type 1 cell surface proteins [96]. Other members of the group include Netrin G1 Ligand (NGL-1), and AMIGO-1 (Amphoterin Induced Gene and Open reading frame (ORF)) which, like LINGO-1, include Ig domains. While LINGO-1 and NGL-1 are well characterised, AMIGO-1 and its family members, are less well understood.

1.8.1. Discovery

The AMIGO genes were identified by several independent research groups in the last decade. Firstly, Kuja-Panula, et al. [97] used ordered differential display [98] to identify AMIGO as a gene in rat hippocampal neurons that was upregulated on an amphoterin matrix but not a laminin matrix. The group subsequently designated the gene as Amphoterin Induced Gene and Open reading frame (ORF), AMIGO. Amphoterin, also known as HMGB1 (high motility group box protein 1) is known to be involved in a number of physiological processes including functioning as a neurite outgrowth promoting factor originally isolated from perinatal rat brain [99]. Sequence data obtained from the AMIGO clone led to the identification of two closely related proteins named AMIGO-2 and AMIGO-3. Independently, another group identified the AMIGO-2 gene in cerebellar granule neurons as an activity-dependent gene that promoted survival of neurons, and termed it Alivin-1 after alive and "activity- dependent leucine- rich repeat and Ig superfamily survival related protein" [100]. The same group also noted the existence of Alivin-2 and Alivin-3 as homologues for Alivin-1 which corresponds to AMIGO-1 and AMIGO-3. The following year AMIGO-2 was described by a third research group as 'DEGA' meaning 'novel cDNA differentially expressed in human gastric

adenocarcinomas' following analyses of cDNA expression levels in normal *versus* tumour tissues, including gastric adenocarcinoma and other cancer cell lines [101].

1.8.2. Expression and function

Each of the AMIGO family members displays discrete expression patterns in mammalian tissues (Figure 1.6a): AMIGO-1 is essentially nervous system-specific, where it is expressed in the cerebellum, cerebrum and retina [97]. AMIGO-2 mRNA is also mainly expressed in the nervous system, with highest levels in the cerebellum; however, expression was also identified in the retina, liver and lung. Finally, AMIGO-3 displays more broad expression and is detected in most tissues [97]. Within the CNS, all three of the AMIGO proteins are found in a wide variety of brain neurons in different areas of the adult brain and spinal cord as well as astrocytes and oligodendrocytes [102]. However, Kuja-Panula et al. [97] found that the AMIGO proteins were specifically detected in axonal fibers. The expression patterns indicate that the proteins may have similar functions in the CNS however the differing expression outside of the CNS indicates that the AMIGO family of proteins may have context dependent functions.

AMIGO-2 is the best studied of the family and appears to possess a diverse range of functions. AMIGO-2 expression in certain areas of the hippocampus particularly resistant to neuronal injury may suggest a role in neuroprotection [100, 103]. Additionally, AMIGO-2 is a downstream target of calcium- dependent survival signals hinting at neuroprotective functions [100, 103]. Similarly, expression of Alivin 1 (AMIGO-2) appears to promote depolarisation dependent survival of cerebellar granule neurons [100].

The above evidence could imply that mutations in AMIGO-2 may result in neurodegenerative effects. Indeed, mutations in Alivin 1 (AMIGO-2) have been identified as possibly playing a role in the onset of the neurodegenerative diseases Alzheimer's and Parkinson's, with genetic loci mapped to within the same region of chromosome 15 as Alivin 1 (AMIGO-2) [100]. It has also been suggested that haploinsufficiency of AMIGO-2 is responsible for mental retardation, seen in a single patient study [104].

As described above, microarray experiments using murine cancer cell lines and corresponding normal tissue found that AMIGO-2 mRNA is expressed in gastric adenocarcinoma [101], and led to the group undertaking the research to name the gene 'DEGA' [101]. DEGA (AMIGO-2) was identified as being differentially expressed in 45% of gastric adenocarcinoma samples, with a very low level of expression in normal tissue. This suggests that DEGA (AMIGO-2) may be required for tumorigenesis in human gastric adenocarcinomas [101]. Furthermore, expression of antisense DEGA (AMIGO-2) clones in a gastric adenocarcinoma cell line was associated with altered morphology, increased size and ploidy, chromosomal instability, decreased cell adhesion and migration and a nearly complete inhibition of tumorigenicity. This therefore suggests that inhibition of AMIGO-2 expression negatively impacts tumour growth [101]. AMIGO-2 is also over expressed in other cancer cell lines when compared to normal tissue, including thyroid, pancreatic, breast, ovary and lung cancers [101].

A possible role for AMIGO-1 in dendritic outgrowth has been suggested due to elevated expression levels being observed during periods of dendritic extension [102]. AMIGO-1 silencing resulted in attenuation of dendritic elongation including a lower dendrite number, and lower total dendrite lengths [102]. Neuroprotective functions for AMIGO-1 were

suggested in experiments using neuroblastoma cell lines, which express AMIGO-1, which were more resistant to apoptotic insult [102].

AMIGO-1 has also been identified as being essential for the development of neural circuits in zebrafish where it is thought to be involved in homophillic interactions [105]. Furthermore, AMIGO-1 was shown to localise at the neuronal plasma membrane with the potassium channel subunit Kv2.1 and is thought to be involved in schizophrenia-related abnormalities [106].

Finally, AMIGO-3 mRNA levels have been shown to be raised in retina immediately following optic nerve crush and dorsal column lesions in rat, additionally AMIGO-3 levels were reduced in models of regeneration suggesting this protein has a dynamic role in the CNS injury response [107].

Structurally, the extracellular part of AMIGO proteins contains 6 leucine rich repeats (LRRs), flanked on either side by cysteine rich LRRCT and LRRNT domains, and one immunoglobulin (Ig) domain next to the transmembrane region (Figure 1.6b) [97]. The AMIGO-1 protein was detected as a 65kDa polypeptide in brain extracts although its calculated molecular mass based on its primary sequence is 56kDa.

The amino acid sequence homology between rat and mouse AMIGO is 95% and these are 89% identical to the human form [97] with the most conserved extracellular regions restricted to LRRs 1-3 and the LRRNT domains, the transmembrane and cytoplasmic tail (Figure 1.6c). AMIGO homologues exhibit lower sequence identity, with AMIGO-1 and -2 48% homologous, AMIGO-1 and -3 50% homologous and AMIGO-2 and -3 48% homologous [97]. Here, the most conserved regions are the LRRs, transmembrane and cytoplasmic regions [97].

BLAST searches [97] using the extracellular domain of the AMIGO proteins indicates that the nearest homologues were NgR [37] and Slit [108]. The Slit family proteins are secreted glycoproteins that play important roles in the development of the nervous system. Slits, like NgR, contain LRR domains, and activate receptors of the Robo family through the binding of the convex face of their LRR domain to the Ig domains of the Robos [109].

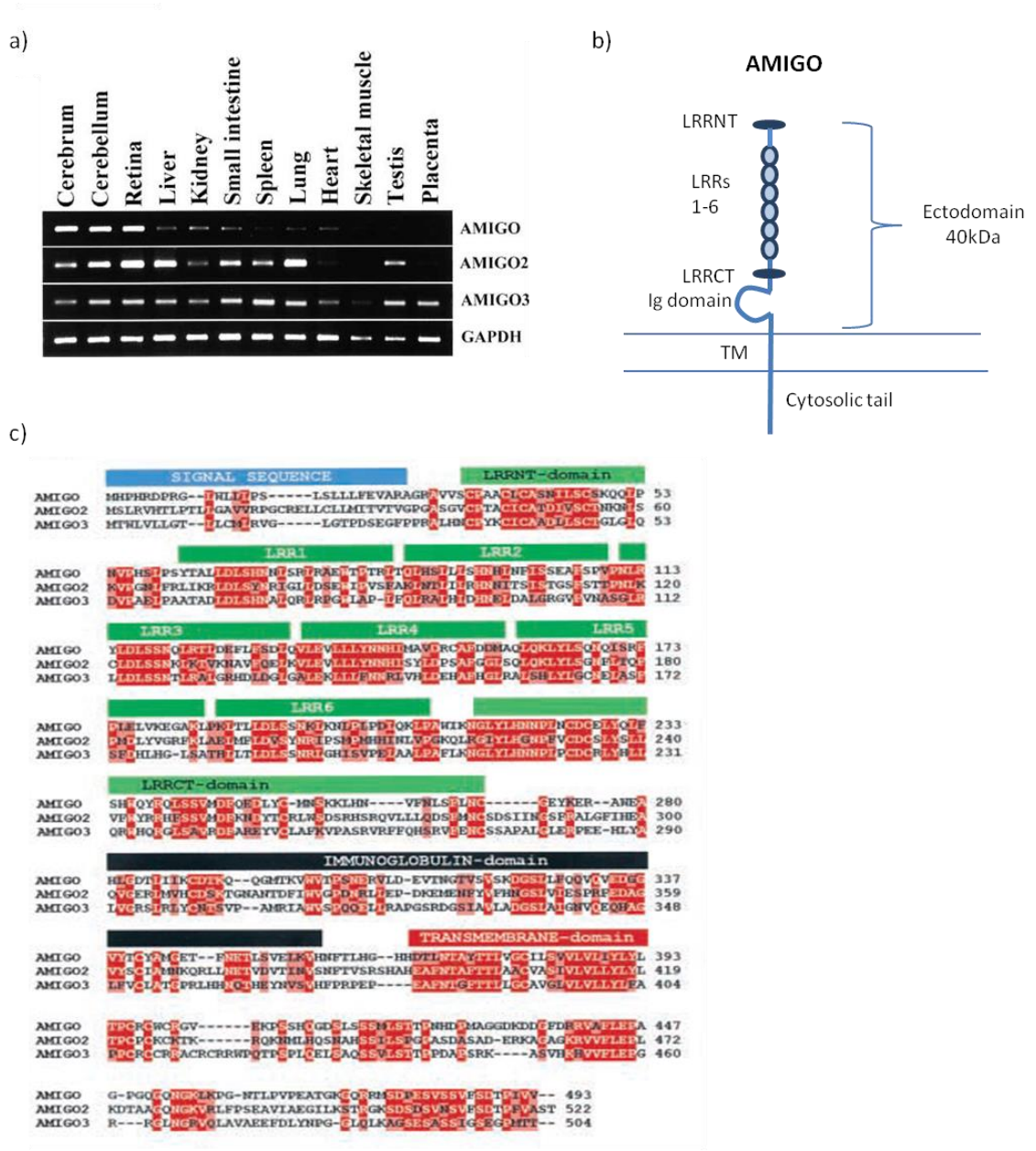

Figure 1.6. Expression, domain organisation and alignment of the AMIGO proteins.

a) AMIGO-1, AMIGO-2 and AMIGO-3 are expressed in many tissues. However different expression patterns are shown, with AMIGO-1 being almost completely nervous system specific and AMIGO-3 being expressed in almost all tissues. b) AMIGO-1, -2 and -3 extracellular domains contain 6 LRRs flanked by LRRNT and LRRCT domains and an Ig domain. The protein also has a transmembrane region and a short cytoplasmic tail. Diagram is not to scale. c) AMIGO-1, AMIGO-2 and AMIGO-3 are 48-50% similar at the amino acid level with the largest similarity in the LRR domain, transmembrane region and cytoplasmic tail.

Images a) and c) taken from [97].

1.9 Treatments in SCI

Therapeutic interventions are most effective in the early stages after injury, i.e. in the acute and sub- acute phases, and should be given as early as possible after injury, before formation of the glial scar. The treatments given in acute and sub- acute phases focus on neuroprotection, compared to those given in the chronic stage focusing on neurorestoration [110]. Neuroprotective treatments must be given alongside treatments which reduce secondary injury caused by inflammation. A number of neuroprotective treatment approaches are being investigated, but basically aim to remove the growth inhibition, manipulate intracellular signalling and deliver neurotrophic factors [13]. There is currently only one drug used in the treatment of SCI, intravenous methylprednisolone is given to reduce inflammation at the site of injury. The drug aids in the reduction of cellular damage if given within 8 hours of injury [110].

1.9.1 Clinical studies

Numerous preclinical and a more limited number of clinical studies have examined the therapeutic potential of multiple drugs and/or protocols to improve recovery after SCI, including those that focus on either the ligands or the receptors that inhibit regeneration. One approach aims to target myelin associated inhibitory factors, for example with an NgR decoy receptor, to attempt to overcome myelin inhibition and improving neurological function [21]. There are two broad approaches to blocking the effects of myelin associated inhibitory proteins (i) removing the intrinsic inhibitory potential of the proteins or (ii) blocking their receptors.

1.9.2 Therapies targeting ligands

Clinical studies targeting Nogo-A and MAG have given promising results, with administration of an anti- Nogo-A antibody in a stroke model associated with an accelerated recovery from neurological damage [111]. An anti- MAG antibody promotes in a stroke model a more rapid recovery of dexterity, the effects are seen as early as 3 days after treatment, suggesting the antibody has a neuroprotective effect rather than a neuroregenerative one. In general, however, the efficacies are relatively low *in vivo* possibly a consequence of the available inhibitory proteins Nogo-66, MAG and OMgp. Treatments that could block all three proteins may therefore be a more attractive therapy.

1.9.3 Therapies targeting the receptors

The human NgR decoy receptor sNgR310-Fc is designed to block the binding of all three myelin associated ligands to NgR. Experimental use has been shown to improve functional recovery and facilitate the growth of axons when used to treat spinal contusion injury in rats [112]. Further, the anti NgR antibody, 7E11 is also a strong inhibitor to NgR and promotes CNS axonal regeneration [113].

Treatments targeting other members of the NgR complex may also give promising results. Clinical trials targeting LINGO-1 are being undertaken for drug companies aiming to find an effective treatment for multiple sclerosis. It is thought that the antibody works by blocking the LINGO-1 protein which inhibits the production of myelin, and in doing so the drug spurs myelin growth [114]. In multiple sclerosis the myelin sheath that insulate axons are damaged by immune mediated processes. Using an anti- LINGO-1 antibody after SCI may help to prevent neurodegeneration by blocking signals from the myelin associated inhibitory proteins

being transmitted into the axon. Phase II clinical trials of an anti-LINGO-1 antibody initially gave promising results (RENEW trial, Biogen), with improved signalling in optic nerves, a possible sign that the myelin sheath had been regenerated [114]. However, results of a Phase II clinical trial for patients with relapsing and remitting MS (SYNERGY trial, Biogen) gave disappointing results, with the treatment failing to provide any improvement in disability or physical or cognitive function. Using an anti- LINGO-1 antibody after SCI may help to prevent neurodegeneration by blocking signals from the myelin associated inhibitory proteins being transmitted into the axon.

1.10. Rationale, hypothesis and aims

It is clear from the literature that further investigations of the NgR complex must be undertaken since *in vivo* treatments targeting the known components do not result in significant regenerative effects. Recent studies determining the intracellular location of LINGO-1 highlights contradictions in the established NgR/p75^{NTR}/LINGO-1 complex. Additionally, the negative response seen in clinical trials and recent indications that the LRR and Ig domain containing protein AMIGO-3 may have a role in the complex, need to be explored further.

1.10.1 Hypothesis

The AMIGO proteins are key members of the NgR complex and can substitute LINGO-1 in the NgR complex to cause axon inhibition.

1.10.2 Aims

To express AMIGO-1, AMIGO-2, AMIGO-3 and LINGO-1, NgR and $p75^{NTR}$ in human cell lines in order to examine their expression and binding profiles.

To produce human AMIGO-1, AMIGO-2, AMIGO-3 and LINGO-1, NgR and $p75^{NTR}$ in *drosophila* in order to determine their binding properties *via* surface plasmon resonance experiments.

Finally, to determine the structures of human NgR, LINGO-1, $p75^{NTR}$ and AMIGO family members, produced in *drosophila*, so that potential ligand binding sites may be determined.

Chapter 2

Materials and Methods

Materials and Methods

2.1: Molecular Cloning

2.1.1 Expression Plasmids

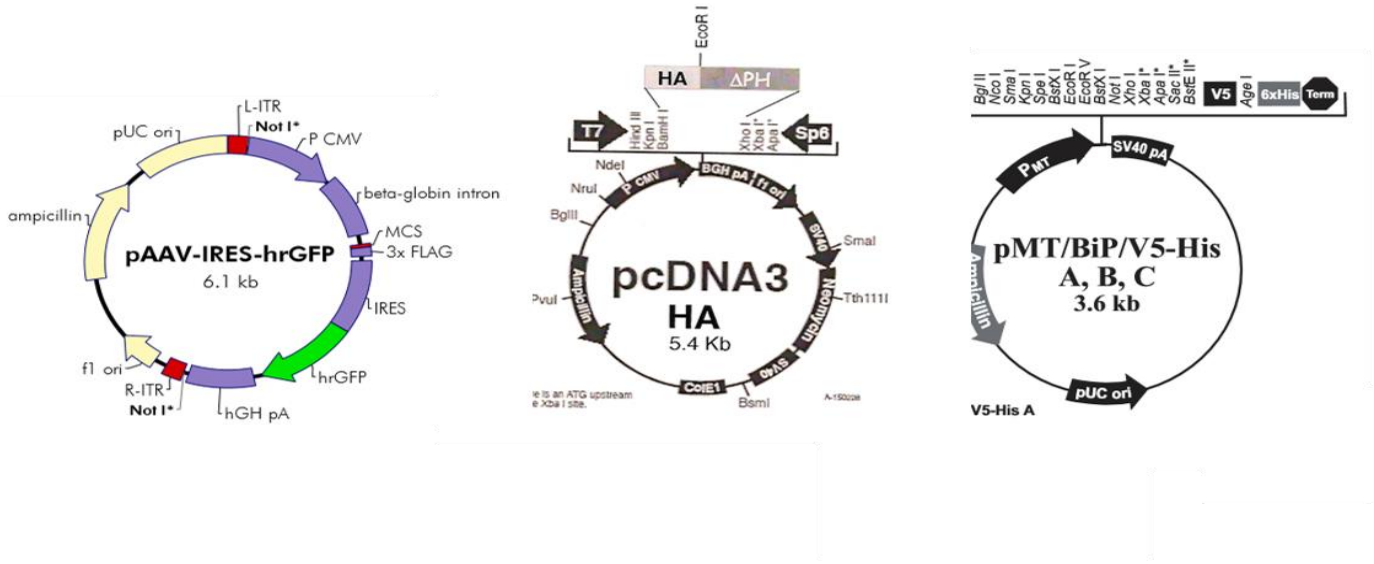

Figure 2.1. Plasmid maps of the expression plasmids used.

Plasmid maps of the pAAV-IRES-hrGFP plasmid (Agilent) and pcDNA3 (Invitrogen) used to express AMIGO-1, -2 and -3, LINGO-1, NgR and $p75^{NTR}$ in HEK293T cells and the pmt-BiP-V5-His plasmid (Invitrogen) used to express human AMIGO-1, -2 and -3, LINGO-1, NgR and $p75^{NTR}$ in *Drosophila* S2 cells.

pAAV-IRES-hrGFP (Agilent) and pcDNA3 (Invitrogen) vectors (Figure 2.1) were used in the eukaryotic expression of human AMIGO-1, AMIGO-2, AMIGO-3, LINGO-1, NgR and $p75^{NTR}$. The pAAV-IRES-hrGFP vector contains a FLAG (3 x FLAG) tag at the 3′ end of the MCS for detection of proteins. pMT/BiP/V-5-His (Invitrogen) was used for eukaryotic expression in S2 *Drosophila* cells, this vector contains a poly-histidine (6 x His) tag for detection and purification of proteins. pCoHygro, a selection plasmid, was co-transfected into Drosophila S2 cells, this plasmid consisted of a bacterial hygromycin B phosphotransferase gene and was used to ensure stable transfections.

2.1.2 PCR

Polymerase chain reaction (PCR) was used to amplify AMIGO-1, AMIGO-2, AMIGO-3, and p75 cDNA (GeneService) and LINGO-1 and NgR cDNA (Thermo Scientific). Primers (Listed in table 1.1 in Appendix) were reconstituted in dH_2O to 20pmol/µl and stored at -20°C. Amplification was carried out using either the Expand High Fidelity enzyme (Roche), Pfu Turbo enzyme (Agilent) or Velocity (Bioline) DNA polymerase enzymes. PCR reactions were performed using a 3770 thermal cycler (Applied Biosystems international) with the following cycling conditions: an initial denaturation step of 96°C, followed by 18 cycles of 96°C for 30 seconds (denaturing), 55°C for 30 seconds (annealing), and 72°C for 90 seconds (extension). A final 5-minute 72°C extension was used to complete the reactions. Typical PCR reactions consisted of 200ng Template DNA, 2µl each of forward and reverse primers (at 20pmol/µl), 200nM dNTPs (Invitrogen), 1 x polymerase buffer (1.5mM $MgCl_2$), 2 units of DNA polymerase enzyme and 1.5µl DMSO.

2.1.3 Overlap extension PCR

Overlap extension PCR was used to introduce mutations or add tags to DNA. This approach uses three PCR reactions, the first two reactions create two halves of the full-length sequence, and the third fuses these together to create the full-length sequence. The first set of reactions used; A: an external forward primer and an internal reverse primer containing a mutation, or B: an internal forward primer containing a mutation and an external reverse primer. The internal primers were designed to have complementary mutations and an overlapping region of 36 base pairs. The third reaction used the products (A and B) from the first set of reactions as template DNA and fused them together using just the external primers. The full-length protein therefore contained the desired mutation.

2.1.4 Restriction digests

DNA was digested using restriction enzymes in their appropriate buffers and at their recommended concentrations according to manufacturer's instructions. Digests were carried out at 37°C for 2 hours.

2.1.5 Agarose gel electrophoresis

Agarose gel electrophoresis was used to separate DNA fragments according to their size; electrophoresis was performed in 1% agarose gels in TBE buffer (89mM Tris base, 89mM Boric acid and 2mM, EDTA), with the addition of 0.5µg/ml ethidium bromide in the gel to allow visualisation of the DNA bands. Electrophoresis was performed using a current of 80mA until clear separation of PCR products, which were prepared by adding an appropriate volume of 10x DNA loading buffer (30% glycerol, 0.25% bromophenol blue) to the DNA sample, was observed. DNA ladders, of appropriate size (100bp and 1kb), were loaded alongside the DNA samples to allow sizing of PCR products. Agarose gels were visualised under a low-level UV light source and recorded using the Syngene documentation system, following which, appropriate bands were excised.

2.1.6 Gel purification

Excised DNA bands were purified using Qiaquick spin columns (Qiagen) based on the standard spin protocol. The purified DNA was eluted into 20µl elution buffer and stored at -20°C until required.

2.1.7 Ligation

Digested vectors were pre-treated with Antarctic Phosphatase (NEB) at 37°C to prevent self-ligation of the vector. DNA inserts were ligated into appropriate vectors digested with the same restriction enzymes as their insert and purified as above. Ligations were carried out at differing insert: vector ratios and in conditions varying from 1 hour at room temperature to overnight at 20°C.

2.1.8 Lysogeny Broth media and pouring plates

Lysogeny broth (LB) media (10g bactotryptone, 10g NaCl and 5g yeast) was mixed with 1 litre deionised water and autoclaved. To make LB agar plates, 15g agar was added to the LB media and autoclaved. The media was cooled to ~55°C and the appropriate antibiotic was added typically ampicillin (100µg/ml) or kanamycin (50µg/ml), the media was poured into plates and left to cool at room temperature before storing at 4°C.

2.1.9 Transformation of bacteria

Ligation mixes were transformed into chemically competent DH5α *E. coli* (Novagen) via heat shock treatment. Cells were thawed on ice for 20 minutes, following which 10-50ng of plasmid DNA was added and left for a further 30 minutes on ice, following this, cells were heat shocked at 42°C for 90 seconds before being placed back on ice for 2 minutes. Next, 250µl of rich growth media SOC (super optimal broth with catabolite repression = SOB+ glucose) was added. The cells were incubated in an orbital shaker at 37°C for 1hr at 220 rpm to allow the antibiotic resistance gene to be expressed and plated onto LB agar plates containing the relevant antibiotic and incubated overnight at 37°C.

2.1.10 Plasmid mini/maxi preparation

Single bacterial colonies were inoculated into 5mls of LB medium containing 100μg/ml ampicillin and incubated overnight at 37°C in an orbital shaker at 220rpm. 3ml of the 5ml culture was centrifuged using a bench top centrifuge (Heraeus Biofuge Fresco 21) and from the resulting pellet, plasmid DNA was extracted using a QIAprep Spin Mini Kit (Qiagen), according to the manufacturer's guidelines. DNA was eluted into 50μl of elution buffer (Tris-EDTA) and stored at -20°C. To obtain higher yields of plasmid DNA, midi (Nucleobond), maxi or mega preps (Qiagen) were performed with correspondingly higher culture volumes (100-500ml). Protocols were followed according to manufacturer's instructions.

2.1.11 Test digests

Test digests were performed on mini prep DNA to ensure DNA inserts had ligated into the plasmid vector prior to sequencing and/or larger scale expression. Briefly, 2μl DNA was added to 1μl appropriate buffer (NEB), 0.1μl bovine serum albumin (BSA, NEB) and 0.5μl each of 5' and 3' enzyme and made up to 10μl with H_2O. Since the volumes are small a master mix of the buffer, enzymes, BSA and H_2O was made up which was then divided equally before the DNA was added. The reactions were incubated at 37°C for 1hr and run by agarose gel electrophoresis to allow separation of vector and insert.

2.1.12 DNA sequencing

DNA sequencing was used to ascertain if any mutations were introduced into the DNA during the PCR and cloning process. Sequencing reactions were set up by adding 2μl of the mini prep DNA to 7μl of H_2O and adding 1μl of the appropriate sequencing primer (4pmol/μl). Sequencing was performed by Functional Genomics (University of Birmingham)

using a high throughput capillary electrophoresis system which can produce read lengths of up to 1000bp. Sequences were analysed using Sequencher software.

2.1.13 DNA quantification

DNA obtained from midi and maxi preps was quantified using Nanodrop apparatus (Thermo scientific) which measures absorbance readings at 260nm. Concentrations were calculated in ng/µl following which all samples were normalised to 1µg/µl using elution buffer (50mM Tris pH7.5).

2.2 Functional studies

2.2.1 Eukaryotic cell transfection

Eukaryotic cell transfection was carried out using HEK293T cells using Polyethylenimine (PEI; Polysciences) in 6 well plates, 10cm dishes or rollerbottles. Cells were plated at a density of 1.2 x 10^5 cells per well in Dulbecco's Modified Eagles Medium (DMEM, Sigma) plus 8% Fetal calf serum (FCS) 48hrs before transfection corresponding to around 90% confluent for transfection. For transfection, for 6 well plates, 2µg DNA was mixed with 15µl PEI (1mg/ml) and 150µl Opti-Mem medium (Invitrogen) and left for 10minutes at room temperature. This was then added drop wise to cells, which had been pre-washed with PBS and were now covered in 3mls Opti-Mem medium. In 10cm dishes the amount of DNA needed was 16µg which was mixed with 100µl PEI (1mg/ml) and 1000µl Opti-Mem. Following transfection cells were incubated for a further 48-72hrs at 37^{o}C before cells and supernatants were collected. Cell supernatants were centrifuged at 13000rpm for 5 minutes to remove cell debris and stored

at -20°C until use. Cells were harvested and washed 3 times in PBS before being lysed with lysis buffer for 30 minutes at 4°C (50 mM Hepes pH 7.5, 150 mM NaCl, 1.5 mM MgCl2, 1mM EGTA, 1% Triton X) following which lysates were stored at -80°C.

For rollerbottle transfection, typically for collection of secreted protein, cells were added to rollerbottles which had been coated with poly-l-lysine, two days before transfection. Cells were transfected with 435µg DNA, 2.7ml PEI (1mg/ml) and 27mls Opti-Mem, into a total volume of 250ml, cells were incubated for 1 week following transfection before the supernatant was collected.

2.2.2 SDS- PAGE

SDS-PAGE was used to separate proteins according to their size. SDS resolving acrylamide gels (12-15%) (0.765M Tris PH8.8, 0.2% SDS, 5ml 30% w/v acrylamide (Geneflow), 0.1% ammonium persulphate and 4ul TEMED (Sigma)) were prepared in 1mm BioRad gel cassettes. Isopropanol was used to cover the resolving gel to level the gel and remove air bubbles. Once the resolving gel had set the isopropanol was removed and the stacking gel (150mM Tris pH 6.8, 0.12% SDS, 0.1% ammonium persulphate, 1% acrylamide and 4ul TEMED) was added on top followed by the insertion of a 1mm 10 well comb.

Protein samples were prepared by mixing protein 1~10µl protein (depending on concentration) with 5x loading buffer (60mM Tris pH 6.8, 10% glycerol, 2% SDS, and 0.01% bromophenol blue, +/- 200mM DTT) and water up to 10-20µl. Reduced samples (+DTT) were boiled at 95°C for 5 minutes and centrifuged for 30 seconds, non-reduced samples (-DTT) were not boiled before loading onto the SDS-PAGE gel alongside an appropriate ladder (medium range protein ladder, BioRad or PageRuler prestained protein ladder, Thermo). Gels were run

in a mini Protean 3 multi casting chamber system (BioRad), 10 x running buffer (0.1% SDS, 90g Tris, 183g glycine) was diluted to 1 x with H_2O and a voltage of 110V was applied while the proteins migrated through the stacking gel and increased to 180V while the proteins migrated through the resolving gel. The current was stopped when the sample had reached the bottom of the gel. To visualise the proteins, the gels were stained with 10ml Coomasie blue stain (Instant blue, Expedeon) for 30 minutes at room temperature then washed in water. Gels were imaged using Syngene gel documentation system (Syngene).

The SDS-PAGE gel was also used to separate proteins for further analysis by western blot, described below. However, in this case, precast gradient gels were used (4-15% TGX stain free protein gels, BioRad) which fit into the same gel chamber and used the same buffer as above.

2.2.3 Western Blotting

Protein samples were separated by SDS-PAGE as described above. Proteins were subsequently transferred via a wet transfer system onto polyvinylidine fluoride (PDVF) membrane (Hybond LFP, GE Healthcare) using transfer buffer (10% methanol, 190mM Glycine, 25mM Tris) and blocked in 5% milk in TBS+ 0.1% Tween-20 (Sigma) for 1hr at room temperature or overnight at 4^{o}C. After blocking the blots were incubated with primary antibody (see table below) in TBS + 0.1% Tween-20 + 3% BSA for 1hr at room temperature. The membrane was then washed again, three times with 0.1% Tween-20 in TBS and the blot was incubated with secondary antibody (HRP conjugated goat anti-mouse mAb) at 1:20 000 (Sigma) or HRP conjugated goat anti-rabbit mAb (1:2000, Sigma) in 5% milk in TBS + 0.1 % Tween-20 for a further 1hr at room temperature before a final 3 washes in TBS + 0.1% Tween-20. Fluorescence was visualised using enhanced chemiluminescence (ECL) reagent (EZ-ECL

Chemiluminescence Detection Kit for HRP, Biological Industries). Briefly, 1ml reagents A and B were mixed in equal measures and incubating at room temperature for 5 minutes, before adding to the membrane and incubating for a further 5 minutes. The membrane was then analysed by autoradiography.

2.2.4 Antibodies

Antibody	Dilution	Supplier
Mouse anti FLAG (Monoclonal)	1:20 000	Sigma F3165
Mouse Anti- HA (monoclonal)	1:1000	Sigma H9658
Rabbit Anti- HA (Polyclonal)	1:1000	Abcam (Ab13834)
Rabbit Anti- β Actin	1:1000	Sigma A5441
Rabbit Anti-AMIGO-1 (Polyclonal)	1:1000	Abcam ab93676
Mouse Anti- AMIGO-2 (Polyclonal)	1:1000	Sigma SAB1400868
Rabbit Anti- AMIGO-2	1:1000	Abcam Ab84416
Rabbit Anti- AMIGO-3	1:1000	Abcam Ab90058

Mouse Anti- AMIGO-3 (Polyclonal)	1:1000	ABNOVA H00386724
Rabbit Anti- LINGO-1	1:1000	Millipore 07-678
Mouse Anti- NgR (Polyclonal)	1:500	R&D systems MAB1208
Rabbit Anti- NgR (Monoclonal)	1:1000	Abcam Ab184556
Rabbit Anti- $p75^{NTR}$	1:1000	Sigma N3908
Rabbit Anti- Na K ATPase (Monoclonal)	1:10 000	Abcam Ab76020
Rabbit Anti- Lamin B1 (Polyclonal)	1:5000	Abcam Ab16048
Mouse Anti-α tubulin (monoclonal)	1:10 000	Abcam Ab7291

Table 2.1. Table of Antibodies used including concentrations used and supplier catalogue numbers.

2.2.5 Quantification of Protein

Protein concentrations produced from HEK293T cell lysates were quantified using a BioRad Dc protein assay kit or by measuring absorbance at OD_{280} using a Biophotometer.

2.2.6 Co-Immunoprecipitation Experiments

For co-immunoprecipitation experiments HEK293T cells were grown in 6 well plates as described above and transfected with 2μg of each DNA construct being assessed. The transfected cells were incubated for 48hrs before they were harvested and lysed using CO-IP lysis buffer (50mM Hepes pH 7.5, 150mM NaCl, 1.5mM MgCl2, 1mM EGTA, 1% Triton X, 10% glycerol). Cell lysates were mixed with 20μl of anti-FLAG (anti-FLAG M2 affinity gel, Sigma) or anti-HA (EZview Red anti-HA affinity gel, Sigma) beads for 2 hours at 4^{o}C. The lysates were then centrifuged and supernatant was discarded, the beads were then washed with 500μl PBS three times before being suspended in 40μl lysis buffer. Next, 10μl of 5 x SDS buffer +DTT was added to the samples which were boiled for 5 minutes at 95^{o}C. Samples were stored at -20^{o}C and analysed by western blot.

2.2.7 Cell fractionation

Cell fractionation allows subcellular protein localisation. Transfected HEK293T cells were divided into 4 subcellular fractions using the Subcellular Protein Fractionation kit for cultured cells (Cell Signalling Technology). The four fractions obtained were; whole cell lysate cytoplasmic, membrane and nuclear. Once divided, fractions were analysed by western blot and stored at -20^{o}C.

2.2.8. MO3.13 cells

The human glial oligodendrocyte cell line MO3.13 (obtained via CELLutions Biosystems Inc, Ontario, Canada) was used to assess the expression of the proteins of interest in the human CNS. Cells were plated at a density of 1.2 x 10^5 cells per well in Dulbecco's Modified Eagles Medium (DMEM, Sigma) plus 8% Fetal calf serum (FCS) and incubated for 48-72hrs (until

~90% confluent) at 37°C before cells were collected. Cells were washed 3 times in PBS before being lysed with lysis buffer for 30 minutes at 4°C (50 mM Hepes pH 7.5, 150 mM NaCl, 1.5 mM MgCl2, 1mM EGTA, 1% Triton X), following which lysates were stored at -80°C until needed when 15µl of cell lysate was analysed by western blot.

2.2.9. Human brain tissue

Human Brain tissue (control tissue) obtained from MS Society Tissue Bank, Imperial College London, Multicentre Research Ethics Committee 08/MRE09/31. Brain tissue was prepared according to standard protocols by MS brain bank staff, with fresh brain was cut into 1-cm-thick coronal slabs before either cryopreserving in cold isopentane on a bed of dry ice. Tissue originated from a donor with a non-primary neurological cause of death (cardiac arrest following pneumonia), considered to be a "non-neurological control" [115]. Upon receipt, brain tissue was lysed, aliquoted into 10µl aliquots and stored at -80°C until needed. Samples were mixed with 5x SDS buffer and analysed by western blot as described previously.

2.3 Protein production in insect cells

2.3.1 Expression in S2 *Drosophila* cells

The *Drosophila* system ensures high level expression of soluble recombinant proteins which, when expressed with a histidine tag, allows quick and simple purification of large quantities of protein. Expression vectors (pMT/BiP/V5-His, Invitrogen) encoding the protein of interest and a selection plasmid, pCoHygro, conferring resistance to Hygromycin B were co-

transfected into the S2 *Drosophila* cell line. Cells were grown in a selecting medium (Schneider's Drosophila Medium modified with L-Glutamine, Lonza) and supplemented with 10% fetal calf serum and 300μg/ml hygromycin. Cells were subcultured every 4-5 days into fresh medium containing 5-10% conditioned medium (media which has been used in growing parental cells and so contains proteins released from parental cells which help enable frozen cells to grow back after a freeze thaw without all the cells dying off), with cells seeded at 1.2 x 10^6 cells/ml in 15-20ml media in T75 culture flasks. For expression, cells were grown in 250mL medium containing 300μl/ml hygromycin plus 0.05% Pluronic F-68 surfactant (Gibco) to prevent the cells from clumping together. Typically, 1 litre of medium split in 4 x 1L Erlenmeyer flasks were produced and incubated at 27°C, gently shaking at 70rpm for 3 days (or reached 4-6 x 10^6 cells/ml). Protein expression was then induced via the addition of 500μM $CuSO_4$ (final concentration) and incubated for a further 4 days before the medium was harvested and cells pelleted by centrifugation at 100g for 15 minutes. Supernatants were stored at 4°c with 0.02% sodium azide until further purification was performed.

2.3.2 S2 cell Protein Test expression

S2 cell expression of protein was tested by inducing a small volume (6ml) of cells with 500μM $CuSO_4$. Supernatant collected at days 2, 3 and 4 was analysed by western blot with a C-terminal anti-His antibody to detect the His tag on the expressed protein.

2.4: Protein purification

2.4.1 Dialysis

In order to successfully purify the expressed protein, smaller compounds present in the culture medium, which can bind to and clog the affinity column, must first be removed. Compounds such as surfactants, free amino acids and excess copper sulphate were removed from the cell media by dialysis. The supernatants were loaded into 10kDa dialysis tubing (Sigma), and dialysed into 10 x volume of PBS buffer overnight at 4^{o}C. Following this the supernatant was removed from the dialysis tubing to undergo further purification.

2.4.2 Nickel affinity chromatography

Econo columns (Biorad) were loaded with 1ml of Nickel beads (Ni-NTA agarose stored in 20% ethanol, Qiagen) per 1 litre of supernatant to be processed over the column. Following this, the column was washed with 1 column volume (10ml) of 1xPBS + 10 mM Imidazole. The dialysed S2 supernatant was flown over the beads by gravity at 4^{0}C overnight with a slow flow-rate (approx 1ml/min). The following day, the column was washed with 1xPBS + 10 mM Imidazole to remove non-specific proteins, and once the UV OD_{280} of the wash flow through was zero (using PBS+ 10mM imidazole as a blank), the beads were incubated with elution buffer (1xPBS + 250 mM Imidazole (~7 ml)) for 30 minutes. After the incubation period the eluted proteins were collected in 1ml fractions and quantified by spectrophotometry using UV absorbance (280nm). The fractions were then either buffer exchanged or filtered and loaded straight onto the FPLC for further purification as described below.

2.4.3 Buffer exchange

PD-10 desalting columns (GE healthcare) were used to buffer exchange the protein into more suitable buffer conditions. PD10 Columns were washed with three column volumes of the desired buffer; the first three fractions of the eluted protein in the 250mM imidazole buffer were then added to the column and the eluate allowed topass through the column. Finally, 3.5ml of the desired buffer was added to the column and the flow through was collected.

2.4.4 Gel filtration

Expression of recombinant proteins with histidine fusion tags is a useful way of facilitating purification of that protein by use of immobilised metal ion affinity chromatography (IMAC).

Size exclusion chromatography was performed using a FPLC system (ÄKTA, GE healthcare), Superdex 200 (>1mg) and HR200 (<1mg) columns were used. Columns were washed and equilibrated with desired buffer prior to the protein being loaded. Samples were filtered using a 0.45μm filter disc immediately prior to gel filtration. The purification step was carried out at room temperature using a flow rate of 3ml/min and fractions were collected as either 0.5ml (HR200) or 5ml (S200) aliquots using the fraction collector. The resulting elution profile showing absorbance (mAu) of the eluted protein fractions were analysed using Unicorn (version 4) software (GE Healthcare), allowing identification of the peak fractions to be analysed by SDS-PAGE to assess purity.

2.4.5 Protein quantification

The concentration of protein at all points during purification was determined by measuring the absorbance of the protein solution at OD_{280} using Biophotometer (Eppendorf) compared to a blank encompassing the buffer alone. From the absorbance reading the concentration of the protein can be determined using the calculation of $OD_{280} = \varepsilon \times c \times l$ where ε is the extinction

coefficient ($cm^{-1} M^{-1}$), c is the concentration (M) and l is the length of light path through the sample (1cm). If the extinction coefficient is known then the concentration of the protein can be worked out using the calculation $c = OD_{280}/ \varepsilon \times l$. The ε value is calculated from the number of tyrosine (Y) and tryptophan (W) residues and the number of disulphide bonds (SB) within the protein using the following calculation; $\varepsilon = ((n_Y \times 1490) + (n_W \times 5500) + (n_{SB} \times 125))$.

2.4.6 Protein concentration

Centrifugal filter units (Millipore) with a 10kDa molecular weight cut off were used to concentrate proteins, 15 ml units were used initially, at a speed of 4000g, to reduce the volume of protein solution to around 1.5ml followed by smaller, 0.5ml units (micron, 10kDa), at a speed of 14000g, were used to further concentrate the protein. Absorbance was calculated after each spin cycle of 10 minutes to check the concentration of the protein at all times.

2.5. X-ray crystallographic studies

2.5.1 Small scale crystallisation trials

Small scale crystallisation trials were initially set up using the 'hanging drop vapour diffusion' method using 100nl protein + 100nl crystallisation buffer aided by the nanolitre mosquito robot (TTP LabTech). To identify the optimal conditions needed for formation of crystals commercial screens were used (Table 2.2), with each screen contained 96 different conditions of which 100µl of each was added to a 96 well plate (Iwaki). The mosquito robot then pipetted 100nl from each condition and 100nl of the concentrated protein onto a plate seal. The plates were then sealed with the protein/buffer drops hanging above their corresponding wells and

incubated at 23°C. After 4 days the 96 well plates were visualised using a light microscope (Leica) to determine crystal formation.

Screen Name	**Company**
JCSG+	Molecular Dimensions Ltd (MDL)
Wizard I + II	Emerald Biosystems
PEG/ ION	Hampton Research
INDEX	Hampton Research
Structure Screen I + II	MDL

Table 2.2. Commercial screen used for small scale crystallisation trials

2.5.2 Large scale crystallisation trials

Large scale trials were set up in 24 well Linbro plates (MDL) using both the 'hanging drop and 'sitting drop' vapour diffusion methods. Briefly, 1ml of crystallisation buffer was added to each well and the edges of each well were coated with vacuum grease (MDL). The protein and the corresponding buffer were mixed on a cover slip or sitting drop columns in ratios of 1:1, 1:2, 1:3 and 2:2 (µl, protein: buffer). For the hanging drop set up the cover slips were then inverted over the wells and sealed. For sitting drops the sitting drop bridges were placed in the well and a clean cover slip was used to seal the well. The 24 well plates were incubated at 23°C and examined after 3 days using a light microscope then subsequently every week. IM50 software (Leica) was used to document crystal formation.

2.5.3 Cryoprotectant soaking

Once protein crystals had formed they were transferred into reservoir solution and allowed to soak for 5 minutes using a 0.2 mm nylon loop. The crystals were then soaked in reservoir solution supplemented with increasing concentrations of glycerol (starting at 5% followed by 15%, 20% and 25%). Crystals were left to soak in for 5 minutes in each condition and soaked for 30 minutes in the final condition of 25% glycerol in mother liquor. Crystals were soaked in a cryoprotectant prior to exposure to X rays in order to prevent the solvent surrounding the protein crystal from forming ice crystals and protect the crystal from radiation damage. Following these series of soaks, the crystals were flash cooled in liquid nitrogen and stored in a cryogenic dewar (MDL), ready for X-ray data collection.

2.5.4 X ray data collection and Processing

X-ray diffraction experiments were performed using either the 'in house' Micromax 007HF rotating anode X-ray generator (Rigaku) and Saturn charged coupled device, or X-ray diffraction data were collected remotely (at University of Birmingham) or the Diamond Light Source (Oxford). All data collection manipulations were carried out using the CrystalClear (Rigaku) software. Intensity data were integrated, scaled and merged using programs of the XDS suite [116].

2.5.5 Structure Determination and Refinement

The structures of hAMIGO-1 LRR and hAMIGO-1 LRR + Ig were determined by molecular replacement with MOLREP (Collaborative Computational Project No 4 1994) [117], AMORE

[118] and CNS [119] packages using the previously determined structure of mAMIGO-1 [120] as the phasing model. For both structures, the molecular-replacement calculations yielded unambiguous rotation and translation function solutions. The molecular models were refined with CNS [119] and REFMAC5 [117], the progress of which was verified by monitoring the reduction in the Rf_{ree} value [119] calculated from an independent set of reflections (5%), set aside for cross validation. The models underwent several rounds of alternating simulated annealing and positional refinement which were followed by isotropic B factor refinement. Examination of the resulting electron-density maps showed unbiased features in the electron density, which confirmed that the molecular replacement solutions were correct. Once R factor values were reduced below 30%, solvent molecules were included in the models, if they appeared in *Fo-Fc* maps contoured at over 3σ and were within hydrogen-bonding distance to chemically accepted groups. Model manipulations were performed with COOT [121]. The quality of final models were verified with PROCHECK [117], structural models were produced using Pymol (http://www.pymol.org), and molecular surfaces generated using DELPhi [122]. All structural analysis were performed with programs of the CCP4 suite [123].

2.6 Surface plasmon resonance (SPR)

SPR is a highly sensitive technique used for the detection of real time binding. The process allows for the determination of binding affinities and kinetic measurements.

2.6.1 Biotinylation of Proteins

The protocols used in surface plasmon resonance binding experiments require that proteins are biotinylated via the BirA tag contained in the expressed constructs. This involved buffer

exchanging soluble proteins purified previously by Ni-NTA +/- size exclusion chromatography, into biotinylation buffer (100mM Tris pH 7.5, 20mM NaCl, 5mM $MgCl_2$) as described in section 2.4.3. For the biotinylation reactions; to the 3ml protein in biotinylation buffer 0.5mM Biotin (Sigma), 1mM ATP (Sigma), 1 x protease inhibitors (25X concentrate, Roche) and BirA enzyme (In house product ([124])) were added and incubated at room temperature for 1 hour, followed by an overnight incubation at 4°C. Excess biotin was removed from the sample by size exclusion chromatography the following day.

2.6.2 Experimental Procedure

SPR studies were performed at 25°C using the University of Birmingham BIAcore 3000 machine (BIAcore, GE Healthcare). To perform a protein binding experiment HBS-EP running buffer (10mM HEPES pH7.4, 150mM NaCl, 3.4mM EDTA. 0.0005% surfactant P20) was used. Firstly, a new CM5 sensor chip was docked in the machine and the system was primed with H_20. Next, BIA normalising solution was injected at 10µl/min to normalise the signals obtained from the instrument and streptavidin was immobilised onto the chip by standard amine coupling at pH 5. This involved injecting a mix of equal volumes of 0.2M N-ethyl-N5 (3-diethylaminopropyl)-carbodimide (EDC) and 0.5M N-hydroxysuccinimide (NHS) over the sensor chip at 10µ/min. Following this, 60µl streptavidin (0.5mg/ml in 10mM Sodium Acetate pH 5.5) was injected over the chip followed by 70µl of 1M ethanolamine pH 8.5 which blocked any remaining active carboxyl-esters on the surface, and 500µl Glycine-HCL pH 2.5 to remove uncoupled streptavidin. Final streptavidin levels were shown in response units on BIAevaluation software. Purified biotinylated protein samples (NgR-Bt) at 1.2mg/ml, were diluted in HBS-EP buffer and injected at 5µl/minute over the immobilised streptavidin, the levels of immobilised protein on each flow cell was kept as consistent as possible over each

cell. Analyte proteins were stored on ice and centrifuged at 13000 rpm immediately prior to injection over flow cells at 10µl/min; a total of 30µl was injected. Serial dilutions of protein were used to obtain affinity measurements. Data was analysed using BIAevaluation software (BIAcore AB) and Origin Pro 8 Software (OriginLab Corperation).

Chapter 3

Functional studies of the AMIGO family of proteins

Functional studies of the AMIGO family of proteins

3.1 Introduction

Unlike those in the PNS, axons in the CNS are unable to regenerate because the environment in the CNS after injury is inhibitory to regeneration. In the initial stages post injury, inhibitory signals originate from the environment created as a result of cell damage whereas in the weeks following injury the formation of a glial scar causes a physical barrier to regeneration. Indeed, it has been well documented that CNS neurons are able to regenerate if given a permissive environment [11, 12]. Inhibitory effects result in part from the release and upregulation of myelin derived axon inhibitory proteins Nogo, MAG and OMgp [125], and cause growth cone collapse via Rho GTPase signalling through the Nogo receptor (NgR) complex.

The tripartite NgR/p75^{NTR}/LINGO-1 complex inhibits axon regeneration in the injured CNS by activating Rho A, with each member of the complex necessary for successful inhibition. *In vitro* expression of NgR and p75^{NTR} alone in non-neuronal cells fails to activate Rho A [68] indicating that another, neuronally expressed, protein is necessary for inhibition. LINGO-1 was identified as an additional essential component of the NgR/p75^{NTR} complex [68] which, when expressed alongside NgR and p75^{NTR} provided responsiveness to the myelin associated inhibitory protein, OMgp. The functional importance of LINGO-1 within the complex is suggested primarily from *in vitro* experiments using a range of methods to manipulate expression or ligand binding (RNAi, dominant negative LINGO-1 transfectants, LINGO-1 Fc fusions or blocking antibodies). Experiments examining the *in vivo* functional consequences of LINGO-1 blockade are limited to a single study using LINGO-Fc in a model of CNS injury [73]. More definitive evidence for an *in vivo* functional role for LINGO-1 is lacking, which is of concern, particularly as the time course of LINGO-1 expression is delayed by up to two weeks following injury [107]. These findings may suggest functional redundancy, either via a LINGO-1 paralog (i.e. LINGO-2, LINGO-3, LINGO-4) or an alternative protein substituting

for LINGO-1. Further complications are evident, with more recent data suggesting that LINGO-1 is in fact intracellular and competes with NgR for binding to $p75^{NTR}$ [126].

In one example examining gene expression profiles in a rat CNS injury model, AMIGO-3 was identified as upregulated following injury [127], and importantly was further identified as downregulated in a modified CNS injury protocol promoting axon regeneration [127]. The same group also confirmed that LINGO-1 expression remained low in all models. Rat AMIGO-3 was also shown to be able to participate in the NgR/$p75^{NTR}$ complex, indicating a potential role for this protein in mediating axon growth inhibition.

3.1.1. LRR proteins and interactions

Leucine rich repeats are frequently involved in the formation of protein-protein interactions. The repeats are present in numerous proteins with diverse functions; both NgR and LINGO-1 are LRR domain containing proteins as are the AMIGO proteins. LINGO-1 and the AMIGO proteins also contain an Ig domain and are referred to as LRR and Ig domain containing proteins.

Three members of the AMIGO family of proteins have been described; AMIGO-1, AMIGO-2 and AMIGO-3, which are single pass transmembrane proteins each containing 6 leucine rich repeats (LRRs) and one Ig domain. AMIGO-2 and AMIGO-3 are homologous to AMIGO-1 with similarities at the amino acid level of 48% and 50% respectively [97]. The most conserved regions of the proteins are the LRR domain, transmembrane region and cytosolic tails, with conserved features observed across mammalian species. The three proteins are differentially expressed, with AMIGO-1 being relatively CNS specific and AMIGO-2 and AMIGO-3 being more widespread [97].

3.2 Specific aims and methods

This chapter outlines several biochemical and cellular approaches to determine whether human AMIGO family members are functional interactors within the NgR/p75^{NTR} complex. cDNA constructs were engineered for protein expression in mammalian cells to permit transient cell expression followed by co-immunoprecipitation studies on cell lysates. The availability of high quality antibodies to AMIGO family members is a major limiting factor, so the majority of the expression studies were therefore performed using constructs which included engineered protein tags to permit efficient immunoprecipitation and/or western blotting analyses. Once transfected into cells, expression patterns (including glycosylation) and the respective subcellular localisations were determined. Protein-protein interactions were determined using co-transfection of differentially tagged proteins. Similar studies were then attempted using cultured cell lines (in which the proteins are endogenously expressed), and native tissue using available polyclonal antibodies to native proteins.

3.3. Determining expression and binding profiles of AMIGO proteins

3.3.1. Cloning of AMIGO-1, AMIGO-2 and AMIGO-3

Homophillic and heterophillic binding between AMIGO family members has been examined via co-immunoprecipitation studies using GFP and V5 tagged AMIGO proteins expressed in HEK293T cells. In a complimentary study, proteins were also bound to protein A-coated beads, and signs of aggregation examined [97]. These experiments demonstrated that the

AMIGO family of proteins display both heterophillic and homophillic binding, as demonstrated by both bead aggregation and immunoprecipitation of corresponding proteins. This approach, although successful is subject to a major limitation, as GFP (used as a tag) forms a dimeric structure. This makes a definitive interpretation of the results complex.

First, two designs were used: AMIGO constructs were produced fused to a C-terminal FLAG tag sequence. The relevant cDNA was inserted into the multiple cloning site (MCS) of pAAV-IRES-hrGFP plasmid (Figure 3.1), leading to fusion with a 3 x FLAG tag. The FLAG epitope can be detected using the highly specific M2 antibody. A second set of constructs were also produced to incorporate an N-terminal HA tag according to Figure 5.1. The HA tag was inserted into the vector following (i) a secretion signal sequence and (ii) a cleavage sequence. The signal peptide derived from preprotrypsin, MSALLILALVGAVAAVA, and epitope tag sequence (HA), YPYDVPDYA, were inserted upstream of the multiple cloning site (MCS), as described previously by Wang et al 2002 [128], inserted into the mammalian expression vector pcDNA3.

Plasmids were transfected into HEK293T cells at 90% confluence using polyethylenimine (PEI) and cells were left to express the protein for 72 hours, whereupon cells and cell supernatants were collected for analysis by SDS-PAGE and western blot.

3.3.2 Cloning of LINGO-1, NgR and p75^{NTR}

LINGO-1, was similarly cloned into (i) pAAV-IRES-hrGFP vectors or (ii) pcDNA3 vectors to produce constructs with either C-terminal 3x FLAG or N-terminal HA tags respectively. NgR and p75^{NTR} were cloned as N-terminal HA tags only. As before, all constructs were transfected

into HEK293T cells using PEI and cell lysates and supernatants were analysed by SDS-PAGE and western blot.

a)

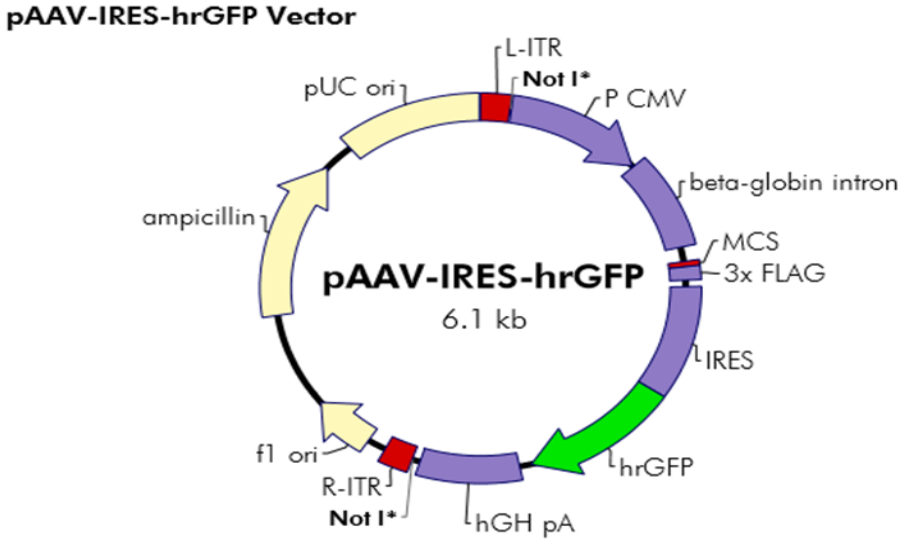

b)

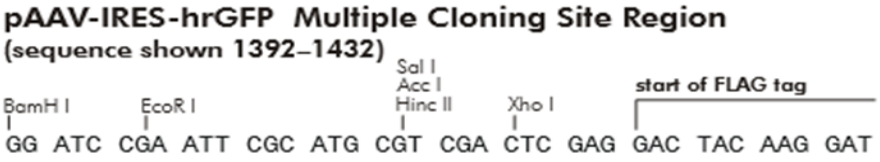

c)

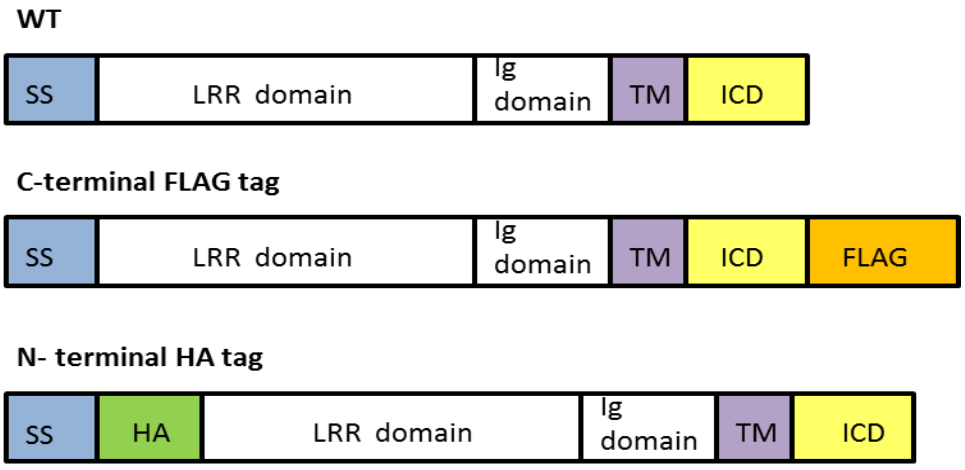

Figure 3.1. Cloning of AMIGO-1 proteins with FLAG and HA tags.

a) Map of paav-IRES-hrGFP vector into which the gene of interest was cloned.
b) Multiple cloning site information
c) Diagrammatic representation of the proteins produced.

3.3.3 Western Blot analysis of HEK293T expression

Following transfection, cells were lysed and analysed by western blot using antibodies against FLAG (Mouse anti FLAG M2) and HA tags. Whilst the FLAG antibody (Sigma F3165) was efficient and reliable, there were initial difficulties with determining the optimal anti-HA antibody. After trials, where the two HA antibodies were added at differing concentrations and developed for varying times the most reproducible antibody was determined to be Mouse Monoclonal Anti-HA, Sigma H9658.

Whole cell lysates were analysed by western blot, to detect AMIGO family members, LINGO-1, NgR and $p75^{NTR}$ (Figure 3.2). The AMIGO family of proteins were shown as doublets at around 70kDa in size when detected using both HA and FLAG tagged antibodies. The predicted mass of the AMIGO proteins are 55.2kDa, 57.9kDa and 55.2kDa respectively. The 3x FLAG tag is around 3kDa in size as is the HA tag, leaving a discrepancy of around 10kDa between the expected sizes and the actual sizes displayed on SDS-PAGE. This discrepancy is likely due to differential glycosylation suggested previously for AMIGO-1 [120]. While the predicted size for the expressed LINGO-1 construct is 67kDa, in the absence of tags, it migrates at around 100kDa, indicating that, like the AMIGO family members, it is also glycosylated. Similarly, the NgR and $p75^{NTR}$ constructs are also expressed as doublets and both are shown at around 70kDa, a similar size to that previously detected [53, 59, 129, 130]. In addition, bands are seen at around 140kDa for AMIGOs -1,-2 and -3 which are likely to be dimers. There doesn't appear to be a similar band in LINGO-1 however there are also large molecular weight bands in NgR and $p75^{NTR}$ which at around 130kDa are also likely to be dimers.

AMIGO-1 has 5 N-linked glycosylation sites, 1 in LRR1, 1 in the LRRCT and 3 in the Ig domain. AMIGO-2 has 8 N-linked glycosylation sites 1 in the LRRNT, 1 in LRR2, 1 in the LRRCT and

5 in the Ig domain. AMIGO-3 also has 5 N-linked glycosylation sites with 1 in LRR2, 1 in the LRRCT and 3 in the Ig domain. Finally, LINGO-1 has 10 N-linked glycosylation sites with 1 in LRR4, 1 in LRR6, 2 in LRR8, 1 in LRR9, 1 in LRR11, and 4 in the Ig domain. Glycosylations are predicted to add around 2kDa each to the mass of the protein they are attached to, therefore the mass of the proteins may be altered substantially [131].

To examine glycosylation dependent effects on gel migration, cell lysates were treated with Peptide N-Glycosidase (PNGaseF), an amidase which removes all N-linked oligosaccharides from proteins. The treated lysates were analysed by western blot, as compared to their untreated counterparts (Figure 3.3) with the deglycosylated cell lysates showing the native size of the expressed proteins. Following deglycosylation AMIGO proteins migrate at around 55kDa, considerably closer to the predicted size of these proteins. Similarly, a large shift in observed sizes for LINGO-1 (100kDa) and the deglycosylated version (70kDa) was observed, with the latter now substantially closer to the predicted size of 67kDa. Finally, NgR and $p75^{NTR}$ were also treated with PNGaseF, which had little effect on the size of $p75^{NTR}$ but altered the size of NgR from around 70kDa to around 50kDa.

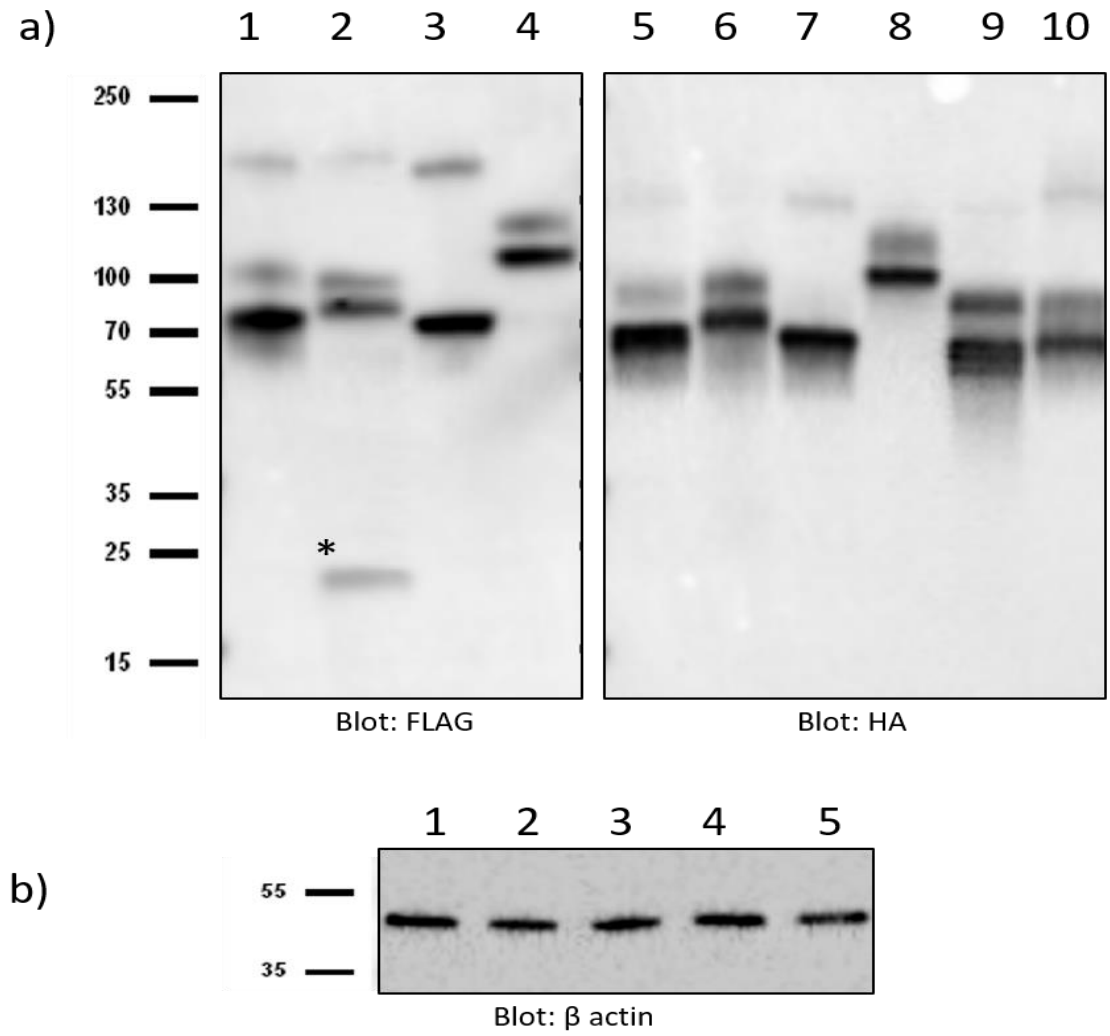

Figure 3.2. Expression of proteins of interest in HEK293T cells.

HEK293T cells were transfected with C-terminal FLAG (Left panel) and N-terminal HA (Right panel) tagged constructs. Cells were lysed and lysates were analysed by western blot. Proteins were detected using antibodies directed against the FLAG (left panel) and HA tags (right panel) demonstrating effective protein expression. * indicates a cleaved form of AMIGO-2 FLAG at around 20kDa in size.

1. AMIGO-1- FLAG
2. AMIGO-2-FLAG
3. AMIGO-3-FLAG
4. LINGO-1-FLAG
5. HA-AMIGO-1
6. HA-AMIGO-2
7. HA-AMIGO-3
8. HA-LINGO-1
9. HA-NgR
10. HA-P75^{NTR}

b) PVDF membranes were stripped and re-probed with β- actin antibody as a loading control.

1. Untransfected HEK293T cells (Negative control)
2. AMIGO-1-FLAG
3. AMIGO-2-FLAG
4. AMIGO-3-FLAG
5. LINGO-1-FLAG

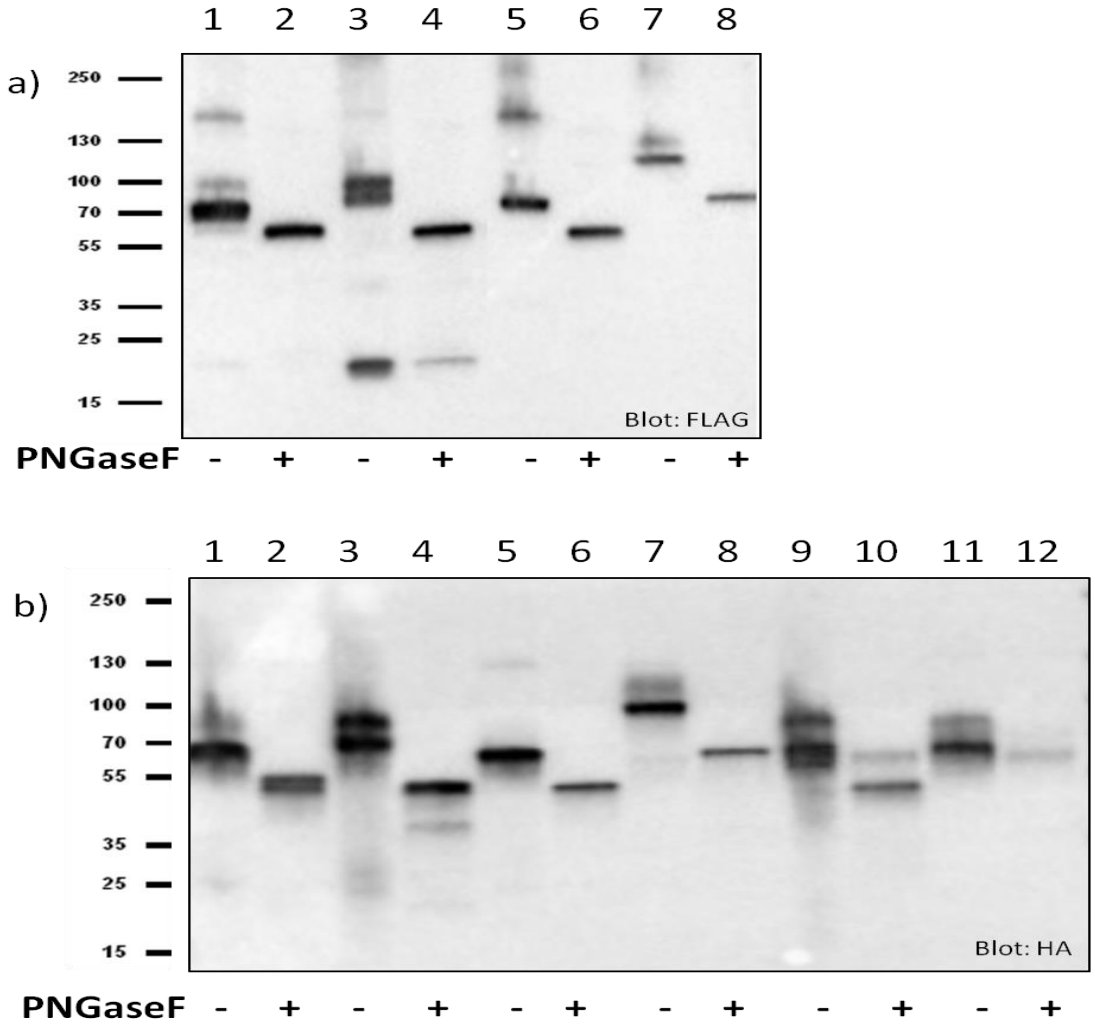

Figure 3.3 Enzymatic deglycosylation of HEK293T expressed proteins
Transfected 293T cell lysates were treated with PNGase F, treated samples were examined by western blot alongside untreated samples. a) FLAG tagged protein lysates analysed using anti-FLAG antibody. b) HA tagged protein lysates analysed using anti HA antibody. Samples treated with PNGaseF are smaller in size than untreated samples and where there are multiple bands in the untreated samples, these are reduced to a single band upon treatment with PNGaseF.

1. AMIGO-1
2. Deglycosylated AMIGO-1
3. AMIGO-2
4. Deglycosylated AMIGO-2
5. AMIGO-3
6. Deglycosylated AMIGO-3
7. LINGO-1
8. Deglycosylated LINGO-1
9. NgR
10. Deglycosylated NgR
11. $p75^{NTR}$
12. Deglycosylated $p75^{NTR}$

3.4 The presence of a band in AMIGO- 2 lysate suggests cleavage and release of the protein cytoplasmic region.

Western blot analysis consistently revealed the presence of a band at around 20kDa in the cell lysate of the C-terminal FLAG tagged AMIGO-2 transfected cells. However, this band was not observed in the N-terminal HA tagged AMIGO-2 cell lysate, indicating that the protein was cleaved and the HA tag was released with the fragment not available for detection in the lysate. Considering the fragment was around 20kDa in size it was most likely that the fragment detected is the intracellular portion of the protein, cleaved extracellularly, adjacent to the cell membrane. Using Expasy and Uniprot to predict molecular weights for different fragment of the protein it was possible to estimate where the protein might be cleaved, for example the cytoplasmic domain of the protein, comprising residues 420-522, is predicted to be 10.8kDa in size. But at around 20kDa in size, the fragment detected was significantly larger than the cytoplasmic domain. The addition of the transmembrane domain (residues 399-419) only increased the predicted fragment size to 13.1kDa indicating that the cleavage must occur somewhere in the extracellular region. If the Ig domain, at 9.1kDa, is included the size becomes somewhat closer to that of the fragment and it is possible that the fragment could be of the intracellular domain plus the Ig domain. This approach is not definitive however, as for example charged amino acids may lead to anomalous migration of the protein fragment through the SDS-PAGE.

To investigate further, the supernatant of HA-AMIGO-2 transfected HEK293T cells was analysed by western blot (Figure 3.4). The HA tag is located at the N-terminal end (ectodomain) of the protein, so western blots were probed using an anti-HA antibody. A faint band was reliably observed at around 70kDa, which is akin to the size of the mature protein identified in cell lysates indicating detection of an intact protein.

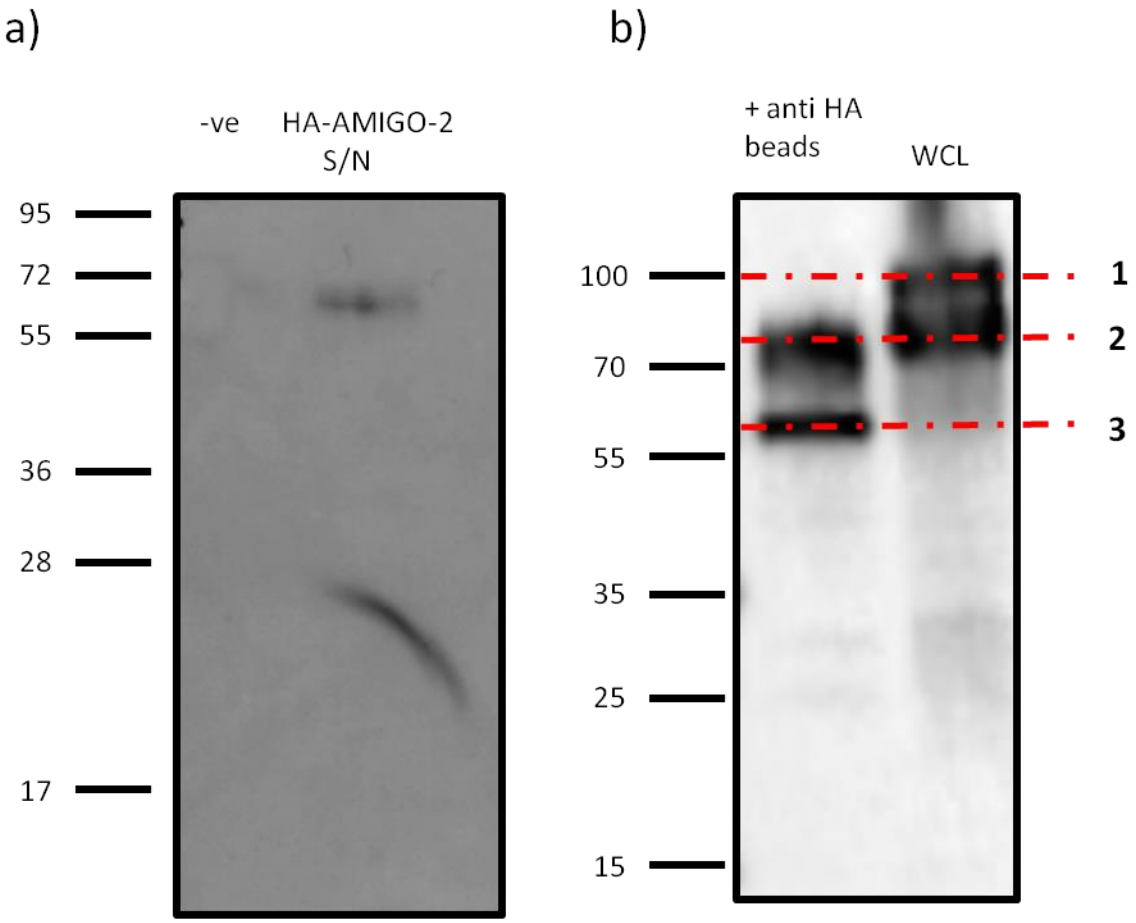

Figure3.4 Western blot analysis of N-terminal HA tagged AMIGO-2 transfected HEK293T cell supernatant.

a) Western blot analysis of HEK293T cell supernatant using anti HA antibody identified a faint single band at around 70kDa which corresponds to the full length glycosylated version of AMIGO-2.

b) Western blot analysis of HA-AMIGO-2 transfected HEK293T cell whole cell lysate (WCL) alongside the transfected cells supernatant treated with anti HA beads (Left lane). A more prominent band is seen at 70Kda after addition of anti HA beads, akin to the band seen in a).

1. Full length AMIGO-2. Glycosylated.
2. Full length AMIGO-2. Partially glycosylated.
3. Full length AMIGO-2. No glycosylation.

Addition of anti-HA beads to the supernatant resulted in the band at 70kDa becoming more prominent, furthermore an additional band was detected at around 60kDa and thought to represent the non-glycosylated form of AMIGO-2.

The release of an intact (full length) protein into the cell supernatant can only really indicate the budding or release of cell fragments or vesicles into the cell supernatant (see Figure 3.5). The physiological significance is uncertain as this phenomenon could be an artefact of cell transfection/ protein overexpression.

LINGO-1 displays similar signs of being degraded in mouse brain tissue lysate, in data provided by Abcam for analysis of the anti-LINGO antibody (ab23631). In western blot analysis, bands are seen at the expected size of 83kDa representing the full-size protein, but bands are also seen at 34kDa and 17kDa potentially representing degradation and cleavage products respectively. It is not known which part of the protein the 17kDa cleavage product represents; it is larger than the predicted size of the intercellular and transmembrane domains (4.2kDa and 2.3kDa) but smaller than the extracellular domain (59.3kDa).

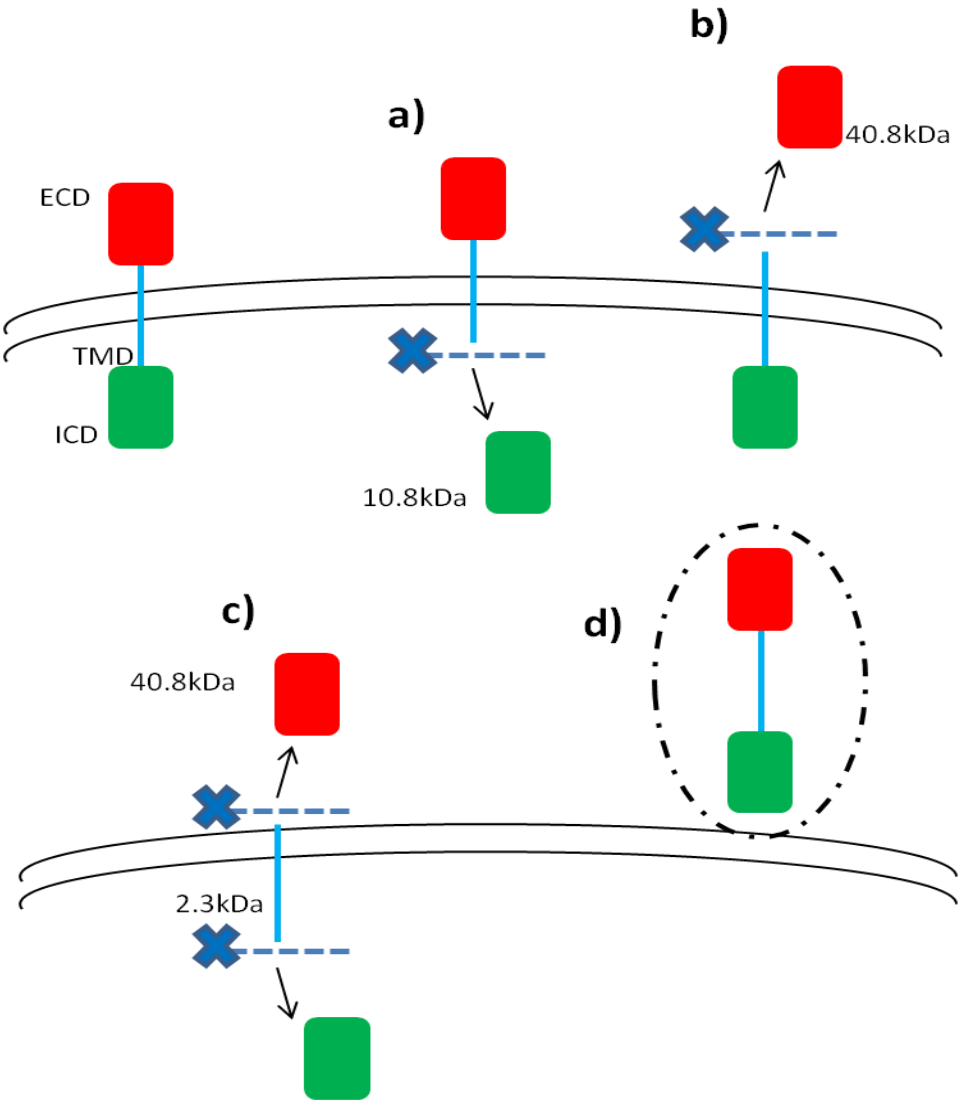

Figure 3.5 Diagram representing possible modes of AMIGO-2 cleavage.

a. Cleavage may occur intracellularly.
b. Cleavage may occur extracellularly.
c. The protein may be cleaved both intracellularly and extracellularly.
d. The protein may be released as a whole, in a vesicle.

ECD = Extracellular domain, 40.8kDa
ICD = Intracellular domain, 10.8kDa
TMD = Transmembrane domain, 2.3kDa
Ig domain – 9.1Kda

cytoplasmic domain of the protein, comprising residues 420-522, is predicted to be 10.8kDa in size. But at around 20kDa in size, the fragment detected was significantly larger than the cytoplasmic domain. The addition of the transmembrane domain (residues 399-419) only increased the predicted fragment size to 13.1kDa indicating that the cleavage must occur somewhere in the extracellular region. If the Ig domain, at 9.1kDa, is included the size

becomes somewhat closer to that of the fragment and it is possible that the fragment could be of the intracellular domain plus the Ig domain

3.5 Subcellular fractionation

It is thought that both NgR and $p75^{NTR}$ are expressed at the neuronal cell surface, where myelin associated inhibitory factors can bind and mediate axon outgrowth inhibition. However, the cellular location of the third member of the axon inhibitory complex, LINGO-1, remains contentious. Recently it has been suggested that LINGO-1 is located intracellularly [126], which questions the tripartite complex model as LINGO-1 would not be freely available to associate with the other proteins in the complex. However, this contradicts previous evidence which appears to show the necessity of the protein at the cell surface- where the actions of LINGO-1 are inhibited when an antibody against LINGO-1 is used [78]. Since the antibody acts extracellularly the protein must presumably be expressed at the cell surface. However, the ability to endocytose antibodies has been reported previously with anti-ganglioside antibodies shown to be endocytosed at nerve terminals [132].

Determining the subcellular location of a protein is critical when examining its biological function, [133]. There are several approaches to separating subcellular compartments, including (i) separation based on centrifugation, using differences in sedimentation co-efficiencies and densities, and (ii) separation based on a chemical properties using a series of detergents with increasing solubilisation efficiencies [133]. It is also possible to use a combination of both approaches, with consideration as to the coverage of the proteome, the reproducibility and ease and speed of processing.

Subcellular fractionation was performed on HEK293T cells transfected with FLAG- or HA-tagged proteins to determine the cellular location of expression. From available options, the Cell Signalling Kit was used which divided the cell into 3 fractions, including cytoplasmic,

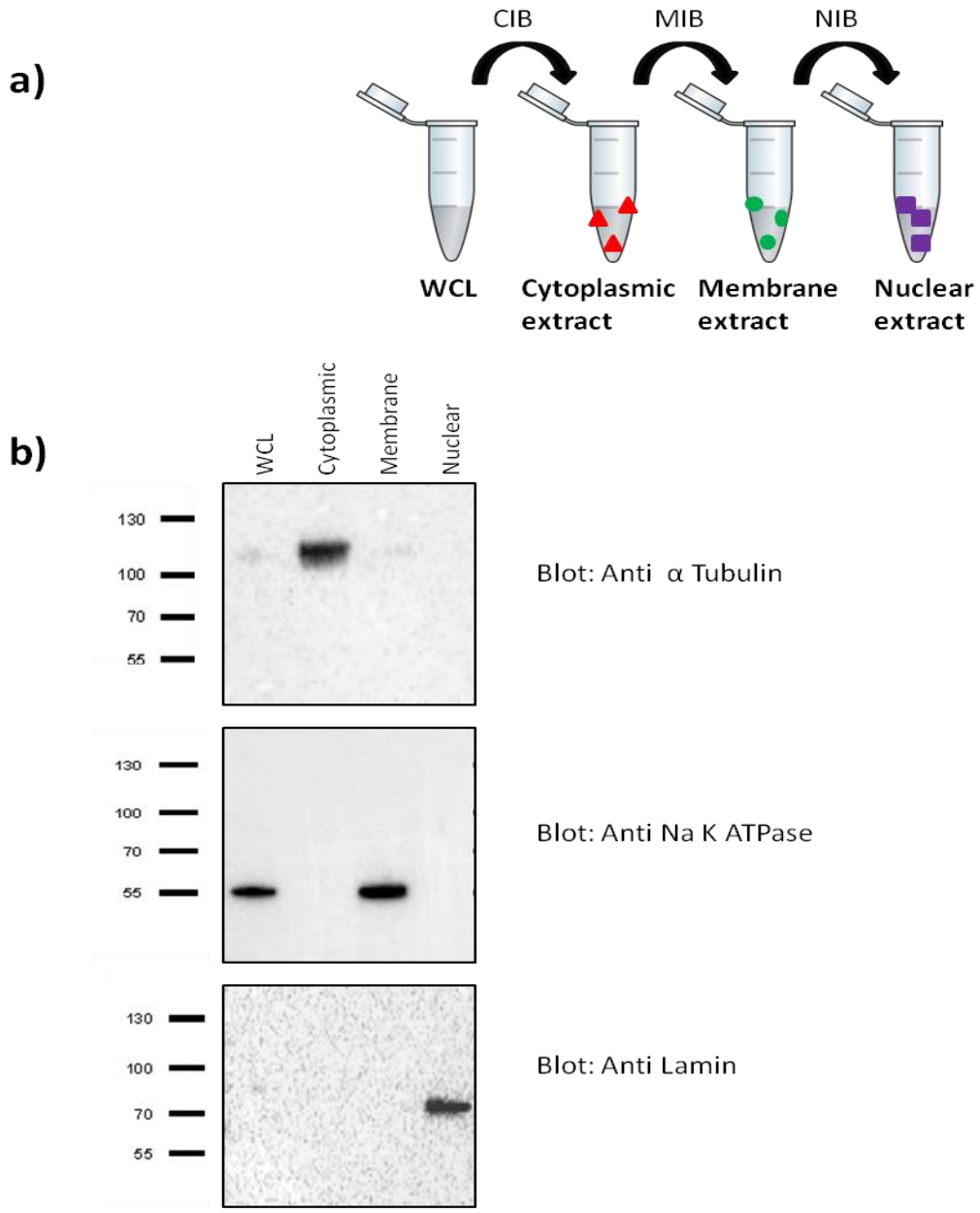

Figure 3.6. Subcellular fractionation controls

a) Subcellular fractionation was performed on HEK293T cells. A series of buffers were added to the cells to extract the cytoplasmic, membrane and nuclear fractions.

b) To ensure efficient fractionation and particularly lack of cross contamination purified fractions were analysed by western blot. Anti-tubulin antibody was used to detect tubulin expressed in the cytoplasmic fraction (top panel), which is where it was detected, with very little seen in other fractions. Anti NA^+ K^+ ATPase was used to detect the NA^+K^+ channel In the membrane fraction (middle panel), no Na+K+ was seen in membrane or nuclear fractions but was seen in whole cell lysate. Finally, anti lamin was used to detect lamin in the nuclear fraction (bottom panel) which is where it was detected, no Lamin was identified in any of the other fractions. Some images appear pixelated due to the longer exposure time required, due to a combination of the low level of expression of the protein of interest and the sensitivity of the antibody used.

membrane and nuclear, followed by analysis by western blot using antibodies against the FLAG or HA tags. The performance of the protocol was tested with proteins with known cellular locations as controls, including tubulin, Na^+ K^+ ATPase and lamin, which are situated in the cytoplasm, membrane and nucleus respectively. Each of these proteins was easily identifiable in the respective fractions predicted (Figure 3.6); furthermore, there was no significant cross-contamination into other fractions. Panels representing α tubulin and lamin appear pixelated due to the longer exposure time needed to identify the proteins; this may be due to the low levels of these proteins in the cells, the poor sensitivity of their antibodies, or a combination of both. The proteins being identified in these panels were likely to be diluted in the WCL samples and so were not of high enough levels to be identified in the western blots. In contrast, Na K ATPase was of high enough concentration to be identified without the need for a long exposure therefore the image is not pixelated, furthermore the level of protein and specificity of the antibody is high enough that it is identified even when its 'diluted' in the WCL sample.

As before, HA- or FLAG- tagged AMIGO-1, -2 and -3 were expressed in HEK293T cells, after 3 days the cells were trypsinised and washed with PBS, a sample was saved corresponding to the whole cell lysate. Next the Cell Signalling Cell Fractionation (Cell Signalling) kit was used to separate the cells into three distinct fractions using a detergent-based method as opposed to other centrifugation methods. A series of buffers, including (i) cytoplasmic isolation buffer, (ii) membrane isolation buffer and (iii) cytoskeletal/nuclear isolation buffers, were added to the cells, which were vortexed and centrifuged according to the manufacturer's instructions. The manufacturers protocol was similar to that of 'Method 2' in Rockstoh et al (2011) [133]. Cytoplasmic, membrane and nuclear fractions were obtained, and samples were mixed with

loading buffer (SDS + 200mM DTT) and analysed by western blot alongside the whole cell lysate sample, using antibodies against either the FLAG or HA tag.

HA-tagged AMIGO proteins were identified at 70kDa in size in the whole cell lysate and membrane fractions, and to a lesser extent the nuclear fraction (Figure 3.7). However, very little expression was observed in the cytoplasmic fractions. This indicates that all of the AMIGO proteins are potentially available at the cell surface where they can interact with other cell surface membrane proteins, and potentially those of the NgR complex. The expression pattern of HA-LINGO-1 differs from that of the AMIGO family, with the majority of the

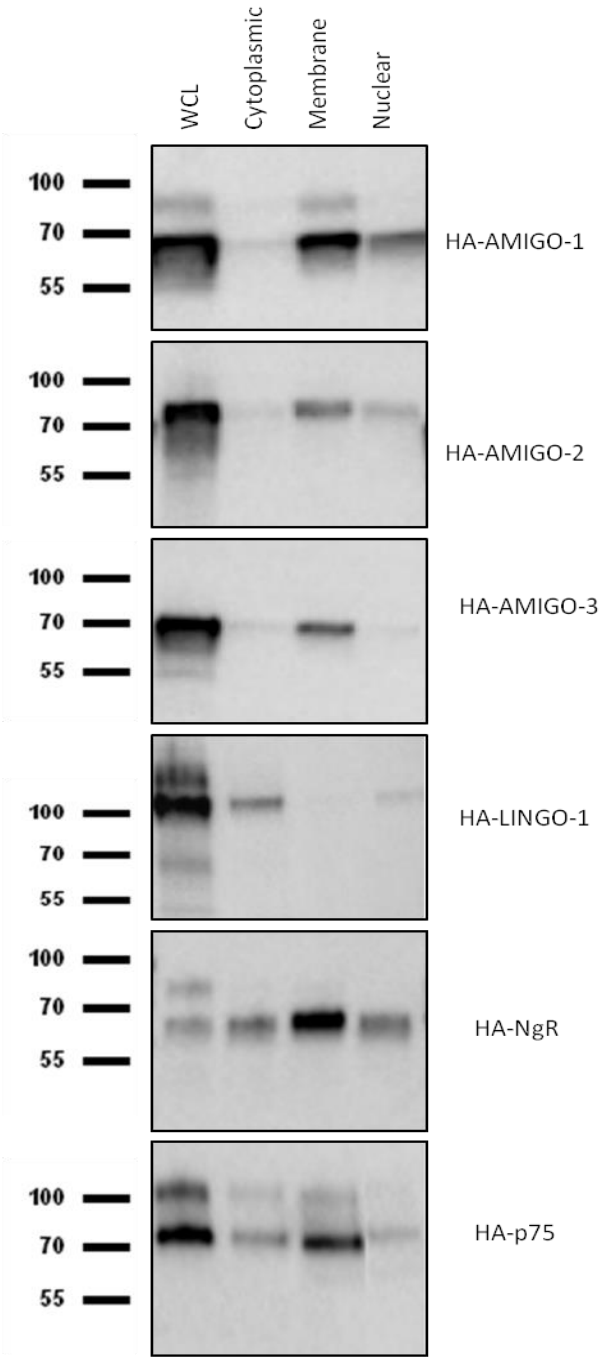

Figure 3.7. Subcellular localisation of HA tagged proteins
N-terminal HA tagged constructs were transfected into HEK293T cells which then underwent subcellular fractionation. Fractions obtained were whole cell lysate (WCL), cytoplasmic, membrane, and nuclear. Fractions were analysed by western blot using an anti-HA antibody to determine the locations of the proteins of interest. All proteins, except LINGO-1, are expressed most predominantly in the membrane fraction. LINGO-1 is absent from the membrane fraction and is seen most predominantly in the cytoplasmic fraction.

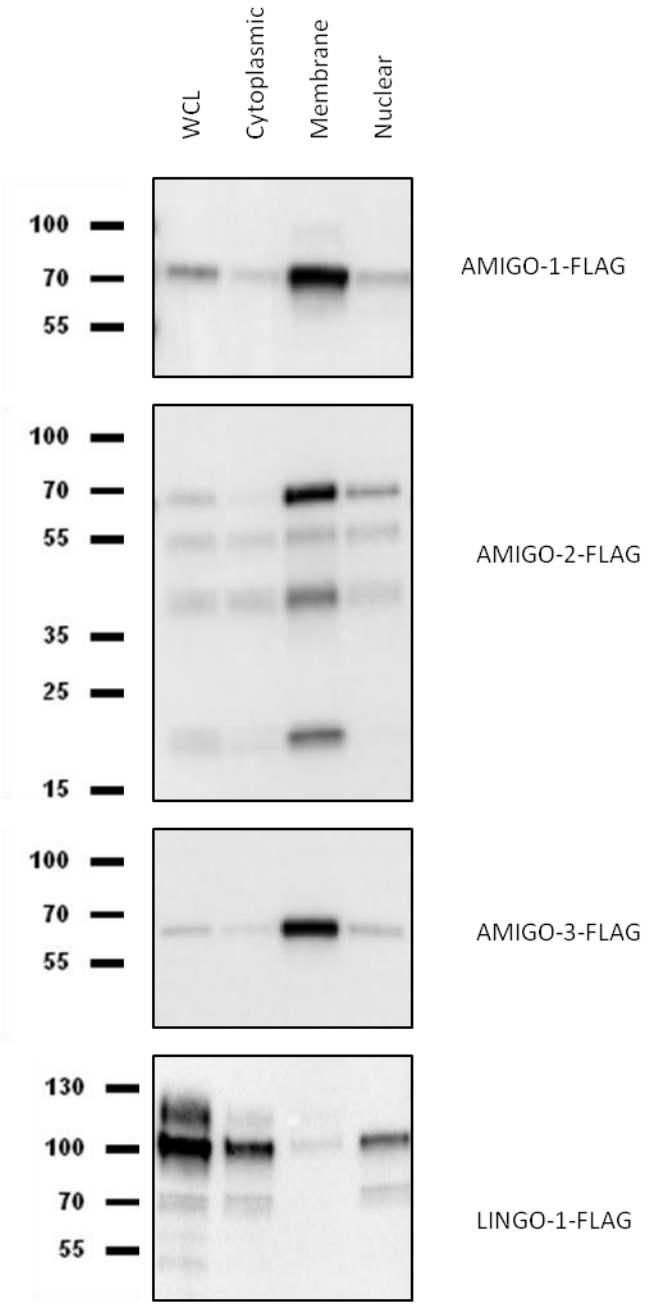

Figure 3.8. Subcellular Localisation of FLAG tagged proteins

C- terminal FLAG tagged constructs were transfected into HEK293T cells which then underwent subcellular fractionation. Fractions obtained were whole cell lysate (WCL), cytoplasmic, membrane , and nuclear. Fractions were analysed by western blot using an anti- FLAG antibody. All three AMIGO proteins are seen predominantly in the membrane fractions ,however very little LINGO-1 is identified in this fraction.

protein being detected in the cytoplasmic fraction, at around 100kDa. Bands are also observed in the whole cell lysate and a small amount is observed in the nuclear fraction, however, no protein was detected in the cell membrane fraction.

Cells expressing HA-NgR and HA-p75^{NTR} were also analysed, and western blots determined that both HA-NgR and HA-p75^{NTR} were expressed in each of the 4 fractions. Larger amounts were observed in the membrane fraction, indicating that the protein is predominantly expressed at the cell surface. p75^{NTR} has previously been identified at the cell surface [134] as has NgR [135].

Western blot analysis of the C-terminal FLAG tagged proteins (Figure 3.8) revealed similar expression patterns. Here, each member of the AMIGO family of proteins was detected in the membrane fraction predominantly, with small amounts visible in the WCL, cytoplasmic and nuclear fractions. Finally, FLAG tagged LINGO-1, akin to HA-LINGO-1 was expressed in the WCL, cytoplasmic and nuclear fractions but was absent from the membrane fraction. This evidence, alongside the HA-LINGO cell fractionation results, supports the findings of the research by Meabon [126] who suggests that LINGO-1 protein expression is predominantly intracellular. The topic of protein transit and localisation has been the subject of intensive study for decades, with the particular importance of signaling endosomes highlighted in neurons, for example regulating the interactions of NGF with its receptor TrkA (Miaczynska2013). To date, there are no detailed mutagenic studies of LINGO-1 permitting an analysis of the sequence specific requirements for intracellular localisation or trafficking. Using antibodies to the extracellular and intracellular regions of LINGO-1, alongside confocal microscopy, de Laat et al (2015) hypothesised that the cytoplasmic region of LINGO-1 binds to cytoplasmic proteins that control trafficking through the secretory and/or endolysosomal

pathway. The evidence for this remains limited. Henceforth, It may be possible that LINGO-1 is expressed in the membrane of small organelles such as mitochondria which because of their size are extracted as part of the cytoplasmic fraction. Another explanation could be that LINGO-1 is rapidly shuttled back and forth from the nucleus to the membrane and therefore appears in the cytoplasmic fraction.

3.6 Co-immunoprecipitation studies

Co-immunoprecipitation experiments were performed using HEK293T cells transfected with N- terminal HA tagged AMIGO-1, -2 and -3, LINGO-1, NgR and $p75^{NTR}$ in combination with C- terminal FLAG tagged AMIGO-1, -2 and -3 and LINGO-1. Three days after transfection, cells were lysed; half the lysate was mixed with anti-FLAG beads and half with anti HA beads. Bound proteins were eluted and analysed by western blot using the antibody to the complimentary precipitating antibody (HA for anti-FLAG beads and FLAG for anti-HA beads).

3.6.1 The AMIGO proteins display homophillic and heterophillic binding

Western blot analysis of co-immunoprecipitated proteins (Figure 3.9) indicates homophillic and heterophillic binding between the AMIGO family members and LINGO-1. These results complement and extend previous studies finding homophillic and heterophillic binding between the AMIGO family in co-immunoprecipitation studies examining binding between GFP- and V5- tagged AMIGO proteins expressed in HEK293T cells.

Western blots produced using protein purified via anti HA beads and processed with anti-FLAG antibody were analysed by dividing the membrane into sections. Panel 1 of the western blot demonstrates the binding between HA tagged AMIGO-1 and FLAG tagged AMIGO-1, -2 and -3 and LINGO-1, with bands observed at around 80kDa in size representing AMIGO-1, AMIGO-2 and AMIGO-3 FLAG. It is worth noting that AMIGO-2-FLAG appears slightly larger in size than AMIGO-1 and AMIGO-3, a likely consequence of the slightly higher Mw of AMIGO-2 (57.9kDa) than both AMIGO-1 (52.2kDa) and AMIGO-3 (52.2kDa) and the larger number of N-Linked glycosylation sites present on AMIGO-2 than AMIGO-1 and AMIGO-3.

Panels 2 and 3 represent binding between HA-AMIGO-2 and FLAG-tagged AMIGO-1, -2 and -3 and HA-AMIGO-3 with the FLAG tagged constructs, respectively. Bands are observed at around 80kDa, demonstrating binding between HA-AMIGO-2 and HA-AMIGO-3 with the FLAG-tagged AMIGO proteins. Differences are observed in the intensity of the bands, this could be due to true differential binding or may be the result of technical artefacts. Panel 4 details the binding between HA-LINGO-1 and the FLAG-tagged AMIGO and LINGO constructs; although the intensity of the bands in this blot are weak, binding can be observed between AMIGO-1-FLAG and AMIGO-2-FLAG and HA-LINGO-1.

Analysis of binding using anti-FLAG beads and anti-HA antibody (Figure 5.10) identifies binding between all members. Here, bands at around 70kDa can be observed in panels 1 and 3, which illustrate binding between HA-AMIGO-1 and HA-AMIGO-3 respectively, with the FLAG-tagged constructs. HA-AMIGO-2 also binds all members of the AMIGO family and LINGO-1-FLAG as observed by bands at 80kDa in panel 2 representing the detection of HA-tagged AMIGO-2. Finally, binding between HA-LINGO-1 and the AMIGO family members was illustrated by bands at around 100kDa in panel 4, representing the HA tagged LINGO-1 proteins.

Further western blots confirmed the already established binding between NgR, $P75^{NTR}$ and LINGO-1 and further demonstrated binding to the AMIGO family members (Figure 3.11). Bands are observed at approximately 70kDa and approximately 100kDa when probed using anti-FLAG antibody corresponding to detection of NgR and $p75^{NTR}$ respectively.

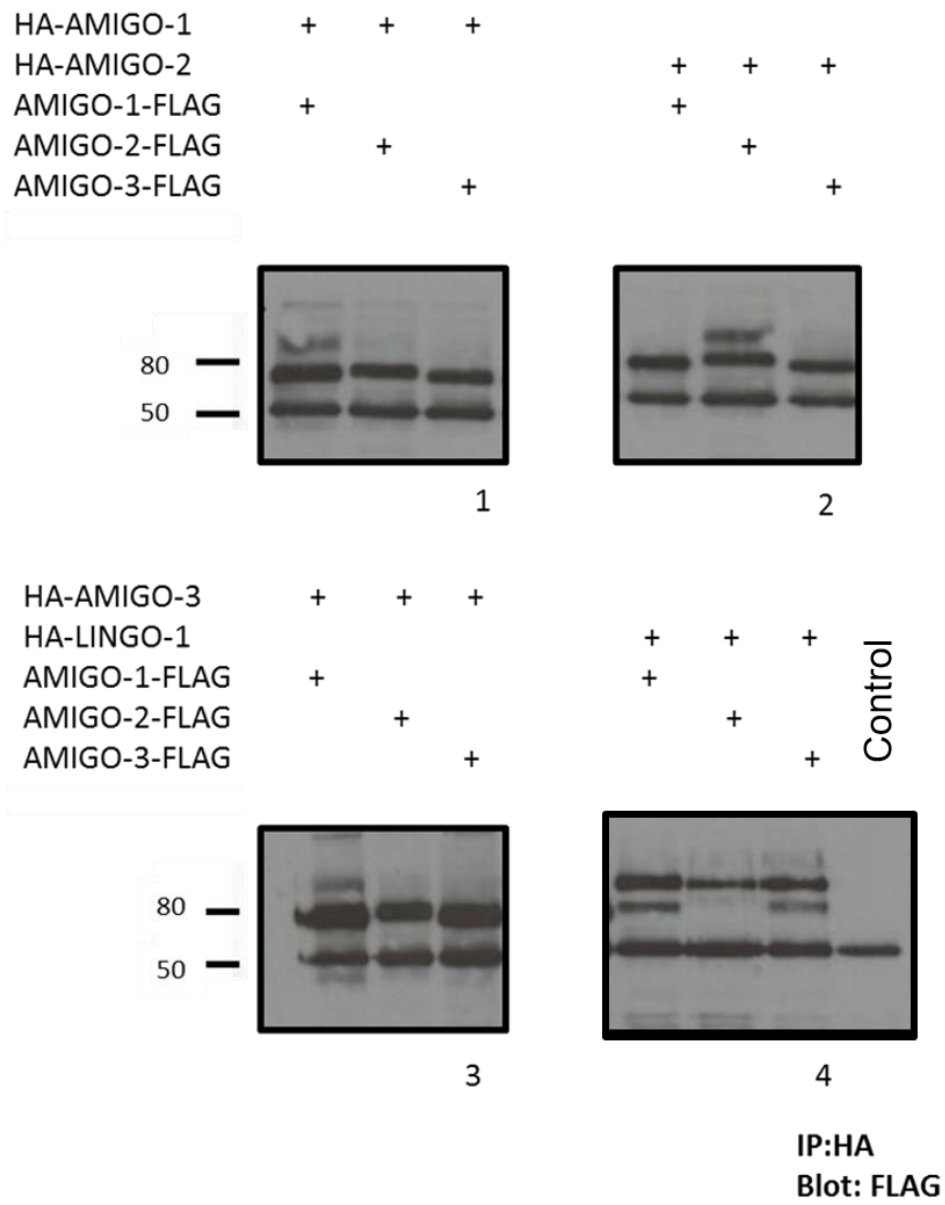

Figure 3.9. Co-immunoprecipitation studies

N-terminal HA tagged and C- terminal FLAG tagged proteins were expressed in HEK293 cells. Proteins were immunoprecipitated using anti-HA beads and analysed by western blot using anti-FLAG antibody. Panels 1,2, 3 and 4 represent binding between N-terminal HA tagged AMIGO-1, AMIGO-2, AMIGO-3 and LINGO-1 respectively, with the FLAG tagged constructs.

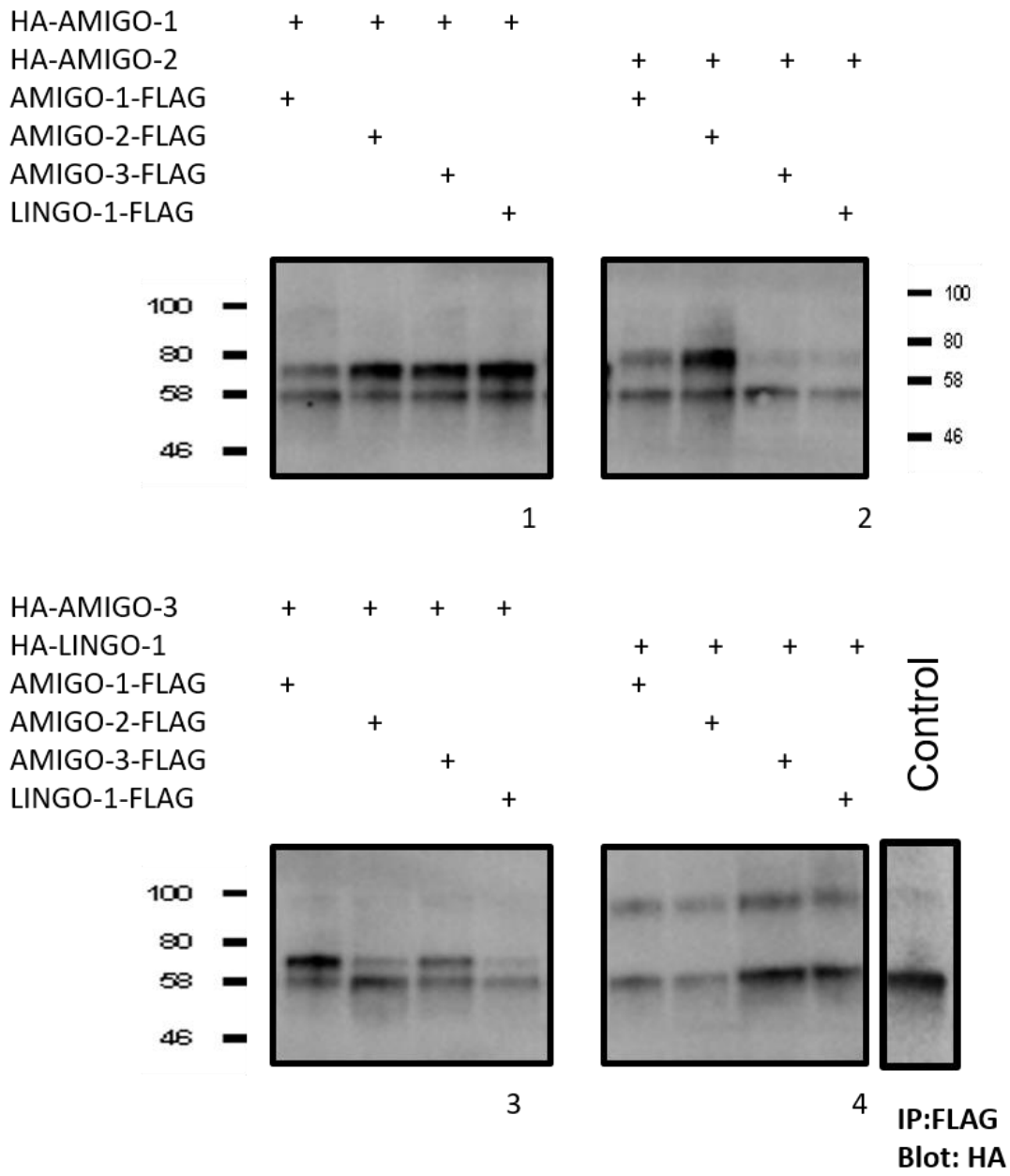

Figure 3.10. Co-immunoprecipitation studies.
N- terminal HA-tagged and C- terminal FLAG-tagged proteins were expressed in HEK293 cells. Proteins were immunoprecipitated using anti-FLAG beads and analysed by western blot using anti-HA antibody. Panels 1,2,3 and 4 represent binding between N-terminal HA tagged AMIGO-1, AMIGO-2, AMIGO-3 and LINGO-1 respectively, with the FLAG tagged constructs.

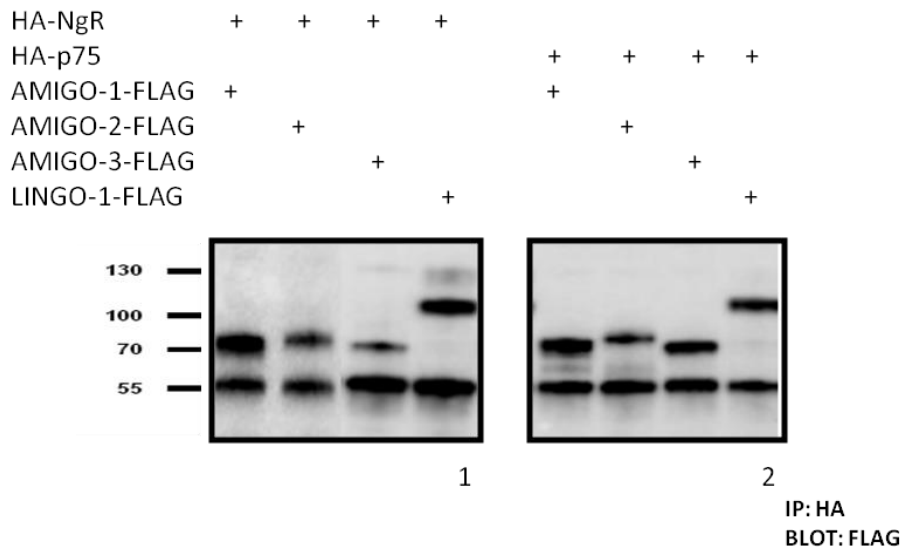

Figure 3.11. Co-immunoprecipitation studies
N- terminal HA-tagged and C-terminal FLAG-tagged proteins were expressed in HEK293 cells. Proteins were immunoprecipitated using anti-HA beads. Samples were analysed by western blot using antibodies against FLAG-tags. Panels 1 and 2 represent binding between N terminal HA tagged NgR and $p75^{NTR}$ respectively, with the FLAG tagged constructs.

3.7. Expression of the members of the NgR complex

The distribution of NgR in the mouse nervous system has been described in detail by Wang et al [129] previously, who described the NgR protein as being present in all layers of the adult, but not neonatal, neocortex, based on western blot approaches. The group also found NgR protein strongly expressed in a number of discrete classes of neurons. Information is also available on the expression of NgR in zebrafish, where NgR homologues are found early during development, and prominently in the adult brain [136]. However, the expression of NgR in human brain is less well established. While the expression of NgR during foetal development has been described to some extent, expression of NgR in the adult brain is less well known. Research by Halabiah et al [137] found that NgR is expressed during foetal development, where the strongest expression is observed in post mitotic cells.

$P75^{NTR}$ expression has been explored at the mRNA level in the mouse and rat CNS where it is detected early during development, however levels of $p75^{NTR}$ decrease in adult stages of development. During development NGFRs are expressed in non-neuronal tissues [138].

LINGO-1 is exclusively expressed in the neurons and oligodendrocytes of the central nervous system [68, 70], whereas it is absent in non-neuronal tissues [68]. Like $p75^{NTR}$, LINGO-1 mRNA levels peak during development and decline thereafter into adulthood where they remain at background levels until after axonal injury, whereupon an increase in expression is seen [68]. At a cellular level, LINGO-1 associates with NgR and $p75^{NTR}$ at the cell surface. Here, the actions of LINGO-1 can be inhibited by antibodies and LINGO-1-Fc fusion proteins, which further highlight the importance of the protein at the cell surface. However, more recently, in more detailed studies it has been suggested that very little LINGO-1 is expressed at the cell surface and that the protein is instead primarily expressed intracellularly [126]. In this study,

cell surface proteins were biotinylated with a membrane impermeable reagent and detected using a fluorescently labelled streptavidin, which failed to detect LINGO-1 at the plasma membrane; instead LINGO-1 was located as intracellular punctae, which presumably represent intracellular membrane vesicles [126]. Further investigations, using a LINGO-1 antibody directed against the extracellular domain of LINGO-1, also failed to detect any LINGO-1 at the surface of non-permeabilized cells of the developing rat cortex [126].

The AMIGO family of proteins exhibit variable tissue expression patterns, with AMIGO-1 and AMIGO-2 highly expressed in the mammalian CNS and AMIGO-3 more widely expressed in a number of tissues [82, 97, 103]. Expression of the AMIGO protein in zebrafish has also been investigated, with AMIGO-1 identified as being the predominant member of the AMIGO family expressed in the zebrafish CNS [105]. The subcellular location of AMIGO-2 has been investigated previously, by fusion with enhanced green fluorescence protein (EGFP). The DEGA/ AMIGO-2-EGFP fusion protein was observed in the plasma membrane [101].

5.7.1. Validating the effectiveness of the native antibodies

Prior to testing for expression of members of the NgR complex in human tissues and cell lines, the antibodies that were to be used were tested on HEK293T cells transfected with N-terminal HA-tagged versions of the proteins. Transfected cells were lysed and analysed by western blot next to untransfected HEK293T cells, using anti-HA antibody and corresponding native antibodies. Detection of each protein would provide an indication of the effectiveness of the antibody as well as information about their expected sizes. Western blot PVDF membranes were then chemically stripped, re-blocked and re-probed with anti-HA antibody in order to a) confirm that the protein was expressed and b) establish the size of the protein for comparison against the native antibodies.

Analysis of cell lysates using native antibodies identified AMIGO-1, and AMIGO-3 around 70kDa (Figure 3.12a); although the AMIGO-1 signal was very weak the apparent size of the respective band appeared to correlate with AMIGO-1. When re-probed with anti-HA antibody (Figure 5.12b) bands were observed at the same size confirming the bands detected in a) represent AMIGO-1 proteins. However, although AMIGO-1 and AMIGO-3 were detected as single bands 70kDa in size, AMIGO-2 was detected as multiple bands, likely representing non-specific binding or alternatively protein degradation products, with a most prominent band observed at around 35kDa. Critically, a similar banding pattern was detected in untransfected cells, suggesting that either the transfection protocol does not work for this specific construct (unlikely as both HA- and FLAG-tagged constructs are detectable), or alternatively that the antibody does not detect AMIGO-2 with any degree of efficiency in western blotting. Analysis of the blot using the anti-HA antibody demonstrated the protein was expressed as it should have been, with a band observed at around 70kDa, slightly larger than those seen for AMIGO-1 and AMIGO-3 as observed previously (Figure 3.2) thereby indicating that the native antibody is poor. Analysis of the anti-NgR and anti-$p75^{NTR}$ antibodies reveals that they are suitable at detecting the protein in the cell lysates. $p75^{NTR}$ was detected as a doublet, with the smaller band observed at around 70kDa and the larger at around 100kDa, likely representing unglycosylated and glycosylated species of the protein respectively. Analysis of the blot using anti-HA antibody shows a single band at 70kDa as observed in previous western blots. The anti-NgR antibody identified the protein in both the transfected and untransfected HEK293T samples, demonstrating that a) NgR is expressed at high enough levels in the untransfected cells to permit detection, and b) the antibody is extremely sensitive. In the transfected samples, NgR is detected as a doublet, with bands observed at 70kDa and 100kDa. Of interest, a significantly weaker single band at 70kDa was

observed in untransfected cells. The reason for this is unclear, but may suggest low levels of endogenous NgR in HEK293T cells, with the smaller MW deglycosylated form of NgR detected by the respective antibody. The presence of a primarily neuronal protein such as NgR might be seen as unexpected in HEK293T cells, which are thought to be of human embryonic kidney (HEK) cell origin. Detailed examination of the RNA and protein expression patterns of HEK cells suggest that, in fact, several neuronal proteins such as Neurofilaments are found in HEK cells [139]. It is not surprising that other proteins, thought primarily to be of neuronal origin, may be found in HEK 293T cells.

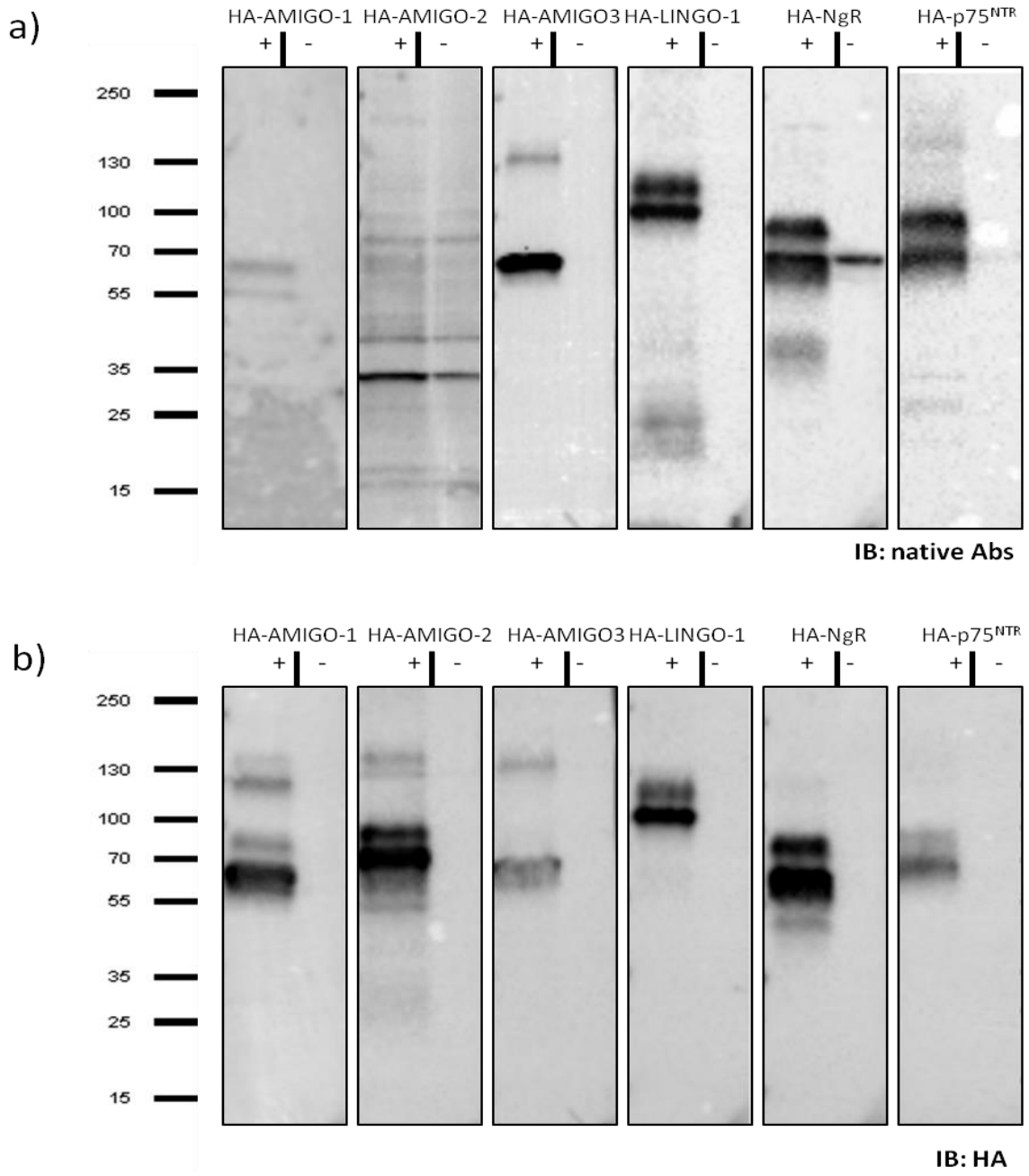

Figure 3.12. Assessing the effectiveness of native antibodies.
HEK293T cells were transfected with N- terminal HA tagged proteins, cell lysates were analysed by western blot alongside untransfected cell lysates (Right lane of each panel, '-').
a) Lysates were probed with; Anti AMIGO-1, Anti-AMIGO-2, Anti-AMIGO-3, Anti-LINGO-1, Anti-NgR and Anti-$p75^{NTR.}$ antibodies.
b) Membranes were then stripped, and re-probed with anti HA antibody.
The blots demonstrate that the antibodies used to detect AMIGO-1 and AMIGO-2 are poor, however those used to detect AMIGO-3, LINGO-1, NgR and $p75^{NTR}$ are satisfactory.

3.7.2. Expression of members of the NgR complex proteins in human oligodendrocyte cell line.

Some of the challenges in detecting native AMIGO family members were highlighted in the HEK293T transfection experiments. Further validation was sought using an immortalised cell line, potentially expressing more physiological levels of the respective proteins.

The human glial oligodendrocyte cell line, MO3.13, was used to test for native expression of each of the NgR complex proteins. MO3.13 cells are derived from a human glial oligodendrocyte hybrid cell line, furthermore they express the characteristics of primary oligodendrocytes and once mature, the cells express myelin basic protein (MBP) [140]. This immortalised cell line was used as the biochemical properties of LINGO-1 have been best characterised in this type of cell, rather than the more limited experiments in neuronal cell lines.

Expression of NgR, $p75^{NTR}$, LINGO-1 and the AMIGO proteins in MO313 cells were determined by western blot analysis of cell lysates using the antibodies for each native protein (Figure 3.13) as discussed in section 3.8. Each protein was detected in MO313 cells at varying levels of signal, but this may be due to the effectiveness of the antibody rather than being an indication of actual expressed levels of protein. NgR was detected at around 70kDa representing the glycosylated form of the protein observed in transfected HEK293T cells, and another less prominent band was also observed at around 200kDa which is possibly a dimeric form of the protein. $P75^{NTR}$ was also detected at 70kDa, as in HEK293T cells, but also at approximately 55kDa, not observed in HEK293T cells, and probably corresponds to a cleaved form of $p75^{NTR}$. The third member of the NgR complex, LINGO-1 was observed as a very faint band of approximately 100kDa, likely representing the glycosylated species. The faintness of

the band may indicate that either the protein is expressed endogenously at low levels, or the antibody is relatively poor. However, having determined the effectiveness of the antibody in transfected HEK293T cells it is more likely that the former is true and the levels of LINGO-1 are low.

Analysis of the expression of the AMIGO proteins was more complex. The AMIGO-1 protein was detected as two bands at 55kDa and 25kDa, the former being akin to the deglycosylated version seen in HEK293T expression. The band at 25kDa may represent a breakdown product detected by the polyclonal antibody, raised to an unspecified epitope in the C-terminus of AMIGO-1. No bands were observed at 70kDa as expected for a mature protein. Multiple bands were detected in the AMIGO-2 western blot, however the most prominent band was observed at around 35kDa, analogous to the species detected previously in HEK293T cells analysed using native antibody (Figure 3.12). Finally, AMIGO-3, like AMIGO-1, was observed as a prominent band of 55kDa, likely representing the deglycosylated form of the protein.

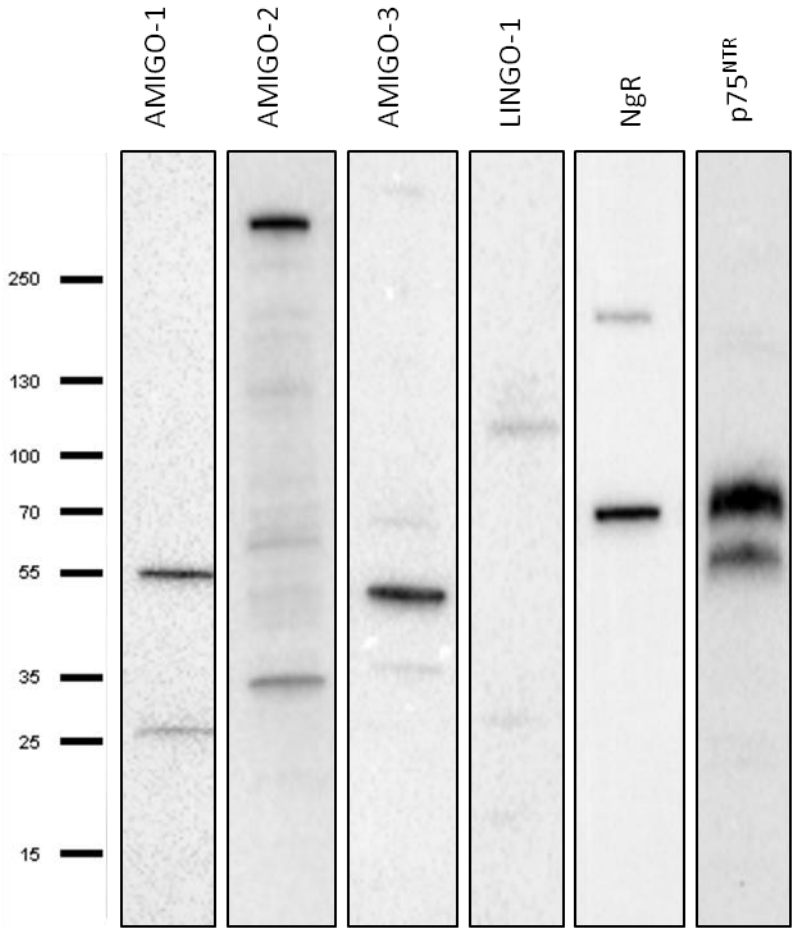

Figure 3.13. Native expression of target proteins in MO3.13 cells

MO3.13 cell lysates were analysed by western blot to test for the expression of AMIGO-1, -2 and -3, LINGO-1, NgR and $p75^{NTR}$ using protein specific antibodies.

3.8 Expression of NgR receptor complex proteins in human brain lysates.

The results from the MO3.13 series of experiments further highlighted some of the difficulties with the use and interpretation of western blotting of proteins using relatively poorly characterised polyclonal antibodies. Furthermore, as the cell line is immortalised and clonal, the expression levels for any given protein may not be representative of the expression seen within native CNS tissue.

To determine if AMIGO was expressed in the human CNS at levels that could be detected in the laboratory, a human brain lysate was analysed by western blot (Figure 3.14). A sample of human brain was lysed and aliquoted, SDS sample buffer was added and SDS-PAGE carried out prior to transfer onto PVDF membrane. Each membrane was tested individually using antibodies directed against AMIGO-1, AMIGO-2, AMIGO-3, LINGO-1, NgR and $p75^{NTR}$. The blots revealed that each of the proteins of interest was detected in the human brain lysate but at varying levels (Figure 3.14). Again, it was difficult to know whether the levels observed on western blot were a true representation of levels of each protein in the brain or due to the differing levels of effectiveness of each antibody.

NgR, which is expressed throughout the CNS, can be observed as a prominent band at around 70kDa, which coincides with the glycosylated form of the protein observed in previous western blots. However, $p75^{NTR}$ was not as easily visualised in the brain lysate using the antibody available and appeared as a number of bands of varying sizes suggesting fragmentation of the protein, a phenomenon that has been shown a number of times previously. $P75^{NTR}$ undergoes a series of proteolytic and intracellular compartmentalisation events, with regulated intracellular proteolysis causing shedding of the ectodomain of $p75^{NTR}$ by α-secretases resulting in the formation of a C-terminal membrane bound fragment (CTF).

The CTF can then be cleaved by γ-secretases, which releases the intracellular domain (p75ICD) [141, 142]. Based on previous western blot analysis of $p75^{NTR}$ expression, the bands identified by western blot represent the full-length protein, the p75 extracellular domain (P75ECD), the p75 C-terminal fragment (p75CTF) and the p75 intracellular domain (P75ICD) [143]. Breakdown of proteins is a key issue when examining post mortem brain tissue samples, which would be subject to apoptosis and/or necrosis.

The western blot shows the third member of the NgR complex, LINGO-1, is also identifiable and appears at around 100kDa in size, which is similar to that observed previously in human brain tissue from MS patients [144]. The AMIGO family members are more difficult to identify in the human brain lysate, however, as mentioned previously, this may be due to their variable expression and/or antibody specificity/sensitivity. AMIGO-3 is difficult to detect in the lysate with no visible bands observed, indicating very little expression as the antibody was previously shown to be fairly sensitive in the MO313 lysate as compared to AMIGO-1 and AMIGO-2. AMIGO-1 was identified, albeit faintly, at around 55kDa in size, corresponding again to the non-glycosylated form of the protein and AMIGO-2 appeared as a more prominent band at around 35kDa in size, which suggests that the band observed represented a fragment of AMIGO-2 rather than the full-length protein.

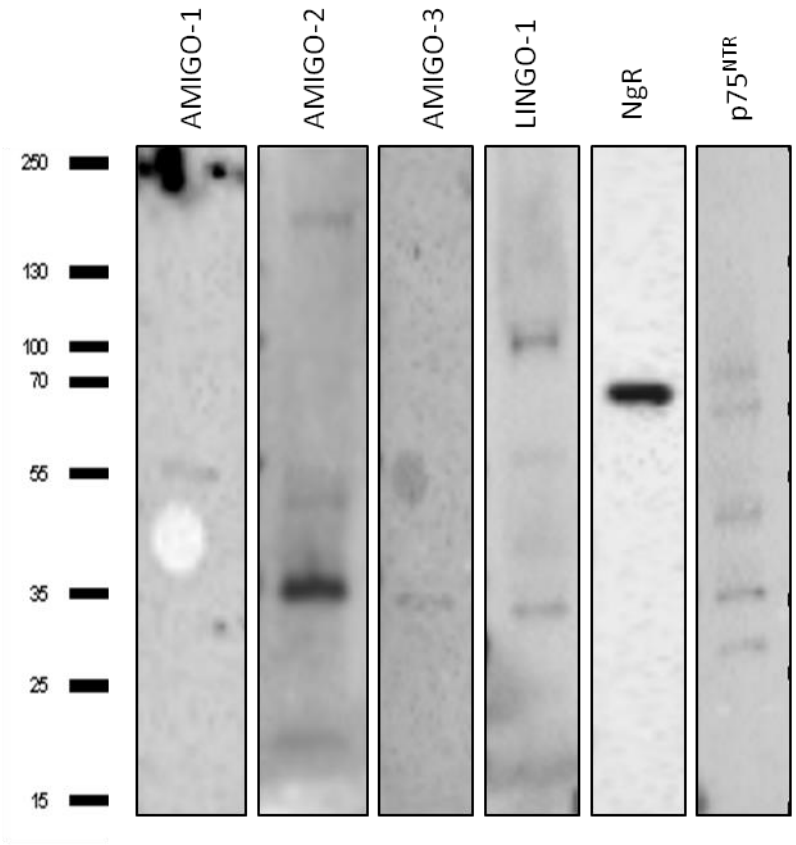

Figure 3.14. Expression of proteins of interest in human brain.

Human brain lysates (non-neurological control) were run on SDS-PAGE and analysed by western blot using native antibodies against human AMIGO-1, AMIGO-2, AMIGO-3 LINGO-1, NgR and $p75^{NTR}$. The results are variable, with NgR being easily identifiable and the other proteins being difficult to identify. AMIGO-1 appears to be present at the expected size of 55kDa however the band is very faint, the same is true for LINGO-1 which can be seen as a very faint band at 100kDa. AMIGO-3 cannot be identified and AMIGO-2 is seen at 35kDa as seen in both the MO313 and HEK293T cell lysates. $p75^{NTR}$ has been cleaved and is seen a s number of different size bands.

3.9. Discussion

The LRR and Ig domain containing proteins AMIGO-1, -2, -3 and LINGO-1 were expressed, alongside NgR and $p75^{NTR}$, and their subcellular localisations, and binding abilities were assessed. Analysis of the proteins' expression in human cell lines and tissues was also examined to determine whether the AMIGO family members could be functional interactors within the NgR/$p75^{NTR}$ complex. The background to this was discussed in the introduction.

Expression of the AMIGO proteins in HEK293T cells demonstrated glycosylation, consistent with previous findings (AMIGO-1 [120, 145]). Indeed AMIGO-1, -2 and -3 contain 5, 8 and 5 predicted N-linked glycosylation sites respectively, which are thought to add around 2kDa per glycan to the mass of the protein [131]. Deglycosylation using PNGaseF demonstrated the proteins were approximately 55kDa in size in their unglycosylated forms. Similarly, LINGO-1, NgR and $p75^{NTR}$ also displayed varying levels of glycosylation. Expression of AMIGO-1 in mammalian cells produces a much more heavily glycosylated form of the protein than that produced in insect cell hosts. *Drosophila* expression of the AMIGO-1 ectodomain produced a 40kDa protein compared to the 70kDa species observed from the mammalian host, and this observation has been described previously [120].

An interesting observation on western blots throughout the expression of the AMIGO proteins was a band of around 20kDa in size consistently detected in AMIGO-2 cell lysates. It is likely that this band represents a cleavage product. By predicting the molecular weights of the AMIGO-2 domains using Uniprot and Expasy it was possible identify where cleavage may occur. It is likely that the fragment detected is the intracellular portion of the protein, cleaved extracellularly. As described in section 3.4 the cytoplasmic domain is predicted to be 10.8kDa in size. The addition of the transmembrane domain increases the predicted fragment size to

13.1kDa, but at around 20kDa in size, the fragment is significantly larger. Additionally, there are no N-linked glycosylation sites present in the intracellular domain so the size difference cannot be attributed to these. Therefore, one can deduce that cleavage must occur somewhere in the extracellular domain, although cleavage is likely to be membrane proximal based on the size of the fragment. It is also worth noting that the migration of proteins through SDS-PAGE is based on both their mass and overall net charge so proteins may not always migrate as expected. To determine the exact nature of the fragment, the band observed at around 20kDa in WCL samples could be excised and analysed by mass spectrometry. Whilst this was planned, it was not performed due to time limitations.

Upon further investigation of the supernatant of HA-AMIGO-2 transfected HEK293T cells, only the mature full-length protein was identified. Addition of anti-HA beads to the supernatant only resulted in making the band at 70kDa, representing the full-length protein, more prominent. By identifying the intact (full length) protein in the cell supernatant I have demonstrated that the protein is released from the cell via budding or vesicles. However, the physiological significance of this phenomenon is unknown. Furthermore, absence of the cleaved protein from the supernatant confirms that the protein fragment is in fact the cytoplasmic portion of the protein. The supernatant was only analysed using an antibody against the N-terminal tag and it would be beneficial to analyse the supernatant of AMIGO-2 transfected HEK293T cells using an antibody directed against the C-terminal end of the protein, to determine if the cleaved fragment, identified in WCL, is released.

It is interesting that the band was observed only in AMIGO-2 lysates and was absent from both AMIGO-1 and AMIGO-3 lysates. Since each protein was subjected to identical protocols, the cleavage must be an intrinsic property of this protein in particular. This leads to the

question of how AMIGO-2 differs from AMIGO-1 and AMIGO-3? The AMIGO proteins display similarity at the amino acid level of 48-50% and although only the structure of AMIGO-1 ectodomain has been determined, those of AMIGO-2 and AMIGO-3 are predicted to be very similar. AMIGO-2 has previously been identified in a number of studies, each identifying the protein's involvement in a different condition. AMIGO-2 mRNA was identified in gastric adenocarcinoma [101], where it was differentially expressed in 45% of gastric adenocarcinoma samples compared to a very low level of expression in normal tissue suggesting that AMIGO-2 may be required for tumorigenisis of human gastric adenocarcinomas [101]. Other studies have demonstrated that overexpression of AMIGO-2 inhibits apoptosis in cerebellar granule neurons [100], thereby promoting survival. More recently, AMIGO-2 was identified as significantly upregulated in rheumatoid arthritis synoviocytes exposed to IL-17A/TNF, in an ERK-dependent manner, with expression correlating with increased cellular adhesion, survival and proliferation [146]. There is no information suggesting the involvement of AMIGO-1 or -3 in these studies, highlighting the differing functions of the AMIGO family members. Determining the structures of AMIGO-2 and AMIGO-3 may provide more information regarding the cleavage of AMIGO-2 and the varying roles each protein has.

Cell fractionation experiments demonstrated the cellular membrane localisation of the AMIGO proteins which also includes plasma, mitochondria and ER-golgi membranes. Similarly, NgR and $p75^{NTR}$ were also identified in the cellular fraction. The matching cellular locations increases the possibility of interactions between the proteins of interest. Interestingly the cellular location of LINGO-1 was identified as predominantly cytoplasmic, supporting previous findings by Meabon et al. [126] who demonstrated native, endogenously expressed

LINGO-1, was found exclusively on intracellular membranes, including on membranes of the endocytic pathway. The group reasoned that the protein may transiently visit the cell membrane.

As detailed in previous chapters, the specific role of LINGO-1 within the NgR/p75^{NTR}/LINGO-1 complex remains the subject of ongoing debate and research, due in part to the expression of LINGO-1 remaining low until 14 days after injury to the CNS [107]. The same group that described the intracellular location of LINGO-1, also describe the apparent competition between LINGO-1 and NgR for binding to p75^{NTR} [126]. Since LINGO-1 and NgR are structurally related, with both containing both LRR and Ig domains, it is plausible to suggest that they bind p75^{NTR} in a similar manner. However, it is difficult to describe a model detailing the sequential binding between NgR/LINGO-1 and p75^{NTR} due to the intracellular expression of LINGO-1. There are two possible solutions to this (i) LINGO-1 is shuttled to the cell surface when needed, as mentioned previously, or (ii) p75^{NTR} is internalised to allow association with LINGO-1 on endosomes [126].

In this chapter, I also confirmed homophillic and heterophillic binding of the AMIGO family of proteins using co-immunoprecipitation experiments, and have demonstrated their ability to bind LINGO-1, NgR and p75^{NTR}. Indeed, binding between the AMIGO proteins has been demonstrated previously [97] and the indication of a role for AMIGO-3 in the complex has also been mentioned before [107]. However, the results in this chapter provide the first evidence that each individual AMIGO family member can interact with both NgR and p75^{NTR} *in vitro,* highlighting the possibility of these proteins playing a role within the NgR complex.

There are numerous methods for analysing protein-protein interactions, each with relative advantages and potential for the introduction of methodological artefacts. A comprehensive

review of the respective merits of each technique is beyond the scope of this thesis, however, it is worth noting that much of the work in this chapter involved overexpression of the proteins of interest, meaning that the assembly of protein complexes may not be a true representation of physiological conditions. Furthermore, overexpression or tagging may cause a protein to become incorrectly localised, therefore it is beneficial to study the localisation of endogenous proteins. However, this requires the availability of highly specific primary antibodies. A problem with detection of endogenous proteins is that the components of the protein complex may not be expressed sufficiently in the cell lines studied [147].

Whilst the results from HEK293T transfected cells are relatively straightforward to analyse, the results obtained from native tissue work were much more challenging, due largely to the reliability and sensitivity of the native antibodies. We were able to identify the expression of some of the proteins of interest in both the human oligodendrocyte cell line, MO3.13, and in human brain tissue lysate but it is difficult to determine if the results obtained were a true representation of expression, or were the result of the success or failure of the native antibodies.

If the effectiveness and reliability of the native antibodies had been better, further tests to identify the subcellular localisations of the proteins of interest in the human cells would have been completed, as would further co-immunoprecipitation experiments.

The results in this chapter have provided the first indications of binding between the AMIGO proteins and NgR and $p75^{NTR}$. However, to confirm such interactions, further experiments to assess direct protein-protein binding, such as surface plasmon resonance, would be beneficial.

Chapter 4

Crystallisation and structure determination of human AMIGO-1 ectodomain

Crystallisation and structure determination of human AMIGO-1 ectodomain

4.1 Transfection of *Drosophila* S2 cells

Previous studies have revealed that LRR and Ig domain containing proteins have been expressed in multiple eukaryotic expression systems [69, 148, 149] For example, LINGO-1 and LRIG-1 have both been expressed in CHO [148] and HEK-293 cells [149]. Notably, the crystal structure of the LINGO-1 ectodomain was generated from protein expressed in CHO cells [69]. However, the mouse AMIGO-1 structure, which is the closest existing homologue to human AMIGO-1, was derived from protein expressed in *Drosophila* S2 cells. Based on these considerations, the human AMIGO-1 ectodomain (Figure 4.1) incorporating residues 28-362 (hereafter referred to as AMIGO-1), was cloned into *Drosophila* expression vectors by the Protein Expression Facility (University of Birmingham).

4.2 S2 cells expression and induction

Initial expression of AMIGO-1 in *Drosophila* S2 cells was performed on a small scale. This involved inducing a small volume of cells (7ml at a density of 1x 10^6/ml) with copper sulphate ($CuSO_4$) and retaining samples of supernatant after 2, 3 and 4 days to determine the optimal time for harvesting cells. Expression levels were analysed by western blot using an anti-His antibody to detect the His tag located at the C-terminal end of the AMIGO-1 ectodomain protein (Figure 4.2a). Human AMIGO-1 was shown to be expressed at equivalent levels at each time course interval examined as demonstrated by bands on the western blot at approximately 40kDa which coincide with the predicted size of the AMIGO-1 ectodomain (40.8kDa). The lack of sizeable shift on the SDS-PAGE gel also indicated that the human AMIGO-1 ectodomain was not heavily glycosylated. This is similar to insect

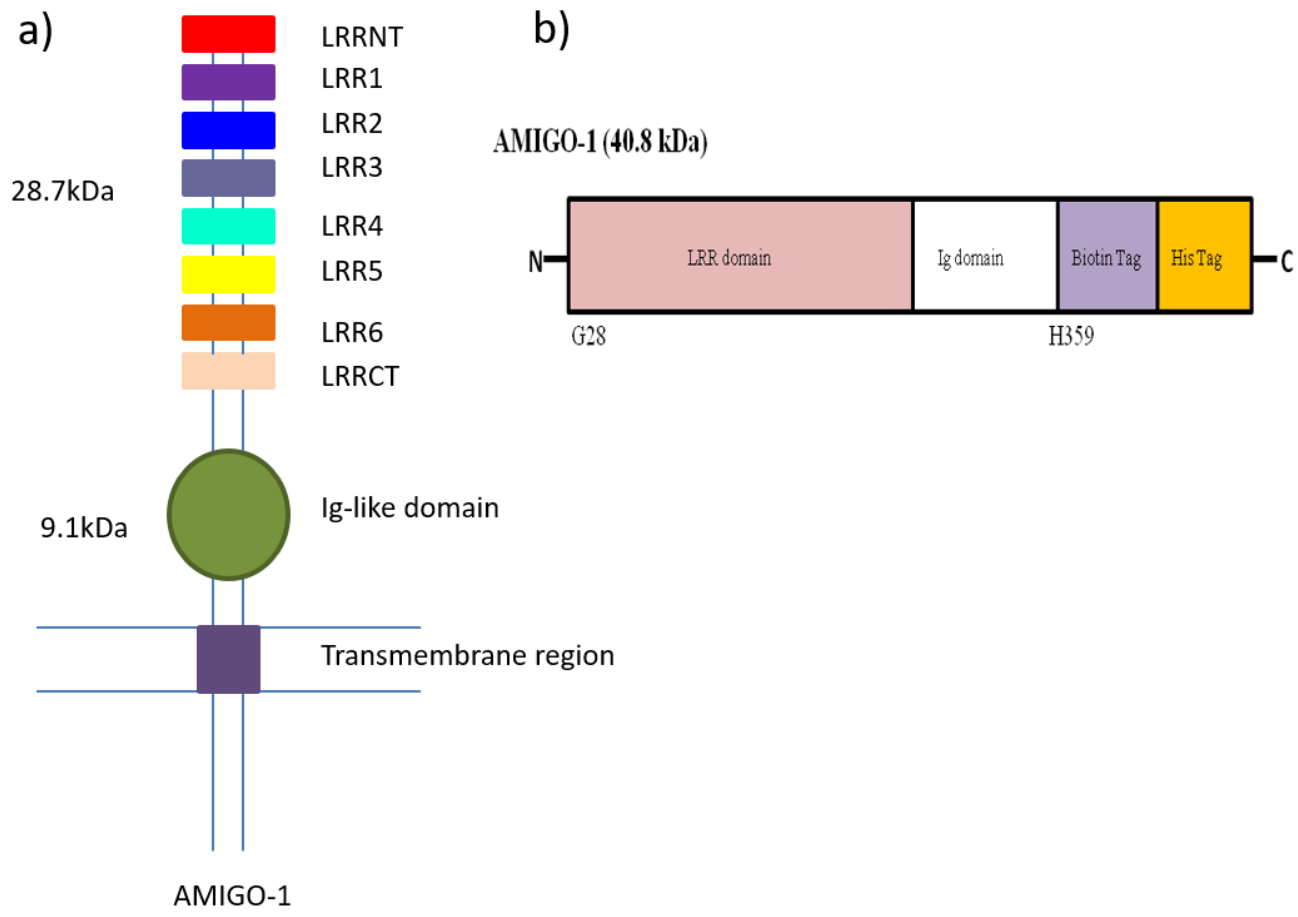

Figure 4.1. Schematic diagram of the domain organisation of AMIGO-1.
The AMIGO-1 ectodomain contains an Ig-like domain and 6 leucine rich repeats (LRR) flanked by cysteine rich capping domains (LRRCT/LRRNT). The predicted size of the Ig –like domain is 9.1 kDa and the LRR domain including capping domains is 28.7 kDa, therefore the predicted size of both domains together is 37.8 kDa. *Drosophila* expressed AMIGO-1 ectodomain is 40.8kDa in size, the difference between these is because the expressed protein also contains biotinylation and 6 x His tags which together are 3kDa in size. The positions of the Biotin tag and the His Tag are shown in b).

derived mouse AMIGO-1 ectodomain which was shown to migrate at approximately 43kDa by SDS-PAGE [120]. Interestingly, this observation contrasts to mammalian (HEK-293) derived full length mouse AMIGO-1 which appears as a band approximately 75kDa in size on SDS-PAGE despite the fact that the predicted size is actually 55kDa thereby indicating heavy glycosylation.

Hence in subsequent large scale preparations, to maximise AMIGO-1 expression levels, *Drosophila* S2 cells were harvested after a 4-day induction interval.

4.3 Purification by Nickel chelate and Size exclusion chromatography

Recombinant human AMIGO-1 containing supernatant from S2 cells was purified by Ni-NTA chromatography. Ni-NTA purification is a simple and a relatively robust technique for purifying proteins with a His-tag in sufficient enough quantities for structural studies as highlighted for mouse AMIGO-1[120]. To achieve optimal binding of His-tagged human AMIGO-1 to the nickel beads, the S2 supernatant was dialysed to remove compounds from the supernatant such as excess $CuSO_4$, surfactant and low molecular weight amino acids, which may compete with the target protein for binding. The dialysed supernatant containing AMIGO-1 was passed over a column containing nickel beads to which the His-tag bound. Typically, between 3-6 mg of protein was eluted off the nickel column with Ni-NTA elution buffer (250mM Imidazole in PBS) from 1L of *Drosophila* S2 cells and stored at -20°C. Unfortunately, SDS-PAGE analysis of Ni-NTA eluted AMIGO-1 was hampered by the fact that approximately 90% of eluted protein was prone to precipitation despite thawing the sample on ice. This highlighted that the Ni-NTA elution buffer containing PBS was unsuitable for stabilising and maintaining AMIGO-1 in solution. In addition, the Ni-NTA elution buffer contained phosphate which has proven in the past to be an undesirable component for

crystallisation as it can readily react with metals found in the commercial crystallisation buffers resulting in the formation of salt crystals. Based on these considerations the protein was buffer exchanged into a suitable buffer free from phosphate. The selection of the appropriate buffer for AMIGO-1 was heavily dependent on its isoelectric point (pI). Generally, selecting a buffer with several pH units away from the pI of the target protein is an ideal start point for identifying a stable buffer that could potentially reduce the precipitation effects. Based on the primary sequence, the pI of AMIGO-1 was calculated to be 6.21 using the EXPASY server [150]. Hence, in the subsequent production of AMIGO-1, the Ni-NTA eluted protein was buffer exchanged into a buffer consisting of 20mM Tris pH 8.5 + 50mM NaCl in readiness for size exclusion chromatography. Notably, the Tris buffer was supplemented with NaCl to further reduce the risk of protein aggregation. Additionally, there was precedence for successfully using a similar buffer in protein purification and crystallisation trials as documented for mouse AMIGO-1 [120]. SDS-PAGE analysis of the eluted protein demonstrated a substantial band migrating at ~40kDa (Figure 4.2b), consistent with the predicted molecular weight of the human AMIGO-1 ectodomain. In addition, there was a noticeable shift in bands observed between the reduced and non-reduced samples suggesting that the protein has fully formed disulphide bonds. Furthermore, the gel illustrated low levels of large molecular weight contaminants, suggesting that additional purification with size exclusion may be necessary before proceeding to crystallisation trials.

Strikingly, there were no visible signs of AMIGO-1 aggregation/precipitation following the buffer exchange step into the new buffer. The size exclusion step was performed with the Superdex 200 column on the FPLC which had been pre-equilibrated with 20mM Tris pH 8.5 + 50mM NaCl. A single peak of 100mAu at 190ml was observed on the resulting S200 elution

profile (Figure 4.2c). However, the monomeric form of human AMIGO-1 ectodomain was expected to elute at 210ml. Based on molecular weight standards, the peak corresponded to a protein that is 80kDa in size. The substantial shift in peak to around 190ml could reflect the fact that the AMIGO-1 protein exists as a dimer in solution. This notion is supported by previous biophysical and structural studies on the mouse AMIGO-1 ectodomain, which formed dimers in solution form and within the crystal lattice [120]. In addition, another member of the LRRIG family, LINGO-1, formed a tetramer in crystal form which can be assembled as either a dimer of dimers or form four monomers [69].

SDS-PAGE analysis of the peak fraction at 190 ml, under reducing and non-reducing conditions, illustrated a single band of approximately 40kDa in size, which was consistent with the predicted size of the AMIGO-1 ectodomain (Figure 4.2d). More importantly, this confirmed that the AMIGO-1 ectodomain forms a dimer in solution. Furthermore, following size exclusion purification, the purity of the protein appeared significantly increased with the high molecular weight contaminants successfully removed. The protein was therefore deemed to be of sufficiently high purity for entering crystallisation trials. The peak S200 fractions were pooled together and concentrated to a final concentration of 10mg/ml. By achieving such high concentrations, it confirmed that the TRIS-NaCL buffer at pH 8.5 was optimal for stabilising and retaining human AMIGO-1 in solution.

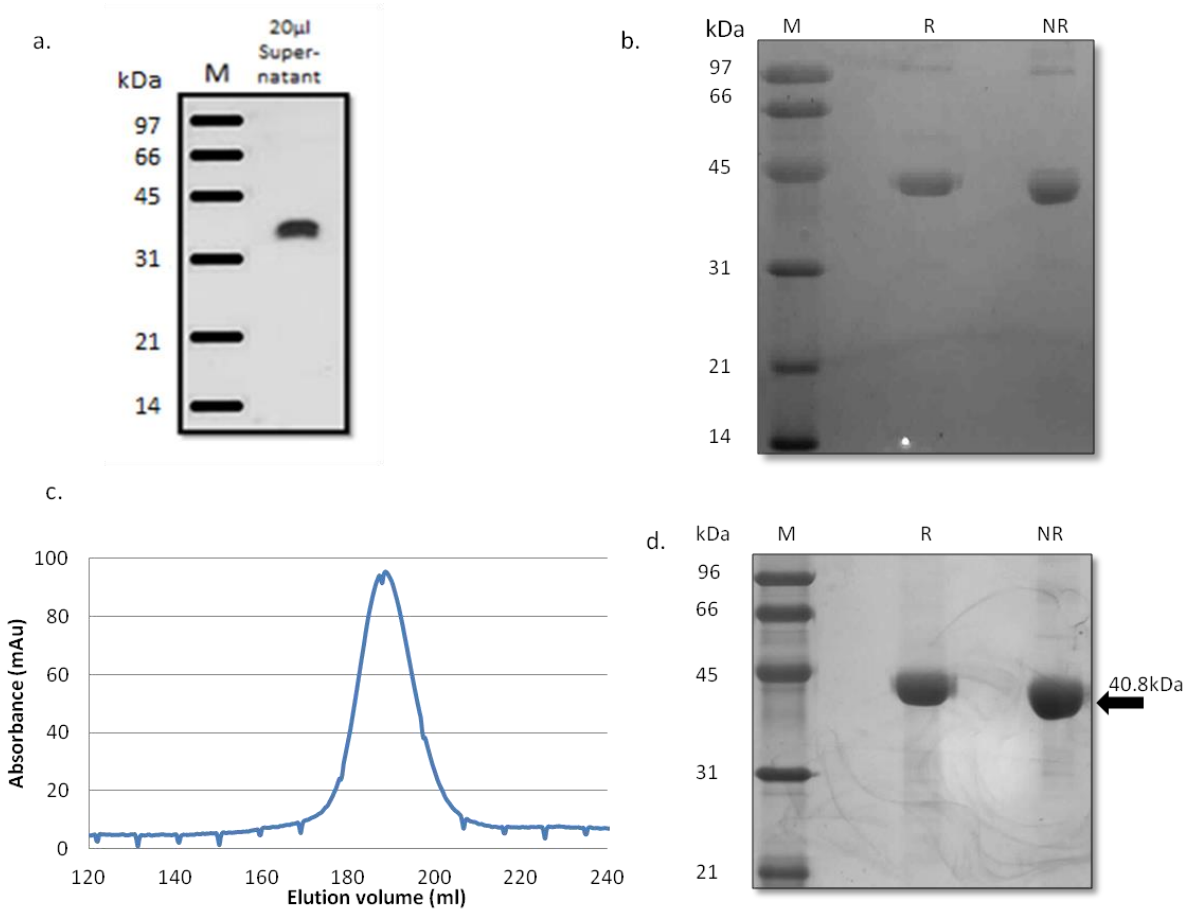

Figure 4.2 Production of human AMIGO-1 ectodomain.
a) Western blot analysis of human AMIGO-1 on day 5 after induction with $CUSO_4$. Sufficient levels of AMIGO-1 can be seen in the supernatant of the *Drosophila*. b) Expressed AMIGO-1 was purified by Ni-NTA and eluted into PBS + 250mM imidazole, following buffer exchange into 20mM Tris pH 8.5 + 50mM NaCl the protein was analysed by SDS-PAGE under reducing (R) and non- reducing (NR) conditions. The SDS-PAGE shows large bands running at the predicted size of the AMIGO-1 ectodomain (40.8Kda) which indicates that the protein is a monomer and is not heavily glycosylated. There are also higher molecular weight bands visible which are contaminants that need to be removed by gel filtration. C) Elution profile of human AMIGO-1 following purification by size exclusion chromatography. AMIGO-1 protein was purified by size exclusion chromatography using the S200 column. A single peak of ~100 mAu is observed at 190ml which corresponds to a protein with a Mw of 80kDa. This suggests that AMIGO-1 ectodomain exists as a dimer in solution. d) SDS-PAGE analysis of human AMIGO-1 following purification by size exclusion chromatography. Following gel filtration peak fractions (elution volume 190ml) were pooled and analysed under reduced (R) and non-reduced (NR) conditions. The high molecular weight contaminants have been removed and only bands at ~40kDa are seen which correspond with AMIGO-1 (40.8kDa, black arrow).

4.4 Overview of X- ray Crystallography

X- ray crystallography is a widely used technique for determining the three-dimensional structure of proteins at a molecular level. The information obtained by X-ray crystallography can be used to ascertain the functions of the protein including identifying how they interact with other molecules and the knowledge obtained can be used in the design of functional studies and drug design. The accuracy of the structures derived by X-ray crystallography can be extremely high; however, the amount of structural data that can be extracted from a structure is heavily reliant on the quality of the protein crystal. There are numerous steps involved in determining the three-dimensional structure of protein using X-ray crystallography (Figure 4.3) and these have been highlighted in further detail below.

4.4.1 Protein crystallisation: Theory

The first requirement for determination of the protein structure is to generate well-ordered diffraction-grade crystals. However, this step represents one of the largest obstacles in X-ray crystallography as the identification of crystallisation conditions appropriate for crystal growth is largely a multi-dimensional search by trial and error. The overall aim in crystallisation is to minimize protein-solvent interactions and maximise protein-protein interactions. This can be achieved by bringing the protein solution to a supersaturated state, thereby increasing the likelihood of protein molecules interacting with each other. Crystallisation occurs in three key stages; nucleation, growth and termination. Nucleation involves the formation of small aggregates, called nuclei which provide a site for crystal growth. The growth of the crystal is achieved by protein molecules being recruited to the growing faces of the crystal, resulting in the formation of well-ordered crystals. The final

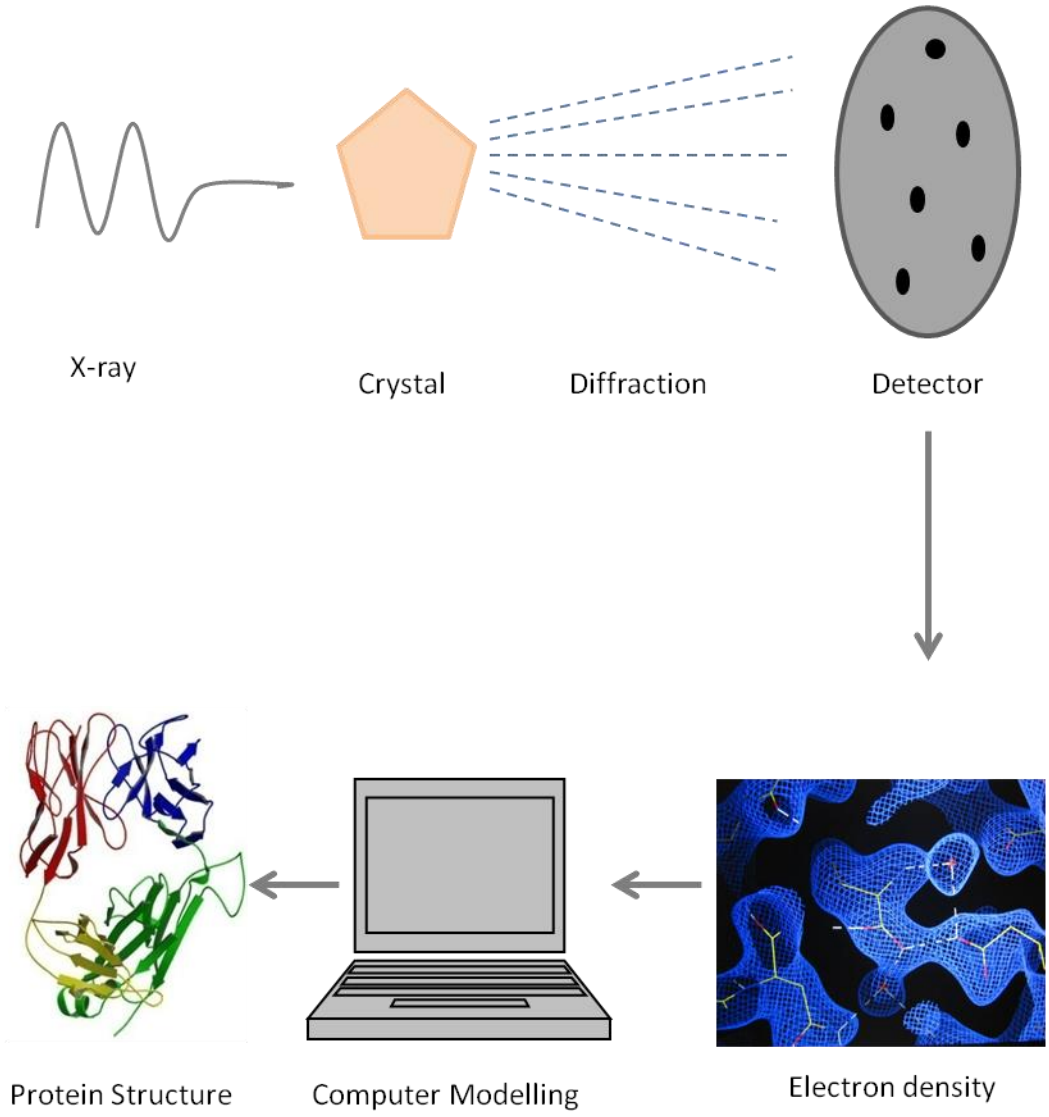

Figure 4.3. An overview of X ray crystallography.
Protein obtained from the drosophila expression system is purified and subjected to crystallisation trials. Suitable crystals are exposed to an X-ray beam which diffracts X-rays that are recorded by an X-ray detector. The diffraction data is processed to produce an electron density map. The electron density map is then interpreted allowing model building and refinement to take place using a computer graphics workstation. The molecular structure is then subjected to numerous cycles of model building and refinement leading to a final protein structure which is analysed.

stage in crystallisation is termination, whereby the crystal ceases to grow due to growth defects, presence of contaminants or depletion of protein molecules.

For proteins to achieve a super-saturation state and potentially crystallise a reduction in their solubility is required. There are several factors that can influence protein solubility including pH, ionic strength and presence of precipitants and these are available as part of commercial sparse matrix based screens. Ideal conditions will force the protein molecules in the solution to interact with one another in a specific manner that may lead to crystallisation. For example, pH has a major influence on crystallisation as the solubility of a protein is at its lowest at a pH close to the isoelectric point (pI) of the target protein. As a result, the number of protein-solvent interactions are minimised and protein-protein interactions are more likely to take place.

4.4.2 Protein crystallisation: Vapour diffusion method

The vapour diffusion method is the most common technique used for protein crystallisation and can be utilised in two ways; hanging drop or sitting drop. Using this approach, it is possible to screen for many different crystallisation conditions with the aim of identifying conditions that yields protein crystals or can at least provide a hint of crystallisation (e.g. straight edged needles). This involves mixing equal volumes of protein solution and crystallisation reagent (reservoir solution) on the surface of a cover slip which is then inverted over the well containing the crystallisation reagent (Figure 4.4a). Since the precipitation concentration in the drop is less than in the crystallisation condition, water diffuses out of the drop by vapour diffusion until equilibrium is reached between the drop and the reservoir solution. As water diffuses out, the protein concentration in the drop slowly increases reaching supersaturated levels at which point protein molecules are forced to interact with

each other which can potentially lead to nucleation (crystal growth) or precipitation. The precipitation effect is a relatively rapid process caused by non-specific protein-protein interactions. In such circumstances, the crystallisation trials are repeated but with a different crystallisation reagent. The initial screening process is performed on a small-scale in 96 well plates utilising nanolitre drop sizes (typically 100nl) with a mosquito nanolitre crystallisation robot. This allows screening of a large number of conditions using small quantities of protein. The buffer conditions that yield promising hits provide a basis for optimisation. This involves altering buffer and/or protein conditions such as salt concentration, precipitant concentration, pH and protein concentration. The optimisation stage can be carried out manually using 24 well Linbro plates with larger drop sizes (typically between 2-3µl in volume). Also at this stage it is possible to use the sitting drop vapour diffusion technique which in principle works in the same manner as the hanging drop method but the drop is placed onto a rod which sits in the well before sealing with the coverslip (Figure 4.4b). Generally, the time duration for crystal growth is heavily dependent on the protein but can typically take between 1 and 14 days.

Once protein crystals of a suitable size have been grown they are subjected to X-ray diffraction experiments. Prior to X-ray data collection, the crystals must be soaked in a cryoprotectant solution which helps to protect the crystal from damage caused by X- ray radiation. The cryoprotectant also serves as anti-freeze and prevents solution surrounding the protein crystal from forming ice crystals which can diffract X-rays and interfere with downstream data processing. The cryoprotectant is made from the reservoir solution supplemented with either glycerol, ethylene glycol, PEG 400 or 2-methyl-2, 4-pentanediol (MPD). The identification of appropriate cryoprotectant conditions is usually performed by trial and error and is

dependent on the components of the mother liquor. Once the crystal has been sufficiently cryoprotected it can then be exposed to X-rays allowing X-ray diffraction experiments to take place.

a. Hanging drop method

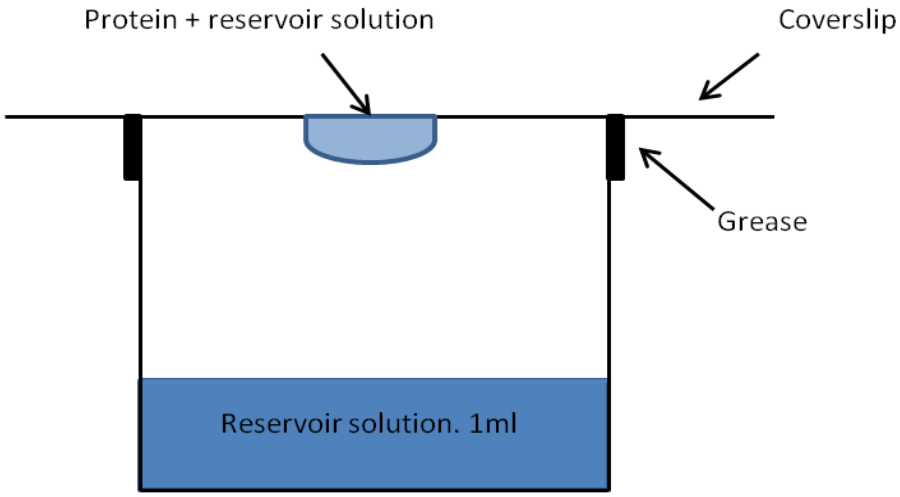

b. Sitting drop method

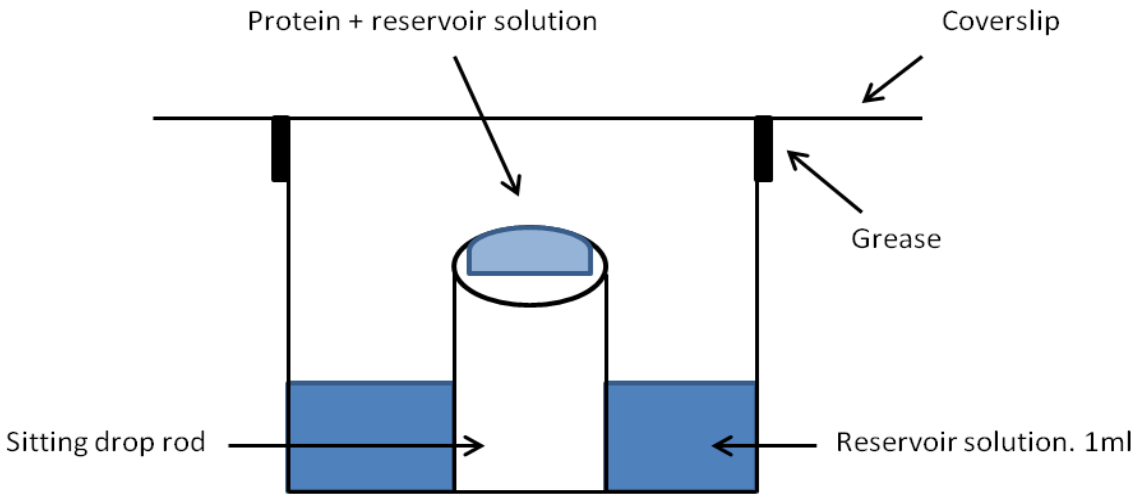

Figure 4.4 Schematic of vapour diffusion set ups using hanging and sitting drop techniques.

Large-scale hanging drops (a.) and sitting drops (b.) are set up by mixing varying ratios of protein: crystallisation reagent (e.g. 1ul +1ul, 2ul + 1ul, 1ul + 2ul and 2ul + 2ul) . The wells are sealed with grease to create an enclosed system. A difference in precipitant concentration between the drop and the reservoir solution causes vapour diffusion where water diffuses out of the drop. This causes the concentration of protein in the drop to increase promoting more protein- protein interactions which may either lead to crystal formation (specific interactions) or aggregate formation (non-specific interactions).

4.4.3 X-ray and data collection

Data collection from protein crystals involves mounting the crystal in a nylon loop and orientating it so that it is in the direct path of an X-ray beam. During this stage crystals are maintained at cryogenic temperatures using a nitrogen gas stream to ensure that the least amount of X-ray damage occurs to the crystal. The X- rays strike the crystal and the electrons surrounding the atoms in the protein diffract the X-ray beam into many discrete beams. The diffracted X-rays are recorded by an X-ray detector. To collect a complete dataset the crystal is rotated with respect to the X-ray beam.

4.4.4 Data Processing

Data processing firstly involves determining the unit cell parameters and space group. The unit cell is the simplest repeating unit and building block of a crystal, of which there are 7 categories. The unit cell dimensions are described by three cell lengths; a, b and c and three angles; α, β and γ. Each of the seven categories of unit cell has different imposed constraints on these lengths and angles. It is essential to determine these parameters before further structure determination can take place. The distances between the spots on the diffraction pattern are used to calculate the unit cell parameters. The space group describes how protein molecules are arranged within the unit cell.

X-rays are simple waves that are described by three parameters; frequency, amplitude and phase, and knowledge of all three parameters allows for determination of the protein structure. The frequency of the wave is known from the wavelength of the X- ray source and the amplitude can be determined during data processing where the intensities of the spots are

measured and converted to amplitude. The phase of the wave however cannot be determined during data collection.

4.4.5 Determining Phase Information

There are several methods available to determine the phase information, the most common being molecular replacement. With this method, phases are borrowed from a known structural homologue as initial estimates for the structure to be determined. The method involves superimposing the phasing model onto the target data, and is highly dependent on the level of sequence identity between the two proteins. The higher the level of sequence correlation between the model and the target structure the easier it is to superimpose. Once the models are superimposed the phase information can be extracted and used for the target structure.

However, in cases with proteins exhibiting novel folds, molecular replacement is not possible and phase information must be determined experimentally. One technique used to calculate experimental phases is multiple isomorphous replacement (MIR) which involves collecting data on a native protein crystal and a crystal that has been soaked in a solution containing heavy atoms. Since heavy atoms are electron dense they have a higher atomic scattering factor and this in turn alters the intensity of the X-ray reflections. These differences in intensity can be used to experimentally determine phase information. Heavy atoms include mercury, gold and platinum which are highly reactive towards cysteine, histidine and methionine, and lanthanides and actinides which bind to glutamic acid and aspartic acid. For this technique to work the unit cell dimensions of the derivative crystal must remain isomorphous to the native crystal. X-ray data is collected on the derivative crystal and the difference between the native and derivative data sets provides the positions of the heavy atoms. A second isomorphous

crystal is then generated using a different heavy atom, to give definitive phase information. MIR is useful for generating phase information for novel structures however the processes involved are time consuming and there is no guarantee that heavy atoms will bind to the atoms after soaking.

Another method used to determine the phase information is multi wavelength anomalous dispersion (MAD). This technique uses anomalous scattering measurements at appropriate energies taking into account the strong variations of the scattering factor near an absorption edge [151], providing useful phase information which in turn can be utilised to solve structures. MAD involves the incorporation of a heavy atom such as selenium into the protein sample prior to crystallisation; a single protein crystal is then exposed to X-rays at three different wavelengths which can be achieved using a tuneable X-ray source such as a synchrotron.

4.4.6 Model building and refinement

The combination of amplitude and phase can lead to calculation of electron density maps. An electron density map is a map showing the distribution of electrons. Since the electrons surround the protein atoms it is possible to interpret the map and build in amino acid side chains of the target protein. Model building is usually performed on a computer graphics display. The model is then refined with refinement software programmes which adjusts the model to best fit electron density and to ensure that bond lengths and angles are correct. Alternate cycles of model building and refinement take place before the refined structure is determined. Crystals that diffract X-rays to a higher resolution have more detailed electron density and therefore amino acid side chains can be placed with a greater degree of certainty.

4.5 Structure determination of AMIGO-1 ectodomain

4.5.1 Crystallisation of AMIGO-1 ectodomain

AMIGO-1 at a concentration of 10mg/ml was used in small scale crystallisation trials with the hanging drop method using 3 sparse matrix based screens; JCSG$^+$ (MDL), INDEX (Hampton Research) and Wizard I+II (Emerald Biosystems). In total 288 different buffer conditions were screened. Positive 'hits' were identified in 3 conditions; JCSG$^+$ condition 20 (0.2M $MgCl_2$, 0.1M Tris pH7, 10% PEG 8000) (Figure 4.5a), INDEX condition 66 (0.2M ammonium sulphate, 0.1M Bis- Tris pH 5.5, 25% PEG 3350) (Figure 4.5b) and INDEX condition 67 (0.2M ammonium sulphate, 0.1M Bis- Tris pH 6.5, 25% PEG 3350) Figure 4.5c). The crystals formed using INDEX conditions 66 and 67 were sparse and non-uniform in shape. In contrast, the crystals formed grown in JCSG$^+$ condition 20 were higher in number and more uniform shape. Negative controls were also set up where the crystallisation buffer was added but protein was excluded to ensure that any crystals formed were not crystallised salt. These controls contained no crystals indicating that the crystals formed in the trials were derived from protein and not salt. Further small-scale crystallisation trials with JCSG$^+$ condition 20 consistently yielded crystals, suggesting that this condition was highly reproducible for producing crystals. Typically, these showers of crystals appeared after 1 day and grew to approximately 40μm x 40μm in size. The size of these crystals was unsuitable for X-ray diffraction experiments and therefore optimisation trials were set up using JSCG$^+$ condition 20.

The optimisation trials were initially set up on a small scale in an attempt to reduce the number of nucleation sites per drop which contributed to the shower of crystals observed. A common strategy employed to reduce the number of nucleation sites is to reduce the precipitant or protein concentration or both. However, equilibration of human AMIGO-1 at

lower protein concentration (7 mg/ml) against home-made screens incorporating reduced concentrations of PEG 8000 (from 10% to 7.5%) failed to generate any crystals. The subsequent strategy involved setting up trials using custom made JCSG$^+$ condition 20 in which the PEG 8000 was unaltered. This large-scale optimisation utilised both hanging and sitting drop techniques and drops were set up using differing ratios of protein: crystallisation buffer including 1:1 (Figure 4.5d), 1:2 and 1:3 (Figure 4.5e). These large-scale optimisation trials resulted in seven large diffraction-grade crystals being formed which were typically 100μm x 100μm in size.

Prior to X-ray diffraction experiments the seven crystals were soaked in cryoprotectants that had previously been used in the structure determination of proteins that had grown in similar crystallisation conditions. Based on this information, four of the crystals were soaked in glycerol and three in ethylene glycol. The crystals were soaked in increasing concentrations of cryoprotectant, spending 5 minutes in 5%, 5 minutes in 15%, 5 minutes in 20% and finally 30 minutes in 25% glycerol or ethylene glycol. Finally, the crystals were flash cooled in liquid nitrogen.

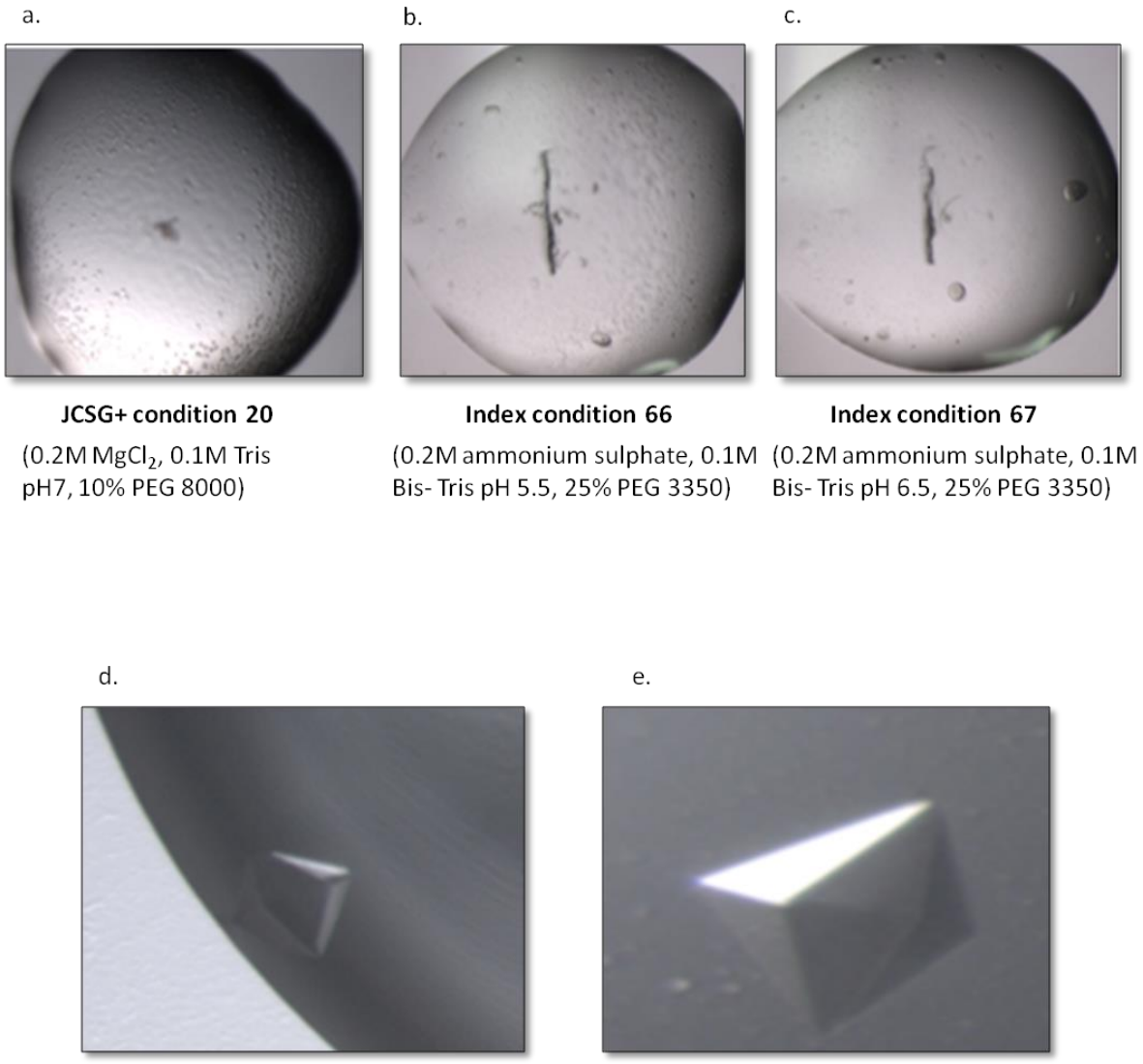

Figure 4.5. Generation of AMIGO-1 ectodomain micro-crystals and large-scale optimisation.

Micro-crystals of the AMIGO-1 ectodomain were identified using the hanging drop method with JCSG+ (a) and Index screens (b, c) commercial screens. Drops were set up by mixing 100nl of AMIGO-1 ectodomain protein with 100nl reservoir solution and micro-crystals appeared after approximately 1 week. Large diffraction-grade crystals were produced by optimising JCSG+ condition 20 (0.2M $MgCl_2$, 0.1M Tris pH7, 10% PEG 8000). Drops were set up using 1:1 (d) and 1:3 (e) ratios of protein: crystallisation reservoir solution.

4.5.2 Data Collection and Processing

X-ray diffraction experiments were performed as described in Chapter 2 (materials and methods). Initial experiments revealed that the ethylene glycol cryoprotectant was sub-optimal compared to glycerol as crystals vitrified with 25% ethylene glycol diffracted to 2.9Å whereas those soaked in 25% glycerol diffracted X-rays to 2.4Å resolution. Approximately 6 data sets were collected (Figure 4.6). Initial data was auto indexed with XDS [116], and the crystal was found to belong to the trigonal/hexagonal space group with unit cell dimensions of; a= 99Å, b= 99Å, c= 103.4Å and α= 90°, β= 90°, γ= 120°. Diffraction data were integrated, scaled and merged using programmes of the XDS suite [116]. The relevant data processing statistics are listed in Table 4.1.

Parameters	AMIGO-1 ectodomain
Space Group	$P3_121$
Unit Cell Length (Å)	a= 99 b=99 c=103.4
Unit Cell Angles (°)	α=90 β=90 γ=120
Resolution (Å)	2.0-2.4 (2.5-2.4)
Observed Reflections	133509 (13944)
Unique Reflections	22199 (2499)
Multiplicity	6.01 (5.58)
Completeness (%)	95 (94.9)
R_{merge} (%)	14 (61.7)
I/σ (I)	13.15 (3.04)

Table 4.1 Data processing statistics for human AMIGO-1 ectodomain.

X-ray data for AMIGO-1 was integrated, scaled and merged using programmes of the XDS suite. Numbers in parentheses represent statistics associated with the highest resolution shell.

In order to circumvent space group ambiguity the data were processed in the lower symmetry space group (P3) and input into POINTLESS [123]. Based on POINTLESS the best possible space group was highlighted to be $P3_121$ however, unequivocal space group determination could only be made following significant translation function solutions during molecular replacement.

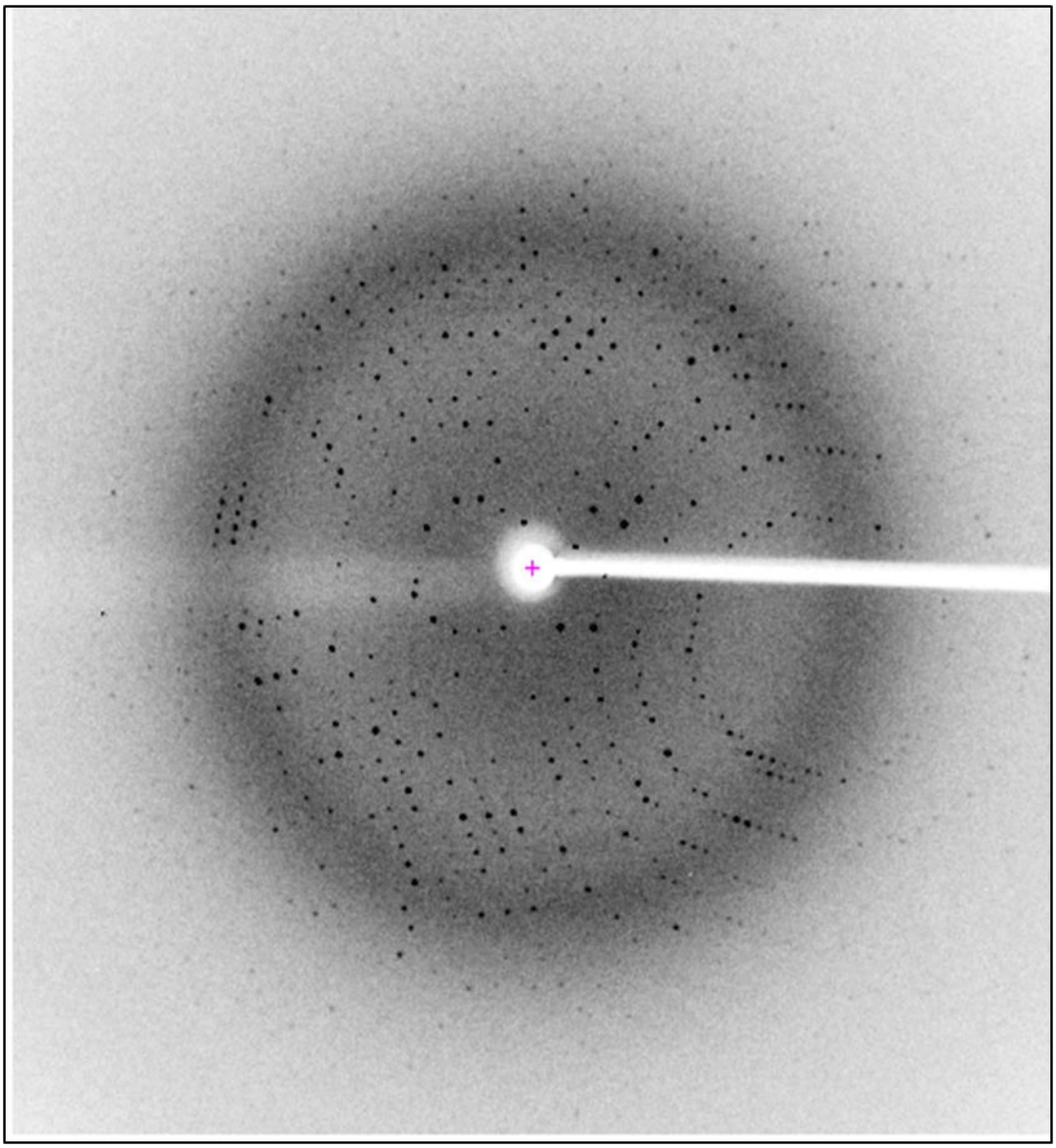

Figure 4.6 X-ray diffraction pattern of human AMIGO-1 ectodomain.
A 0.5° oscillation image of the human AMIGO-1 crystal which diffracted X-rays to 2.4Å resolution. The data was collected using an in house Micro-Max 007HF rotating anode X-ray generator (Rigaku) using a Saturn CCD detector (University of Birmingham Macromolecular X-ray Facility).

4.5.3 Determination of Phase Information

Assuming the AMIGO-1 crystals possess a dimer in the asymmetric unit, a solvent content of 31.9% was calculated [152]. Initial determination of phase information for AMIGO-1 was carried out by molecular replacement using the mouse AMIGO-1 ectodomain (PDB ID code: 2XOT) as a search model with MOLREP [117]. The choice of search model was based on the high degree of sequence identity (89%) that exists between mouse and human AMIGO-1. Unsurprisingly, molecular replacement calculations yielded unambiguous rotation and translation function solutions (data not shown) for two AMIGO-1 molecules consistent with AMIGO-1 crystallising as a dimer. However, the resulting model failed to refine with R-factors stalling at around 50% suggesting that there were significant differences between the human and mouse AMIGO-1 structures. One possibility was that the AMIGO-1 protein had become cleaved during the crystallisation process, and the crystals corresponded to a fragment of either the LRR or Ig domain. To investigate this further, samples of AMIGO-1 at 10mg/ml were stored at either -20^{o}C or at 23^{o}C for 17 days and analysed by SDS-PAGE. The samples were run alongside each other on an SDS-PAGE gel which illustrated a noticeable size difference between the two samples (Figure 4.7). The sample stored at -20^{o}C ran at the predicted size of the AMIGO-1 ectodomain, 40.8Kda, but the sample stored at 23^{o}C appeared to run at ~30 kDa. This lower sized band probably corresponds to the LRR domain of human AMIGO-1 which is predicted to be 28.7 kDa in size, indicating that the protein has been cleaved; this could be tested by removing the band and analysing it by mass spectrometry. Interestingly the band appearing at ~30 kDa is made up of multiple bands which is also a sign of degradation. The Ig domain of AMIGO-1 is predicted to be 9.1 kDa in size; however, this is not visible on this SDS-PAGE gel. The SDS-PAGE gel has confirmed

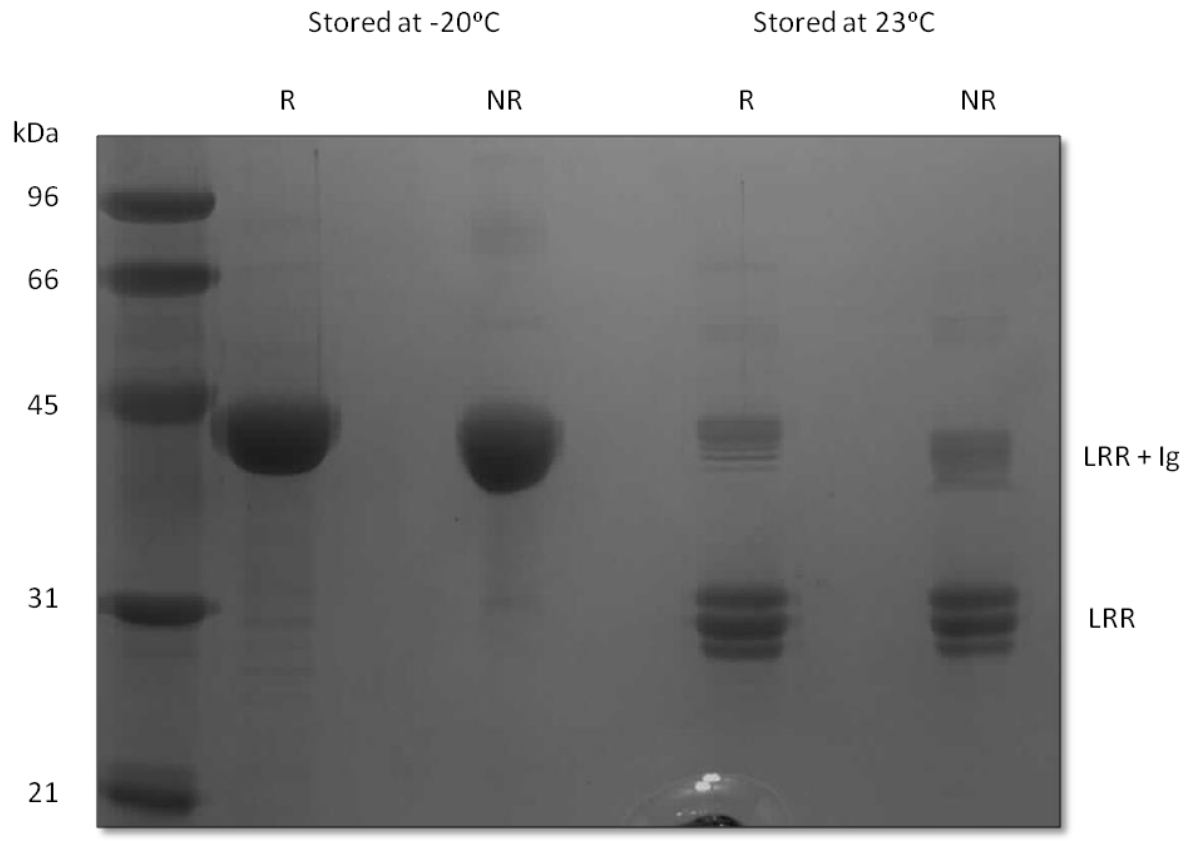

Figure 4.7 Cleavage of the AMIGO-1 protein under crystallisation conditions.
SDS-PAGE analysis of AMIGO-1 (10mg/ml) stored at either-20°C or at 23°C for 18 days. The sample of AMIGO-1 stored at -20°C continued to run at ~40kDa, however, the protein stored at 23°C appeared to shift in size to ~30kDa. This band is believed to represent the LRR domain of the protein which is 28.7kDa in size which indicates that the protein has become cleaved and therefore demonstrates that the protein is not stable at 23°C.

that the AMIGO-1 protein had become cleaved during storage under X-ray crystallography conditions, illustrating the protein is not stable at this temperature.

With this in mind, molecular replacement was repeated using the mouse AMIGO-1 model with the Ig domains omitted. Once again significant rotation and translation function peaks were determined for two human AMIGO-1 molecules (Tables 4.2, 4.3 and 4.4). Following the first round of refinement of the model the R-factors dropped to 28.7 and R-free to 32.2 with a revised solvent content of 45.9% for the AMIGO-1 LRR domain.

Peak number	α	β	γ	RF/σ
1	8.25	101.50	329.87	8.41
2	51.65	101.55	48.71	8.32
3	55.74	109.63	60.58	4.16
4	119.40	104.95	332.13	3.76
5	114.12	105.57	60.67	3.73

Table 4.2 Rotation function statistics for human AMIGO-1 ectodomain.

The table shows the 5 highest rotation function peaks using the mouse AMIGO-1 (LRR domain) monomer as the search model. The correct solutions are shown in red as determined by an increase in RF/σ scores.

Peak number	TX	TY	TZ	RFcnt	R factor
1	0.634	0.241	0.175	24.53	0.526
2	0.212	0.354	0.336	16.29	0.541
3	0.995	0.610	0.342	2.11	0.590
4	0.750	0.445	0.172	1.55	0.592
5	0.366	0.532	0.344	2.90	0.591

Table 4.3 Translation function statistics for human AMIGO-1 LRR ectodomain.

The table shows the 5 highest translation function peaks using rotation function angles from Table 4.2. The correct solutions are shown in red as determined by a decrease in R factor.

Peak number	TX	TY	TZ	RFcnt	R factor
1	0.212	0.353	0.331	27.01	0.443
2	0.272	0.386	0.305	4.02	0.541
3	0.389	0.267	0.692	2.25	0.554
4	0.633	0.955	0.628	4.87	0.557
5	0.905	0.664	0.279	3.01	0.556

Table 4.4 Translation function statistics for human AMIGO-1 ectodomain.

The table shows the 5 highest translation function peaks after fixing the first molecule. The correct solutions are shown in red as determined by a further decrease in R factor.

The molecular replacement solution was validated further by examination of the resulting electron density maps which showed distinct features that were associated with human AMIGO-1 ectodomain but absent from mouse AMIGO-1 ectodomain (Figure 4.8). For example, clear and unambiguous electron density can be observed for residue 123 which is an Arginine in human AMIGO-1 but a histidine in the mouse form.

Model building and refinement demonstrated that the crystals formed and the data that was collected was on the LRR domain of the human AMIGO-1 protein; however, data could not be collected on the full-length protein (containing the Ig domain) as this did not crystallise.

Following several rounds of refinement interpreted with manual model building the structure of human AMIGO-1 was built. The relevant refinement statistics are listed in Table 4.5. The structure was verified using PROCHECK [153] and revealed that most residues were present in the allowed regions of the Ramachandran plot (Figure 4.9). Ser-42 of both molecules was found in disallowed regions despite well-defined electron density. The residue is located in a hairpin loop within the N-terminal capping domain which may account for the distortion. The structure confirmed that human AMIGO-1 lacks the Ig domain.

Parameters	LRR
Resolution Range (Å)	20-2.4
Ref. In working set	21114
Ref. In test set	1081
R_{cryst} (%)	21.4
R_{free} (%)	25.7
Number of protein residues	484
Average B-factor (Å^2)	
Monomer A	21.6
Monomer B	23.4
Number of water mol.	113
RMS Bond Length (Å)	0.00658
RMS Bond Angle (°)	1.395
Ramachandran Plot	
Most Favourable (%)	72.3
Additionally allowed (%)	26.2
Generously Allowed (%)	1.3
Disallowed (%)	0.2 (Ser 42 for both subunits)

Table 4.5 Refinement Statistics for human AMIGO-1

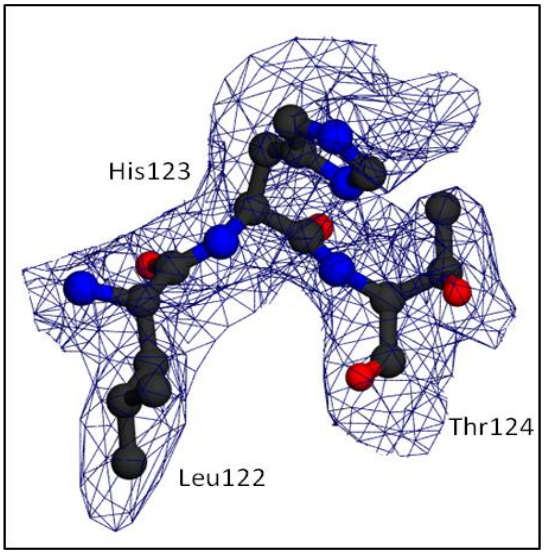

Mouse AMIGO-1
His 123

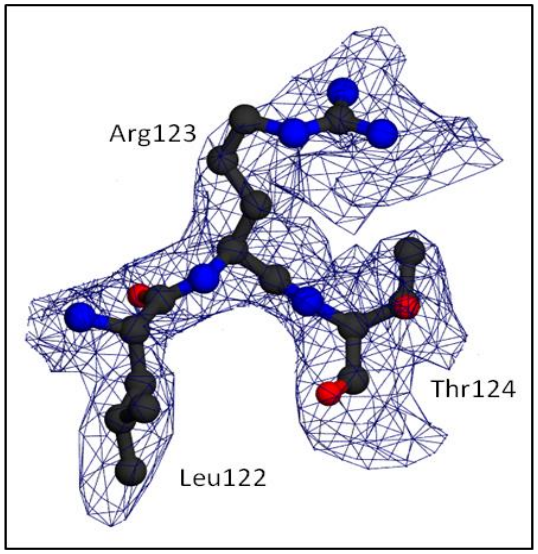

Human AMIGO-1
Arg 123

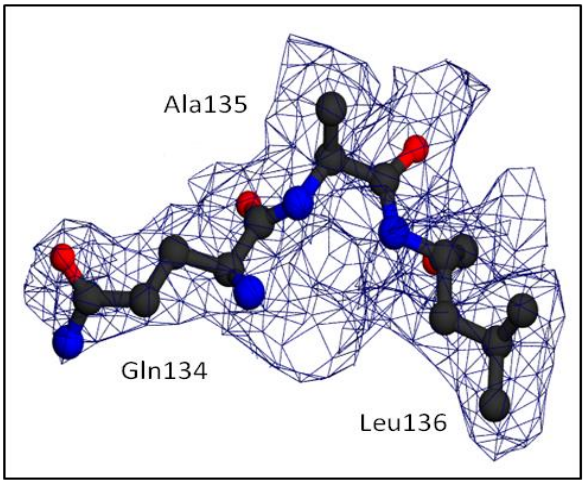

Mouse AMIGO-1
Ala 135

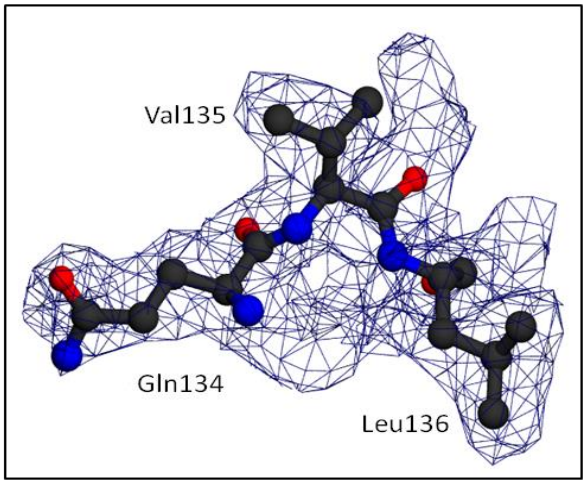

Human AMIGO-1
Val 135

Figure 4.8 Electron density maps showing differences between the mouse AMIGO-1 phasing model and the human AMIGO-1 target structure following molecular replacement.

Confirmation of the correct molecular replacement solution for hAMIGO-1. The pictures display 2Fo-Fc density contoured at 2σ for features that are present in the hAMIGO-1 model and not apparent in the mAMIGO-1 structure. In the hAMIGO-1 structure 2Fo-Fc density for the Arginine side chain can be seen at position 123, whereas in the mAMIGO-1 structure there is Histidine. Similarly, in the hAMIGO-1 structure 2Fo-Fc density for the Valine side chain at position 135 can be seen, whereas in the mAMIGO-1 structure there is Alanine.

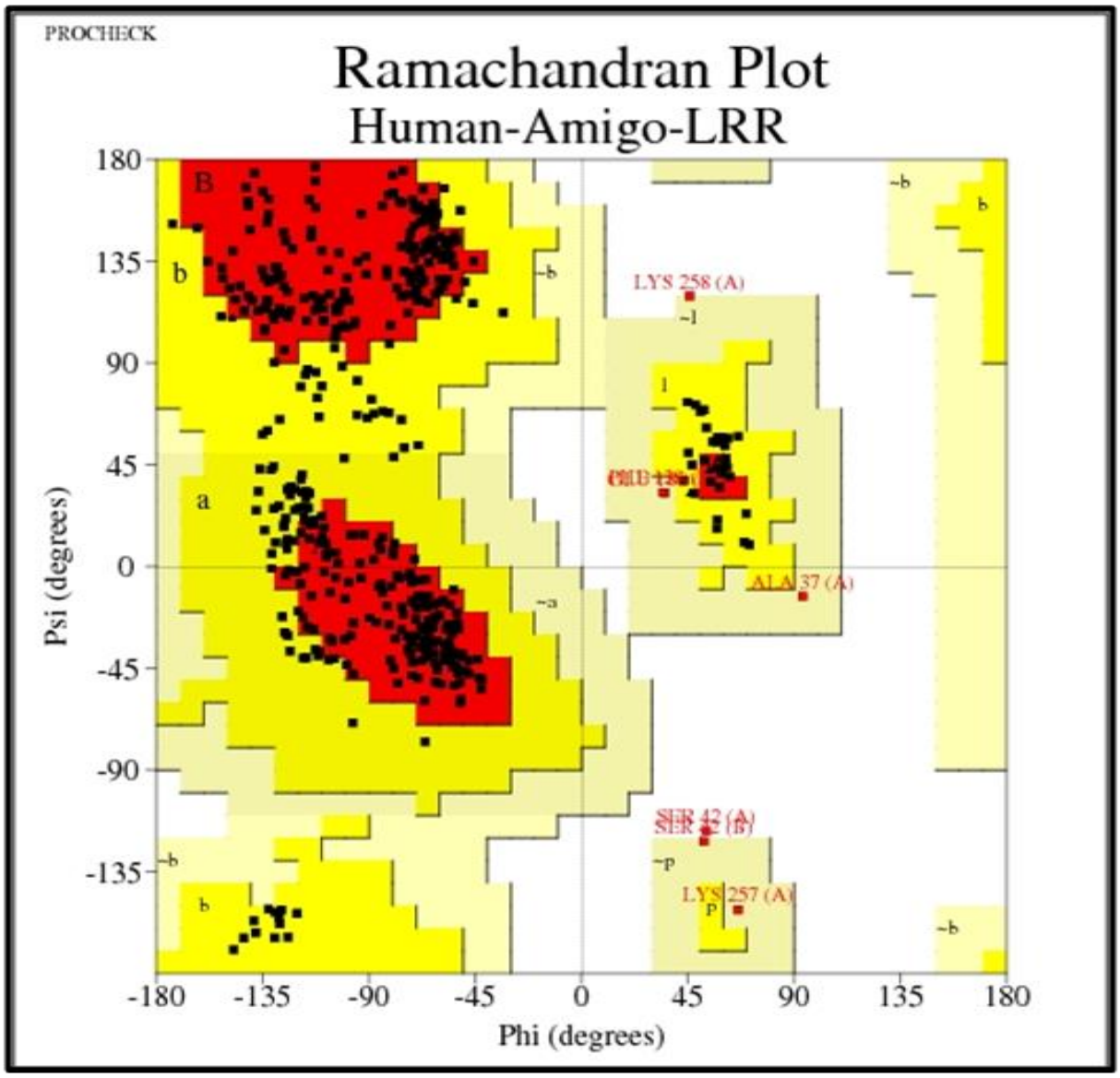

Figure 4.9 Ramachandran Plot for human AMIGO-1 ectodomain
The Ramachandran plot allows visualisation of the angles Phi and Psi of amino acids in a peptide. The top left quadrant is the region where β sheets lie, the bottom left quadrant is where right handed α- helices lie and the top right quadrant is where left handed helices lie.

4.6 Discussion

This chapter will be discussed in greater detail in Chapter 5, where we will analyse the human AMIGO-1 structure in detail.

Chapter 5

Analysis of the hAMIGO-1 LRR domain structure

Analysis of the hAMIGO-1 LRR domain structure

5.1 Overall structure of the hAMIGO-1 LRR domain.

The crystal structure of the hAMIGO-1 LRR ectodomain (R29-C270) was solved at 2.4 Å resolution with R factors of R_{cryst}/R_{free} = 21.4/25.7%. The crystallographic asymmetrical unit contains two molecules in an anti-parallel dimeric arrangement (Figure 5.1). The two monomers display an extremely similar conformation with a root mean square deviation of 0.35Å for 241 Cα atoms. Therefore, unless otherwise stated, molecule A was subjected to structural analysis. Strikingly, no electron density was observed for the Ig domain (G271-T362) of each monomer despite the fact that the hAMIGO-1 *Drosophila* construct incorporated residues G29-H359. Consistent with the structures of mAMIGO-1[120], hLINGO-1 [69] and hNgR [32, 46], hAMIGO-1 adopts a typical curved LRR domain fold with the LRR module flanked by cysteine rich capping domains (Figure 5.2a, Table 5.1). The N-terminal capping subdomain (LRRNT, residues G29-L59) is characterised by two β-strands that run anti-parallel to each other and is stabilised by two disulphide bridges mediated between residues C34 and C40 and C38 and C47.

The LRRNT domain is followed by six LRRs (Figure 5.2). Each repeat consists of an 11 residue fragment with the consensus sequence LxxLxLxxNxL, followed by a variable stretch of 10-12 residues (Figure 5.2b). The concave side of this LRR domain encompasses one β-strand per repeat which run parallel to each other forming a banana shape, consistent with previously determined structures of LRR domain- containing proteins with similar length repeats [94]. The location of the β strands on the concave face is a defining feature of LRR domains. Typically these strands are interwoven with various forms of helices, β turns and even short

β strands, which are predominantly found at the convex face of the protein [154]. In hAMIGO-1 each LRR contains the 21-23 residue conserved repeat motif; xLxxLxLxxNxLxxLxxxxFxxLx (Figure 5.2b), where L can be substituted with V, I, F, M and T, and F (Phenylalanine) can be interchanged with L, V and T. The length of LRRs determines the type of secondary structural motif adopted at the convex face. Indeed, longer repeats (27-29 residues) tend to contain an α helix on the convex side whereas shorter repeats are more likely to possess a main chain arrangement with interwoven polyproline II helices [154]. Consistent with these characteristics, the hAMIGO-1 convex surface is composed mainly of variable loops with three short helices. During the course of this study, a crystal structure of mouse AMIGO-1 (referred to as mAMIGO-1 from now on) was published. During this chapter, I shall analyse the structure of hAMIGO-1 alongside mAMIGO-1 and, later, alongside other structural homologues.

Similar to mAMIGO-1, the C-terminal capping subdomain (LRRCT) of hAMIGO-1 (residues G215-C270) adopts an irregular fold containing a 12-residue alpha-helix and several short 310 helical segments [120, 155]. The LRRCT is stabilised by two disulphide bridges, the first of which is located immediately after the LRR domain (mediated by C225 and C253) and the second at the C-terminal end of the LRRCT (formed by residues C227 and C270). These capping domains have important functional roles which include shielding the hydrophobic LRR core from solvent [156] and providing protection against *in vitro* proteolysis [157].

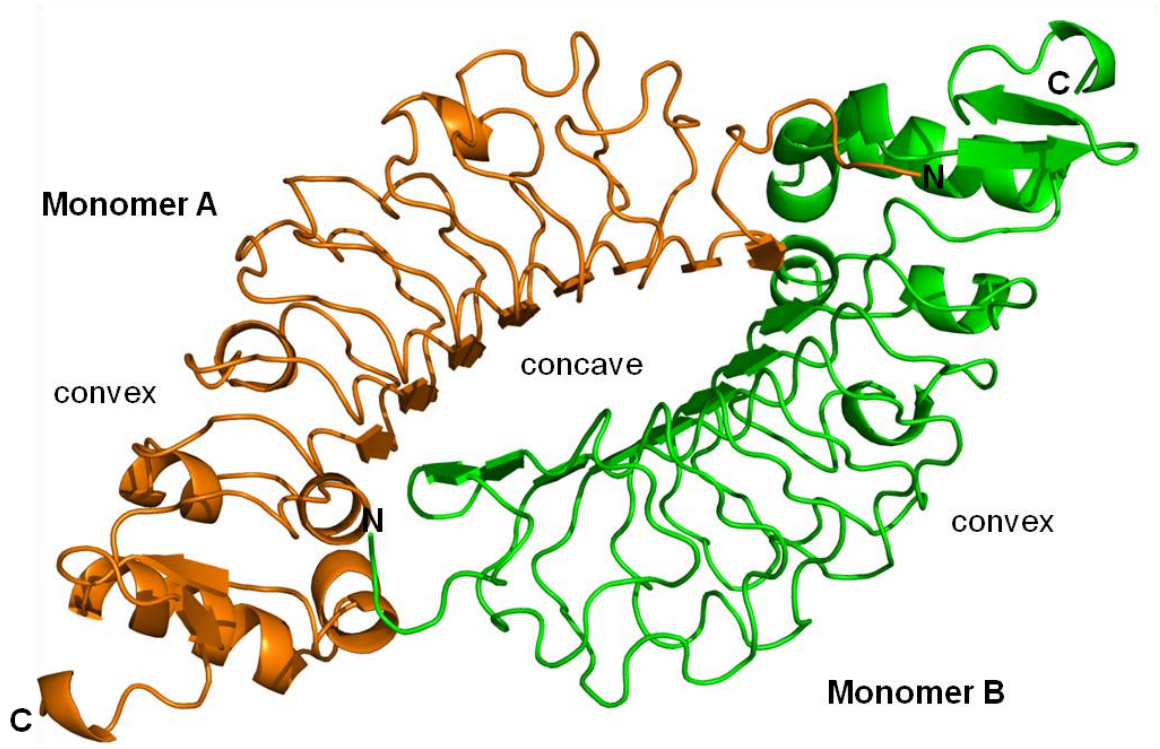

Figure 5.1 Overall structure of the hAMIGO-1 LRR dimer.
The hAMIGO-1 crystal possesses two molecules in the asymmetric unit (highlighted in orange and green). Each monomer adopts a banana shaped fold, with a parallel β-sheet contributing to the inner concave face and various secondary structural elements forming the outer convex face. The N- and C-terminus for each monomer are highlighted.

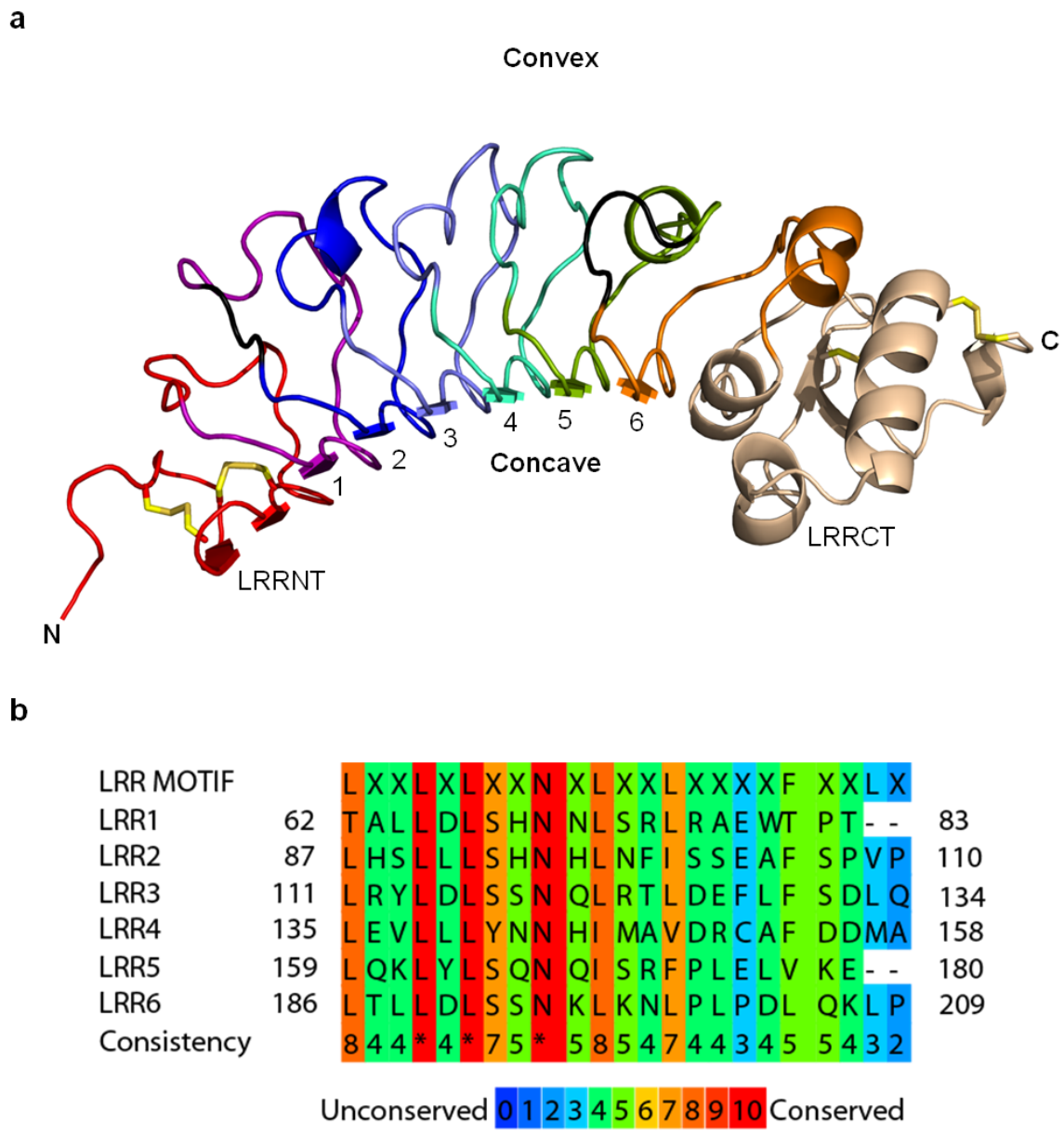

Figure 5.2 Structural characteristics of the hAMIGO-1 LRR domain.
a) LRR domain structure showing LRRNT (red) LRR1 (pink), LRR2 (blue), LRR3 (grey), LRR4 (cyan), LRR5 (green) LRR6 (orange) and LRRCT (beige). Disulphide bridges that stabilise the LRRNT and LRRCT are highlighted (yellow). b) Sequence alignment of the six leucine rich repeats of hAMIGO-1 calculated by PRALINE. The consensus motif for LRR's is also highlighted. The hAMIGO-1 sequence was obtained from Uniprot (accession number Q86WK6). The colour scheme of the alignment is for amino acid conservation.

5.2 Identification of hAMIGO-1 LRR structural homologues

Proteins with similar structural homology to hAMIGO-1 were identified using DALI software [158]. With the exception of mAMIGO-1, the most structurally homologous proteins to hAMIGO-1 included Variable Lymphocyte Receptor A [159], Leucine-rich repeat-containing G-protein coupled receptor 4 (LGR4) [160], Biglycan [161], Toll Like Receptor 4 (TLR4) [162], glycoprotein 1bα [163] and Decorin [94] (Figure 5.3). The Z scores for these proteins, which correspond to degree of structural identity, ranged between 21.7 and 25.5 (35.1 for mAMIGO-1). Despite all homologues encompassing an LRR module, there was a striking variability in the number of LRRs found within these domains which ranged between 6 and 22 (Figure 5.3). Consequently, this impacts on the overall shape of the LRR domain with proteins encompassing a large number of repeats adopting a horseshoe arrangement, whereas those with fewer repeats form a banana-like fold. Also, these proteins exhibit contrasting functions relative to neuronally-associated hAMIGO-1. For example, LGR4 has been shown to be crucial in mediating signalling during both embryonic development and in the adult organism. Additionally, it regulates adult stem cell maintenance by associating with proteins involved in Wnt signalling [160]. In contrast, biglycan is found in cartilage and plays a key role in osteogenesis [161]. Decorin is found in most connective tissues where it regulates the formation and organization of collagen fibrils. A second role attributed to decorin is that it inhibits calcification of soft connective tissues, thereby preventing calcinosis [161]. Finally, TLR4 is an important immune receptor that binds to lipopolysaccharide, which activates the innate immune response to microbial infection [162]. Interestingly, neuronally expressed proteins that also encompass the LRR fold, namely LINGO-1 and NgR, were found further down the DALI-derived list of structurally homologous proteins to hAMIGO-1 with Z scores of 21.3 and 21.2, respectively.

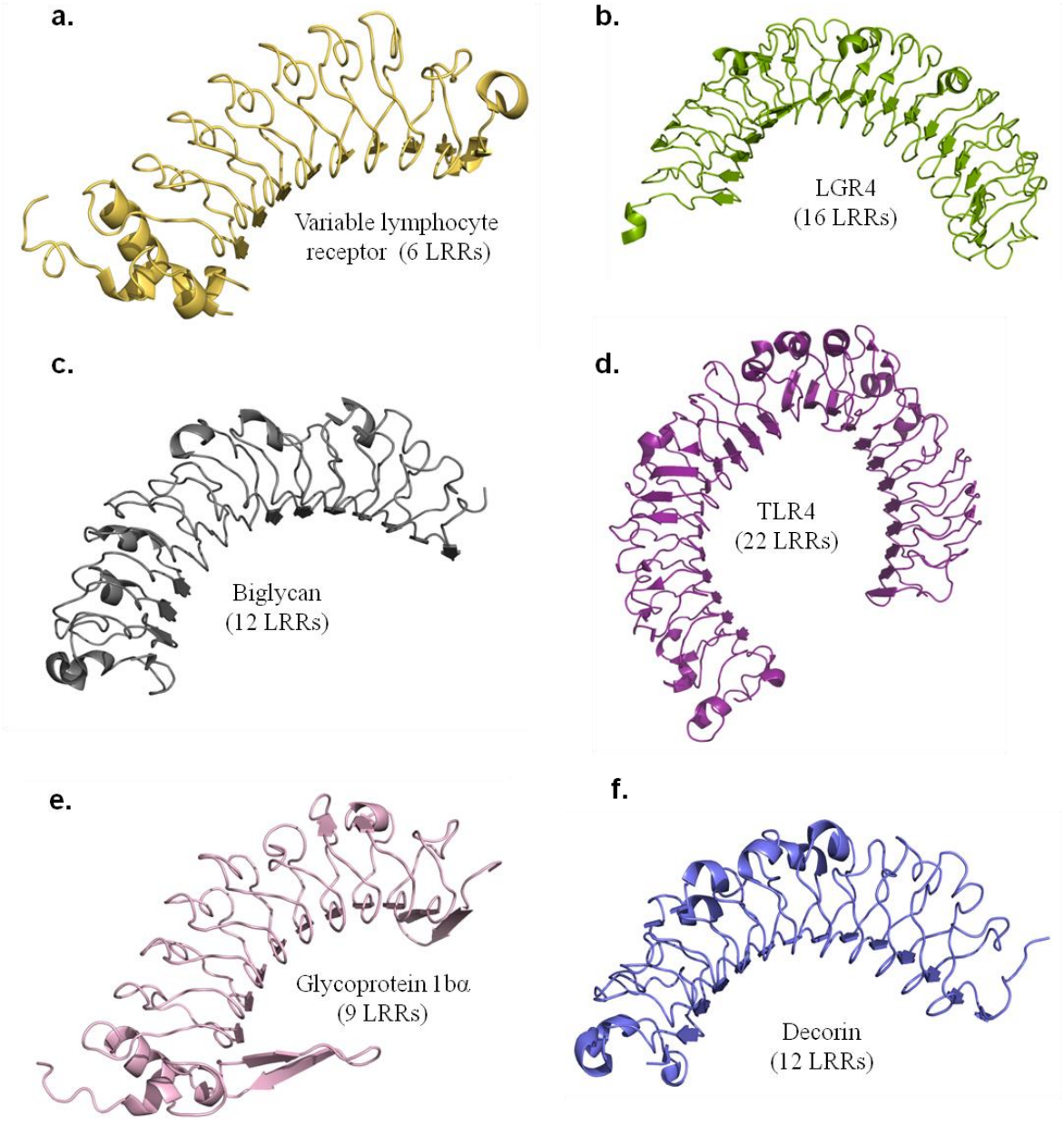

Figure 5.3 Structurally homologous proteins to hAMIGO-1.

The six most homologous proteins to hAMIGO-1 identified with DALI are highlighted a) Sea lamprey variable lymphocyte receptor (pdb code 3M19), b) Western clawed frog LGR4 (pdb code 4LI1), c) bovine biglycan (pdb code 2FT3), d) Mouse TLR4 (pdb code 3VQ2), e) Human glycoprotein 1b*α* (pde code 1U0N) and f) Bovine decorin (pdb code 1XCD). All adopt a banana-shaped fold except for TLR4 which exhibits a horse shoe arrangement. The number of LRRs found in each homologue is indicated.

5.3 Comparison of the overall structures of mouse and human AMIGO-1 LRR

Structural comparisons between mouse and human AMIGO-1 have revealed striking similarities for the LRR domain (Figure 4.4). This is not entirely unexpected given the high levels of sequence identity (89%) that exists between the homologues. Comparison of hAMIGO-1 LRR monomers A and B with the equivalent domains of mAMIGO-1 provided an r.m.s.d of 0.88 Å (for human A versus mouse A; 237 C atoms), 1.05 Å (for human A versus mouse B; 240 C atoms), 0.96 Å (for human B versus mouse A; 237 C atoms) and 1.11 Å (for human B versus mouse B; 240 C atoms). The most significant difference occurs between residues 180-182, where the Ca positions deviate by as much as 2.4 A°. This corresponds to the LRR5 loop found on the convex side which adopts a distinct conformation in mAMIGO-1 monomer B and is absent in monomer A, suggesting extreme flexibility in this segment of the molecule (Figure 5.4). The equivalent region of hAMIGO-1 participates in crystal contacts which may account for the contrasting conformations. In addition, further conformational differences between mouse and human AMIGO-1 are observed at the extreme C-terminal end of the LRRCT in the vicinity of the LRR-Ig linker region (Figure 5.4).

The hAMIGO-1 LRR structure was subjected to temperature factor analysis to further investigate the conformational flexibility of this molecule. Temperature factors (also referred to as B-factors) are a measure of thermal vibration and provide useful information with respect to the degree of flexibility exhibited by different regions of a protein. For example, regions with higher B- factors reflect considerable flexibility or poor fitting of the model into the electron density, whereas areas exhibiting lower B-factors are less mobile and increasingly ordered. It was possible to rule out poor fitting as well-defined electron density was observed for the LRR domains of each molecule. Consistent with the mAMIGO-1 structure [120],

temperature factor analysis for hAMIGO-1 revealed lower B-factors (<15 Å^2) for regions that contribute to stabilising the core dimer interface, particularly the β-sheet on the concave face (Figure 5.5). In contrast, higher B-factors (> 30Å^2) were observed predominantly in the cysteine rich capping domains and in several loop segments found on the outer convex face, particularly in LRR5. Hence, extended conformational flexibility exists in specific parts of the outer convex face and also with the C-terminal LRR-Ig domain linker region. Consistent with this, the lack of the Ig domain within the hAMIGO-1 crystal lattice is presumably due to the LRR-Ig linker region exhibiting higher conformational flexibility which renders it increasingly susceptible to proteolytic cleavage during crystallisation trials [32]. Strikingly, although there was no data published on the B factors in the linker region for mAMIGO-1, the temperature factor analysis of the Ig domain of mAMIGO-1 highlighted higher B-factors associated relative to the LRR module [120],

Finally, comparison of the human and mouse AMIGO-1 LRR at the primary sequence level revealed 27 amino acid differences of which 9 are non-conservatively substituted and 18 are conservatively substituted (i.e. the hydrophobicity of the amino acids and molecular bulk of the side chain are similar). The majority of these differences when mapped onto hAMIGO-1 are located on the convex face of the LRR domain (Figure 5.6), further demonstrating that the concave faces are highly conserved and are likely to play a key functional role.

Figure 5.4 Comparison of the human and mouse AMIGO-1 LRR homodimer.
The mAMIGO-1 LRR structure (teal, PDB code 2XOT) was superimposed onto hAMIGO-1 LRR (orange) using Pymol. Regions that significantly differ are highlighted (red dotted circles).
Loop located at the convex face of LRR5.

a.

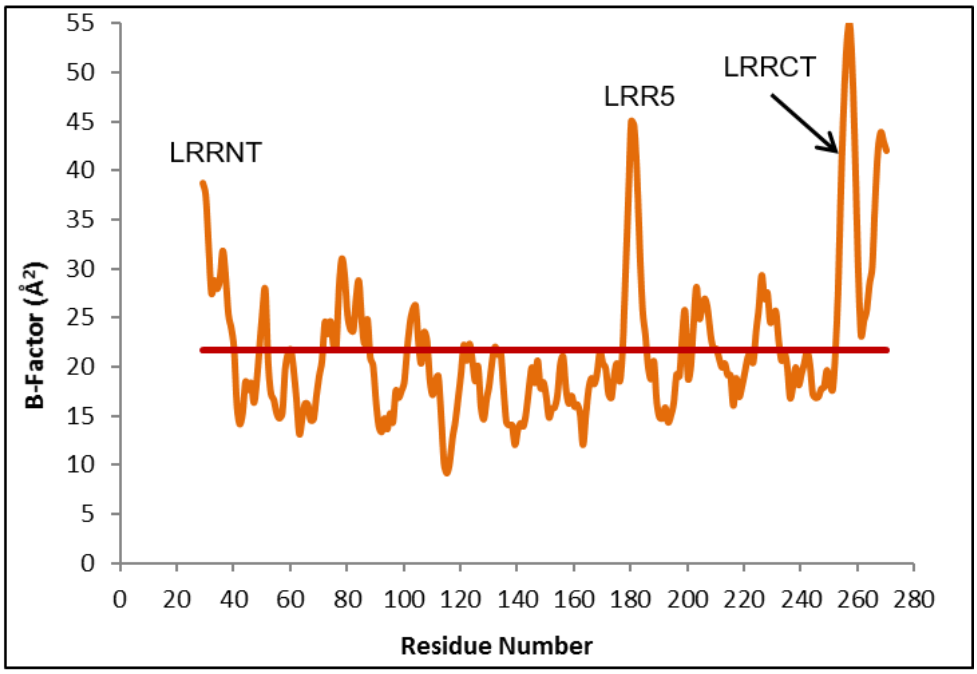

b.

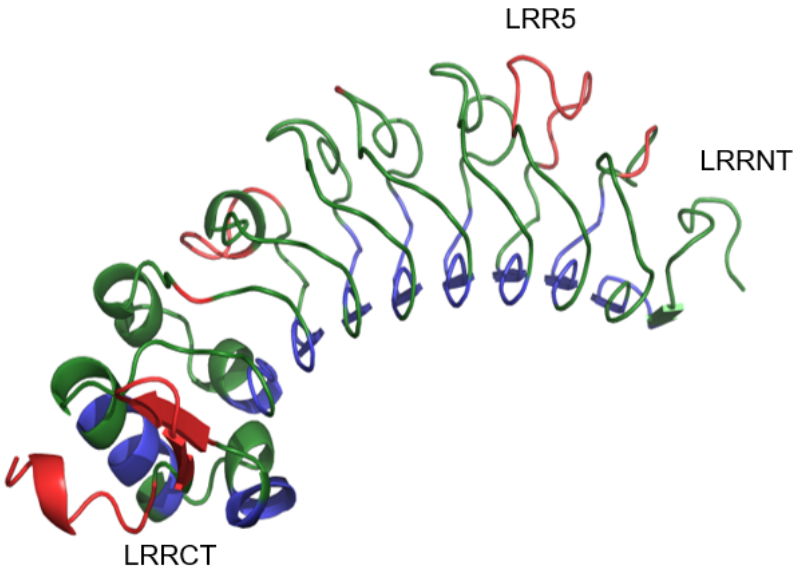

Figure 5.5 Temperature factors analysis of the hAMIGO-1 LRR domain.

a**)** Temperature factors were plotted against hAMIGO-1 residue number. There are several regions with above average B-factors which include the N- and C- terminus capping domains and several loops found on the outer convex surface. The red line indicates the average B factor. b) Residues with high B-factors (highlighted in red) are mainly located on the outer convex face of each monomer and at the extreme C terminal end. Residues with low B-factors (highlighted in blue) are found on the inner concave face of the monomer.

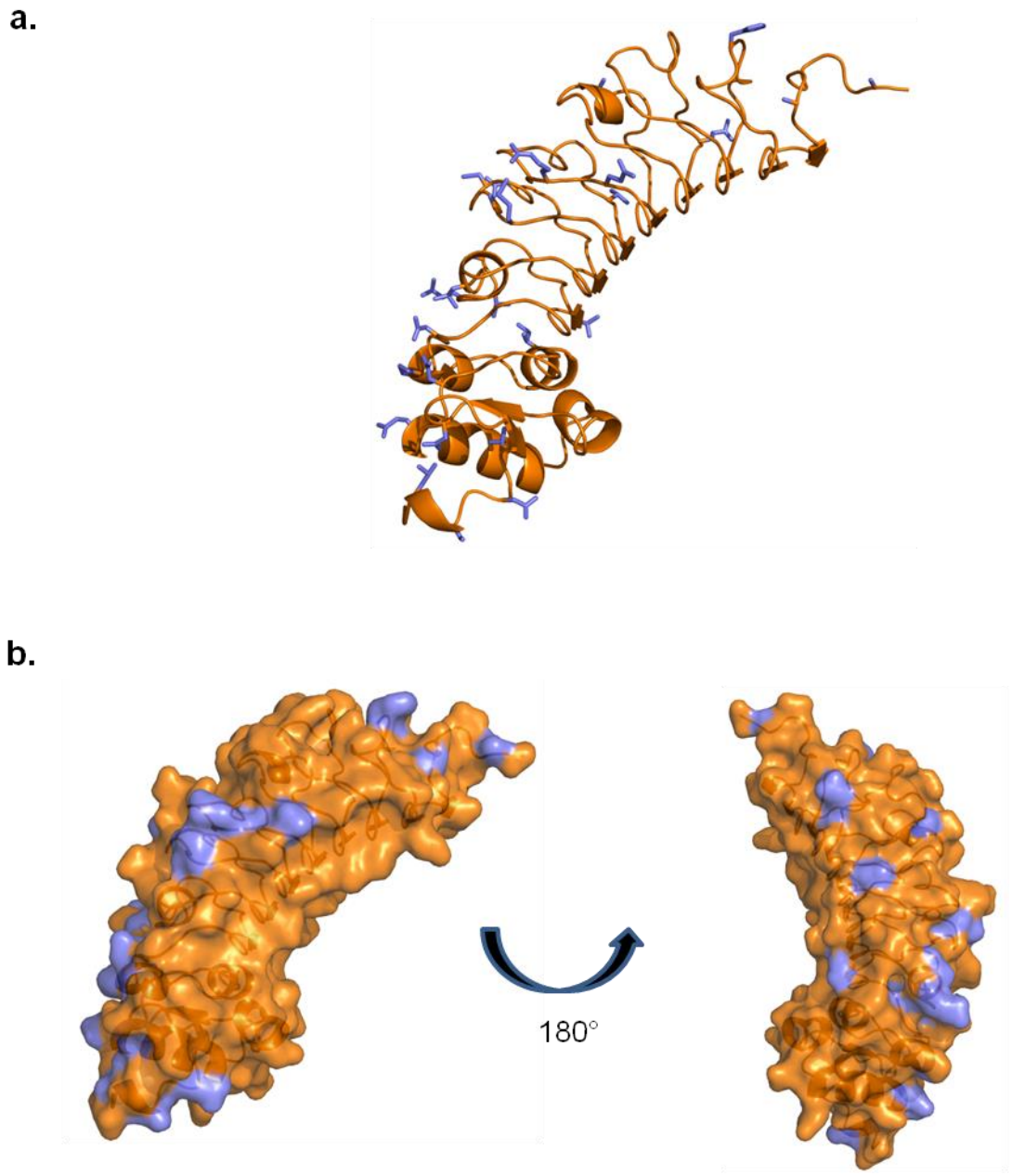

Figure 5.6 Mapping of mAMIGO-1 LRR residues that differ from hAMIGO-1.
a) Structure of hAMIGO-1 with residues that differ from mouse highlighted (blue stick format). b) Molecular surface representation of hAMIGO-1 (orange) with regions that differ from mAMIGO-1 highlighted (blue). The concave face is more conserved relative to the convex face.

5.4 Molecular interactions at the hAMIGO-1 LRR dimer interface

The hAMIGO-1 structure exists as a dimer within the crystal lattice (Figure 5.7a), consistent with size exclusion data described in Chapter 3. The hAMIGO-1 dimer interface is centred on the concave face of each LRR module and buries a total of 2964 $Å^2$ solvent accessible surface area. The buried surface area in the mAMIGO-1 dimer is 1350$Å^2$ [120]. Interestingly a number of other LRR domain containing proteins have also been crystallised as dimers, including decorin and the fourth Slit2 domain (D4) whose buried surface areas are ~2300 $Å^2$ and 2480$Å^2$ respectively [94, 155]. Both decorin and Slit2 D4 dimerize *via* their concave face, but in distinct modes. The decorin dimer is predominantly mediated by contacts involving the N-terminal capping domain, LRR1 and the central LRRs (Figure 5.7b). In contrast, similar to hAMIGO-1, the entire ectodomain of Slit 2 D4, including the C-terminal cap, contributes to stabilizing the dimer interface (Figure 5.7c). Interestingly, the ectodomain of LINGO-1 crystallises as a tetramer which buries a very extensive surface area that corresponds to 9200$Å^2$ (Figure 5.7d) [69]. It has been proposed that large contact surfaces are associated with high binding affinities between individual monomers [94].

The overall mode of dimerization adopted by hAMIGO-1 is very analogous to that of its mouse counterpart. Indeed, with the exception of S30A substitution, the majority of residues that contribute to stabilising the hAMIGO-1 interface are conserved with mAMIGO-1 (Figure 5.8). The hAMIGO-1 dimer interface is stabilised by nine hydrogen bonding interactions located in three distinct clusters between the concave face of each monomer (Figure 5.9, Table 5.2). The first of these clusters is formed by LRRNT of monomer A and the LRR5, LRR6 and LRRCT regions of monomer B. More specifically, the main chain of V32 and S42 in monomer A mediate hydrogen bonding interactions with the carboxyl groups of D191 and D250 in

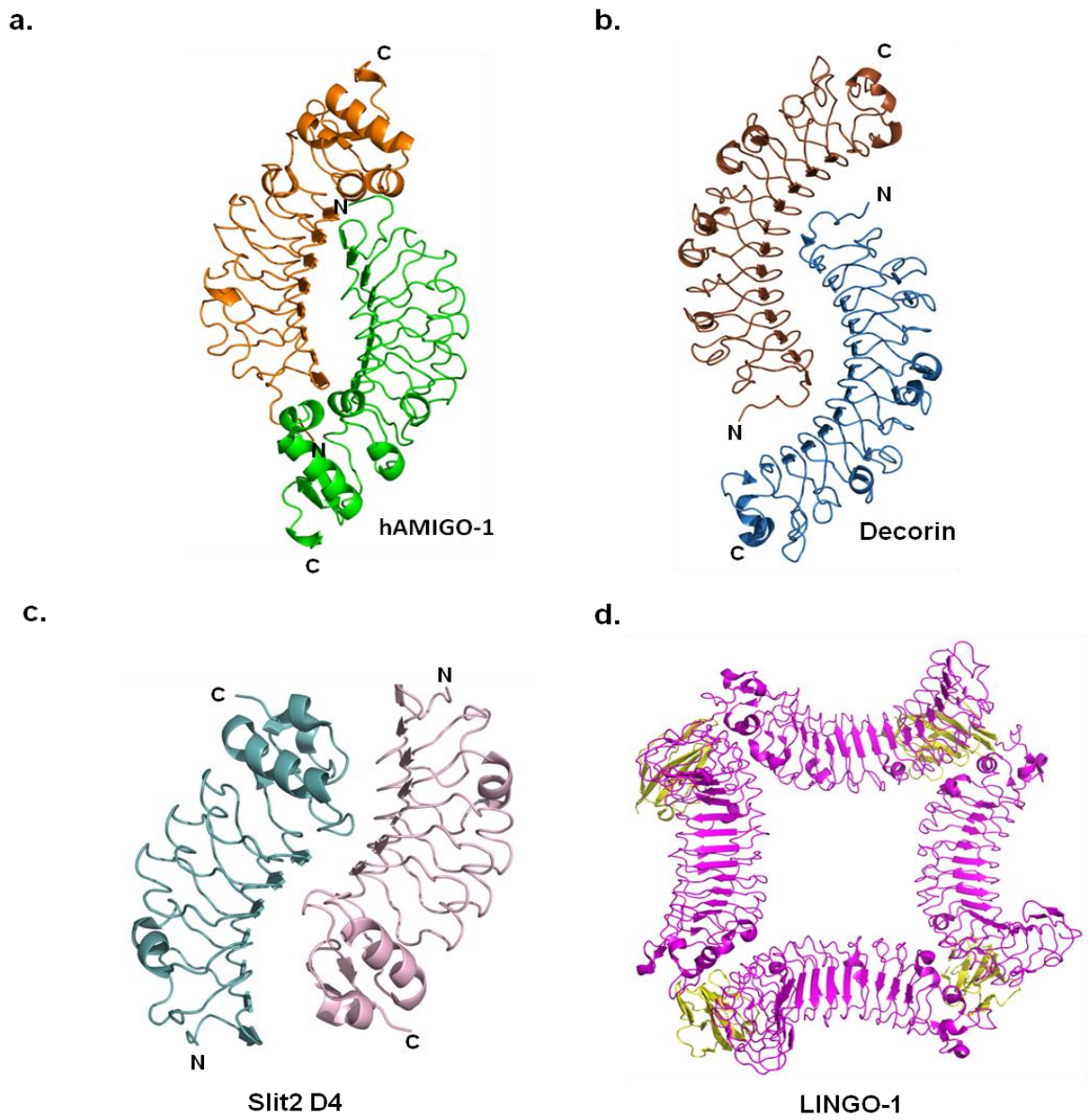

Figure 5.7 Homo oligomerisation of LRR containing proteins.

a) hAMIGO-1 forms a homodimer via association with the concave face. Each monomer is depicted in orange and green. b) Decorin forms a homodimer mediated by residues of its concave face (pdb code 1XCD). Each monomer is depicted in brown and sky blue. c) Slit-2 domain 4 (pdb code 2WFH) also forms a homodimer via its concave face. Each molecule is coloured in teal and light pink. d) Crystal lattice of the LINGO-1 ectodomain (pdb code 2ID5) is comprised of a tetramer formed by residues of the convex face. The LRR module is shown in magenta and the Ig domain in yellow.

monomer B. In addition, N43 of monomer A forms a hydrogen bond with Y164 (LRR5) of monomer B. The second cluster is focused on the centre of the dimer interface and is comprised of residues S48, K49 and H70 which are located in the LRRNT and LRR1 on monomer A and form polar interactions with residues H70 and S48 on monomer B (LRR1 and LRRCT). The third cluster is the reverse of the first cluster with residues at the C-terminal end of monomer A packing against residues at the N-terminal end of monomer B. Comparison with the mAMIGO-1 dimer interface reveals subtle differences in the number of polar contacts. For instance, mAMIGO-1 surface exposed residues R29, C40, Q167 and N220 mediate hydrogen bonding interactions that are absent in the human counterpart. Conversely, K49 and H70 in hAMIGO-1 form a polar interaction that is lacking in the corresponding region of mAMIGO-1.

In addition to the polar contacts, the hAMIGO-1 interface is further stabilised by a series of non-polar interactions chiefly mediated by core hydrophobic residues that include V31, I44, Y62, L140, Y142, Y217, H219 and F247 (Figure 5.10). These hydrophobes form comparable contacts within the mAMIGO-1 dimer interface. Despite these similarities, the mAMIGO-1 interface exhibits a greater number of non-polar interactions relative to hAMIGO-1 (271 versus 243 contacts) and is likely to be more stable in solution. Finally, 29 well-ordered water molecules mediate an extensive network of hydrogen bonds, which further stabilize the hAMIGO-1 LRR dimer interface.

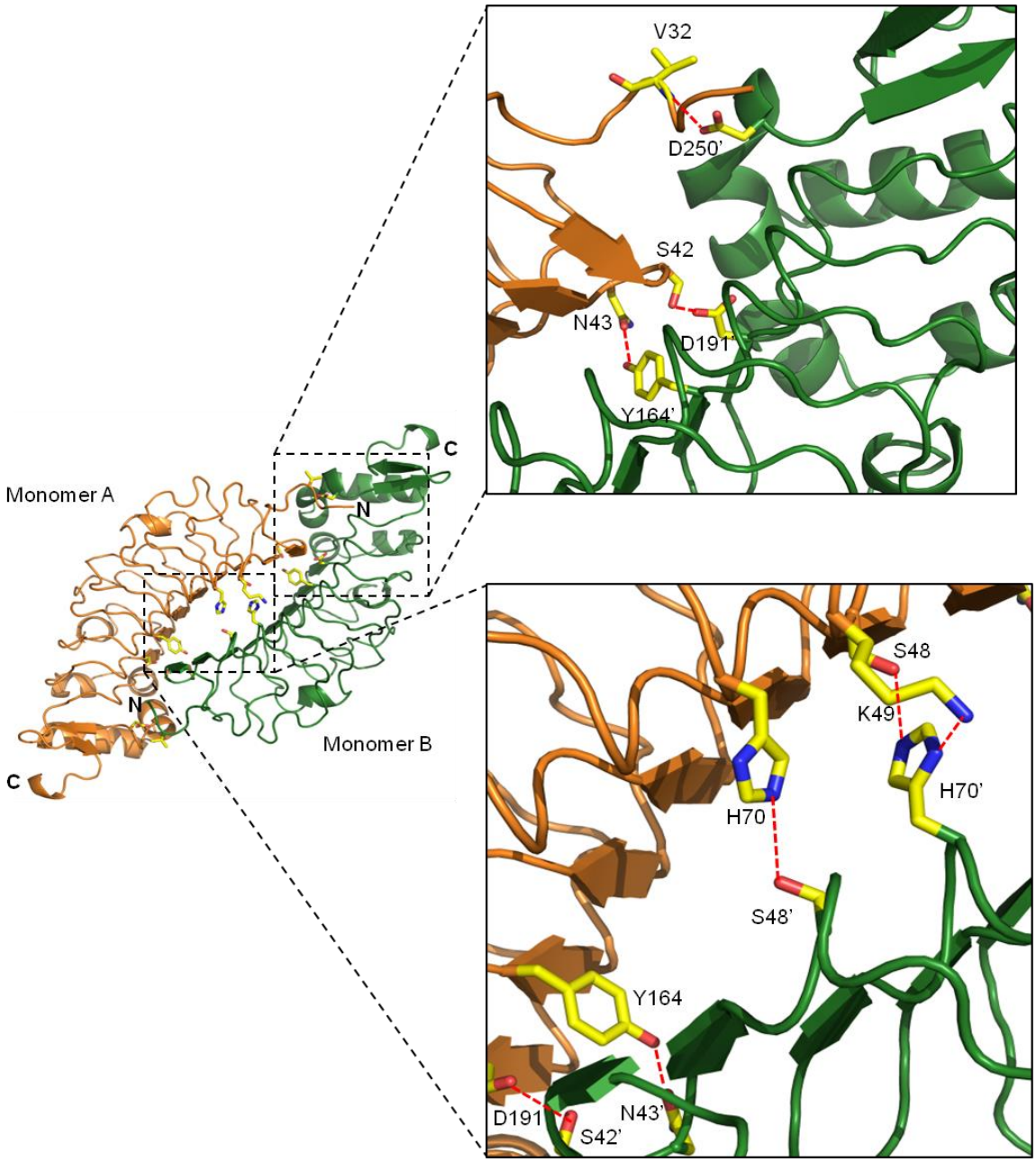

Figure 5.8 Polar interactions that stabilise the hAMIGO-1 LRR dimer interface.
There are nine hydrogen bonding interactions within the hAMIGO LRR dimer interface. Residues that contribute to hydrogen bonds are shown in stick format and labelled. The polar contacts at the interface are predominantly mediated by the upper region of LRR and the N- and C- terminal capping domains. Hydrogen bonds are highlighted as red dashed lines.

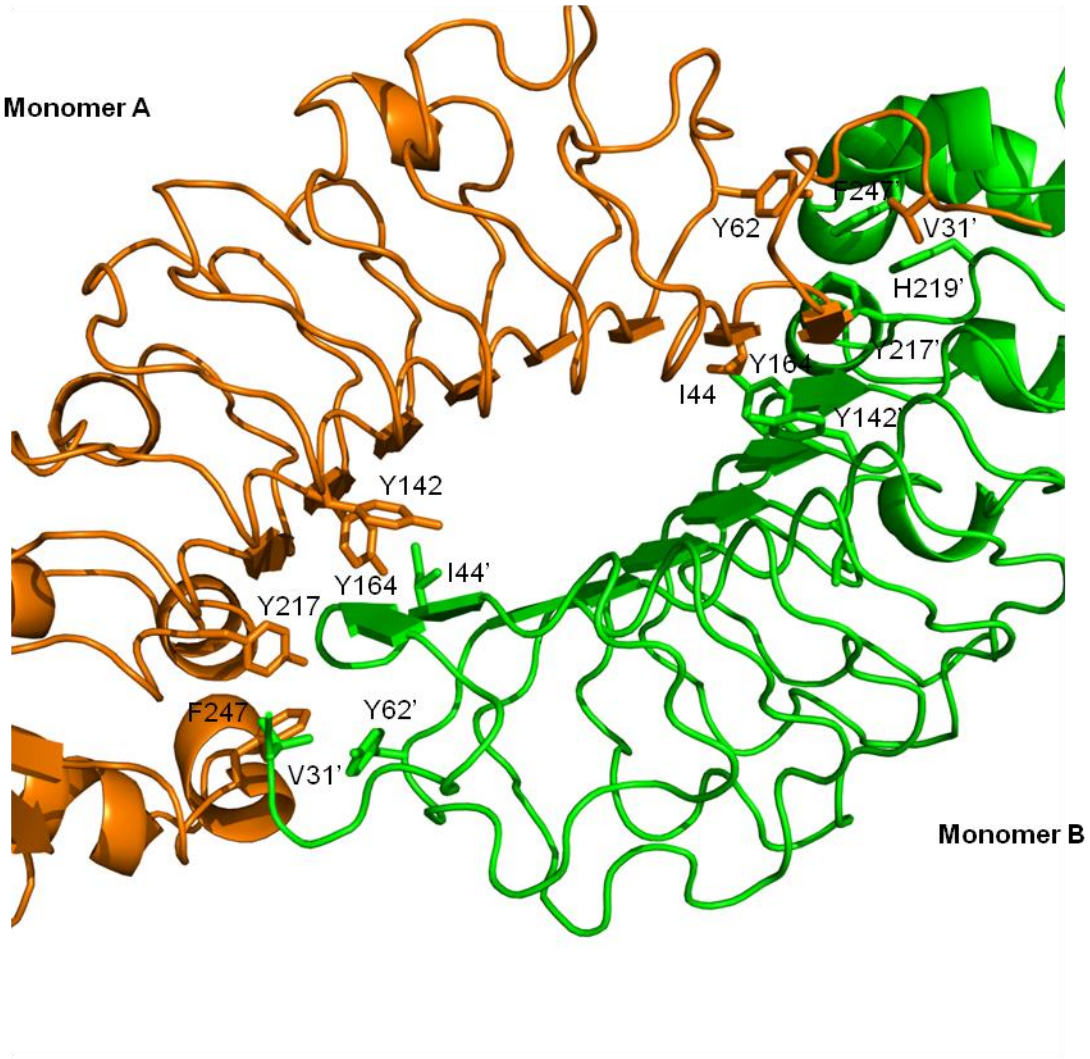

Figure 5.9 Hydrophobic interactions that stabilise the hAMIGO-1 LRR dimer interface. There are several core aromatic residues that mediate non-polar interactions within the hAMIGO LRR dimer interface. Residues that chiefly contribute to hydrophobic interactions are shown in stick format and labelled. The non-polar contacts at the interface are mainly formed by the upper region of the LRR and the N- and C- terminal capping domains**.**

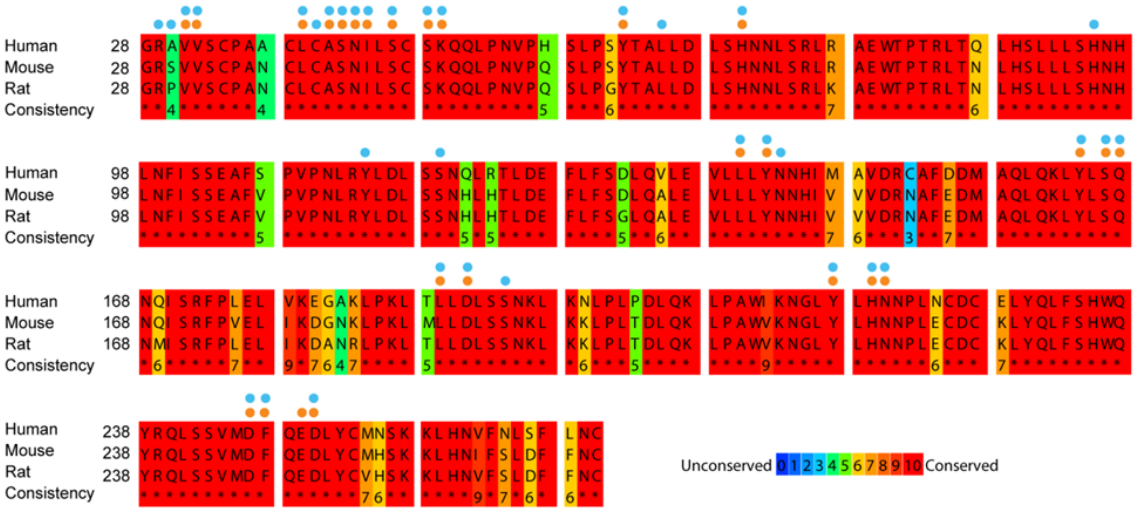

Figure 5.10 Sequence alignment of human, mouse and rat AMIGO-1 LRR domain. Sequences were obtained from Uniprot (accession numbers Q86WK6 (hAMIGO-1), Q802D8 (mAMIGO-1) and Q802D7 (rAMIGO-1) and aligned with Praline. The colour scheme of the alignment is for amino acid conservation. Residues that contribute to stabilising the AMIGO-1 dimer interface are shown (hAMIGO-1 (orange circles) and mAMIGO-1 (cyan circles).

5.5 Sequence comparison of the hAMIGO family

Similarity at the primary amino acid sequence level for the LRR domain between hAMIGO-1 to hAMIGO-2 is 52%, hAMIGO-1 to hAMIGO-3 is 50%, and hAMIGO-2 to hAMIGO-3 is 44% (Figure 5.11a). The most highly conserved residue positions map to the concave dimerization surface of the molecule, whereas the convex face is considerably less conserved (Figure 5.11b). Strikingly, the majority of residues that mediate non-polar contacts in the hAMIGO-1 dimer are invariant across the hAMIGO family. In contrast, out of the 9 residue positions that mediate hydrogen bonding interactions, seven are either identical (residues Y164 and D191) or demonstrate highly conservative (residues S42, N43, S48, H70 and D250), substitutions across homologues (Figure 5.11a). Only two positions (residues V32 and K49) demonstrate chemically distinct variations and these reside in the LRRNT. Notably, the residue at position 32 participates in dimer formation exclusively through main-chain atoms. Hence, variation at this position is unlikely to significantly compromise dimerization. In summary, the conservation of residues in the hAMIGO-1 interface along with the large accessible surface area buried on dimerization, strongly suggest that all AMIGO family members dimerize in an analogous fashion, via their LRR module.

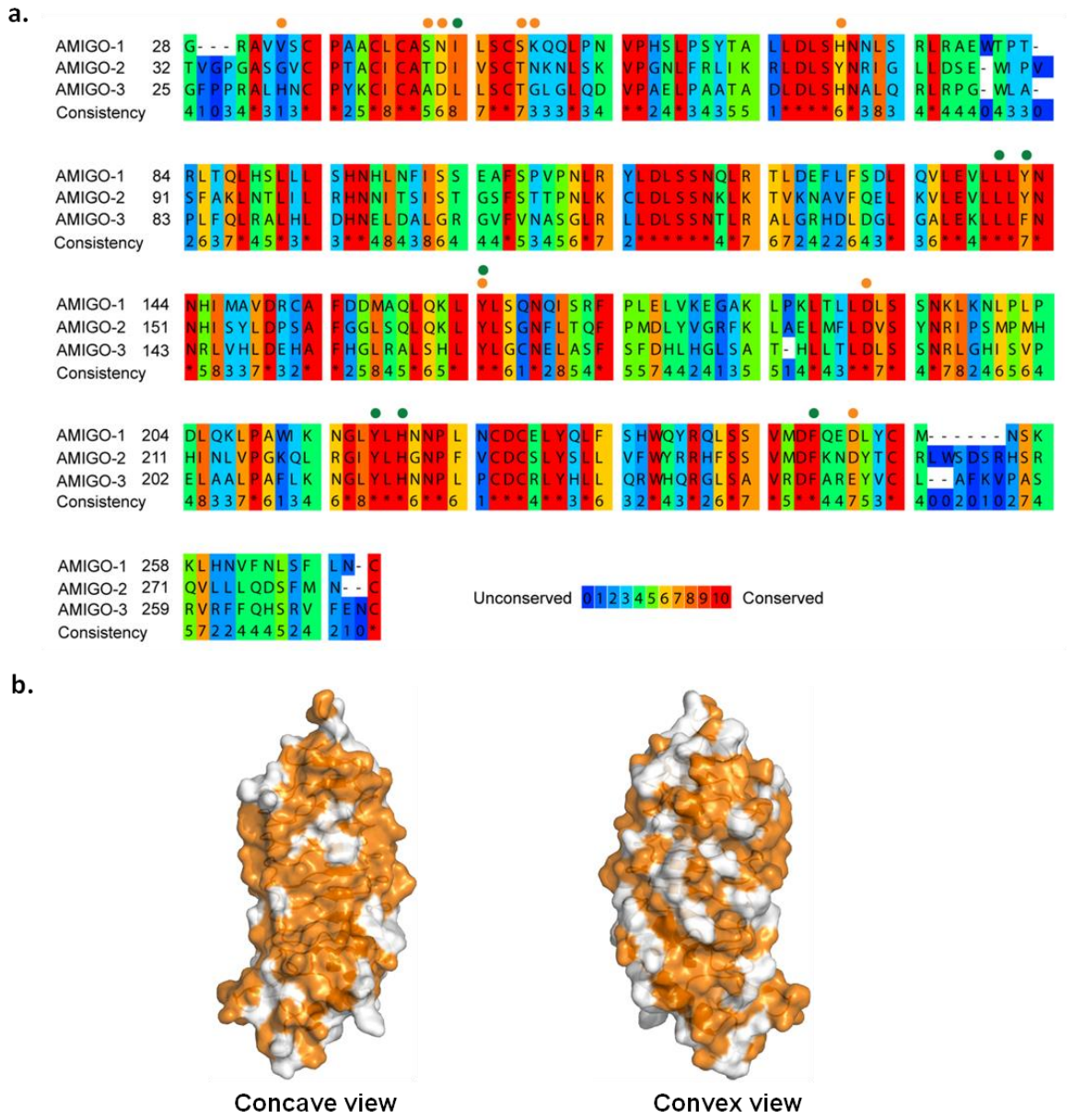

Figure 5.11 Sequence comparisons of the human AMIGO-1/-2/-3 LRR domain.
a) Sequences were obtained from Uniprot (accession numbers Q86WK6 (hAMIGO-1), Q865J2 (hAMIGO-2) and Q86WK7 (hAMIGO-3) and aligned with Praline. The colour scheme of the alignment is for amino acid conservation. Residues that contribute to stabilising the AMIGO-1 dimer interface are shown (polar contacts (orange circles) and core hydrophobic interactions (green circles)). b) Molecular surface representation of the hAMIGO-1 LRR (orange) with residue positions that are non-conservatively substituted across the hAMIGO family mapped (white).

5.6 Identification of putative ligand binding sites for the hAMIGO family

Information garnered from previously reported structures of LRR containing proteins in complex with their ligands has offered indications of putative hAMIGO ligand binding sites. Generally, the solvent exposed concave face of LRR proteins provides an ideal surface for ligand binding [95, 154]. Indeed, such an arrangement has been documented for ribonuclease inhibitor-angiogenin [164], glycoprotein 1bα-von Willebrand factor [165, 166], Slit2-D2-Robo [166] and netrin G2-NGL2 [167] protein-ligand complexes (Figure 5.12). Further evidence that the concave surface of LRR domain is involved in ligand binding is provided by LINGO-1, which forms a tripartite complex with NgR and p75 and is structurally analogous to AMIGO-1. Based on the LINGO-1 structure, the convex face is buried upon tetramer formation (Figure 5.13a), raising the question of whether the concave face may be used in binding to other ligands such as NgR and $p75^{NTR}$ (discussed in further detail in Chapter 6). Consistent with the importance of the convex face in oligomerisation, LINGO-1 in complex with Li81 (Figure 5.13b), an anti-LINGO-1 antibody used therapeutically in repairing damaged CNS neurons, revealed that it binds to the convex face of the LRR domain and prevents LINGO-1 tetramer formation [77]. Furthermore, binding of Li81 to LINGO-1 reduced the affinity of LINGO-1 for the non-competitive antibody, 1A7 [77].

To examine these issues further, the hAMIGO-1 structure was used as a template to generate molecular models of hAMIGO-2 and hAMIGO-3 LRR domains with I-TASSER [168]. These molecular models together with the crystal structure of hAMIGO-1 were subjected to electrostatic potential analysis to identify putative ligand binding sites for NgR and $p75^{NTR}$/TROY. The convex surface of hAMIGO-1 LRR domain exhibited no remarkable electrostatic properties. In contrast, the concave surface of hAMIGO-1 LRR module

demonstrated a striking electrostatic potential distribution, with the centre surface being highly negatively charged (Figure 5.14). Contributing to this negatively charged patch are residues D67, D116, D191, D246, E249 and D250. Next to this patch there is another remarkable electrostatic surface characterised by a single negative patch surrounded by three positively charged regions. Here, the contributing residues include E137, R113, K162 and K186. Notably, the equivalent region of hAMIGO-3 also demonstrated a similar striking electrostatic potential distribution despite the fact that it exhibits ~50% sequence identity to hAMIGO-1. The electrostatic surface profile for hAMIGO-2 slightly resembles that of hAMIGO-2 and 3 suggesting that it may exhibit a different function. Moreover, this prominent pattern was also a characteristic feature of the concave mAMIGO-1/2/3 molecular surfaces (Figure 5.15). In summary, the conservation of residues that contribute to this unique motif across the human and mouse AMIGO family suggest that it may represent a potential evolutionary conserved ligand binding site for NgR and $p75^{NTR}$/TROY.

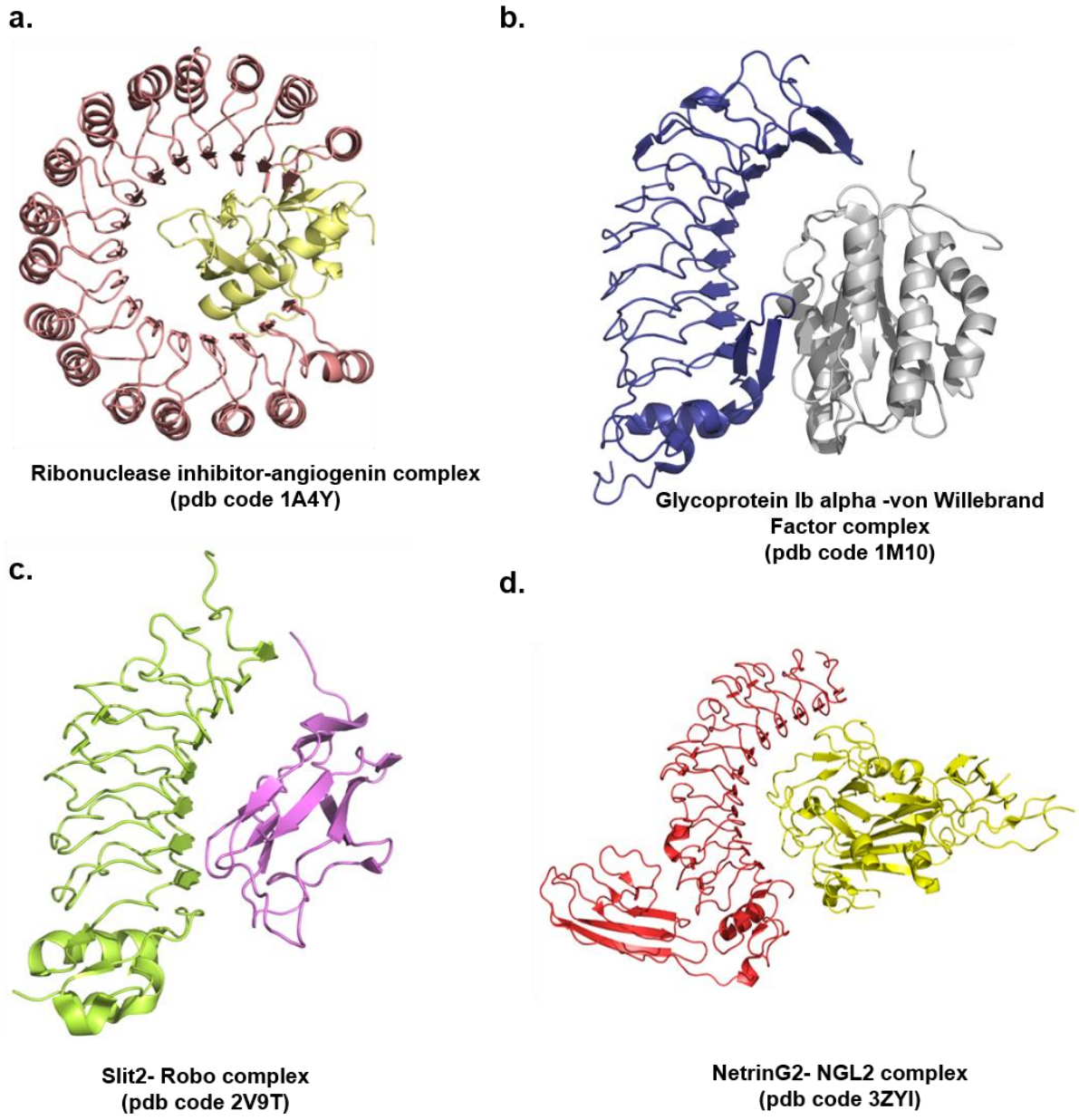

Figure 5.12 Structures of LRR containing protein/ligand complexes.
a) Structure of ribonuclease inhibitor (salmon) in complex with angiogenin (pale yellow). b) Structure of glycoprotein 1bα (deep blue) in complex with its ligand von Willebrand factor (grey). c) Structure of Slit S2 (limon) in complex with Robo (violet). For each complex the concave face of the LRR module mediates interactions with the ligand. D) Structure of netrinG2 (yellow) in complex with NGL2 (red).

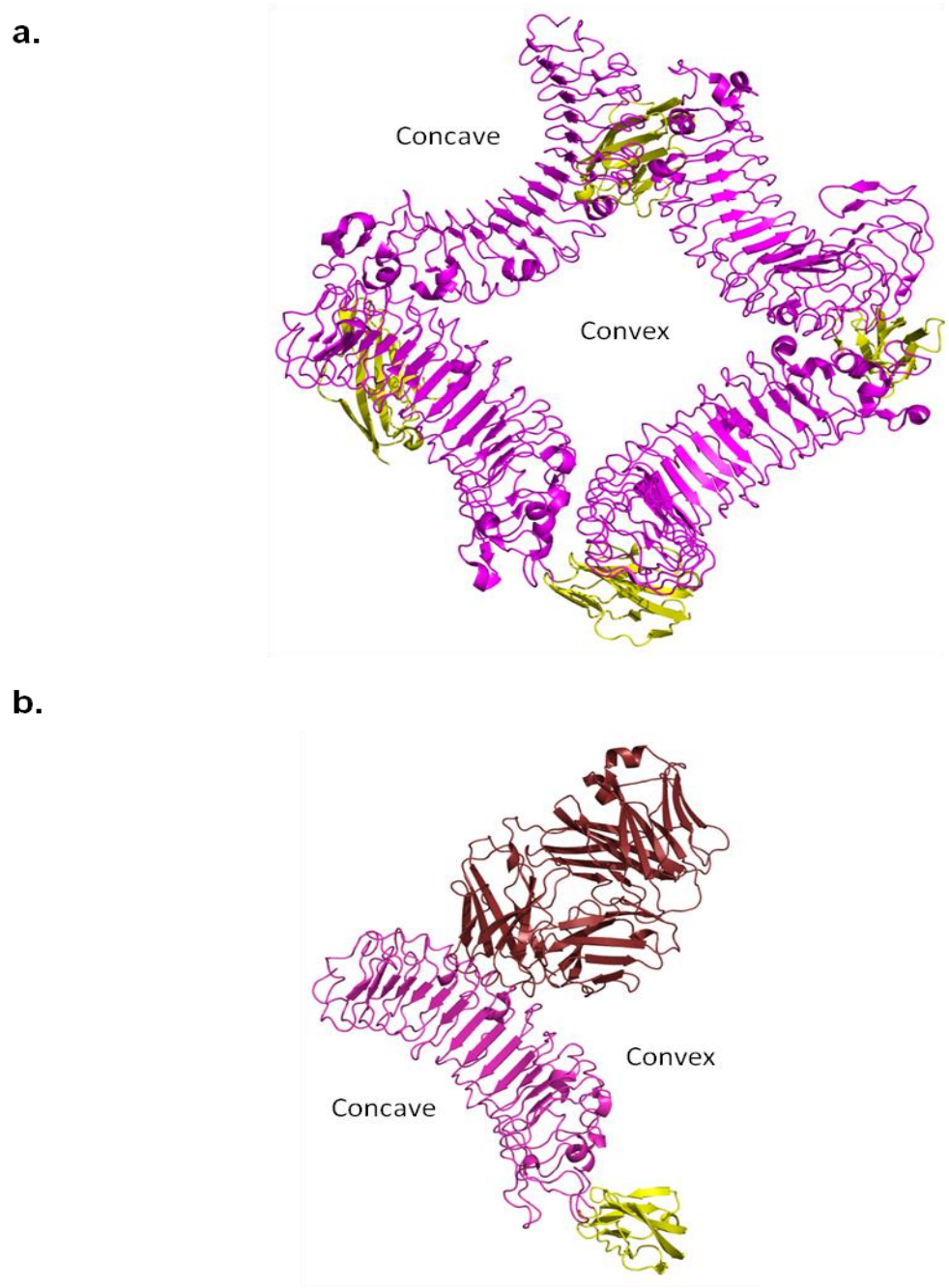

Figure 5.13 Human LINGO-1 ligand binding.

a) Structure of the hLINGO-1 ectodomain (pdb code 21D5). hLINGO-1 forms a tetramer through the convex faces of its LRR domains leaving the concave faces potentially available for ligand binding. b) Structure of the hLINGO-1 in complex with anti-hLINGO-1 antibody Li81 (pdb code 4OQT). The anti-hLINGO-1 antibody (brown) binds to the convex face of the hLINGO-1 LRR domain (magenta). The Ig domain of hLINGO-1 is depicted in yellow.

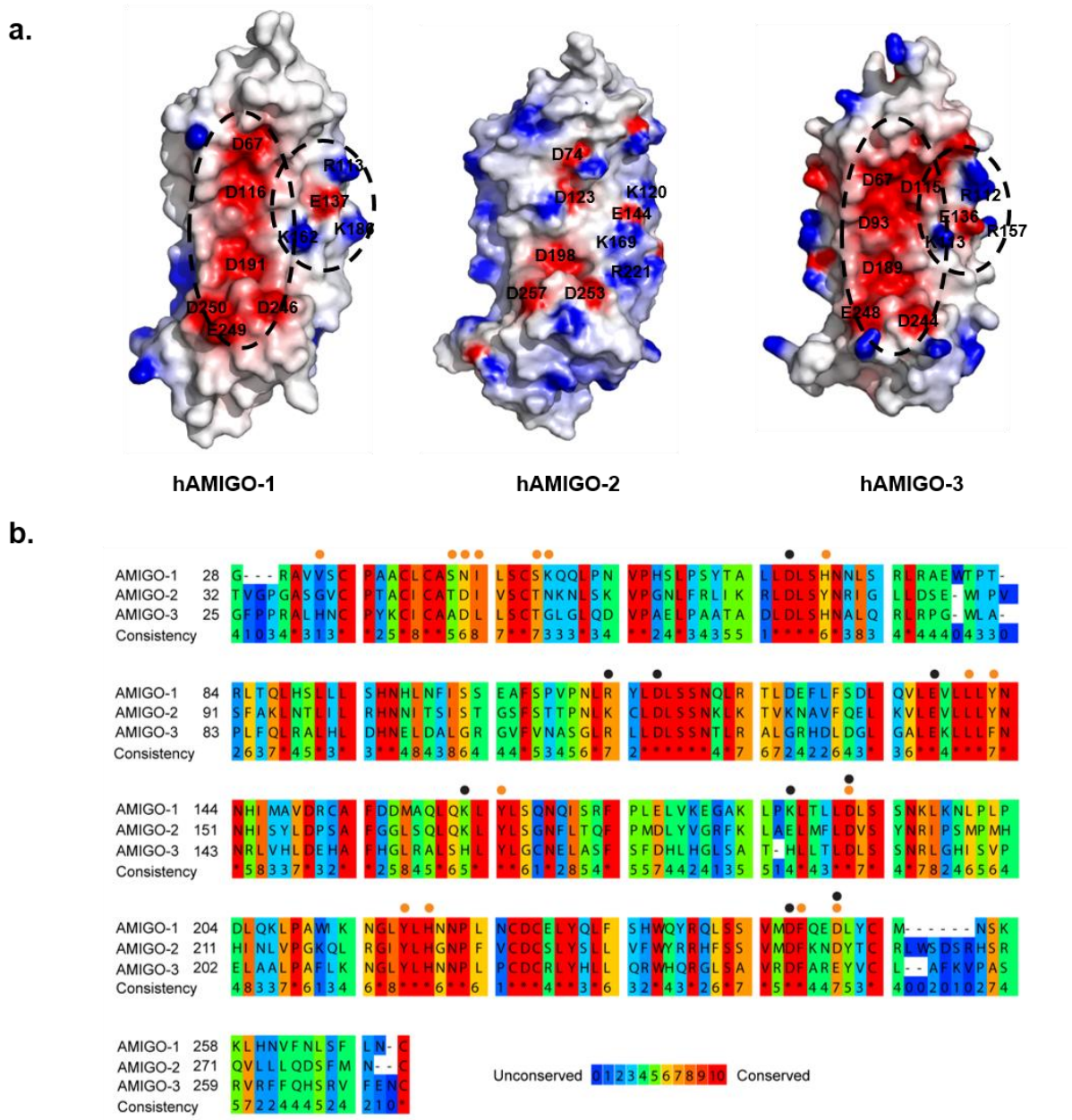

Figure 5.14 Identification of putative ligand binding sites for human AMIGO-1/-2/-3 LRR. a) Comparison of the molecular surface electrostatic potential for human AMIGO-1/-2/-3 LRR. The molecular models of hAMIGO-2 and hAMIGO-3 were generated with I-TASSER. The electrostatic potential was calculated using Delphi. There are two striking electrostatic patches (residues labelled, black dashed circles) observed on the concave face which may represent a putative ligand binding site. The potential scale ranges from -7 (red) to +7 (blue) in units of kT/e. b) Sequence alignment of the human AMIGO-1/-2/-3 LRR domain. Sequences were obtained from Uniprot (accession numbers Q86WK6 (hAMIGO-1), Q86SJ2 (hAMIGO-2) and Q86WK7 (hAMIGO-3) and aligned with Praline. The colour scheme of the alignment is for amino acid conservation. Residues that contribute to hAMIGO-1 homodimerisation (orange circles) differ from those that are form the potential ligand binding site (black circles).

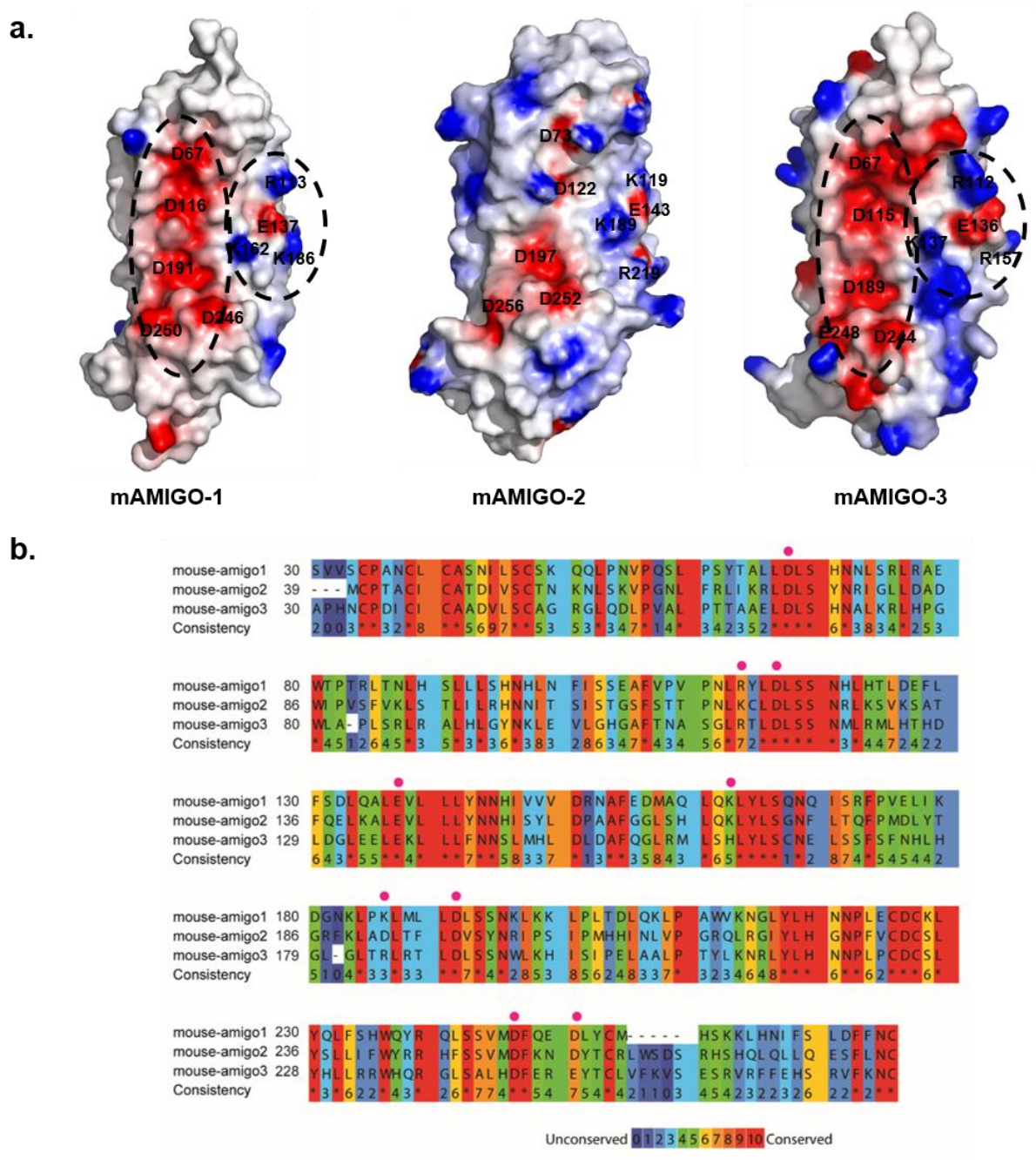

Figure 5.15 Identification of putative ligand binding sites for mouse AMIGO-1/-2/-3 LRR. a) Comparison of the molecular surface electrostatic potential for mouse AMIGO-1/-2/-3 LRR. The molecular models of mAMIGO-2 and mAMIGO-3 were generated with I-TASSER. The electrostatic potential was calculated using Delphi. There are two striking electrostatic patches (residues labelled, black dashed circles) observed on the concave face are conserved across the mouse and human AMIGO family and may represent a putative ligand binding site. The potential scale ranges from -7 (red) to +7 (blue) in units of kT/e. b) Sequence alignment of the mouse AMIGO-1/-2/-3 LRR domain. Sequences were obtained from Uniprot (accession numbers Q802D8 (mAMIGO-1), Q802D9 (mAMIGO-2) and Q8C2S7 (mAMIGO-3) and aligned with Praline. The colour scheme of the alignment is for amino acid conservation. Residues that contribute to the potential ligand binding site are highlighted (pink circles).

5.7 Discussion

In this chapter, the crystal structure of the hAMIGO-1 LRR domain was determined and analysed with the aim of gaining an in depth understanding of the molecular basis of hAMIGO function as part of the NgR-p75^{NTR} receptor complex, and how it compares to other related receptors including LINGO-1.

The structure of the hAMIGO-1 LRR-Ig ectodomain was determined to 2.4Å resolution but was found to lack the Ig domain. To explore this further, purified hAMIGO-1 LRR-Ig domain was incubated at a temperature mimicking the crystallisation trials (22 °C) for several weeks and subsequently analysed by SDS-PAGE. The resulting SDS-PAGE analysis highlighted a major band corresponding to the LRR domain (~30 kDA) but no band at the desired molecular weight for the fully intact ectodomain (40.8 kDa) suggesting that the protein was susceptible to significant proteolytic cleavage. Indeed, temperature factor analysis of the extreme C-terminal end of hAMIGO-1 LRR revealed high B-factors relative to the core LRR domain. It is possible that these high B-factors can be solely attributed to the lack of the LRR domain. However this can be ruled out as high B-factors were observed in the equivalent region of the mAMIGO-1 counterpart [120] which contains the entire LRR-Ig module. It is possible that the short LRR-Ig hinge region within human and mouse AMIGO-1 is uniquely flexible and in the absence of ligands adopts a conformation that is prone to cleavage.

Consistent with gel filtration data (see Chapter 4), structural studies of the hAMIGO-1 LRR domain have established that the protein exists as a dimer. This dimer assembly is facilitated by residues that protrude from the concave face of each LRR domain. This arrangement is consistent with previous structural studies for the closely related mAMIGO-1 [120] and other

LRR containing proteins including decorin [94], and biglycan [161]. In addition, the LINGO-1 crystalline state revealed a tetramer that was assembled via the convex face of each LRR module. This poses a key question as to whether the dimeric or tetrameric forms of these neuronal proteins represent a crystal packing artefact or exhibit a physiological role. There is considerable evidence that points to the latter. Firstly, the dimer interfaces identified in the crystal lattice of hAMIGO-1, mAMIGO-1 have robust interfaces with an extensive surface area. Secondly, mutagenesis studies have demonstrated that mAMIGO-1 dimerisation is necessary for stable folding and cell surface expression [120]. Thirdly, the oligomeric state of LINGO-1 in solution is highly dynamic as monomeric, dimeric and tetrameric states were readily detected using dynamic light scattering, size exclusion chromatography and SDS-PAGE [69]. Finally, there is a high degree of evolutionary conservation in residues that contribute to stabilising the dimer interface, across the AMIGO and LINGO family members, despite low sequence identity. Collectively, this suggests that oligomerisation of these neuronal associated proteins plays a precise biologically relevant function.

The crystal structure of hAMIGO-1 was also used to identify putative hAMIGO-1 ligand binding sites. This involved consideration of evolutionary conserved regions, electrostatic surface potentials, N-linked glycan exposure and extrapolating from knowledge of previously determined LRR-ligand complex structures. Generally, the concave surface of LRRs are predominantly involved in ligand binding [154] as observed for the ribonuclease inhibitor-angiogenin [164], glycoprotein 1bα- von Willebrand factor [169] and Slit2-D2-Robo [166] protein-ligand complexes. These studies have highlighted the critical role of both electrostatic attraction and non-polar interaction following protein-ligand complex engagement. Mapping the calculated electrostatic surface potentials on the molecular surface of hAMIGO-1 crystal

structure has provided potential indications as to the p75^{NTR} and/or NgR ligand binding site. This analysis revealed a striking electrostatic potential distribution which is dominated by a negative patch that runs along the concave face. More importantly, the equivalent regions of the Phyre derived hAMIGO-2 and hAMIGO-3 molecular models demonstrated a comparable electrostatic potential distribution in spite of exhibiting low sequence identity to hAMIGO-1. This remarkable electrostatic potential distribution also appeared to be conserved across the mouse AMIGO family. Collectively, this suggests that both the mouse and human AMIGO family all have the potential capability of binding NgR and/or p75^{NTR}. Indeed, a recent limited study using closely related rat AMIGO-3 constructs revealed interactions with NgR andp75^{NTR} in non-neuronal cells and in brain lysates, culminating in RhoA activation in response to stimulus with CNS myelin [107].

Interestingly, the amino acid side chains contributing to the proposed ligand binding site on the concave face differed from residues implicated in the dimerisation motif. Despite this there is a distinct possibility that the hAMIGO-1 dimerisation site could also correspond to or overlap with the putative ligand binding site. Therefore, an unresolved issue is whether dimerisation of hAMIGO-1 is important in the formation of the tripartite complex with NgR and p75^{NTR}. Molecular and biochemical studies of decorin, which adopts a similar mode of dimerisation to hAMIGO-1, provide further insights on this issue [94]. Since decorin forms a tight dimer *via* the concave face of its LRR domain, it was initially inferred that the outer convex face represented the likely collagen binding site [94]. However, there have been suggestions that decorin may transition from dimeric to monomeric in order to allow ligand binding at the concave face [94]. Indeed, decorin is easily denatured and is less stable than many other globular proteins. Heat denaturation of decorin is fully reversible, demonstrated

by a reduction in molecular weight by half during thermal denaturation, representing the transition from dimer to monomer, followed by the reverse during cooling [161]. This indicates that decorin may be able to transition from a dimer to monomer to enable ligand binding as suggested previously. Furthermore, more recent studies have established that mutations on the concave face of decorin abolished collagen binding irrespective of whether the mutants retained their ability to dimerise or not [131]. Here, the authors concluded that the concave face of decorin is involved in binding to collagen and the decorin dimer dissociates to mediate binding collagen *via* the concave face [131]. Unfortunately, due to time constraints it was not possible to analyse AMIGO-1 by heat denaturation but it may be possible that, similar to decorin, hAMIGO-1 can mediate ligand interactions *via* its inner concave surface.

Further evidence supporting the involvement of the concave faces of LRR domains in ligand binding is provided by the neuronal LRR-Ig domain containing protein, LINGO-1. LINGO-1 forms a tripartite complex with NgR and $p75^{NTR}$ and is structurally analogous to AMIGO-1 [96]. Based on the LINGO-1 structure, the authors reported that the concave face is likely to play a significant role in ligand binding since the convex face is buried upon tetramer formation. However, an unresolved question is whether the LINGO-1 tetramer represents a physiologically relevant form or a crystallisation artefact. More recent data favours the former, as tetramers have been observed both in solution and in cells expressing the full-length LINGO-1 indicating that the ability to form oligomers is an intrinsic property of LINGO-1 [77]. In addition, a recent structure of LINGO-1 in complex with Li81, an anti-LINGO-1 antibody used therapeutically to facilitate repair of damaged CNS neurons, revealed the antibody binds to the convex face of the LRR domain and prevents LINGO-1 tetramer formation [77]. The

tetramer arrangement of LINGO-1 leads to a large surface area being buried, it is suggested that it serves as an efficient and stable scaffold for assembly of the LINGO-1/NgR/p75^{NTR} complex [170]. Accordingly, knowledge of the LINGO-1 oligomeric status may shed light on unresolved questions about the stoichiometry of the LINGO-1/NgR/p75^{NTR} complex; it has been hypothesized that each signalling complex may be comprised of four of each receptor component (4:4:4) rather than one (1:1:1) [170]. The formation of a supramolecular assembly of this type would have significant implications for the binding properties (affinities/avidities) for the trimeric complex, likely resulting in signal amplification. This process could increase the sensitivity of this molecular "stop" signal dramatically, leading to rapid growth cone collapse in the presence of even limited amounts of myelin-derived inhibitors.

Another important factor to consider is whether the orientation of the Ig domain with respect to the LRR module could shield the putative ligand binding site on the concave face. Unfortunately, this was difficult to determine with the current hAMIGO-1 structure as the Ig domain has been cleaved during crystallisation trials. However, for the closely related fully intact mAMIGO-1 ectodomain, the Ig module is orientated in a manner that partially covers the convex face of the LRR domain, rendering this region unavailable for ligand binding. In addition, potential N-linked glycosylation sites map onto the convex surface of hAMIGO-1. Collectively, this further reduces the likelihood that the hAMIGO-1 convex face represents a functional ligand binding site.

Chapter 6

Molecular and structural studies of NgR complex interactions

Molecular and structural studies of NgR complex interactions

6.1. Introduction

A wealth of studies suggest that interaction of NgR with partner proteins is essential to transmission of growth inhibitory signals, with both the signalling adapter $P75^{NTR}$ and the neuronally-restricted LINGO-1 protein emerging as critical partners in the NgR complex. Interestingly both NgR and LINGO are members of a group of proteins containing both LRR and Ig domains (see chapter 1), members of which frequently are involved in interprotein interactions via these domains. Notably, the large ectodomains of LRR proteins such as TLRs are critically involved in ligand engagement [171], and similarly the ectodomains of LRR and Ig domain containing proteins such as LINGO-1 and NetrinG Ligands are known to interact with co-receptors or ligands through their LRR domains [75, 172]. This consideration raised the possibility that the extracellular domains of NgR are also involved in and may be important for NgR complex formation and function. In addition, the results in chapter 5 suggested that certain members of the AMIGO family may be able to substitute for LINGO-1 in the NgR complex, however they did not establish a role for the AMIGO ectodomains in these interactions. Although some studies have provided evidence for NgR/LINGO-1 interactions[68, 69], this area is understudied, and no convincing molecular evidence has confirmed AMIGO/NgR interactions. A key aim for this chapter was to test whether AMIGO ectodomains could interact directly with other components of the NgR complex, as has been suggested for LINGO-1. Ultimately, understanding the molecular architecture of the trimeric NgR/LINGO-1/$P75^{NTR}$ complex is a significant goal and could shed light on how inhibitory

signals are initiated, establishing a key component of the knowledge base from which novel therapeutic interventions can be generated.

This chapter aimed to establish whether AMIGO proteins can interact with NgR directly via their ectodomains, and also attempted to probe the structural basis of interactions between NgR and LRR and Ig domain containing proteins.

6.2 Surface Plasmon Resonance studies of NgR/LINGO and NgR/AMIGO interactions

The interactions between NgR/LINGO-1 and NgR/AMIGO were examined using a BIAcore machine, which exploits the phenomenon of surface plasmon resonance (SPR). SPR relies on exploits laser light directed at a sensor surface under conditions of total internal reflection. At a specific 'resonance angle', there is dip in the intensity of the reflected light, due to some of the energy being passed into a wave of delocalised electrons (a 'plasmon') in a gold layer adjacent to the surface. The angle at which this resonance angle occurs depends on the refractive index of the solution adjacent to the sensor, which is directly related to the concentration of macromolecules (eg proteins) in the solution itself. As there is a linear relationship between the resonance angle and the solution's refractive index, by detecting changes in resonance angle (converted to 'Resonance Units or RU), SPR provides a powerful route to measuring changes in refractive index, and this allows the technique to be exploited for the study of ligand binding interactions. SPR is a powerful and sensitive technique used to study diverse ligand binding interactions, and can be exploited as an accurate 'real time' method to measure protein-protein interactions, and potentially allows quantitative data to be collected, allowing measurement of affinity and kinetics. Importantly however, SPR is susceptible to a number of different artefacts. These include artificially slow kinetic values,

which can result from the presence of protein aggregates in solution, which can be avoided with careful experimental design. Valid SPR experiments are also dependent on the availability of high quality recombinant protein.

6.2.1 Expression of proteins

Human AMIGO-1 (G28-H359), AMIGO-3 (T20-H372), LINGO-1 (C42-S516), and NgR (P26-V311) were expressed in *Drosophila* S2 cells. Expression of human AMIGO-2 was attempted, however the protein failed to express in *Drosophilla* S2 cells, possibly due to the cleavage of the protein identified in Chapter 5, which would be expected to prevent the protein from being purified by His tag purification. Human $p75^{NTR}$ was expressed in *Drosophilla* by the University of Birmingham Protein Expression Facility (PEF). Ectodomains including LRR and Ig domains were expressed with biotin and histidine tags at the C- terminal end of the protein (Figure 6.1). Constructs were introduced into S2 cells by calcium phosphate transfection as described for AMIGO-1 in Chapter 3. Each protein was expressed in the same way. Expression was confirmed by western blot analysis of small scale cultures of each protein, before larger quantities of S2 cells were grown. Ni-NTA purified proteins were analysed by SDS-PAGE and optical density, $OD_{280,}$ was used to determine the quantities of protein produced. From 1 litre cultures of S2 cells, 3-6 mg of protein was typically eluted from the nickel column.

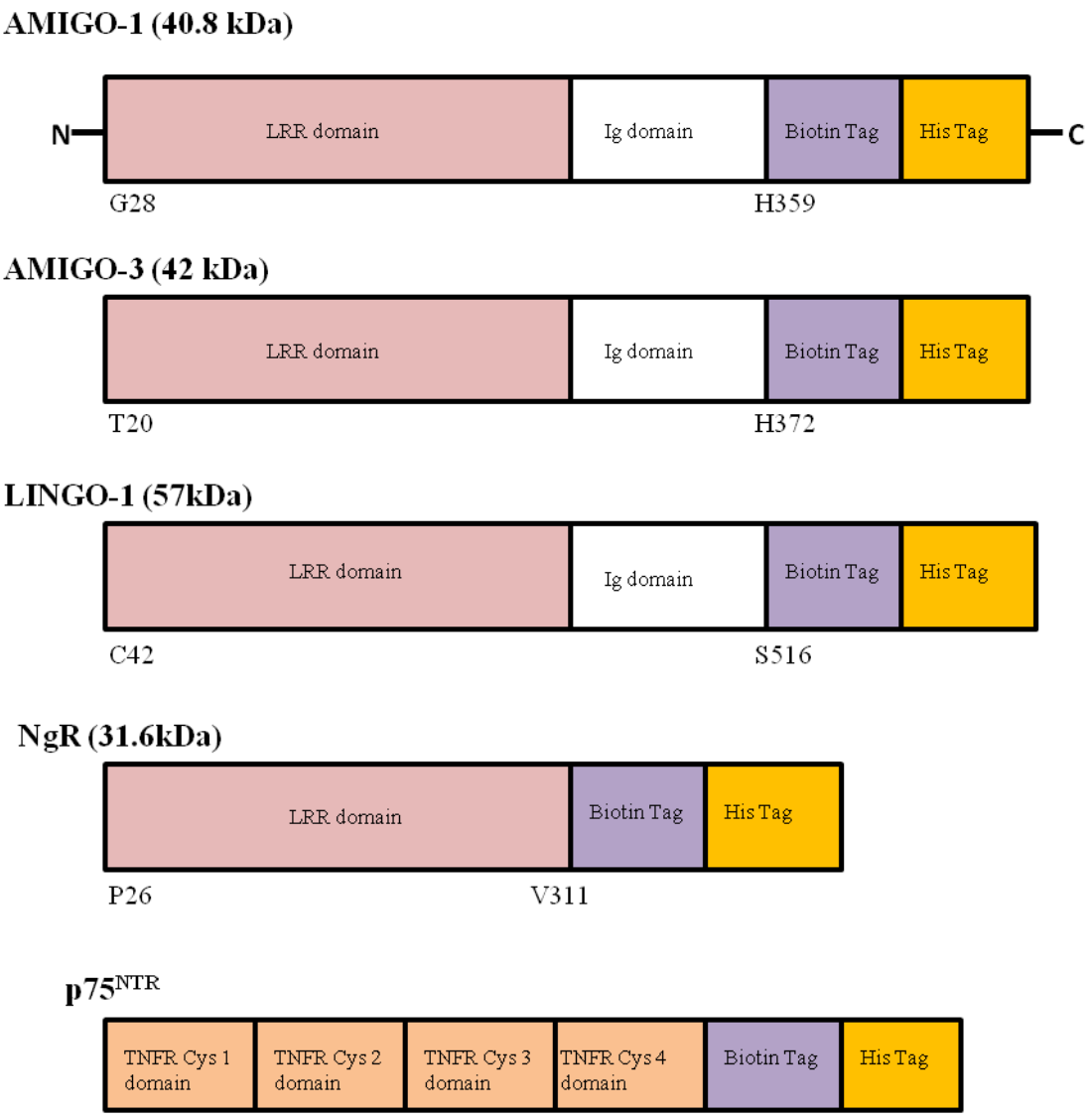

Figure 6.1. ***Drosophila*** **expressed protein constructs**

AMIGO-1, AMIGO-3, LINGO-1, NgR and p75^{NTR} proteins were expressed in Drosophila S2 cells. The most N- and C- terminus amino acids for each construct are labelled, and each protein is followed by a biotin tag and a histidine tag at the C terminal end. For BIAcore, the NgR protein was biotinylated. Domains are not to scale.

6.2.2 Purification of AMIGO-1, AMIGO-3 and LINGO-1

AMIGO-1, AMIGO-3 and LINGO-1 were to be used as analytes, and injected over the chip in surface plasmon resonance experiments. Following Ni-NTA purification, these proteins were loaded onto the Superdex S200 column which had been pre- equilibrated with the appropriate buffer. This provided additional separation from impurities. AMIGO-1 was exchanged into 20mM Tris pH 8.5, 50mM NaCl, AMIGO-3 into 20mM Tris pH 8.5, 100mM NaCl and LINGO-1 was exchanged into 20mM Tris pH 7.4, 150mM NaCl. Following size exclusion chromatography, peak fractions were collected and samples were analysed by SDS-PAGE to confirm size and purity.

Prior to SPR, proteins were required to be concentrated prior to SPR, in order to obtain concentrations likely to result in detectable binding. However, this can result in protein aggregates, which can cause grossly inaccurate interpretation of SPR results if the data generated are assumed to derive from *bona fide* monomeric protein/ligand interactions. For this reason, an additional HR200 'polish' step was introduced, prior to SPR data collection. This ensured maximum purity of the samples that were to be analysed, and excluded aggregates. For the concentration step, proteins were concentrated using an AMICON Ultra centrifugal filter (Millipore 0.5ml, 10kDa) to a volume 245µl and loaded onto the Superdex HR200 column pre-equilibrated with appropriate buffer. Following size exclusion chromatography, peak fractions were analysed by optical density (OD_{280}) for use in the SPR experiment. Although ideally no further concentration steps would be required, in some cases additional post-HR200 concentration (carried out in centrifugal filter units as above) were necessary but were kept to a minimum. It was important to keep the samples on ice

throughout purification to reduce the likelihood of protein aggregation, which could alter binding to the ligand.

Purification of AMIGO-1 by size exclusion chromatography was described in Chapter 3, the elution profile identified that AMIGO-1 was a dimer in solution. The S200 elution profile of AMIGO-3 (Figure 6.2a) illustrates two peaks 'a' and 'b' of 20mAu and 40mAu at 130ml and 190ml respectively. Peak 'b' correlates to a protein of approximately 80kD in size which, like AMIGO-1, indicates that AMIGO-3 is a dimer in solution because the predicted size of the expressed protein is 42kDa. The HR200 elution profile (Figure 6.2b) illustrates that AMIGO-3 is eluted at 15-16ml which correlates to a protein of around 80kDa size, again identifying the protein as a dimer. Further analysis of peak fractions by SDS-PAGE (Figure 6.2c) revealed single bands at approximately 45kDa in reduced and non-reduced forms indicating that the protein is not glycosylated, as its predicted size is 42kDa, and demonstrating that the AMIGO-1 dimer is non-covalent. The S200 elution profile of LINGO-1 (Figure 6.2d) reveals that the protein eluted at 200ml, which corresponds to 66kDa, suggesting that it exists in a monomeric state in solution (Figure 6.3). Furthermore, the HR200 elution profile (Figure 6.2e) identifies two peaks 'a' and 'b' at 15ml and 23ml respectively; the former corresponds to a protein of 60kDa in size which confirms the protein is monomeric in solution. The later peak corresponds to small cleavage products which are the result of freeze thawing of the sample, indicating the buffer that the protein was stored in was perhaps not ideal. When analysed by SDS-PAGE (Figure 6.2e), peak fractions were visible as single bands migrating at ~66kDa in size, which differs from the expected size of 57kDa. It is possible that this difference can be attributed to N-linked glycosylation. Interestingly, the LINGO-1 elution profile differed from previous

published results in which it was described to exist as a tetramer in solution based on cross-linking studies and gel filtration [69].

6.2.3 Biotinylation of NgR

NgR and $p75^{NTR}$ were biotinylated to enable binding to the surface of the BIAcore CM5 chip. Biotinylation involved buffer exchanging the soluble proteins into biotinylation buffer containing biotin, ATP and BirA enzyme, after collection from the Ni-NTA column, described in Chapter 2. Following biotinylation, excess biotin was removed from the sample by size exclusion chromatography. Human NgR was applied to the S200 column which had been pre equilibrated with 20mM Hepes pH 7.2 150mM NaCl, following biotinylation. The elution profile (Figure 6.2f) revealed a peak at 225ml corresponding to a protein of 35kDa in size which is similar to the estimated size of 32kDa for NgR revealing that the protein is a monomer in solution, as documented previously [32]. When purified by HR200 (Figure 6.2g) two peaks 'a' and 'b' at 16ml and 20ml respectively were detected, peak 'a' corresponds to the eluted protein being around 30kDa in size, which is in the correct range for the expressed NgR protein and again suggests it is a monomer in solution. Peak 'b' is probably buffer components such as excess biotin and ATP. Peak fractions were analysed by SDS-PAGE in reduced and non-reduced forms, which identified the proteins as single bands at approximately 35kDa in size and also determined the protein was very clean with little contamination (Figure 6.2h).

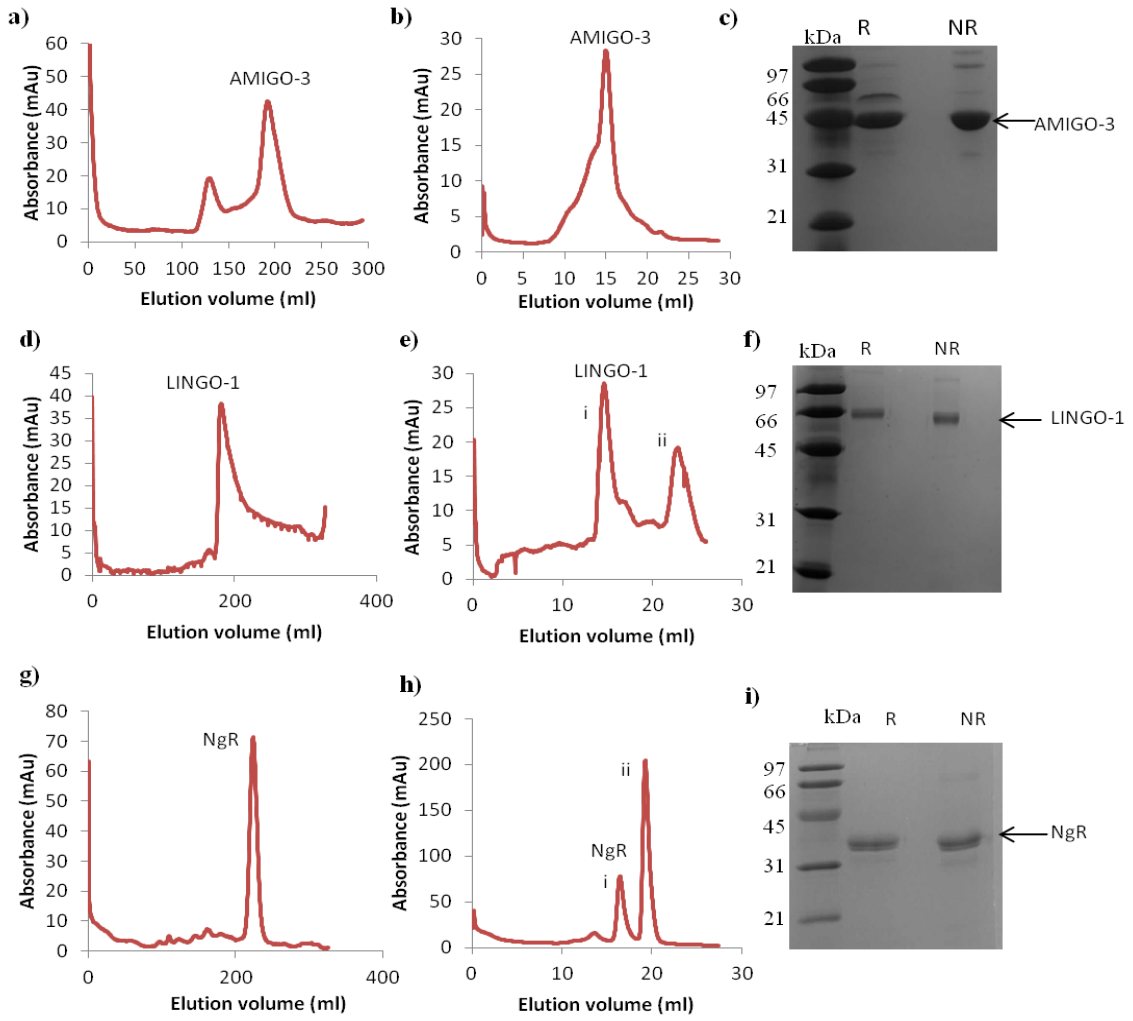

Figure 6.2. Purification of hAMIGO3, hLINGO-1 and hNGR by size exclusion chromatography.

a) Size exclusion elution profile for hAMIGO-3 using the S200 column. hAMIGO-3 elutes as a dimer at ~190ml. b) Size exclusion elution profile for hAMIGO-3 using the HR200 column. hAMIGO-3 elutes at ~15ml consistent with a dimeric species. The rationale for dual S200/HR200 purification is outlined on page 7. c) SDS-PAGE analysis of hAMIGO-3 peak fractions eluted from the HR200 column under reducing (R) and non-reducing (NR) conditions. d) Size exclusion profile for hLINGO-1 using the s200 column, the protein is eluted as a monomer at ~200ml. e) Size exclusion **e**lution profile for hLINGO-1 using the HR200 column, two species are eluted at ~15ml (i) and ~22ml (ii) the former corresponds to hLINGO-1 monomer and the latter corresponds to low molecular weight buffer components. f) SDS-PAGE analysis of hLINGO-1 peak a fractions eluted from HR200 under reducing (R) and non-reducing (NR) conditions. g) Size exclusion elution profile for hNgR using the S200 column. hNgR elutes as a monomer at ~210ml. h) Size exclusion elution profile for hNgR using the HR200 column., two species are eluted at ~18ml (i) and ~20ml (ii), the former corresponding the protein in monomeric form and the latter representing buffer components. i) SDS-PAGE analysis of hNgR peak a fractions eluted from the HR200 column under reducing (R) and non-reducing (NR) conditions

Protein	Mw (Da)	Elution Volume (ml)	Log (Mw)
Ribonuclease A	13700	255	4.14
Carbonin anhydrase	29000	233	4.46
Ovalbumin	44000	212	4.64
Conalbumin	75000	194	4.88
Aldolase	158000	171	5.20
Ferritin	440000	140	5.64

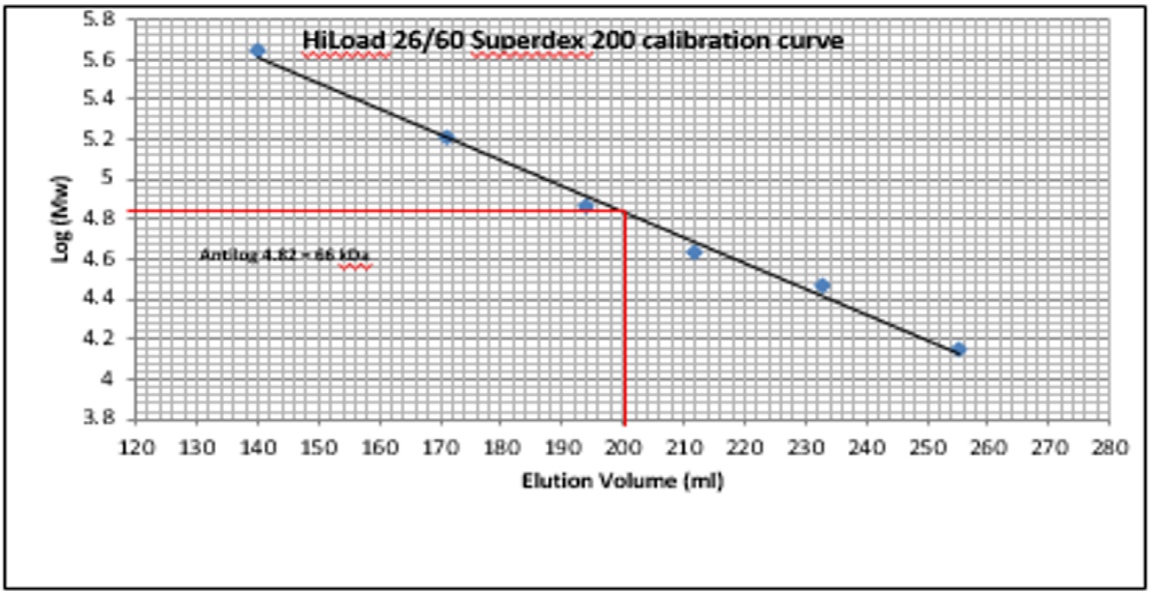

Figure 6.3 Calibration curve for standard proteins eluted from the Hiload 26/60 Superdex 200 size exclusion column.

Lingo-1 elutes at 200 ml which corresponds to 66 kDa.

6.3 Testing interaction of LINGO-1 to NgR-Fc and P75^{NTR}-Fc fusion proteins

Choice of strategy for immobilisation of ligand to the sensor surface is a critical factor in establishing an experimental system for SPR analysis. Various different methods are commonly used for directly coupling proteins to the sensor surface, including amine coupling, sulphydryl group coupling, and a range of tag-based coupling methods including His-NTA chips [173]. Alternatively, proteins of interest can be coupled indirectly, by first immobilising a protein capable of binding tightly to the protein of interest. Common examples of this strategy include immobilisation of biotinylated proteins to chip surfaces to which streptavidin has been coupled, and coupling of antibodies to the chip surface, allowing specific target antigens to be captured. One important consideration in these experimental systems is whether the strategy enables oriented/semi-oriented or non-oriented coupling. Amine coupling methods rely on the presence of primary amine groups on the immobilised protein (ie Lysine residues). Depending on their location on the protein in question, immobilisation via such groups can reduce/eliminate activity of the ligand on the chip surface for binding target analytes. In contrast, oriented/semi-oriented methods typically result in higher levels of activity of the protein surface, which can be critical to downstream detection of interaction with partner proteins.

Before testing interaction of AMIGO proteins with NgR, an experimental system that could detect NgR interaction with P75^{NTR} and/or LINGO-1 was established. For these experiments, initially LINGO-1 had been expressed, in-house, using a well-established Drosophila expression system; in contrast neither the NgR nor P75^{NTR} Fc fusion proteins had been produced in-house, and had instead been obtained commercially. The presence of Fc tags on both P75^{NTR} and NgR suggested an immobilisation strategy exploiting the presence of this tag.

Previously, the anti-human-Fc antibody Rz108e9 has been successfully used to capture Fc-fusion proteins for BIAcore analysis, by first amine coupling the antibody, allowing Fc-fusion proteins to be injected in solution, capturing them in a semi-oriented fashion for subsequent binding experiments. This method was therefore selected in a first attempt to establish a system to study NgR/LRR domain containing protein interactions.

Reproduction of a previously reported method [174] for amine coupling Rz108e9 successfully immobilised relatively large quantities (16-19,000RU) of the antibody on two chip surfaces (Fig 6.4a). First, the CM5 chip surface was activated with EDC/NHS, and then Rz108e9 was injected over the activated surface at 10ug/ml; subsequently unused groups were quenched using ethanolamine, and finally the surface was cleaned to remove any uncoupled Rz108e9 stuck to the surface. Subsequently, injection of commercially available NgR-Fc fusion protein over Fc2 resulted in capture of ~2000RU of bound protein, whereas Fc1 acted as control surface (Figure 6.4b).

To test interaction with LINGO-1, recombinant LINGO-1 was injected at 400µg/ml (~3.5µM) over both surfaces (not shown). Although a substantial increase in the signal was observed during the injection, indicative of the relatively high protein concentration used, almost exactly equivalent responses were obtained over both flow cells, indicating that no binding was detected. To test if higher concentrations of LINGO-1 were required to detect binding, LINGO-1 was injected over both surfaces at a concentration of 1mg/ml (Figure 6.4c). Again, no binding was detected, however, interestingly at this concentration of LINGO-1, a relatively slow association response was observed, and a higher response was observed over Fc1, despite the absence of NgR on this flow cell. This suggested that at this higher concentration

of LINGO-1, a weak stickiness to the Rz108e9-coated was occurring, and that this was marginally impeded by the immobilisation of NgR-Fc. Following failure to detect LINGO-1 interaction with NgR-Fc, $P75^{NTR}$-Fc was immobilised to Fc1 (Figure 6.4d), and following this LINGO-1 injected over Fc1 and Fc2, exploiting the lack of interaction with NgR (Fc 2) as a control surface (Figure 6.4e). As observed before $P75^{NTR}$ immobilisation, there was a somewhat higher signal over Fc1 than Fc2, however the traces closely matched those before $P75^{NTR}$ immobilisation, with similar slow association and closely matched dissociation phases observed. This indicated that there was no detectable binding to $P75^{NTR}$.

These experiments failed to detect any convincing binding of recombinant LINGO-1 to immobilised NgR-Fc or $P75^{NTR}$-Fc proteins. One possible explanation for lack of expected interaction on BIAcore could be use of an immobilisation method that resulted in a highly inactive protein surface. However, in this case, the use of the well-established Rz108e9 method, allowing semi-oriented coupling of proteins via C-terminal Fc tags, suggested this explanation was unlikely. One alternative explanation was that one or more of the proteins was not folded correctly. While the quality of in-house-produced LINGO-1 could be tested, it was more difficult to establish for the commercially obtained NgR-Fc and $P75^{NTR}$-Fc proteins, although they were clearly able to bind to the Rz108e9 antibody. One concern with fusion proteins involving relatively large fusion partners is that even if the target protein is misfolded, the presence of a large, highly soluble fusion partner moiety can mask such problems, enhancing solubility. In contrast, proteins bearing only relatively short tags are likely to rely mostly on correct folding of the target protein itself for acceptable solubility. These considerations led us to produce recombinant forms of NgR and $P75^{NTR}$ without the presence of Fc tags, for using in BIAcore and structural studies.

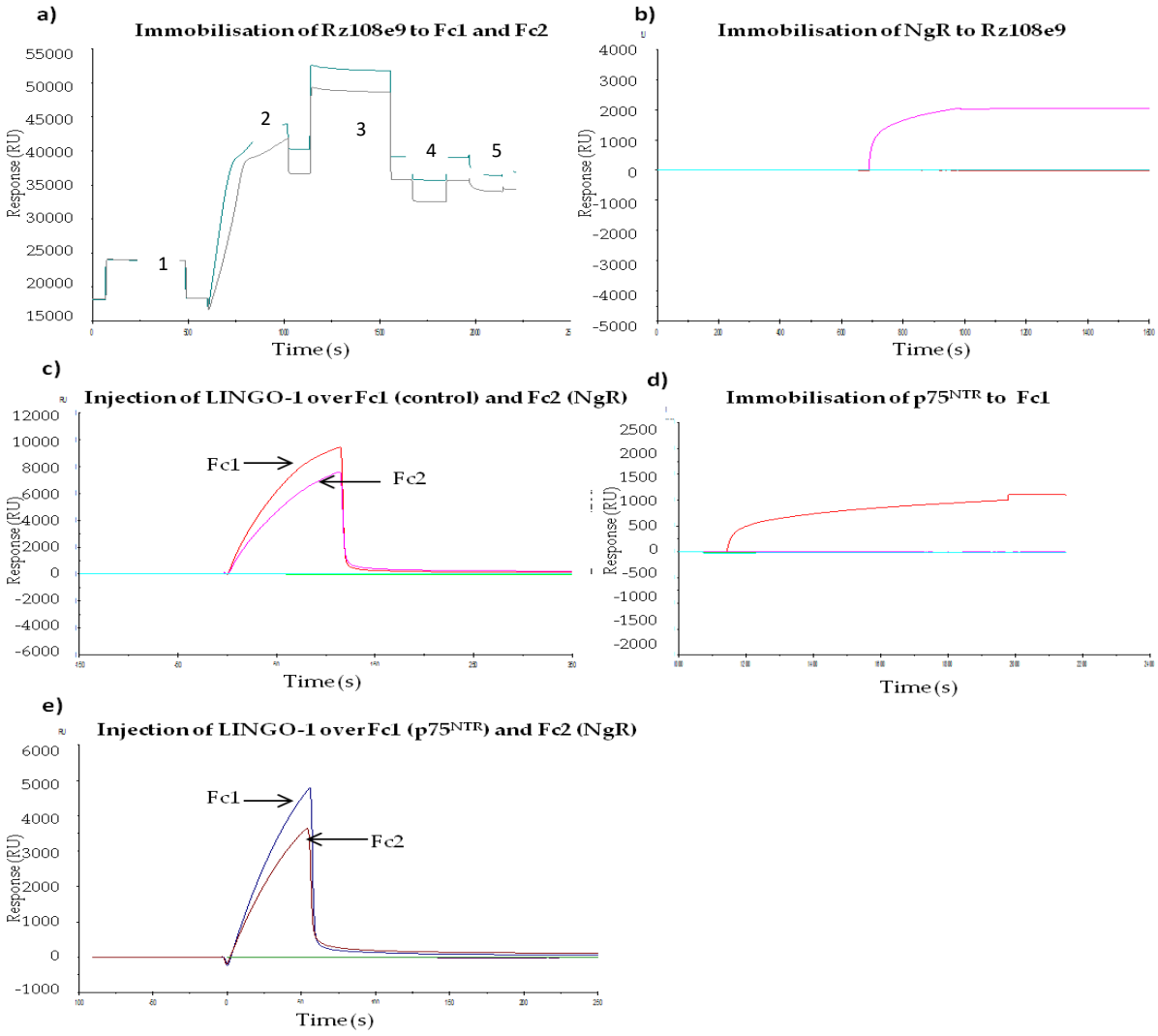

Figure 6.4. Establishing NgR/p75^{NTR}/LINGO-1 interactions.

Prior to testing AMIGO/NgR interactions, it was important to establish an experimental method to detect the NgR/p75^{NTR}/LINGO-1 interactions. NgR-Fc and p75^{NTR}-Fc were immobilised to the sensor chip via amine coupling using the anti-Fc antibody, Rz108e9. LINGO-1, made in house, was then injected over the flow cells and binding detected.

a) Immobilisation of Rz108e9 over flow cells 1 and 2, indicating activation step (1), antibody injection (2), quenching with ethanolamine (3), and surface cleaning steps (4,5) to remove protein that was not covalently coupled.
b) Immobilisation if NgR over flow cell 2 (pink trace) indicates ~ 2000RU of NgRFc immobilised in around 300 seconds.
c) Injection of LINGO-1 over flow cells 1 (control) and 2 (NgR-Fc immobilised), resulting in broadly similar traces over both surfaces (marginally high signal was obtained over the control surface relative to NgR-Fc surface).
d) Immobilisation of p75^{NTR} over flow cell 1. Approximately 1000RU of p75^{NTR} was immobilised in ~ 900 seconds.
e) Injection of LINGO-1 over flow cells 1 (p75^{NTR}) and 2 (NgR). Again, broadly similar traces are obtained over both surfaces (marginally higher signal was obtained over the control surface relative to NgR-Fc surface).

6.4 Establishing an experimental system for detecting LINGO-1/NgR interaction

To produce NgR and $P75^{NTR}$ proteins in a form lacking Fc domains, we engineered these with C-terminal bt-His tags, permitting both affinity purification via Nickel-NTA chromatography, and subsequent enzymatic site-directed biotinylation, *via* the action of the enzyme BirA on the biotinylation tag. These proteins were expressed recombinantly in Drosophila cells, purified, and biotinylated, with the aim of capturing them onto streptavidin-coated chips.

To test interaction with NgR, streptavidin was first immobilised to two flow cells, using a standard amine coupling protocol (Figure 6.5a). NgR-bt was then injected over a single streptavidin-coated flow cell (Fc2), and was captured at relatively high levels (~5000RU). A control protein, WT1bt, was immobilised to a second flow cell (Fc1) at similar levels (Figure 6.5b), and non-biotinylated LINGO-1 was then injected over both surfaces. Injection of LINGO-1 (for 1 minute) at 3.5uM resulted in substantially higher responses over Fc2 (with NgR immobilised) than over Fc1 (with the control protein WT1 immobilised), indicating specific binding (Figure 6.5c). Interestingly, a negative buffer signal was observed, a phenomenon observed relatively frequently in BIAcore assays (eg Fig 6.6, due to differences in refractive index between the buffer the analyte is in, and the running buffer for the experiment), and after subtraction of the buffer signal, a more easily interpretable binding trace was revealed, featuring an association phase culminating over 500RU of bound LINGO-1, after which the dissociation phase lasted around 4mins. Importantly, the interaction did not reach equilibrium after 1 minute, and secondly essentially all LINGO-1 protein dissociated from the NgR surface ~ 4 minutes after the end of the injection. Notably, essentially no protein 'sticking' was observed to the control surface. This result was reproduced in a separate experiment (comparing responses over flow cells bearing NgR-bt, and streptavidin alone

(Figure 6.5d). In addition, longer, 2-minute injections were carried out, in an attempt to extend the detection period during the association phase such that the interaction reached equilibrium (Figure 6.5e). During a 2-minute injection period, the binding detected reached a plateau (of around 800RU), indicating that equilibrium had been reached. Non-specific sticking of LINGO-1 was observed to the NgR surface with higher signals being seen 2 minutes after the end of the injection, indicating the presence of aggregates.

These results both confirmed direct interaction of the ectodomain of LINGO-1 with that of NgR, but also confirmed that this experimental system was appropriate for detection of NgR/LRR interactions, and one that could in principle be sufficiently robust to determine affinity measurements.

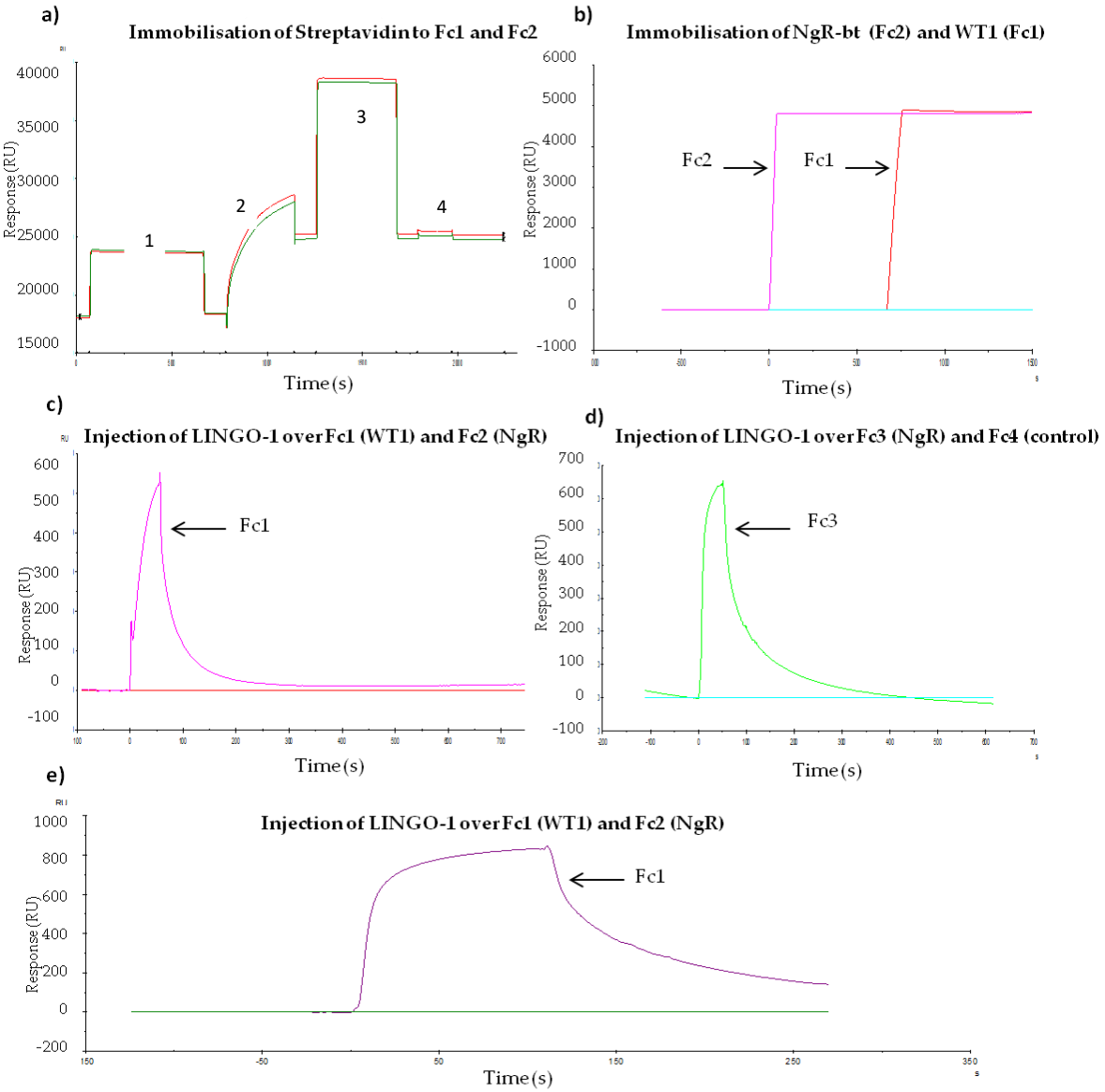

Figure 6.5. Establishing NgR/LINGO-1 interactions.

In order to test the interaction between NgR and LINGO-1, NgR was produced in house with a C-terminal Bt-His tag. NgR-Bt was immobilised over the sensor chip via amine coupling using streptavidin, LINGO-1 was injected and binding was assessed.

a) Immobilisation of Streptavidin over flow cells 1 and 2, highlighting activation phase (1), streptavidin injection (2), quenching with ethanolamine (3), and clean-up step to remove any non-covalently-associated protein (4).
b) Immobilisation if NgR-Bt over flow cell 2 (purple, ~4800 RU immobilised) and WT1 (control protein, red, 4800 RU immobilised) over flow cell 1.
c) Injection of LINGO-1 (3.5μM) over flow cells 1 and 2. Negative buffer signals have been subtracted from both flow cell 1 and 2 traces.
d) Injection of LINGO-1 (3.5μM) over flow cells 3 (NgR-Bt, immobilisation not shown) and 4 (Blank control). Negative signals have been subtracted from both flow cell 3 and 4 traces.
e) Injection of LINGO-1, diluted 1:2 in HBS-EP over flow cells 1 and 2. Negative signals have been subtracted from both flow cell 1 and 2 traces.

6.5 Detection of AMIGO protein interactions with NgR

To test interaction of NgR with $P75^{NTR}$ and AMIGO proteins, an additional experiment was conducted. Streptavidin-coated flow cells were prepared, and both NgR-bt and P75-bt immobilised to separate surfaces, alongside WT1bt control protein. Unfortunately, the attempt to immobilise recombinant biotinylated $p75^{NTR}$ was largely unsuccessful, with only a relatively small amount of $p75^{NTR}$ protein successfully captured. The reasons for this were unclear, but may have related to cleavage of the biotinylation tag after protein purification. As a result, subsequent analyses focussed largely on NgR interactions with LINGO-1 and AMIGO proteins.

To validate detection of LINGO-1/NgR interactions, LINGO-1 protein was injected over all four flow cells, one coated with NgR, one coated with $p75^{NTR}$, one was coated with WT1 control protein and one was left blank (streptavidin-alone). LINGO-1 was subjected to size exclusion chromatography immediately prior to injection. Interestingly, a 3-minute injection 0.58μM over NgRbt-coated and control flow cells confirmed specific binding but was not sufficiently long to reach equilibrium (Figure 6.6a). The likely explanation for this is the much-reduced protein concentration (as a result of dilution during size exclusion), which would be expected to reduce the speed of the association phase (which is dependent on analyte concentration) considerably.

Having established that LINGO-1/NgR binding was detected broadly as expected, AMIGO-1 was then injected over all four flow cells, at 14.7μM (Figure 6.6b). Clear binding was observed to the NgR flow cell, with no binding or sticking observed to other flow cells. Interestingly, the interaction failed to reach equilibrium during the injection. In addition, dissociation

appeared relatively slow, occurring (essentially to completion) over ~ 4000 seconds (albeit under slow flow rate conditions). A subsequent injection at a 5-fold lower concentration (i.e. 2.9μM) also resulted in clearly detectable interaction (Figure 6.6c). These injections confirmed that the ectodomain of AMIGO-1 is capable of directly interacting with the ectodomain of NgR.

Following detection of AMIGO-1/NgR interactions, AMIGO-3 was injected over all four flow cells 11.8μM (Figure 6.6d). AMIGO-3 injection yielded higher responses over NgRbt-coated flow cells, relative to all controls, indicating specific binding to NgR (~500RU of binding). Subtraction of negative background signals indicated the interaction did not reach equilibrium (Figure 6.6e), and indicated a fast and slow phase to the dissociation period, potentially indicative of the presence of aggregated protein in the analyte. Injection of AMIGO-3 immediately post-size-exclusion chromatography also yielded detectable binding, despite the low concentration used 0.69μM (Figure 6.6f). These experiments provide the first direct evidence that the ectodomains of AMIGO-1 and AMIGO-3 are able to directly interact with that of NgR, and confirm the results presented in chapter 5 suggesting that NgR can associate with AMIGO proteins.

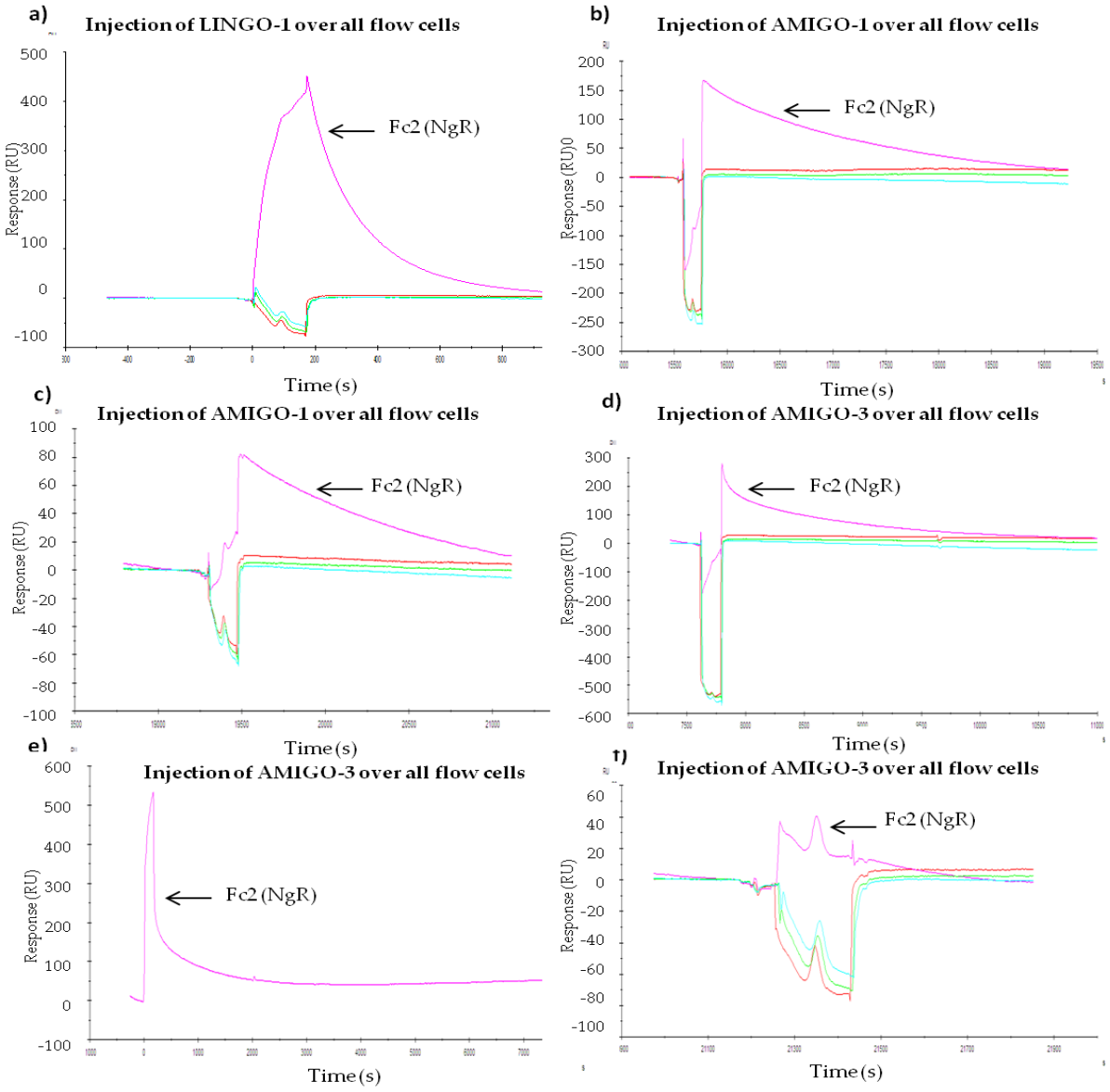

Figure 6.6. Establishing NgR/AMIGO interactions.

In order to test the interaction between NgR and the AMIGO proteins, NgR-Bt was immobilised over the sensor chip on the indicated flow cells onto streptavidin-coated CM5 chips, and following this step, LINGO-1, AMIGO-1 and AMIGO-3 were injected in separate experiments, and binding responses were assessed.

a) Injection of LINGO-1 0.58µM over immobilised NgR (Fc2), and control streptavidin-coated flow cells. A substantially higher signal is evident over Fc2 compared to Fc1,Fc3 and Fc4, indicating clear binding of LINGO-1 to NgR.
b) Injection of AMIGO-1 14.7µM over all flow cells. Again, a far higher signal was obtained over Fc2 compared to control flow cells, indicating specific binding to AMIGO-1 to NgR.
c) Injection of AMIGO-1 diluted in HBS-EP 2.9µM over all flow cells, again indicating specific binding to NgR.
d) Injection of AMIGO-3 11.8µM over all flow cells, indicating specific binding of AMIGO-3 to NgR.

e) Injection of AMIGO-3 11.8μM. Negative signals in the responses over the NgR-coated and control flow cells have been subtracted.
f) Injection of AMIGO-3 0.69μM. Negative signals in the responses over the NgR-coated and control flow cells have been subtracted. Data are relatively noisy due to the low signals detected, and a blip in the sensorgram is observed, due to pressure effects in the internal flow cell.

6.6 Structural studies of AMIGO-1/NgR complex.

Having both confirmed direct interactions of NgR with the LINGO-1 ectodomain and established NgR interaction with AMIGO ectodomains, structural studies were then attempted to further probe the precise mode of binding between the Nogo tripartite complexes comprised of NgR, AMIGO-1, AMIGO-3 and LINGO-1. Initial attempts at crystallising AMIGO-3/NgR were hampered by the fact that AMIGO-3 was prone to aggregation at high concentrations. To address this issue ThermoFluor stability assays were performed to identify buffer conditions that could improve protein solubility and, in turn, crystallisation success. This assay provides a fluorescence readout measurement of thermally-induced protein melting. Briefly, AMIGO-3 was heated in the presence of 96 unique solubility reagents (varying buffer, pH and ionic strength) and Sypro Orange dye to identify sample buffer formulations that increase the melting temperature (Tm) and therefore relative stability of the protein. The fluorescence of the hydrophobic dye Sypro Orange increases considerably when the dye binds to internal hydrophobic protein regions that become exposed following protein denaturation. Protein stability or Tm is then measured by analysing the temperature dependence of protein denaturation and subsequent increase in fluorescence intensity. Using this approach, several candidate solubility reagents were identified including 0.1M Na cacodylate pH 6.5 (Figure 6.7). However, based on successive spectrophotometric measurements of protein concentration and visual evidence of protein precipitation, none of these conditions allowed AMIGO-3 to remain in solution at high concentrations sufficient for complex crystallisation trials. Additionally, a previous study had highlighted the extreme difficulty in crystallising LINGO-1 [69], which was ultimately overcome by subjecting the protein to limited proteolysis, where flexible areas of the protein were cleaved to provide a more stable fragment.

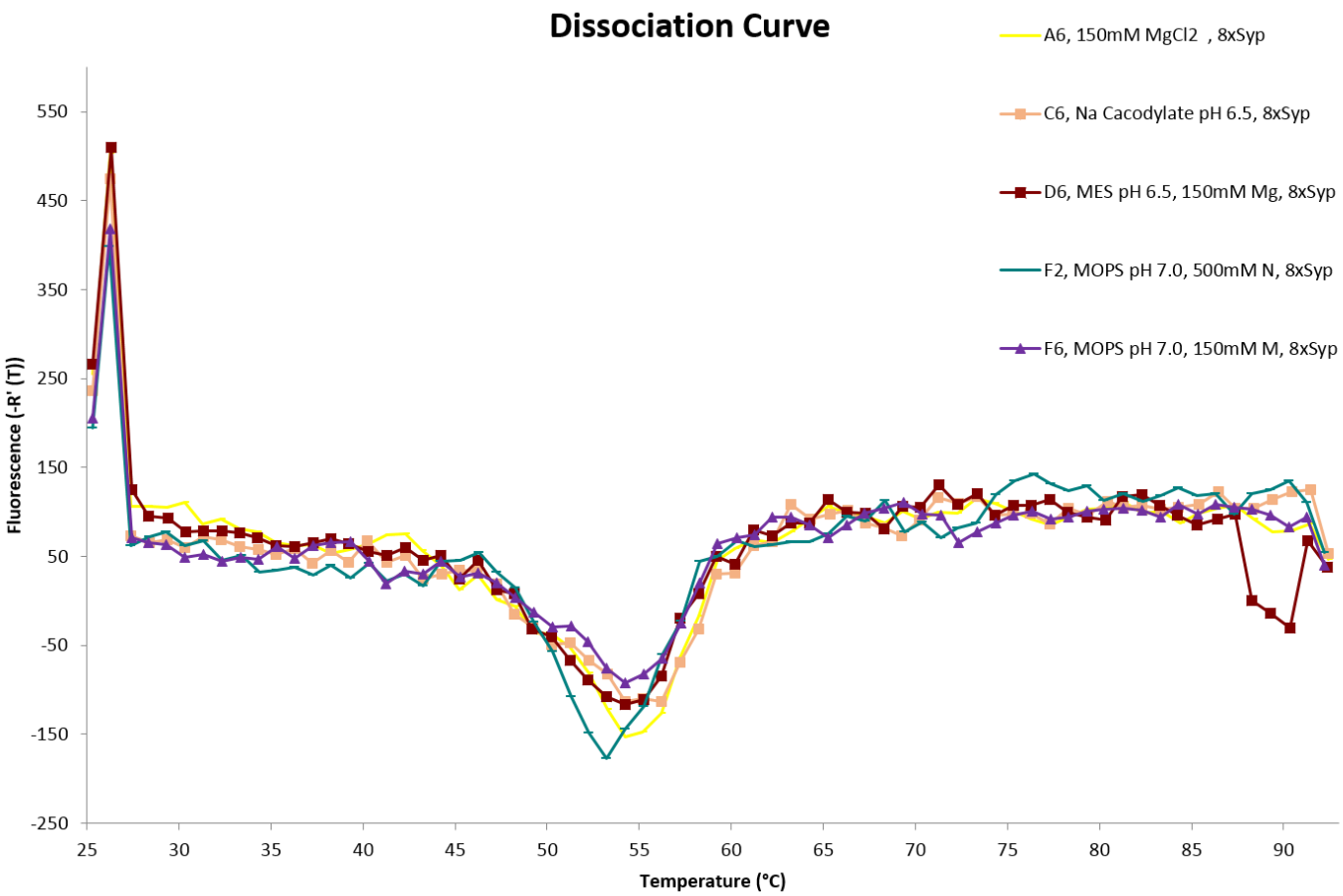

Figure 6.7. ThermoFluor stability assay dissociation curve for hAMIGO-3.

Stability assays were performed to identify buffer conditions that could improve protein solubility. The assay provides a fluorescence readout measurement of thermally-induced protein melting. AMIGO-3 was heated in the presence of 96 unique solubility reagents and Sypro Orange dye. The fluorescence of the hydrophobic dye increases considerably when the dye binds to internal hydrophobic protein regions that become exposed following protein denaturation. Protein stability or Tm is then measured by analysing the temperature dependence of protein denaturation and subsequent increase in fluorescence intensity. Using this approach, several candidate solubility reagents were identified including 0.1M Na cacodylate pH 6.5.

Based on these considerations and due to time constraints my focus was to determine the three dimensional structure of the AMIGO-1/NgR complex. Indeed, this endeavour was helped by the fact that unlike AMIGO-3, both AMIGO-1 and NgR were not prone to aggregation at high concentrations.

6.6.1 Production of AMIGO-1 and NgR in *Drosophila* S2 cells

The hAMIGO-1 ectodomain (residues G28-T362) was expressed in *Drosophila* S2 cells as described in Chapter 3 and was identified as a dimer in solution. The human NgR ectodomain comprised of residues Q26-P448 was also expressed in *Drosophila*, as described above. Both proteins were initially purified by Ni-NTA chromatography followed by further purification by size exclusion chromatography. Briefly, human NgR was loaded onto the Superdex 200 column on the FPLC which had been pre-equilibrated with 20mM Hepes pH 7.2, 150mM NaCl. Typically, a single peak of 70mAu was observed at ~220ml which is consistent with the predicted size of 31kDa for NgR and confirmed that the protein exhibits a monomeric state in solution (Figure 6.2**)**. The peak fractions were pooled, concentrated and analysed by SDS-PAGE under reducing and non-reducing conditions. Examination of the resulting gel revealed a single band for NgR at ~30kDa, suggesting that glycosylation, if present at all, was minimal (Figure 6.8a). Moreover, the high purity evident on SDS-PAGE, combined with monomeric behaviour in solution, suggested the NgR sample was of sufficient quality for co-crystallisation screening trials with hAMIGO-1.

6.6.2 hAMIGO-1/NgR Co-crystallisation trials

hAMIGO-1and NgR were mixed at a 1:1 molar ratio to a final concentration of 11.5mg/ml, and screened against several commercial sparse- matrix based screens with the mosquito nanolitre

crystallisation robot. In total 288 conditions were screened (derived from Structure Screen 1 and 2, MIDAS and JCSG$^+$), using the hanging drop vapour diffusion method. The initial screening process identified four conditions (Figure 6.8b-e) that yielded promising crystallisation hits; JCSG$^+$ conditions 1.5 (0.2M Mg formate, 20% PEG3350) and 1.42 (0.2M $MgCl_2$, 0.1M Tris pH8.5, 20%PEG 8000), MIDAS 1.40 (10% Pentaerythritol ethyoxylate) and Structure Screen C9 (0.2M $MgCl_2$, 0.1M Tris pH8.5, 30%PEG 4000). These conditions were subsequently screened against AMIGO-1/NgR, AMIGO-1, NgR and buffer alone. Importantly no crystals appeared in the drops containing AMIGO-1 and NgR alone suggesting that the initial crystal hits were most likely comprised of the AMIGO-1/NgR complex. Additionally, no crystals were observed in drops in the absence of protein suggesting that salt crystals could be excluded. Of the 4 conditions, JCSG$^+$ 1.5 (0.2M Mg formate, 20% PEG 3350) reproducibly yielded micro-crystals which typically appeared after 2-3 days. Hence, in order to grow diffraction grade crystals optimisation trials were undertaken.

The overall aim of the optimisation trials was to reduce the number of nucleation sites per drop in order to achieve larger diffraction-grade crystals. This involved varying the AMIGO-1/NgR complex concentration, the PEG 3350 precipitant concentration and the ratio of the protein: reservoir solution. Crystallisation trials were performed with AMIGO-1/NgR complex at 11.5, 10 and 9mg/ml and the PEG 3350 concentration was varied between 20-16%. These trials were set up on a large scale (1µl + 1µl) using both hanging and sitting drop techniques with drops derived from differing ratios of protein: crystallisation buffer (1:1, 2:1, 3:1, 3:3, 4:1, 4:2 and 4:3). Following these optimisation trials a number of larger crystals were observed that were typically 100µm x 100µm in size (Figure 6.9). The condition yielding the most optimal crystals comprised 0.2M Mg formate and 17% PEG 3350. These were grown

using the sitting drop method with a drop ratio of 4:2 (protein: reservoir solution) at a final AMIGO-1/NgR concentration of 9mg/ml. Four of these crystals were soaked in cryoprotectant in reservoir solution supplemented with 20% glycerol for 30 minutes as a cryoprotection step and subsequently flash cooled in liquid nitrogen.

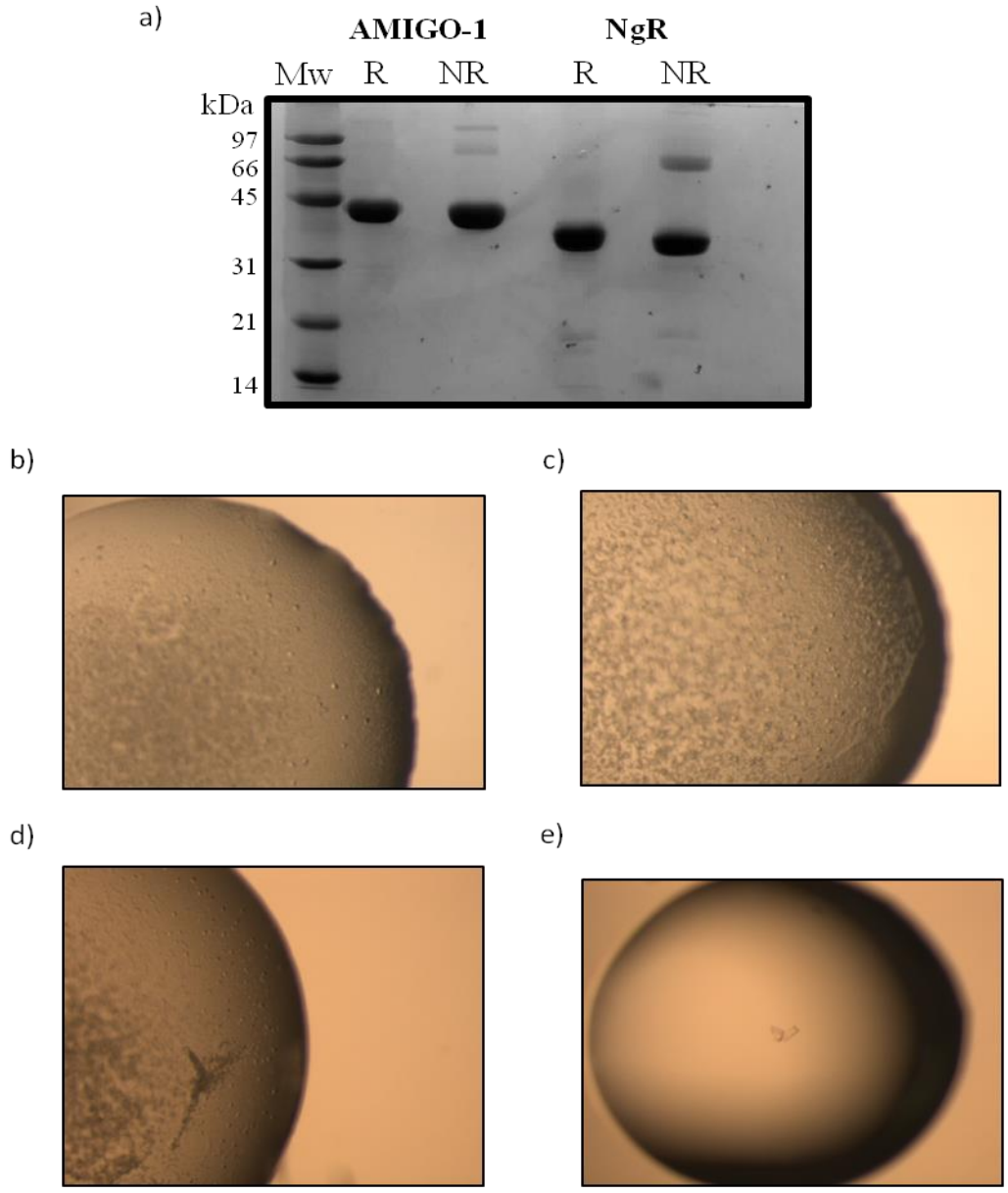

Figure 6.8 Crystallisation trials of the hAMIGO-1/NgR complex.

a) SDS-PAGE analysis of purified hAMIGO-1 and NgR for complex crystallisation trials. Both proteins demonstrate sufficient purity for crystallisation trials and migrate to their expected molecular weights. b-e) hAMIGO-1/NgR co-crystallisation trials with commercial screens using the hanging drop vapour diffusion method yielded micro crystals in a number of conditions; JCSG$^+$ condition 1.5 (0.2M Mg formate, 20% PEG3350), JCSG$^+$ condition 1.42 (0.2M $MgCl_2$, 0.1M Tris pH8.5, 20%PEG 8000), Structure screen condition C9 (0.2M $MgCl_2$, 0.1M Tris pH8.5, 30%PEG 4000) and MIDAS condition 1.40 (10% Pentaerythritol ethyoxylate). 100 + 100 nl drops were set up at 11mg/ml. Micro-crystals appeared after approximately 4 days.

a)

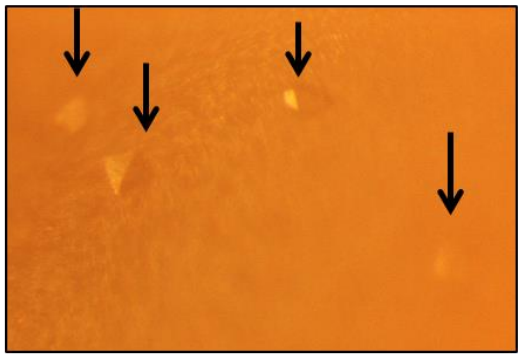

b)

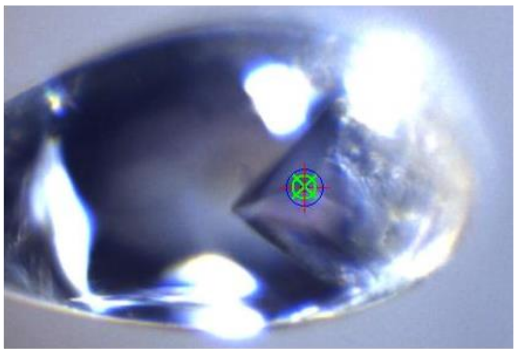

c)

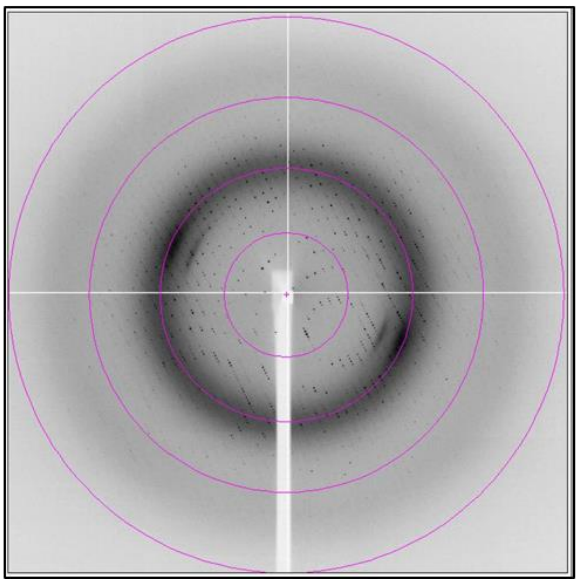

d)

Parameters	AMIGO-1 ectodomain
Space Group	$P4_32_12$
Unit Cell Length (Å)	a= 94.3 b=94.3 c=95.2
Unit Cell Angles (°)	α=90 β=90 γ=90
Resolution (Å)	42.2-1.9
Observed Reflections	365930 (24367)
Unique Reflections	34261 (4789)
Multiplicity	10.6 (5.10)
Completeness (%)	99.5 (99.4)
R_{merge} (%)	10.7 (70.7)
I/σ (I)	13.6 (2)

Figure 6.9. Production of diffraction-grade hAMIGO-NgR complex crystals

a) Large crystals were generated following optimisation of the JCSG+ condition (black arrows). These were grown in sitting drops with a 4:2 (protein: reservoir solution) ratio at 9 mg/ml. The final optimised crystallisation condition comprised of 0.2M Mg formate and 17% PEG 3350. **b)** Mounted hAMIGO-1.NgR crystal that was soaked for 30 minutes in reservoir solution supplemented with 20% glycerol and subsequently flash cooled in liquid nitrogen. **c)** A 0.05° oscillation image of hAMIGO-1-NgR crystal diffracting X-rays to 1.9Å resolution collected at the Diamond light source synchrotron facility (Oxford). **d)** Data processing statistics for human AMIGO-1. X-ray data for hAMIGO-1 LRR-Ig was integrated, scaled and merged using programmes of the XDS suite. Numbers in parentheses represent statistics associated with the highest resolution shell.

6.6.3 Data Collection

X-ray diffraction data were collected remotely (at University of Birmingham) using the Diamond Light Source Synchrotron facility (Oxford). One of the crystals diffracted X-rays to 1.9 Å resolution and several data sets were collected. The crystal was found to belong to the tetragonal space group $P4_32_12$ with unit cell dimensions of; a= 94.3Å, b= 94.3Å, c= 95.2Å and α= 90°, β= 90°, γ= 90°. Diffraction data were integrated, scaled and merged using programmes of the XDS suite [116]. The relevant data processing statistics are listed in Figure 6.9d.

6.6.4 Determining Phase Information, Model Building and Refinement

Attempts to determine initial phase information for the hAMIGO-1/NGR complex were performed with molecular replacement using previously determined hAMIGO-1 (Chapter 3) and NgR (pdb code 1OZN) [46] as phasing models. Unfortunately, initial searches with the NgR phasing model yielded no significant rotation function solutions with the MOLREP [117], AMORE [118] and CNS [119] software packages. However, molecular replacement calculations with only the newly refined hAMIGO-1 LRR structure provided a single unambiguous rotation and translation function solution, consistent with a monomer in the asymmetric unit. The model was subjected to a round of refinement with CNS (simulated annealing and individual isotropic B-factor) and the R-factor and Rfree were reduced to 27.8 and 30.9%, respectively. Examination of the resulting *2Fo-Fc* and *Fo-Fc* maps revealed substantial electron density at the C- terminal end the AMIGO-1 LRR domain (Figure 6.10). This electron density was attributed to the hAMIGO-1 Ig domain which was manually built with COOT (Figure 6.10). Following several rounds of refinement interspersed with manual model building the structure of hAMIGO-1 LRR-Ig ectodomain was determined to 1.9Å resolution (Figure 6.11). The relevant refinement statistics for the hAMIGO-1 LRR-Ig structure

are listed in Table 6.1. All residues were built except for the extreme C-terminal end of the LRRCT subdomain (S266-C270) and the C'D loop (E312-V313) of the Ig domain which is characterised by a lack of associated electron density. The hAMIGO-1 ectodomain structure was verified using PROCHECK [153] and revealed that most residues were present in the allowed regions of the Ramachandran plot.

Parameters	hAMIGO1 LRR-Ig
Resolution Range (Å)	42.2- 1.9
Ref. In working set	32555
Ref. In test set	1705
R_{cryst} (%)	23.2
R_{free} (%)	25.5
Number of protein residues	325
Average B-factor (Å^2)	39.2
Number of water mol.	129
RMS Bond Length (Å)	0.007
RMS Bond Angle (°)	1.151
Ramachandran Plot	
Most Favourable (%)	76.7
Additionally allowed (%)	22
Generously Allowed (%)	1.3
Disallowed (%)	0

Table 6.1 Refinement statistics for full length AMIGO-1 (LRR+Ig)

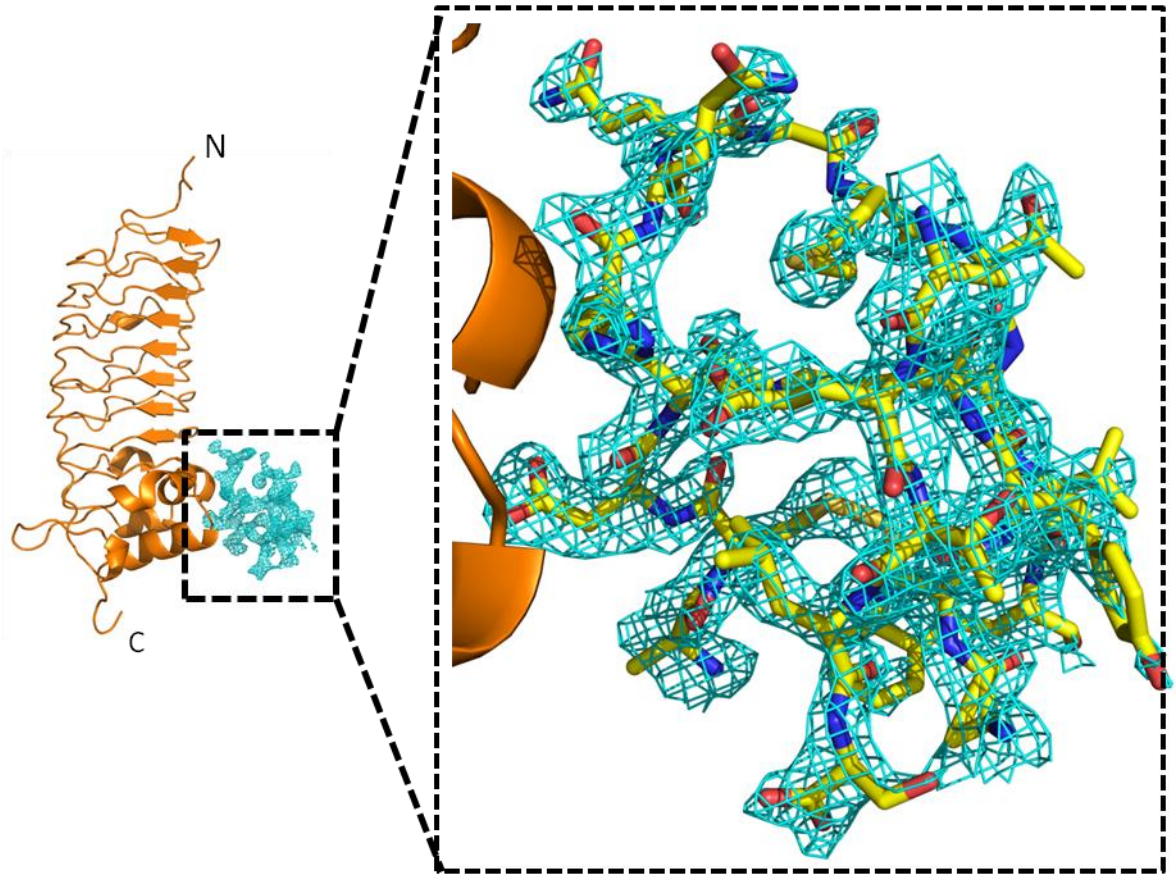

Figure 6.10. Electron density for the hAMIGO-1 Ig domain

Substantial electron density was observed at the C terminal end of theAMIGO-1 LRR domain. The electron density was assumed to belong to the missing AMIGO-1 Ig domain which was manually built in using COOT. All residues were built in except for the extreme C-terminal end of the LRRCT subdomain (S226-C270) and the C'D loop (E312-V313).

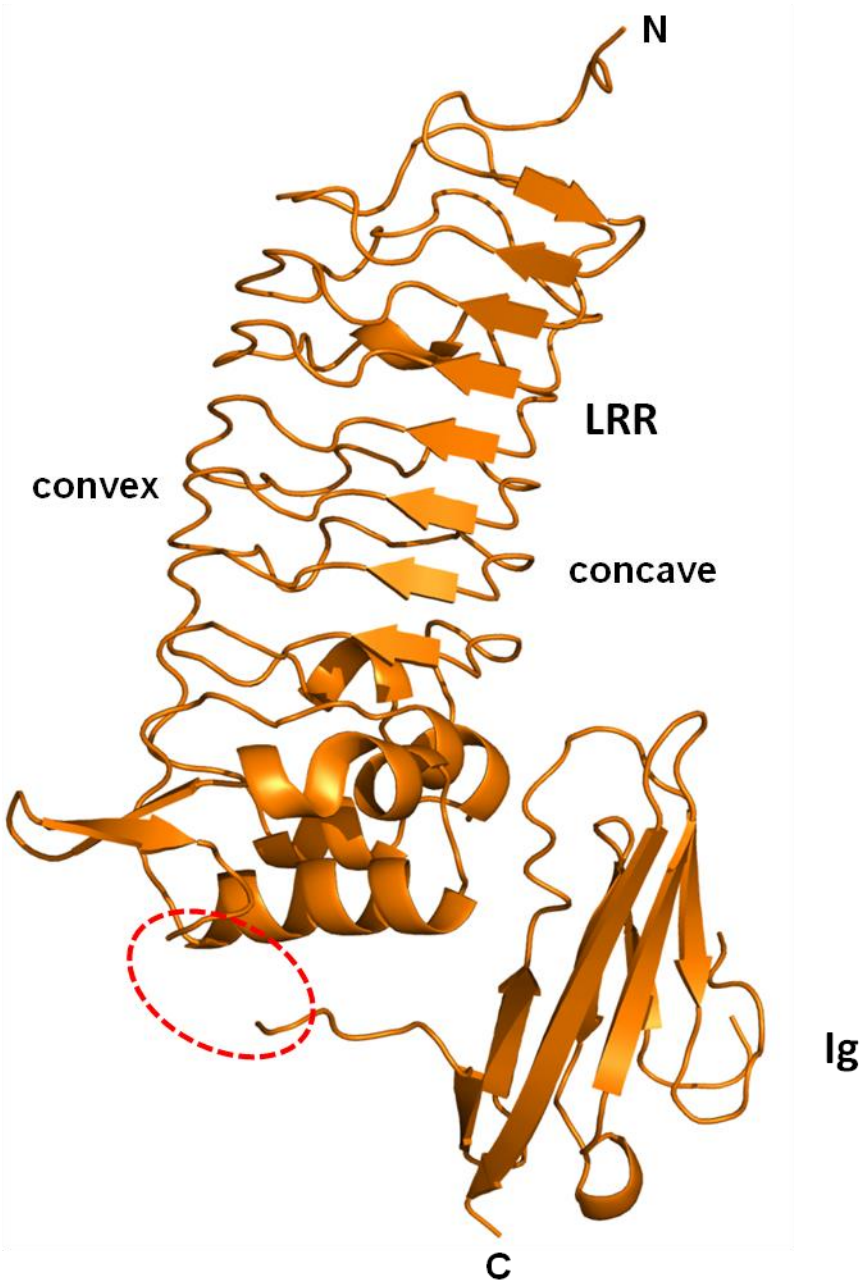

Figure 6.11 Overall structure of the hAMIGO-1 LRR-Ig ectodomain.

The hAMIGO-1 LRR-Ig crystal possesses one molecule per asymmetric unit (highlighted in orange). The LRR domain (labelled) adopts a banana shaped fold with a parallel β-sheet contributing to the inner concave face and various secondary structural elements forming the outer convex face. The Ig domain (labelled) adopts a closely packed β-sandwich encompassing two anti-parallel β-sheets. The N- and C- terminus are highlighted. The red dashed circle represents the disordered LRR-Ig hinge region.

6.7 Structural analysis of the full length ectodomain of hAMIGO-1

The crystal structure of the full length hAMIGO-1 ectodomain including the LRR and Ig modules has been solved to 1.9 Å with R factors of R_{cryst}/R_{free} = 23.2/25.5 %. Despite the crystal form containing one hAMIGO-1 LRR-Ig monomer per asymmetric unit, the hAMIGO-1 LRR-Ig exits as a dimer generated through the crystallographic two-fold axis (Figure 6.12). The dimer interface is formed by interactions mediated by residues that protrude from the LRR module of each monomer as described previously (see Chapter 3). The presence of the Ig domain does not affect formation of the dimer through the LRR domain. The linker region that connects the LRR and Ig domains also exhibits weak electron density suggesting that it is highly flexible, thereby permitting the connecting domains to freely twist and rotate which may be essential in the formation of the AMIGO-NgR-p75 tripartate complex.

6.7.1 Overall structure of the hAMIGO-1 LRR-Ig ectodomain

The hAMIGO-1 LRR domain fold has previously been described in detail (see Chapter 3) and hence this section will predominantly focus on analysing the Ig module. Structural analysis reveals the hAMIGO-1 Ig domain adopts a C2-type immunoglobulin (Ig) fold, consisting of eight β stands, with a single 3^{10} α helix positioned between the E-F strands (Table 6.2, Figure 6.13. Consistent with its homology to the Ig superfamily, the hAMIGO-1 Ig structure adopts a compact beta sandwich domain encompassing two anti-parallel sheets (one comprising of strands B, D, E, the second A', C, C', F, G) (Figure 6.12). A large hydrophobic core, generated by inward facing hydrophobic residues from the B (L286 and I288), E (L326, F328 and V331), C (W301) and F (Y339) strands, contributes to stabilising the interior of the Ig domain (Figure 6.14b). The hAMIGO-1 Ig module is further stabilised by an intra-chain disulphide bridge (mediated by residues C290 and C341) that links strands B and F (Figure 6.14b). This

prominent feature, which connects the beta sheets, is similar to other Ig-like domain containing proteins and is a structural hallmark of Ig-folds [175].

As highlighted with other Ig domain containing proteins, the internal core region of the hAMIGO-1 Ig module is further stabilised by a conserved tryptophan residue (W301) that packs against the disulphide bond (Figure 6.14). In addition to these non-polar interactions, the core region is further stabilised by a hydrogen bonding interaction mediated by the indole ring nitrogen of W301 and the backbone carbonyl group of G324.

Residue	Secondary structure	Residue	Secondary Structure
G271-A277	Random coil	L310-G316	Random coil
W278-A280	β Strand A'	T317-S321	β Strand D
H281-G283	Random coil	K322-D323	Random coil
D284-C290	β Strand B	G324-V331	β Strand E
D291-M297	Random coil	Q332-G336	3^{10} helix
T298-T303	β Strand C	G337-G345	β Strand F
P304-N306	Random coil	A346-T347	Random coil
E307-V309	β Strand C'	F348-H359	β Strand G

Table 6.2 Secondary structure assignments for the hAMIGO-1 Ig domain

6.7.2 Sequence comparison of the Ig domain across the hAMIGO family

Similarity at the primary amino acid sequence level for the Ig domain between hAMIGO-1 to hAMIGO-2 is 49%, hAMIGO-1 to hAMIGO-3 is 48%, and hAMIGO-2 to hAMIGO-3 is 39% (Figure 6.13). The most highly conserved residue positions map to the Ig core region, whereas the surface exposed residues are considerably less conserved (Figure 6.15). Interestingly, the majority of residues that contribute to the hydrophobic core are either highly conserved or semi-invariant across the hAMIGO family. For example, out of the 7 residues that form hydrophobic interactions in AMIGO-1, three are identical (residues L286, W301 and L326) and four demonstrate semi-conservative (residues I288 (V and I in hAMIGOs-2 and 3), F328 (I in

hAMIGOs-2 and 3), V331 (P in hAMIGO-2) and Y339 (F in hAMIGO-3) substitutions across the hAMIGO family (Figure 6.15). Collectively, this suggests that the internal Ig hydrophobic core is stabilized in an analogous manner across the hAMIGO family. The precise role of the Ig domain within the AMIGO family is yet to be established. One possibility is that it plays a structural role orienting the LRR domains correctly on the cell membrane for optimal binding interactions with ligands.

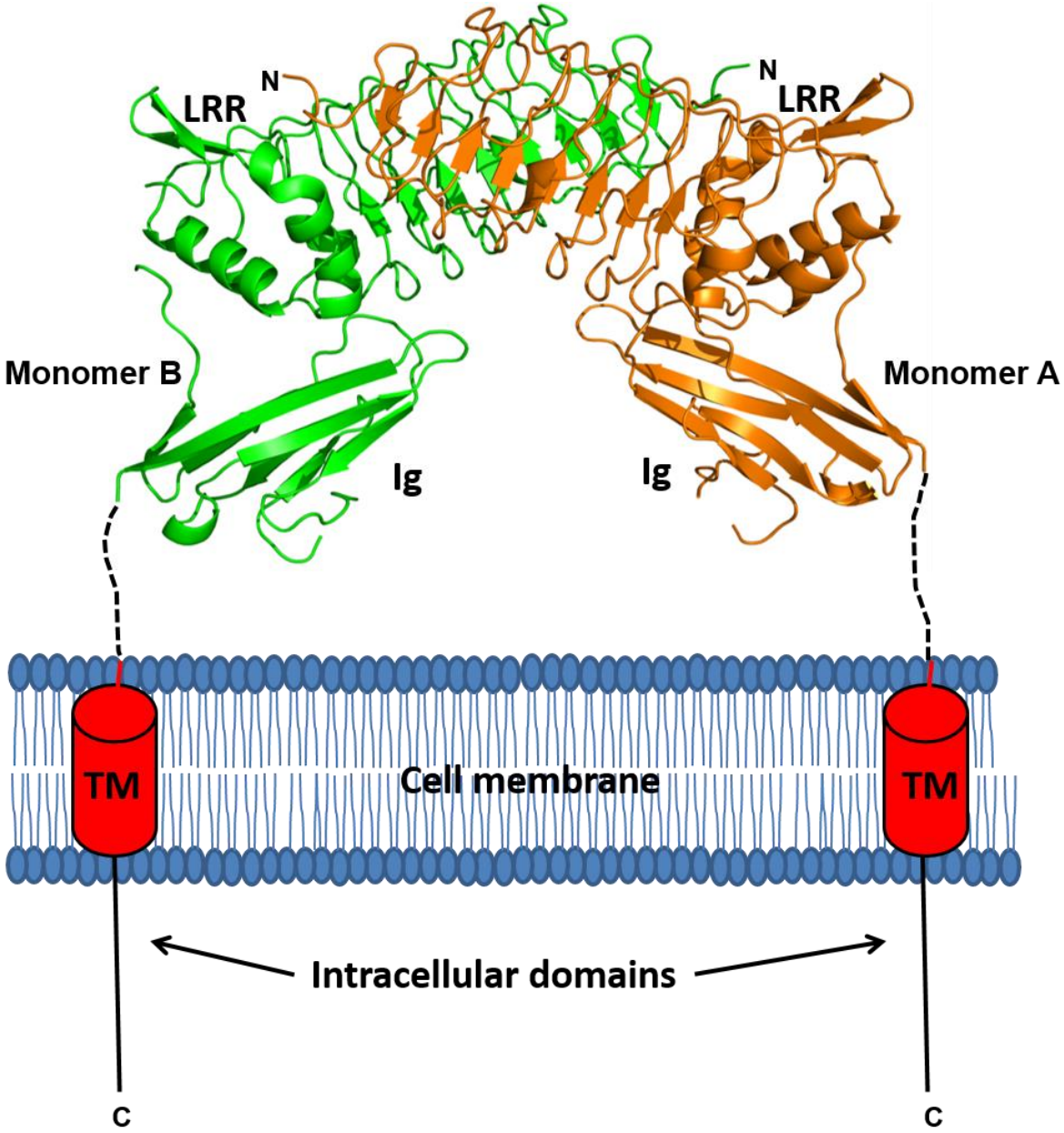

Figure 6.12 Overall structure of the hAMIGO-1 LRR-Ig dimer.

The hAMIGO-1-LRR Ig dimer is generated by a crystallographic 2–fold axis. Each monomer is highlighted (orange and green). The dimer interface is mediated by residues that protrude from the LRR module of each monomer. The N- and C- terminus for each monomer is highlighted. The membrane proximal region (black dashed line), short transmembrane helix segment (elongated tubes; red), and the intracellular domain (thick black line) for each monomer are also highlighted. The cell membrane is also shown to indicate the potential orientation of the C-terminal Ig domain.

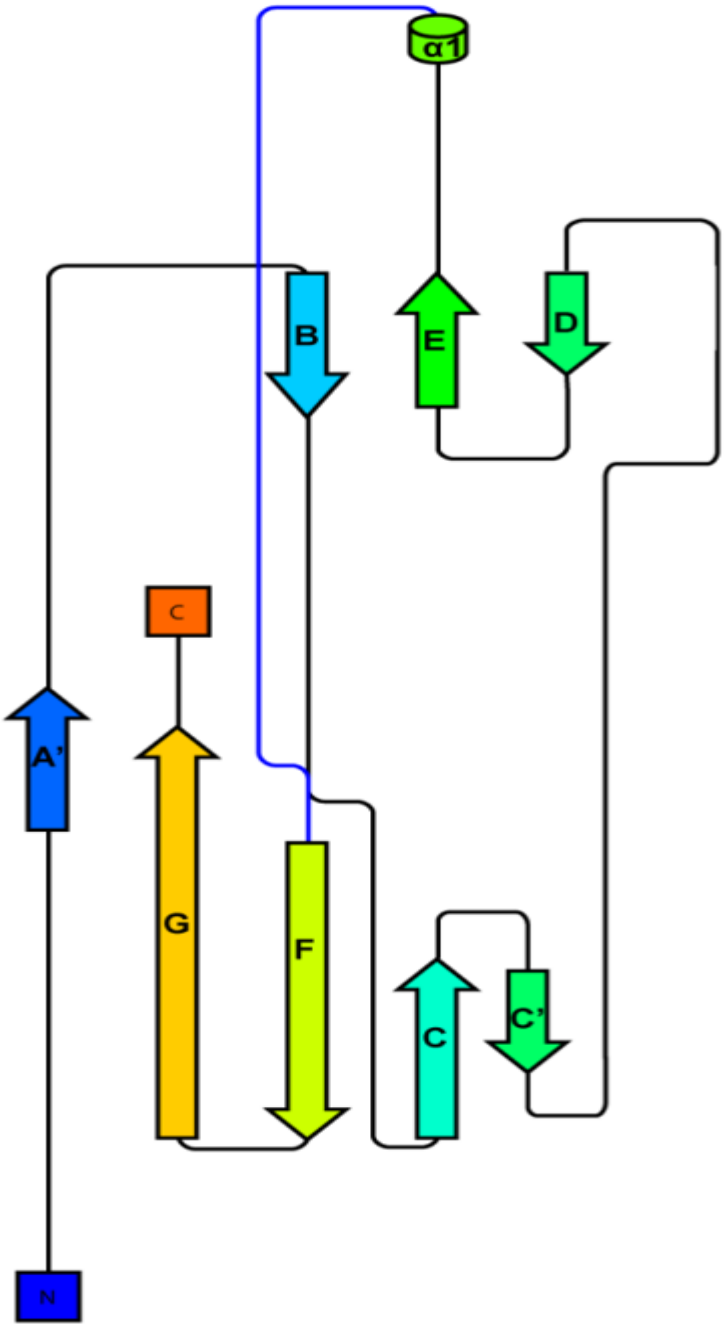

Figure 6.13 Topology diagram for the hAMIGO-1 Ig domain.

The secondary structure elements for the hAMIGO-1 Ig domain are labelled (strands represented as arrows and helix shown as a short tube). The N- and C- terminus for the Ig domain are also highlighted.

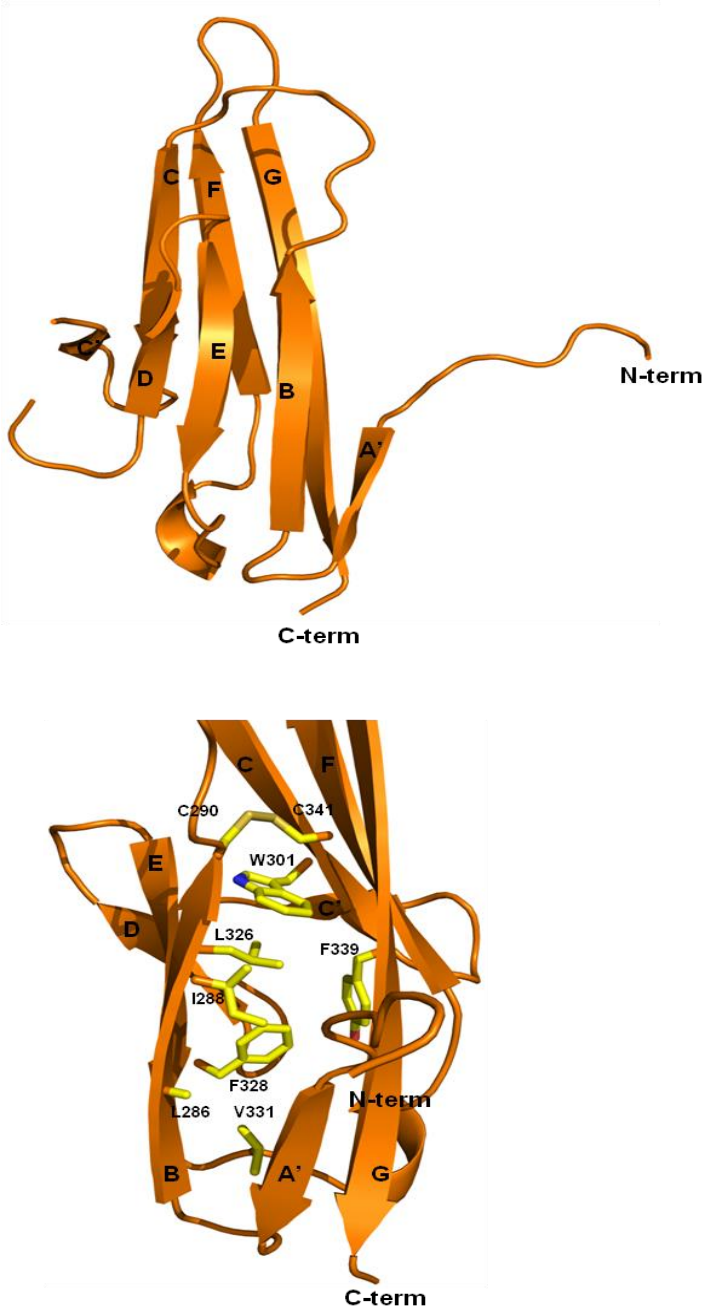

Figure 6.14 Stabilisation of the hAMIGO-1 Ig core.

The beta sheets are stabilised by an inter-chain disulphide bond (mediated by C90 and C341), an invariant tryptophan residue (W301) and multiple non-polar interactions mediated by inward facing hydrophobic residues (labelled) from the core B, E, F and C strands.

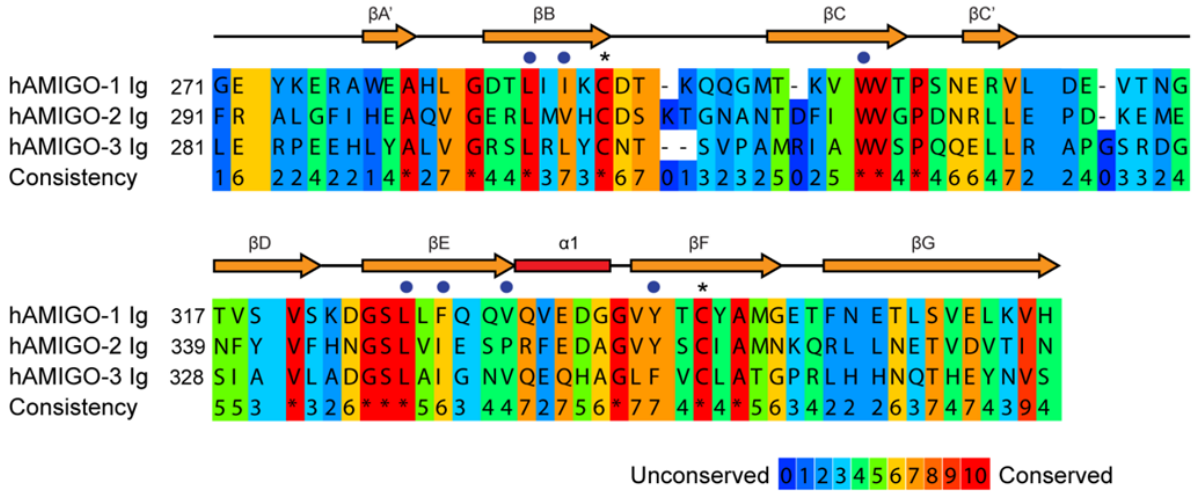

Figure 6.15 Sequence alignment of human AMIGO Ig domain.

Sequences were obtained from Uniprot (accession numbers (hAMIGO-1), (hAMIGO-2) and (hAMIGO-3) and aligned with Praline. The colour scheme of the alignment is for amino acid conservation. The cysteine residues that form an internal disulphide bridge are highlighted (black star). Residues that contribute to stabilising the Ig core are shown (blue circles). hAMIGO-1 Ig structure based secondary structural elements are colour coded (β sheets are shown as orange arrows and helices are highlighted as red rectangles).

6.7.3 Identification of homologous proteins to hAMIGO-1 Ig domain

Similarly, to mAMIGO-1, the hAMIGO-1 LRR–Ig structure reveals an arrangement in which a C2-type Ig domain folds slightly back onto the convex face of a horseshoe-shaped LRR domain. This domain composition is also observed, albeit in a rather more extreme fashion, with the neuronal Nogo-66 receptor-binding glycoprotein LINGO-1 [69] and netrinG ligand 2 (NGL2) [167] (Figure 6.16). These differences could be attributed to the considerably larger LRR-Ig linker regions which allow LINGO-1 and NGL2 to adopt distinct conformations relative to hAMIGO-1. The hAMIGO-1 LRR-Ig linker region (G271-Y273) packs against the LRR domain via non-polar interactions involving Y230, H235 and Y238. In addition, the hAMIGO-1 LRR-Ig interface is further stabilized by multiple hydrogen bonding interactions involving the B-C loop of the Ig domain (D291, T292, K293 and Q295) and the C-terminal regions of the LRR (P185, A210, W211 and R239).

Proteins that were closely related to the hAMIGO-1 Ig domain were identified using the DALI automated structural comparison software [158]. With the exception of mAMIGO-1 (Figure 6.17), the most structurally homologous proteins included neuronal cell adhesion molecule 1 (NCAM1; pdb code 5AEA) [176], LINGO-1 (pdb code 2ID5) [69] and NGL2 (pdb code 3ZYI) [167], with Z scores (conforming to degree of structural identity) of 12.3, 12.0 and 11.4, respectively. Notably, despite displaying very low levels of sequence conservation (> 20 %), all structural homologues adopt a C-type Ig fold [177] and the structure of each can be superimposed onto hAMIGO-1, resulting in an RMSD of 1.37 Å for Lingo-1 (over 77 Cα aligned atoms), 1.47 Å for NGL2 (over 77 Cα aligned atoms) and 1.59 Å (over 82 Cα aligned atoms) for NCAM1 (Figure 6.17**)**. Also, barring NCAM1, each homologue associated with a LRR domain. The highly conserved feature of the Ig domain within LRR-Ig family members

implies that it serves an indispensable function that is yet to be established but most likely involves orientating the LRR modules away from the membrane to facilitate ligand interactions.

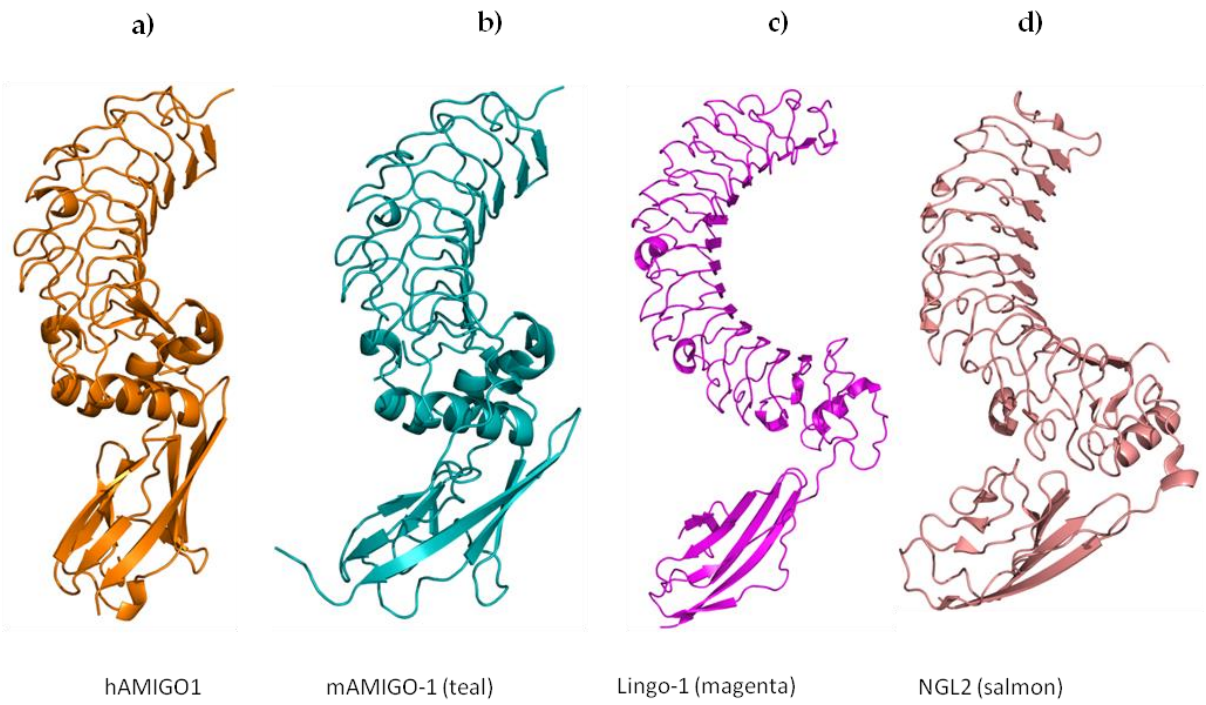

Figure 6.16 Structurally homologous proteins to hAMIGO-1 LRR-Ig.

Proteins homologous to the hAMIGO-1 ectodomain, including LRR and Ig domains, are highlighted. a) hAMIGO-1 (Orange), b) mAMIGO-1 (PDB code 2XOT), c) LINGO-1 (PDB code 2ID5) and d) NGL2 (PDB code 3ZYI). All proteins adopt a banana- shaped fold in their LRR domains. The largest variation is observed in the LRR-Ig linker region which exhibit distinct conformations.

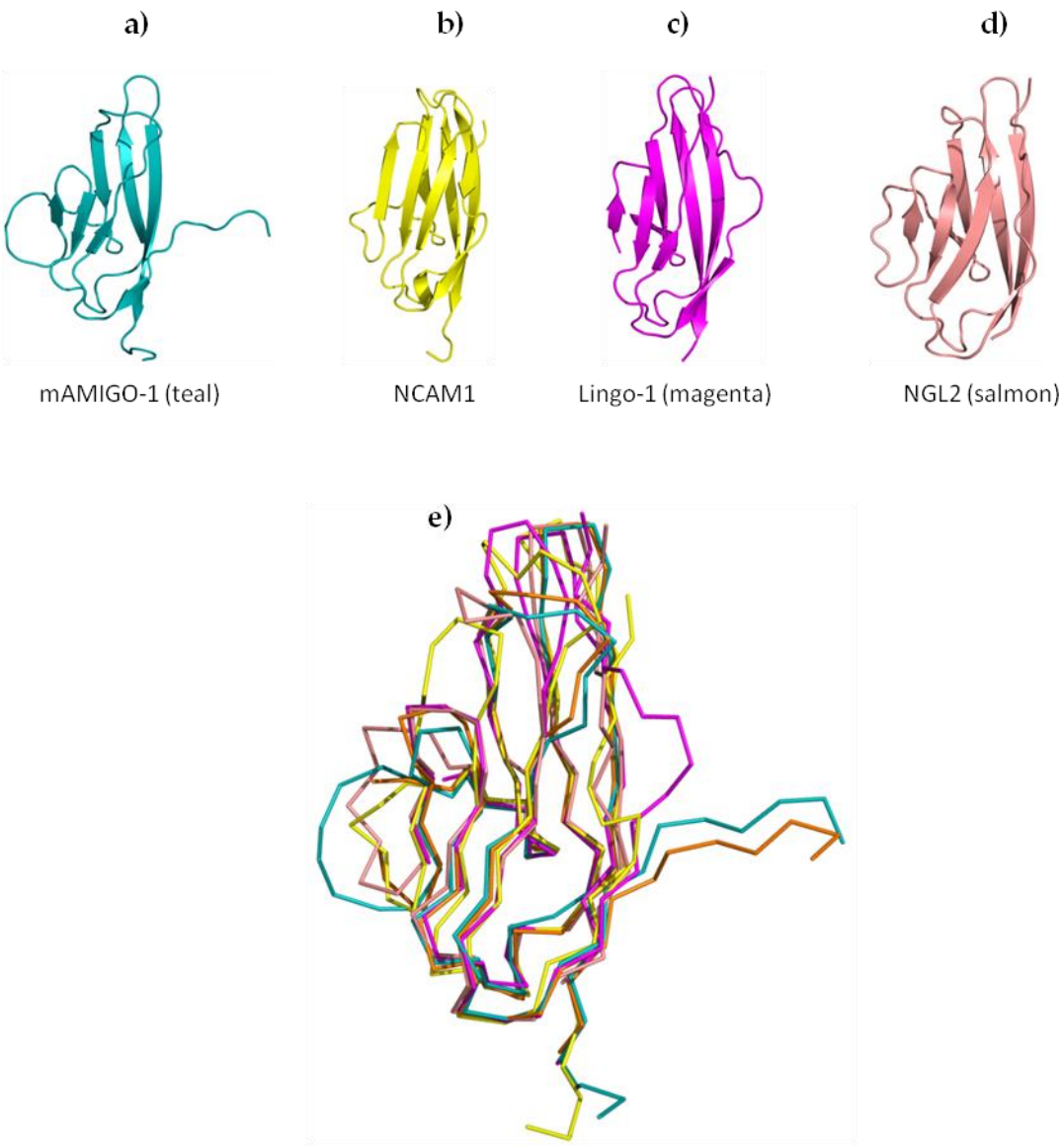

Figure 6.17 Identification of structural homologues for the hAMIGO-1 Ig domain using the Dali server.

Protein Ig domains homologous to the hAMIGO-1 ectodomain identified by DALI analysis are highlighted. a) mAMIGO-1 (PDB code 2XOT), b) NCAM1 (PDB code 5AEA), c) LINGO-1 (PDB code 2ID5) and d) NGL2 (PDB code 3ZYI). Despite low levels of sequence identity the protein domains all adopt a C2-type Ig fold. e) All DALI identified structural homologues superimposed on hAMIGO-1 Ig domain (orange).

6.7.4 Comparison with mAMIGO-1

Structural comparisons between mouse and human AMIGO-1 have demonstrated considerable similarities for the Ig module (Figure 6.18). Indeed, structure-based alignments of the hAMIGO-1 Ig domain with the equivalent region of mAMIGO-1 revealed a RMSD of 1.37 Å (for 80 Cα atoms). The largest structural variation was observed in the loop regions that flank strand D (Figure 6.18a). These differences could be accounted for by crystal packing elements although this region demonstrated considerable sequence variation between the homologues (Figure 6.18b). Consistent with the high levels of sequence identity between the Ig domains of hAMIGO-1 and mAMIGO-1, the electrostatic molecular surface properties were remarkably similar (Figure 6.18c).

6.7.5 Temperature factor analysis of hAMIGO-1 LRR-Ig domain

Temperature factor analysis of the hAMIGO-1 LRR-Ig ectodomain revealed distinct differences in the average main chain B-factors for the LRR domain (33.6 Å^2) and the Ig module (54 Å^2) (Figure 6.19a, 6.19b). The highest B-factors were mapped to residues located near the LRR-Ig linker leading to a paucity of electron density for residues in this region. Interestingly, this difference in the average B-factors between the LRR and the Ig domain was also observed for mAMIGO-1 (26.4 Å^2 and 38 Å^2 for the LRR and Ig domain, respectively; Figure 6.19c, 6.19d), but not for other proteins that exhibit a LRR-Ig fold including LINGO-1 and NGL2. It is possible that within AMIGO-1 the LRR-Ig linker region is highly flexible in the unliganded state but rendered more stable following interactions with ligands such as NgR or p75^{NTR}.

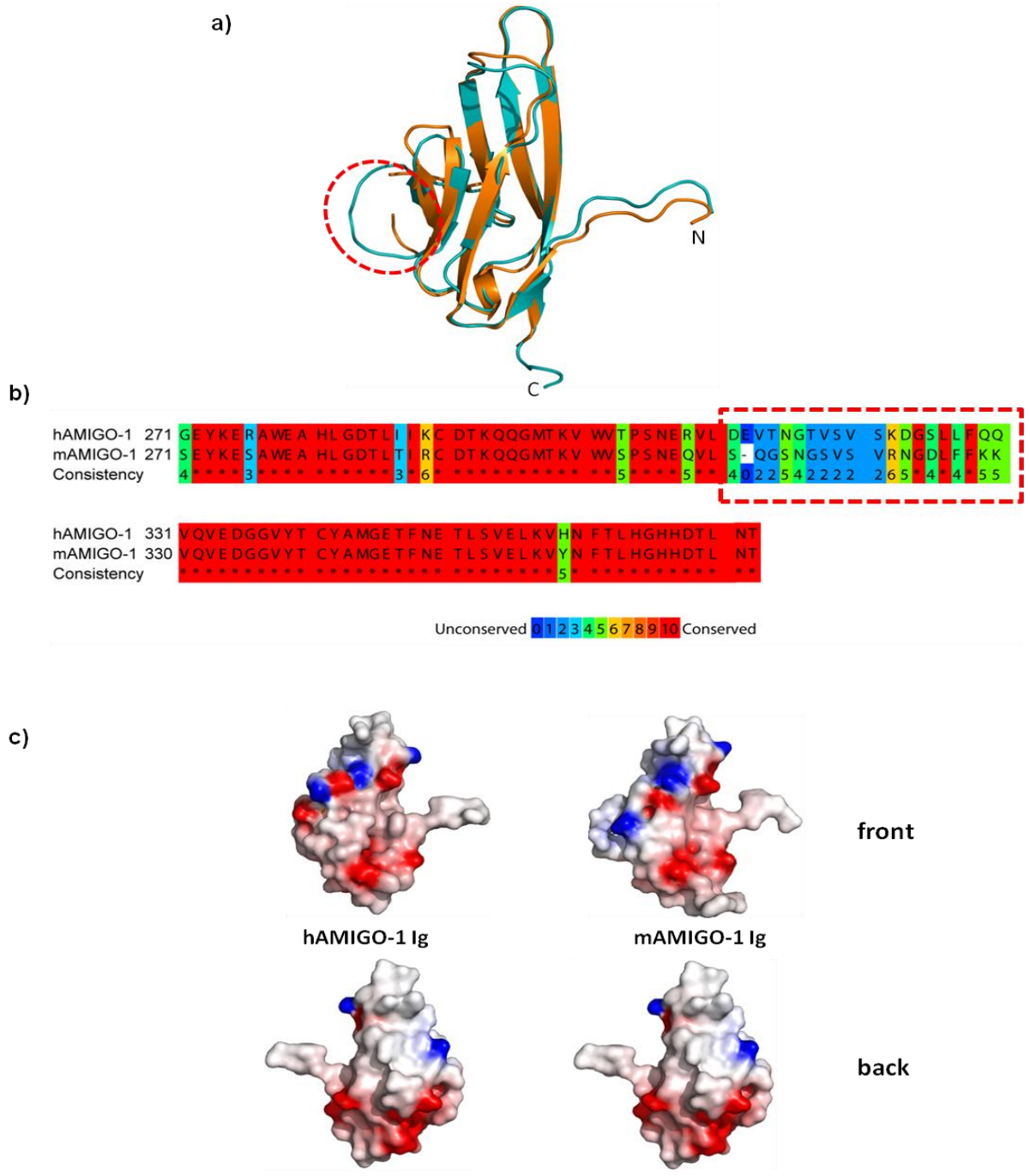

Figure 6.18. Comparison of the human and mouse AMIGO-1 Ig domain.

a) Superimposition of the hAMIGO-1 (orange) and mouse AMIGO-1 (teal) Ig domains. The red dashed circle highlights the area with the largest structural variations. b) Sequence alignment of human and mouse AMIGO-1 Ig domains, interestingly the area which demonstrates most sequence variation (red dashed box) corresponds to the looped region highlighted in a). c) Comparison of the molecular surface electrostatic potentials of human AMIGO-1 and mouse AMIGO-1. The electrostatic potential was calculated using Delphi. The potential scale ranges from -7 (red) to +7 (blue) in units of kT/e. The electrostatic surface properties between the two proteins are remarkably similar.

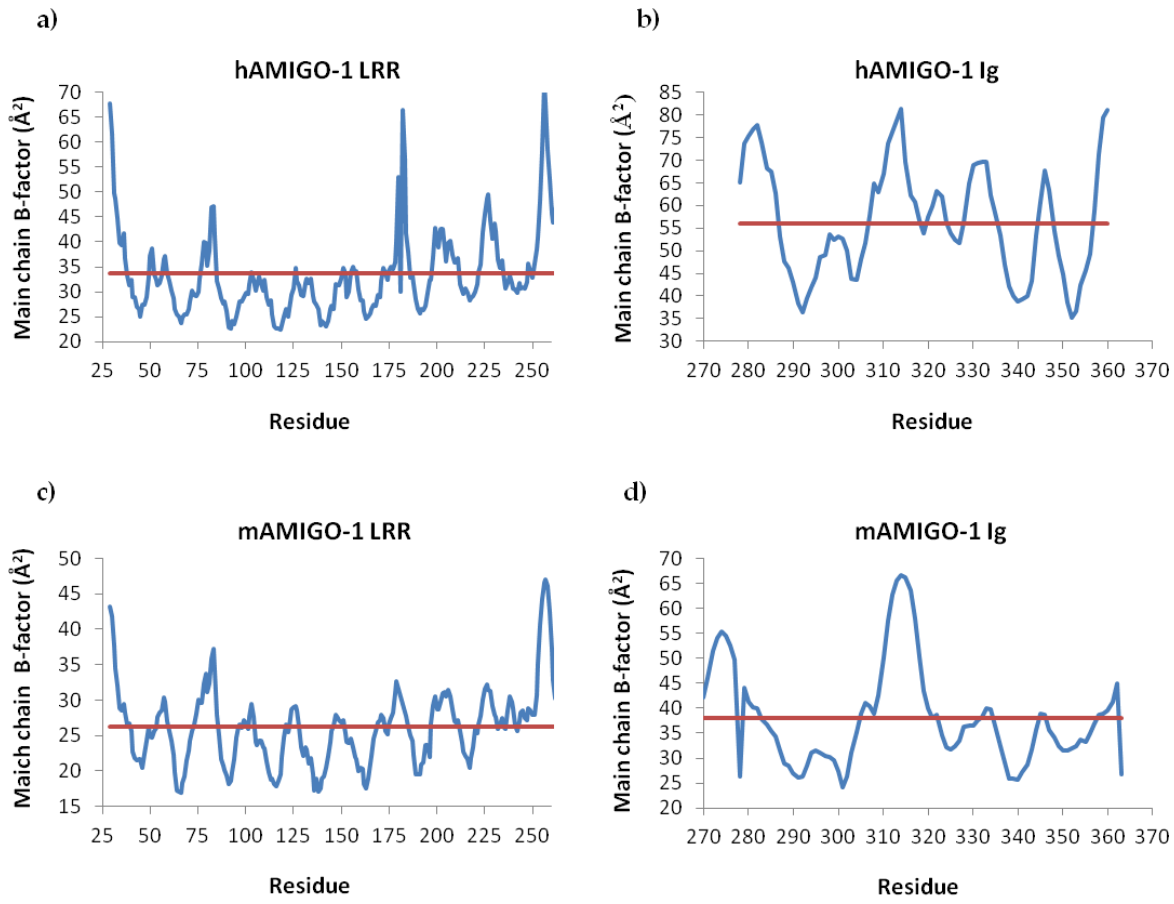

Figure 6.19. Temperature factor analysis of hAMIGO-1 and mAMIGO-1 LRR-Ig domains.

The main chain temperature factors as a function of amino acid residues for the hAMIGO-1 LRR (a), hAMIGO-1 Ig (b), mAMIGO-LRR (c) and mAMIGO-1 Ig (d) domains. The solid red line represents the mean B-factor which comprised of 33.6Å^2 (hAMIGO-1 LRR), 54Å^2 (hAMIGO-1 Ig), mAMIGO-1 LRR domain which are around 26.4Å^2 (mAMIGO-1 LRR) and 38Å^2 (mAMIGO-1 Ig). In both cases the B-factors for the LRR domains are considerably lower than those for the Ig domains.

6.7.6 Electrostatic molecular surface properties of hAMIGO and mAMIGO Ig domains.

Three dimensional models of the hAMIGO-2, and -3 Ig domains were generated with PHYRE using the hAMIGO-1 crystal structure as a modelling template. Despite low levels of sequence identity between the Ig domains of hAMIGO-1 and hAMIGOs-2 and -3 (26-27%), an extremely large degree of structural identity was evident. The majority of the non-conservative amino acid substitutions found in hAMIGOs 2 and 3, when mapped onto the hAMIGO-1 structure, are located on the surface. Hence, the high level of sequence diversity observed in solvent accessible positions suggested the possibility that the Ig domain may not be a conserved feature of NgR/p75 interactions with hAMIGO-1, or may not be directly involved at all. . To evaluate this further, an electrostatic potential map for the hAMIGO-2 -3 models was calculated with DELPHI. Comparison of the surface electrostatics between hAMIGO-1 and hAMIGOs-2 and 3 demonstrated distinct electrostatic properties, particularly on each face of the β-sheet **(**Figure 6.20**).** Similarly, the crystal structure of the Lingo-1 Ig domain, which has previously been implicated in binding NgR [77, 84], demonstrated a distinct surface electrostatics compared with hAMIGO-1 (Figure 6.17).

A similar pattern emerged when examining the primary sequence and electrostatic surface properties of mAMIGO family members. Indeed, sequence comparison of mAMIGO-1 with mAMIGOs 2 and -3 revealed low levels of sequence identity at 21-25% (Figure 6.21). The majority of the non-conservative substitutions were focused on the surface when mapped onto the mAMIGO-1 structure. However, similar to the hAMIGO family, there was a distinct lack of surface electrostatic conservation across the mAMIGO family (Figure 6.21) further leading credence to the notion that the AMIGO Ig domain may not be directly involved in forming a tripartite complex with NgR and $p75^{NTR}$.

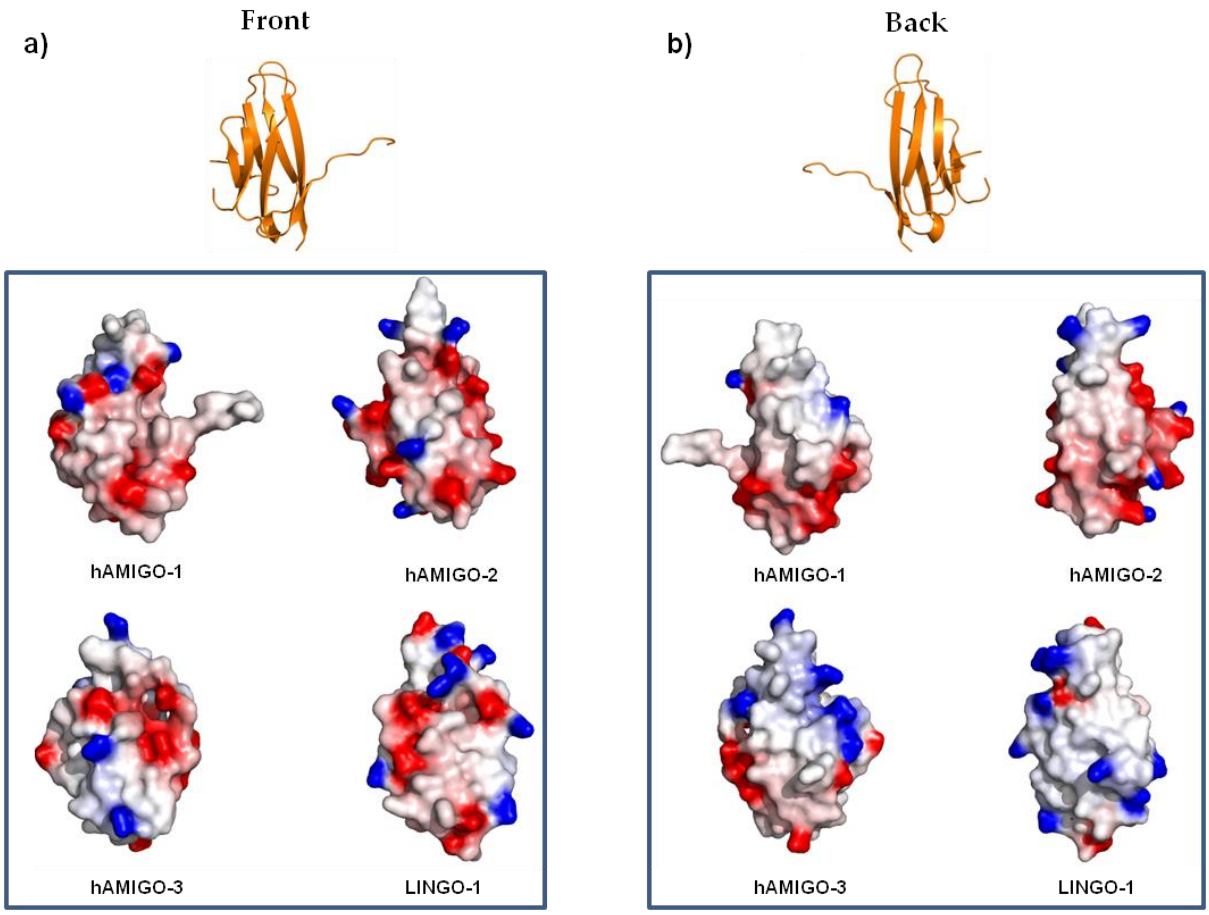

Figure 6.20. Comparison of the molecular surface electrostatic potentials of hAMIGO-1/-2/-3 and LINGO-1 Ig domains.

The molecular models of hAMIGO-2 and hAMIGO-3 were generated using PHYRE and electrostatic potentials were calculated using Delphi. The potential scale ranges from -7 (red) to +7 (blue) in units of kT/e. a) front view, b) rear view. Each Ig domain displays distinct surface electrostatics which highlights the lack of conservation across the protein surfaces.

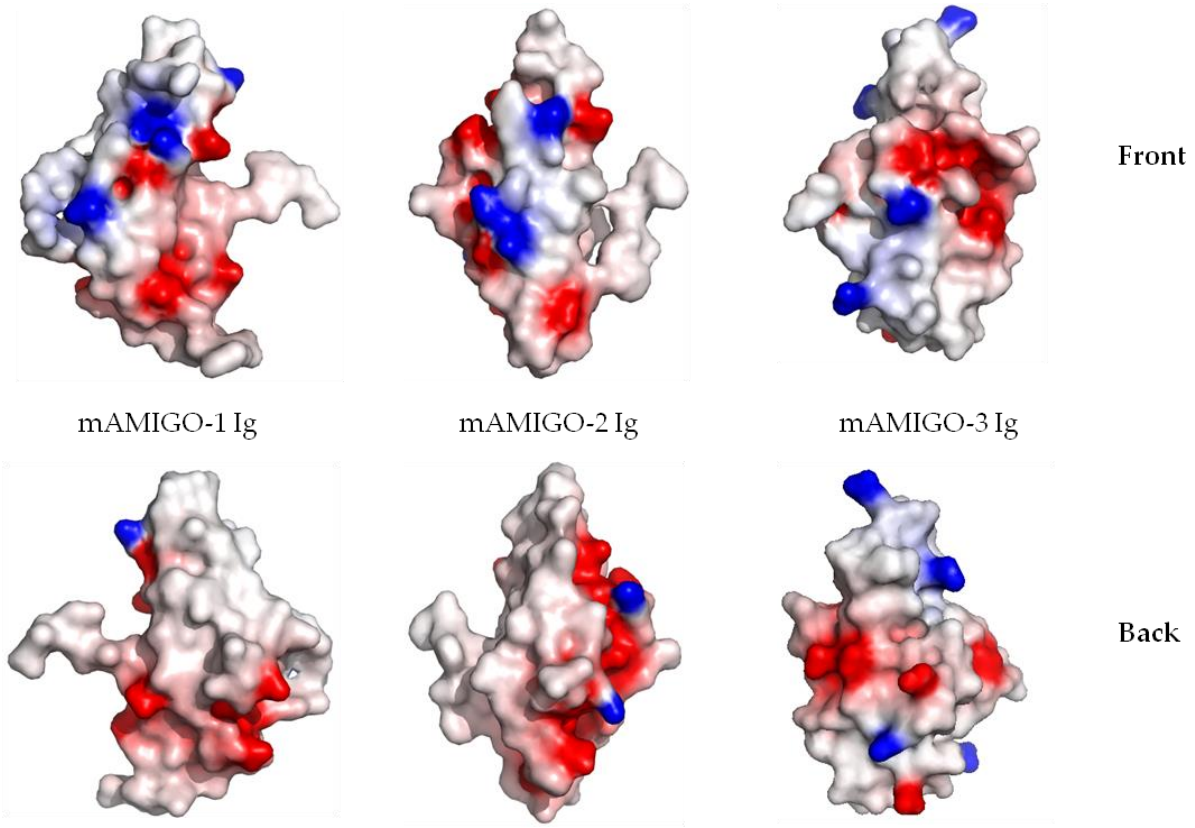

Figure 6.21. Comparison of the molecular surface electrostatic potentials of mAMIGO-1/-2/-3 Ig domains.

The molecular models of mAMIGO-2 and mAMIGO-3 were generated using PHYRE and electrostatic potentials were calculated using Delphi. The potential scale ranges from -7 (red) to +7 (blue) in units of kT/e. Similar to the hAMIGO family, each Ig domain exhibits distinct surface electrostatics highlighting the lack of conservation across the mAMIGO family.

6.7.7 Comparisons with LINGO-1

There are six N-linked glycosylation sites (N144, N202, N264, N274, N293, N341) present within the LRR of LINGO-1 which are likely to restrict surfaces available for interactions between LINGO-1 and its ligand binding partners (Figure 6.22). These sites appear to be conserved across LINGOs 2-4. Although the concave surface of most LRR proteins is used for ligand engagement and/or dimerization [120, 154], N-linked glycans on N293 and N341 in LINGO-1 are expected to block this surface thereby dictating that the convex face represents a potential site for binding (Figure 6.22). It is anticipated that this will also hold true for LINGOs 2–4. More recent studies have suggested that the Ig domain is important for NgR binding based on domain deletional mutagenesis of the LINGO-1 ectodomain [84]. Furthermore, intact LINGO-1 ectodomain constructs incorporating the RKH to EKV mutation within the Ig domain prevented MBP expression in OPC differentiation studies when trying to identify functional epitopes in the LINGO-1 ectodomain. . Interestingly, the RKH sequence motif is not only absent in LINGOs 2-4 but also from the AMIGO family (Figure 6.22).

The predicted N-linked glycosylation sites on hAMIGO-1 LRR-Ig ectodomain may also provide hints as to which region of the exterior surface is likely to recognise NgR and $p75^{NTR}$. In total there are 5 predicted N-linked glycosylation motifs in the hAMIGO-1 ectodomain; two in the LRR domain (N72 and N264) and three in the Ig module (N315, N349 and N360). Interestingly, N-linked glycans on N72 and N264 are distal to the putative ligand binding site identified on the convex surface and therefore unlikely to interfere with ligand engagement (Figure 6.23). The 3 predicted N-linked glycosylation sites present in the Ig domain would likely prevent this domain from being able to form protein-ligand interaction. Also, the predicted LRR N-linked glycans of hAMIGO-2 (N58 and N104) and hAMIGO-3 (N107) can be

mapped on to the convex face suggesting that these surfaces do not contribute to protein-protein interactions. Furthermore, the Ig domains of hAMIGO-2 and hAMIGO-3 are likely to be heavily glycosylated as they exhibit 6 and 4 predicted N-linked glycosylation motifs, respectively.

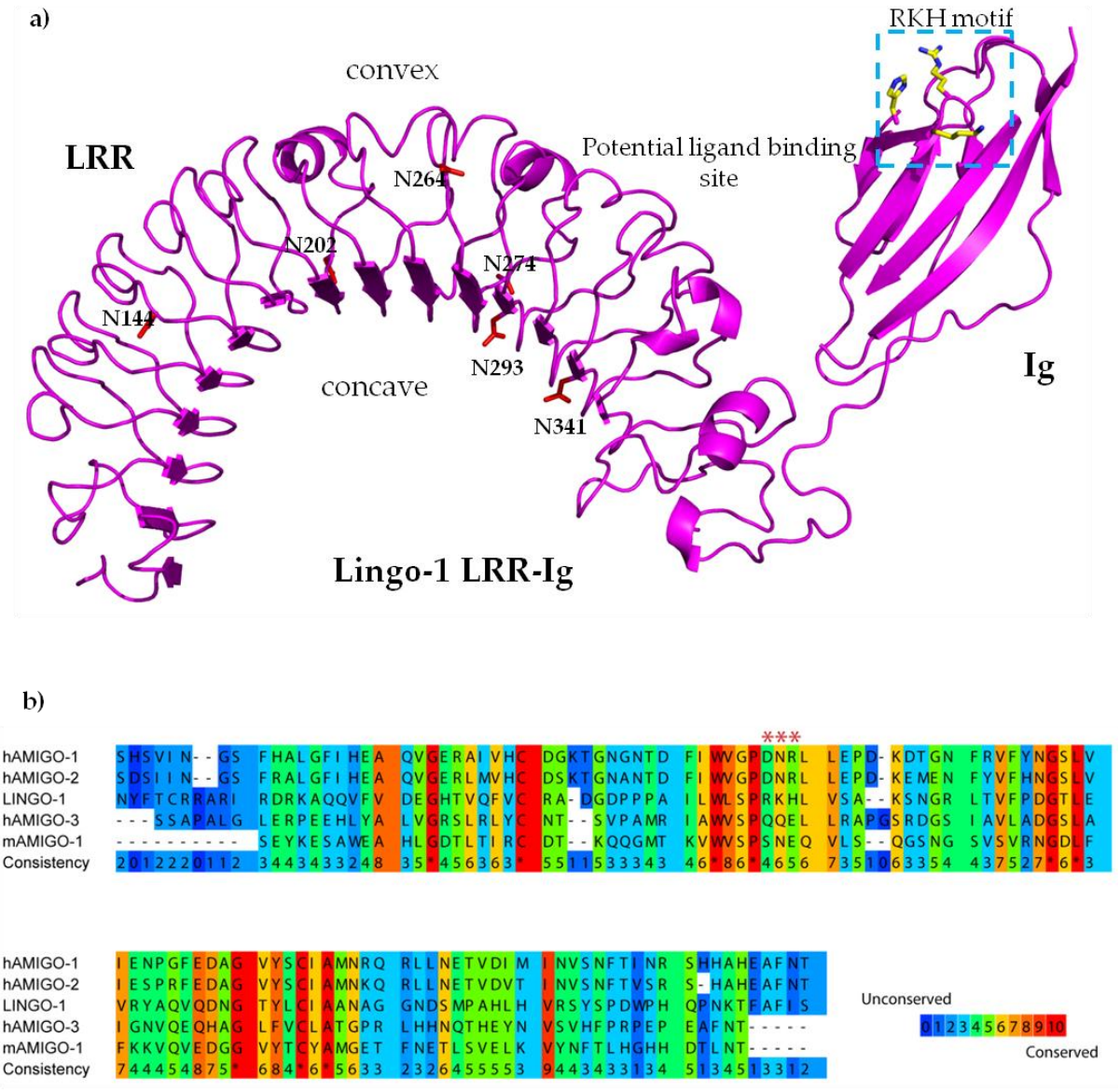

Figure 6.22. Comparison of AMIGO-1 and LINGO-1 ectodomains.

a) The LINGO-1 ectodomain including LRR and Ig domain with N-linked glycosylation sites mapped on. Two N-linked glycosylation sites are located on the concave face of the LRR domain indicating that this area is unavailable for ligand binding. The RKH motif in the Ig domain is also highlighted (blue box), which has been identified as being necessary for binding to NgR [77].

b) Sequence alignment of hAMIGOs-1/-2/-3, LINGO-1 and mAMIGO-1. The RKH motif is highlighted with red asterisks; these residues are not conserved between LINGO-1 and any of the AMIGO family of proteins, mouse or human.

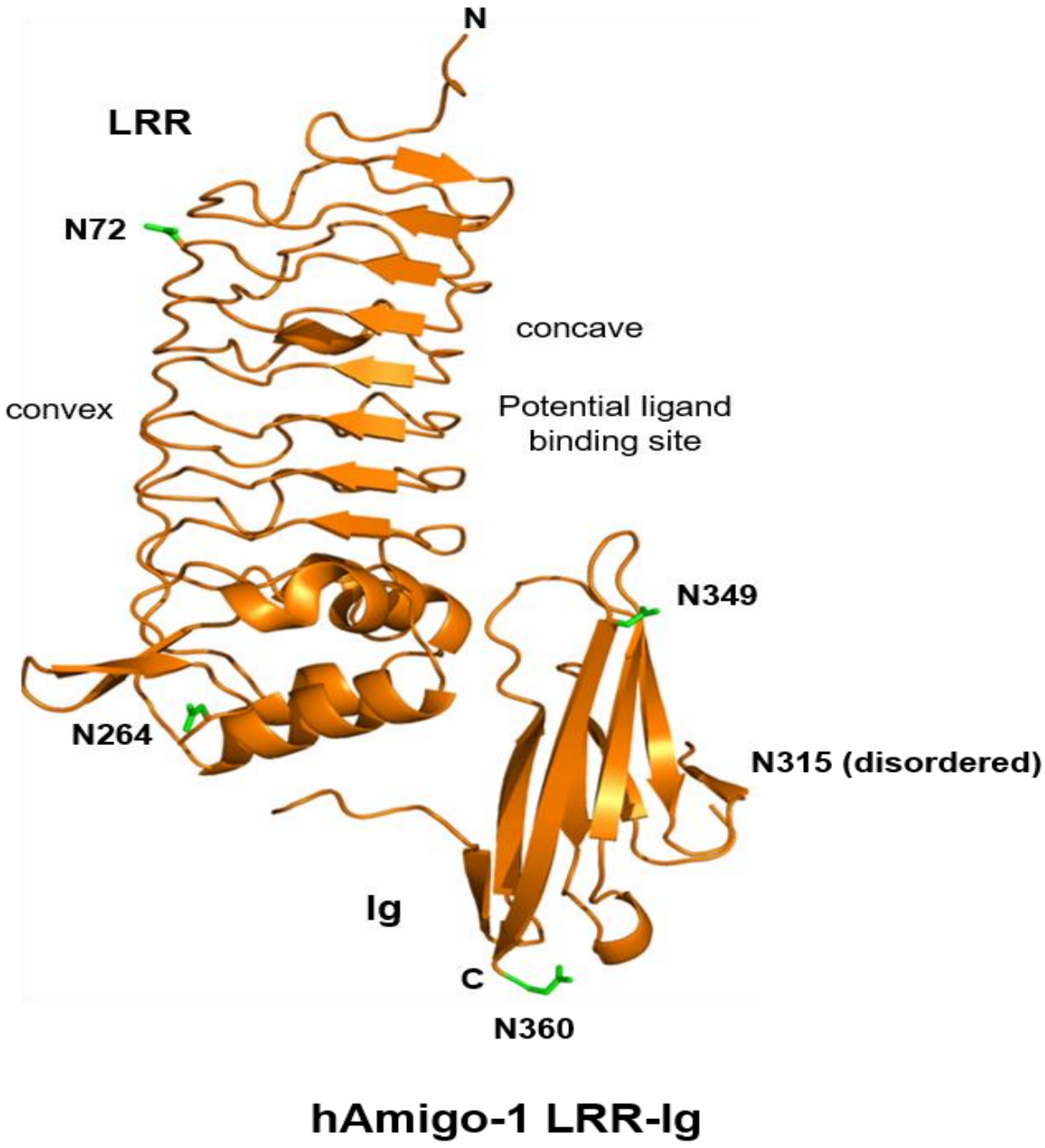

Figure 6.23. The hAMIGO-1 ectodomain with N-Linked glycosylation sites mapped.

The hAMIGO-1 ectodomain including LRR and Ig domain with N- linked glycosylation sites mapped in green. Two N-linked glycosylation sites (N72 and N264) are located on the convex face of the LRR domain indicating that this area is likely to be unavailable for ligand binding. Three other N-linked glycosylation sites (N315, N349 and N360) are located on the Ig domain. N-linked glycosylation site N315 is located within the C′-D loop which is disordered.

N-linked glycosylation sites present on AMIGO-2 (N58, N104, N281, N288, N345, N373 and N381 and AMIGO-3 (N107, N272, N301, N362 and N368) can also be modelled onto their predicted structures. In both cases, the N-linked glycosylation sites are either on the convex face of the LRR domain or on the Ig domain indicating, that similar to AMIGO-1, the concave face represents the most likely ligand binding site.

6.8 Discussion

In this chapter protein-protein binding assays and structural techniques were used to probe interactions of key components of the NgR receptor complex.

6.8.1 BIAcore

A key aim was to establish whether the AMIGO proteins studied in chapters 3-5 are able to interact directly with NgR via their ectodomain regions, as has been demonstrated for LINGO-1, and as immunoprecipitation results suggested in Chapter 5. The BIAcore studies first established an experimental system involving immobilisation of recombinant NgR protein to a streptavidin-coated chip surface, via a site specific biotinylation incorporated into a C-terminal tag. In contrast to other approaches tried, this enabled oriented coupling, enabling interactions between NgR and putative partners in the Nogo receptor complex, LINGO-1, and the AMIGO family proteins, to be tested.

These BIAcore experiments provided the first unequivocal evidence that AMIGO proteins directly interact with NgR, and indicate the AMIGO ectodomains are involved in such NgR/AMIGO interactions. In doing so, they provide independent validation of the IP experiments in chapter 5, which suggested AMIGO proteins associate with NgR, and extend the findings by establishing a direct interaction. Specifically, both AMIGO-1 and AMIGO-3 bound immobilised NgR, and LINGO-1 was also confirmed as capable of directly binding immobilised NgR. Unfortunately, data on AMIGO-2 were not collected, as recombinant AMIGO-2 was not successfully produced using the *Drosophila*-based expression system employed. Similarly, binding to $p75^{NTR}$ could not be tested satisfactorily, as the recombinant protein was poorly expressed. In addition, despite detecting both AMIGO and LINGO-1 interaction with “in-house” recombinant NgR, commercial NgR-Fc and $p75^{NTR}$ both failed to interact with these target proteins. These observations underline the importance of high quality

recombinant proteins for meaningful direct protein-protein binding assays. The reasons why AMIGO-2 and $p75^{NTR}$ were not successfully expressed in the *Drosophila* expression system are unclear, but could include misfolding, and/or the requirement for human-specific glycosylations.

Although this was not the primary aim, in principle, the experimental BIAcore system established could be exploited to shed further light on NgR/ligand interactions. One possibility would be to develop it further to carry out quantitative measurements of NgR/ligand interactions and determine affinity and kinetic measurements. This was not carried out largely due to time constraints. Notably, affinity measurements have been reported previously for LINGO-1/NgR interaction [69] (K_d of ~1μM), although the activity levels of immobilised NgR was extremely low in this study, and far higher in the experimental system I established; AMIGO/NgR interaction has not previously been tested by BIAcore and the affinity of such interactions is unclear. Future experiments to determine affinities could include equilibrium binding. Although higher concentrations of LINGO-1/AMIGO injections reached equilibrium, suggesting such approaches might be feasible, some sticking to flow cell surfaces was observed – likely resulting from protein aggregation under these conditions. These could be eliminated by size exclusion chromatography, after which much less sticking was observed, however the low concentrations meant that binding responses did not reach equilibrium, and therefore kinetic analyses might be preferable in order to determine K_d values. Although kinetic measurements would have been interesting, these can be time-consuming to obtain robust measurements and other workpackages, some of which required large amounts of recombinant protein (like NgR/LINGO and NgR/AMIGO complex trials) were prioritised over these experiments. However, in the future, kinetic measurements would require high flow rates and low levels of immobilised ligand (NgR) in order to eliminate mass transport effects that limit efficient delivery of analyte to (or removal from) the surface, artefactually constraining the

kinetic constants measured. This may be of interest in the future, and might potentially allow AMIGO-1/-2/-3 affinities/kinetics for NgR to be correlated with functional potency in the Nogo receptor complex.

A second possible use of the system would be to use it in conjunction with mutational studies on NgR and AMIGO/LINGO-1 proteins to test hypotheses regarding NgR/ligand binding modes. These would include testing the hypothesis (Chapter 4) that AMIGO proteins use the concave face of their LRR domain to interact with NgR. Site-directed mutants could be selected based on their amino acid type, phylogenetic conservation and location on the surface of the domain. The mutant proteins could be expressed and their ability to bind NgR (and also $p75^{NTR}$ if direct binding could be established) could be assessed by BIAcore and parallel functional assays. Initially, it would also be beneficial to produce whole domain deletion mutants to assess if the Ig domain of AMIGO-1 is redundant or critical for binding to NgR and $p75^{NTR}$. More in-depth analysis would follow, by selecting a residue or group of residues to mutate in order to pinpoint a ligand binding site. In determining where to commence these more in depth mutational studies it would be prudent to start at the concave face which we have suggested is the most likely ligand binding site.

6.8.2. Co-crystallisation and Structural studies

Structural studies initially aimed to determine the crystallographic structure of AMIGO/NgR complex, with a series of co-crystallisation trials. Although crystals were obtained from AMIGO-1/NgR trials, a lack of molecular replacement solutions for NgR in the processed data, combined with a successful solution for AMIGO-1 LRR, suggested the crystals may only contain AMIGO-1. Initial inspection of electron density maps indicated unaccounted for

density that appeared to be the AMIGO-1 Ig domain. The favourable statistics for refinement of a protein model consisting solely of AMIGO-1 LRR-Ig confirmed that the crystals had resulted from selective crystallization of the AMIGO-1 LRR-Ig from the AMIGO-1/NgR complex trial conditions. This ultimately resulted in structure determination of the full-length AMIGO-1 ectodomain including the LRR and Ig domain to 1.9Å. In Chapters 3 and 4, the Ig domain of AMIGO-1 was cleaved under crystallization conditions meaning only the structure of the LRR domain was determined. One possibility is that the presence of NgR in the crystallization trials helped to stabilize the AMIGO-1 protein ectodomain, preventing cleavage of the Ig domain. However, other possibilities, such as differences in buffer composition or contaminants from the NgR preparation inhibiting proteases responsible for cleaving the AMIGO-1 LRR-Ig domain cannot be excluded. It is also unclear why AMIGO-1 selectively crystallised rather than crystallising as complex with NgR as intended, however this might conceivably relate to AMIGO-1 LRR-Ig intermolecular protein-protein interactions being particularly favourable. Given more time for additional recombinant protein production, more efforts could have been devoted to obtaining either AMIGO-1/NgR or LINGO-1/NgR complexes. Despite this, the full length AMIGO-1 LRR-Ig domain structure provided additional information relative to the AMIGO-1 LRR structure.

The full length, LRR and Ig domain containing structure, like the LRR domain structure, is a dimer in crystallographic form. The Ig domain is a C2- type Ig domain containing a large hydrophobic core which helps stabilise the domain with hydrogen bonding and a disulphide bridge also contributing. Temperature factor analysis of the hAMIOGO-1 ectodomain demonstrates differences between the LRR and Ig domain components with higher B factors seen in the Ig domain and the highest B factors observed in the linker region, indicative of

increased flexibility. Therefore, it is possible that there is considerable flexibility in LRR-Ig linker under physiological conditions, and this may allow AMIGO-1 to accommodate different ligands, such as NgR and $p75^{NTR}$. Consistent with this, conformational flexibility has been observed with mAMIGO-2 based on SAXS analysis [120]. Furthermore, the finding that the hydrophobic core residues of AMIGO-1 Ig are conserved across AMIGO-2 and -3, whereas non-conservative substitutions are predominantly surface localised, suggests a conserved core structure of this domain across the AMIGO family, but also hints that the electrostatically diverse Ig domain surfaces may have a limited role in binding to NgR. Interestingly, LINGO-1 does not share the same pattern indicating the protein has a less flexible Ig domain despite the fact the linker region is shorter in AMIGO-1 than LINGO-1.

Among the more interesting structural findings was the location and orientation of predicted N-linked glycosylation sites on the hAMIGO-1 ectodomain, which may provide hints as to which region of the exterior surface is likely to recognise NgR and $P75^{NTR}$. In total there are 5 predicted N-linked glycosylation motifs in the hAMIGO-1 ectodomain; two in the LRR domain (N72 and N264) and three in the Ig module (N315, N349 and N360). Previously in chapter 4, it was shown that the N-linked glycans on N72 and N264 were located on the convex face of the LRR domain, distal to the putative ligand binding site identified on the concave surface (see chapter 4). In addition, comparable predicted N-linked glycans on the LRR of hAMIGO-2 (N58 and N104) and hAMIGO-3 (N107) were also mapped on to the convex face. The full length LRR and Ig domain containing structure of AMIGO-1 reveals the localisation of these sites with respect to the Ig domain, and also reveals the likely orientation of N-linked glycosylations on the Ig domain itself (N315, N349 and N360). N-linked glycosylation sites on the Ig domain (N315, N349 and N360) were distal to the concave face of

the LRR domain, but oriented in different directions. This is consistent with the idea that the concave face of the AMIGO-1 ectodomain is used for binding and is also consistent with the idea that the Ig domain may play a limited role in ligand interactions.

Crystallographic studies also shed light on the key question of which region of hAMIGO is responsible for binding NgR and $p75^{NTR}$. Sequence analysis of the hAMIGO-1 Ig domain reveals very low levels of sequence identity compared to other family members. However, the minority of conserved amino acids were preferentially localised to the hydrophobic core. In contrast, the surface of the Ig domain preferentially comprises residues that are chemically distinct between each AMIGO family members, suggesting the Ig domain is highly unlikely to form a common ligand binding site. In contrast, the concave exterior surface of the LRR module, which unlike that of LINGO-1 is devoid of N-linked glycosylation sites, contains a region of evolutionarily conserved patches of charged residues, possibly suggestive of common ligand binding sites. It is therefore possible that LINGO-1 and the AMIGO proteins use distinct regions of their homologous domains to achieve comparable functions in hindering neuronal regeneration. In the last decade LINGO-1 binding to NgR1 and $p75^{NTR}$ to form the inhibitory tripartite LINGO-1–NgR1–$p75^{NTR}$ signalling complex through RhoA activation has been subject to in-depth investigation [52, 68, 69, 178]. Indeed, epitope mapping data, which employed ELISA assays to study which domains of LINGO-1 were involved in ligand interactions, revealed that individual LINGO-1 LRR- and Ig constructs bound NgR1 with relatively lower affinity (EC50 values of 120 and 60 nM, respectively) compared to the full-length ectodomain (EC50 value of 6nM). In addition, mutation of an RKH-to-EKV motif within the Ig domain of the intact ectodomain (residues 462-464) led to a 20-fold reduction in EC50, suggesting that the RKH within the Ig domain contributes to the binding [77]. Bourikas

et al. (2010) [84] also used domain truncation analysis to map binding of $p75^{NTR}$ and demonstrated that the LINGO-1 LRR module was not essential for the inhibitory actions of the protein but that the Ig domain and stalk region were sufficient in inhibiting oligodendrocyte progenitor cell (OPC) differentiation. While these studies may shed some light on LINGO-1/ligand interactions, the crystallographic data presented here indicate that the AMIGO proteins may use a completely different binding mode (relative to LINGO-1) to bind ligands, employing the concave rather than the convex surface of the LRR domain. Based on the evidence provided, we suggest that it is most likely that the AMIGO family of proteins bind ligands using their concave faces, similar to the majority of LRR domain containing proteins. In contrast, it is less clear which face of LINGO-1 is most heavily involved in ligand engagement.

Finally, recent studies have shown that rat AMIGO-3, an LRR- Ig domain containing protein implicated in CNS axon growth inhibition, also forms NgR–$p75^{NTR}$ and NgR–Troy signalling complexes [107]. I have shown in Chapter 5 that human AMIGO- 1 and -3 co-localise, based on IP analysis, with NgR and $p75^{NTR}$ in cell membranes. In this chapter, I was able to confirm direct AMIGO-1/-3 interaction with NgR via BIAcore technology. Unfortunately, I was unable to concentrate AMIGO-3 to high enough levels to allow crystallography studies, due to the instability of the protein at high concentrations, despite solubility screens giving clues as to an appropriate buffer for the protein. As mentioned previously, limited proteolysis was used to enable crystallisation of LINGO-1 [69], this established method could be employed in the future to facilitate crystallisation of hAMIGO-3.

Collectively, these results now provide a detailed framework for future structure-function studies aimed at assessing the physiological relevance of AMIGO-mediated protein-protein interactions to axon regeneration inhibition.

Chapter 7

Overall Discussion

Overall Discussion

7.1. Understanding the role of the AMIGO family in the Nogo receptor complex

Central Nervous System tissues exhibit only limited regeneration after tissue injury resulting from trauma, stroke or inflammatory conditions (such as Multiple Sclerosis). The key constraints on CNS regeneration and the underlying molecular mechanisms have emerged in the last decade, involving myelin derived breakdown products, such as the "Nogo" protein, transmitting potent anti-regenerative signals to adjacent neurons by binding to a tripartite receptor complex comprised of NgR, $p75^{NTR}$/TROY and LINGO-1 on the neuronal cell surface. Disruption of the NgR inhibitory signalling axis *via* either antibody approaches or small molecule inhibitors represents a major therapeutic avenue for potentiating CNS regeneration after injury or disease. However, inhibition of LINGO-1 alone does not completely reverse neuronal inhibition [68, 73, 74] and it has been suggested that the AMIGO proteins may also be critical in modulating the negative response to regeneration after injury. However, a comprehensive understanding of the molecular basis of human AMIGO receptor function is currently lacking, but is likely to be critical to such efforts. In this thesis, I investigated the hypothesis that AMIGO proteins are key members of the NgR complex, and carried out molecular, structural and cellular experiments to probe both the involvement of AMIGO proteins in the complex, and the underlying molecular mechanisms.

7.2. Structural studies on AMIGO-1

In Chapters 3 and 4 I employed X-ray crystallography to shed light on the structure of AMIGO-1, which culminated in solving the structure for the LRR domain of AMIGO-1. The resolution of the structure (2.4Å) was sufficient to allow detailed structural comparisons with other proteins, to analyse involvement of surfaces in oligomerisation, and to assess molecular surface properties that might be involved in ligand binding interactions.

Aside from establishing a domain architecture for the AMIGO-1 LRR domain broadly in keeping with those of other LRR proteins, two key findings emerged from this work. Firstly, the structure supported the idea that AMIGO-1 is a dimer, as it highlighted a dimer interface within the crystal. As outlined in chapter 4, several reasons suggest this dimer is physiologically relevant, not least the substantial size of the interface region, the conservation of amino acids involved across AMIGO family members and in LINGO-1, and also the observation that the size exclusion profile of AMIGO-1, which is consistent with a dimeric oligomerisation state. These considerations support the idea that human AMIGO-1 can form a dimer that is biologically relevant, although its precise role in engagement of ligands is currently unclear.

A second key area the structure has contributed to is consideration of which areas of AMIGO-1 might be involved in engaging ligands. A substantial body of studies on LRR proteins has established that ligand engagement often occurs via the concave face of the LRR domain, and electrostatic analyses of the structure suggests this may also be the case for AMIGO-1, highlighting notable electronegative patches on the concave face of the molecule, in contrast to a somewhat electrostatically featureless convex face. Consistent with involvement of the

concave face of the molecule, N-linked glycosylation sites on the LRR domain mapped to the convex face, leaving the concave face unhindered for potential protein-protein interactions. Importantly, the electronegative patches observed on this concave face were not only distinct from those residues involved in AMIGO-1 dimerisation, but were also conserved strongly across the AMIGO family. These observations provide strong circumstantial evidence for the importance of the concave face of AMIGO-1 in ligand interactions, and suggest that this involvement is likely to apply to other AMIGO proteins.

Although I was not able to test these hypotheses in the work presented in this thesis, the availability of the hAMIGO-1 structure can now facilitate a number of experiments to address whether they are correct. To systematically evaluate whether any of the proposed AMIGO-1 ligand binding residues are critical (or to probe importance of the AMIGO-1 dimerisation site) directed mutagenesis could be used to generate a series of hAMIGO-1 mutants, each incorporating a specific point mutation, and assessed for binding candidate partners using either immunoprecipitation methods in whole cells (see Chapter 5 discussion below) , or using a direct protein-protein assay such as SPR (see Chapter 6 discussion). These analyses would identify and define the limits of such functionally important 'hot spot' regions, including residues highlighted as important for AMIGO-1 dimerisation and putative ligand binding regions, and in doing so provide further insights into how hAMIGO-1 recognition of binding partners might modulate neuronal regeneration. In addition, where structures of partner candidate ligands are available, approaches such as computational docking might provide useful hypotheses around which to plan such mutagenesis studies.

7.3. Characterising involvement of AMIGO proteins in the NgR complex

In Chapter 5, I extended my approaches to a set of cellular experiments aimed at directly assessing the involvement of AMIGO proteins in the NgR complex. Initial expression studies successfully achieved expression of AMIGO- 1,-2 and -3 in HEK293T cells, and also highlighted a novel cleavage product for AMIGO-2.

Subsequent cell fractionation studies were then carried out, and confirmed that the AMIGO proteins are present in cell membranes. Although this would be expected given they are type I transmembrane glycoproteins, this finding is important because as both NgR and $p75^{NTR}$ are membrane-associated, localisation to membranous compartments is likely to be a prerequisite for physiological association with either protein as part of the NgR complex. In addition, the finding that LINGO-1 was mainly cytoplasmic supports previous findings on LINGO-1 [126], and raises questions as to which subcellular compartments are involved in mediating LINGO-1 association with $p75^{NTR}$ and NgR.

Arguably the most important set of findings were based on immunoprecipitation assays applied to HEK293T cells expressing various combinations of AMIGO proteins and NgR complex components, utilising recombinant tags, namely FLAG and HA. These studies have provided the first evidence that each individual human AMIGO family member is able to interact with both NgR and $p75^{NTR}$. These findings are potentially important, particular given the observation that following injury, expression of AMIGO family members (eg AMIGO-3) can be increased to levels that are substantially higher than LINGO-1 in rat neuronal injury models. However, various caveats should be noted, particularly the use of overexpression systems and tags, which can potentially affect localisation of transfected components, and

could conceivably lead to artefactual results. Attempts were made to use AMIGO-specific mAbs to detect these interactions in human tissue samples, however the results were somewhat ambiguous and clearly further studies are required in this area. In addition, immunoprecipitation approaches provide little information about whether interactions detected are direct or whether they are indirect. To resolve this, direct protein-protein binding assays are more informative and this was part of the reason for developing SPR-based approaches to directly test AMIGO/NgR/p75^{NTR} interactions, as outlined below in relation to Chapter 6.

One promising avenue for future studies would be to combine the immunoprecipitation approaches developed in this chapter to assess AMIGO/NgR/p75^{NTR} interactions, with structurally informed mutagenesis approaches (see above). This could help confirm which regions of AMIGO-1 (or other family members) are important for interactions with either NgR or p75^{NTR}, and could reciprocally be used to identify regions of NgR or p75^{NTR} that might also be involved in NgR complex interactions.

A second important development would be to address whether AMIGO interactions with NgR complex proteins could mediate Nogo receptor signalling in response to myelin breakdown products. In principle this is relatively feasible and would exploit identical co-expression systems developed in this chapter with commercially available Rho signalling assays following exposure to myelin-associated inhibitory proteins. Attempts were made to establish these assays, however despite the fact they have been successfully applied to confirm the contribution of rat AMIGO-3 proteins to NgR complex signalling [107]; unfortunately substantial background signals were evident, precluding their use on the human AMIGO

proteins I have focussed on. However, additional efforts focussed on establishing systems with which to validate the importance of human AMIGO proteins to NgR complex signalling are clearly warranted.

7.4. Understanding AMIGO/ligand interactions in the NgR complex

Following my studies that highlighted human AMIGO proteins could be co-immunoprecipitated with both NgR and $p75^{NTR}$, I exploited surface plasmon resonance (SPR) to test whether these associations were the result of direct protein-protein interactions. A significant achievement was to establish an experimental system that enabled oriented coupling of NgR components, facilitating detection of ectodomain interactions. Importantly this enabled me to both confirm direct interaction of LINGO-1 ectodomain with NgR, and also to establish for the first time that AMIGO-1 and AMIGO-3 are able to interact directly with NgR. Unfortunately, poor expression of both $p75^{NTR}$ and AMIGO-2 precluded interactions with these proteins being analysed.

While these experiments were important in both confirming the co-immunoprecipitation results outlined in Chapter 5 and establishing direct AMIGO/NgR interactions, future studies could extend these findings by exploiting the BIAcore experimental system established to carry out quantitative measurements of the relevant interactions, including affinity and/or kinetic measurements. In addition, as highlighted earlier, SPR could be combined with mutagenesis approaches to define which regions of the AMIGO-1/-3 and LINGO-1 proteins are involved in NgR interaction, and to define regions of NgR involved. The importance of AMIGO-1 residues involved in dimerization could also be probed using this approach. Parallel information on the relative potency of the proteins in NgR complex signalling would

also be desirable (see above) and could be correlated with affinity and kinetics of the underpinning interactions.

Having established direct AMIGO/NgR interaction using SPR, a key additional aim was to carry out co-crystallisation experiments with the aim of determining an AMIGO/NgR complex structure. These efforts were focussed on AMIGO-1, and yielded crystals, although these ultimately transpired to contain only AMIGO-1, illustrating the challenge of successful complex crystallisation. Nevertheless, the structure obtained is the first structure of the complete ectodomain of human AMIGO-1 (Chapter 4 described the structure of the LRR domain alone), and allowed the LRR and Ig domain components to be analysed in the context of each other. Importantly, the AMIGO-1 LRR-Ig protein remained a dimer in the crystal, consistent with the suggestion that AMIGO-1 dimers may be physiologically important. Notably, the core of the Ig domain, but not its surface amino acids, was conserved across the AMIGO family, suggesting the Ig domain may have a limited role in engaging ligands. In addition, the full length structure enabled all N-linked glycosylations to be mapped on the structure, including three located on the Ig domain. Importantly, all of these glycosylation sites were distal to the concave face of the molecule hypothesised to be important for ligand engagement, highlighting that the concave face is a likely surface for ligand interactions.

Clearly major questions remain to be answered before a clear molecular understanding of the NgR complex is achieved. A solid knowledge base of the structural basis of key interactions involved is critical, and future studies could devote additional efforts to achieving either LINGO-1/NgR or AMIGO/NgR crystal complexes. While the structural results in Chapters 4 and 6 strongly implicate the concave face of AMIGO-1 in ligand binding, it is still somewhat

unclear how LINGO-1 ligand engagement takes place. In addition, studies on other LRR domain proteins, including decorin, which forms a dimer analogous to AMIGO-1, have suggested that decorin may transition from a dimer to a monomer to enable ligand binding [94]. Structural studies on LINGO-1/NgR or AMIGO/NgR complexes could clarify how LINGO-1 and AMIGO-1 oligomerisation relates to ligand interaction. A coordinated approach aligning such studies to functional assays and mutagenesis would have a significant impact on understanding of the NgR receptor complex, and would undoubtedly shed light on downstream therapeutic approaches.

References

1. Neuroscience, T.S.f. *Recovering from Spinal cord injuries*. 2015 [cited 2015 13 Jan].
2. Jensen, M.P., et al., *Secondary health conditions in individuals aging with SCI: terminology, concepts and analytic approaches.* Spinal Cord, 2012. **50**(5): p. 373-8.
3. Liu, N.K. and X.M. Xu, *Neuroprotection and its molecular mechanism following spinal cord injury.* Neural Regen Res, 2012. **7**(26): p. 2051-62.
4. Rowland, J.W., et al., *Current status of acute spinal cord injury pathophysiology and emerging therapies: promise on the horizon.* Neurosurg Focus, 2008. **25**(5): p. E2.
5. Sabapathy, V., G. Tharion, and S. Kumar, *Cell Therapy Augments Functional Recovery Subsequent to Spinal Cord Injury under Experimental Conditions.* Stem Cells Int, 2015. **2015**: p. 132172.
6. Tanaka, E.M. and P. Ferretti, *Considering the evolution of regeneration in the central nervous system.* Nat Rev Neurosci, 2009. **10**(10): p. 713-23.
7. Weil, Z.M., et al., *The injured nervous system: a Darwinian perspective.* Prog Neurobiol, 2008. **86**(1): p. 48-59.
8. Rhona Seijffers, L.B., *Intrinsic determinants of axon regenration.* CNS Regeneration (Second edition), 2008: p. 1-39.
9. Berry, M., *Post-injury myelin-breakdown products inhibit axonal growth: an hypothesis to explain the failure of axonal regeneration in the mammalian central nervous system.* Bibl Anat, 1982(23): p. 1-11.
10. Berry, M., et al., *Regeneration of axons in the visual system.* Restor Neurol Neurosci, 2008. **26**(2-3): p. 147-74.
11. David, S. and A.J. Aguayo, *Axonal elongation into peripheral nervous system "bridges" after central nervous system injury in adult rats.* Science, 1981. **214**(4523): p. 931-3.
12. Richardson, P.M., U.M. McGuinness, and A.J. Aguayo, *Axons from CNS neurons regenerate into PNS grafts.* Nature, 1980. **284**(5753): p. 264-5.
13. Horner, P.J. and F.H. Gage, *Regenerating the damaged central nervous system.* Nature, 2000. **407**(6807): p. 963-70.
14. Fawcett, J.W. and R.A. Asher, *The glial scar and central nervous system repair.* Brain Res Bull, 1999. **49**(6): p. 377-91.
15. Filbin, M.T., *Myelin-associated inhibitors of axonal regeneration in the adult mammalian CNS.* Nat Rev Neurosci, 2003. **4**(9): p. 703-13.
16. Carulli, D., et al., *Chondroitin sulfate proteoglycans in neural development and regeneration.* Curr Opin Neurobiol, 2005. **15**(1): p. 116-20.
17. Ohtake, Y., et al., *Two PTP receptors mediate CSPG inhibition by convergent and divergent signaling pathways in neurons.* Sci Rep, 2016. **6**: p. 37152.
18. Bradbury, E.J., et al., *Chondroitinase ABC promotes functional recovery after spinal cord injury.* Nature, 2002. **416**(6881): p. 636-40.
19. Barritt, A.W., et al., *Chondroitinase ABC promotes sprouting of intact and injured spinal systems after spinal cord injury.* J Neurosci, 2006. **26**(42): p. 10856-67.
20. Winzeler, A.M., et al., *The lipid sulfatide is a novel myelin-associated inhibitor of CNS axon outgrowth.* J Neurosci, 2011. **31**(17): p. 6481-92.
21. Cafferty, W.B., et al., *MAG and OMgp synergize with Nogo-A to restrict axonal growth and neurological recovery after spinal cord trauma.* J Neurosci, 2010. **30**(20): p. 6825-37.
22. Bartsch, U., et al., *Lack of evidence that myelin-associated glycoprotein is a major inhibitor of axonal regeneration in the CNS.* Neuron, 1995. **15**(6): p. 1375-81.
23. Schnell, L. and M.E. Schwab, *Axonal regeneration in the rat spinal cord produced by an antibody against myelin-associated neurite growth inhibitors.* Nature, 1990. **343**(6255): p. 269-72.

24. Caroni, P. and M.E. Schwab, *2 Membrane-Protein Fractions from Rat Central Myelin with Inhibitory Properties for Neurite Growth and Fibroblast Spreading.* Journal of Cell Biology, 1988. **106**(4): p. 1281-1288.
25. Bongiorno, D. and S. Petratos, *Molecular regulation of Nogo-A in neural cells: Novel insights into structure and function.* International Journal of Biochemistry & Cell Biology, 2010. **42**(7): p. 1072-1075.
26. Li, M. and J. Song, *The N- and C-termini of the human Nogo molecules are intrinsically unstructured: bioinformatics, CD, NMR characterization, and functional implications.* Proteins, 2007. **68**(1): p. 100-8.
27. Schwab, M.E., *Nogo and axon regeneration.* Curr Opin Neurobiol, 2004. **14**(1): p. 118-24.
28. He, Z.G. and V. Koprivica, *The Nogo signaling pathway for regeneration block.* Annual Review of Neuroscience, 2004. **27**: p. 341-368.
29. Wang, X.X., et al., *Localization of Nogo-A and Nogo-66 receptor proteins at sites of axon-myelin and synaptic contact.* Journal of Neuroscience, 2002. **22**(13): p. 5505-5515.
30. Caroni, P. and M.E. Schwab, *Antibody against Myelin-Associated Inhibitor of Neurite Growth Neutralizes Nonpermissive Substrate Properties of Cns White Matter.* Neuron, 1988. **1**(1): p. 85-96.
31. GrandPre, T., et al., *Identification of the Nogo inhibitor of axon regeneration as a Reticulon protein.* Nature, 2000. **403**(6768): p. 439-44.
32. Barton, W.A., et al., *Structure and axon outgrowth inhibitor binding of the Nogo-66 receptor and related proteins.* Embo Journal, 2003. **22**(13): p. 3291-3302.
33. Atwal, J.K., et al., *PirB is a functional receptor for myelin inhibitors of axonal regeneration.* Science, 2008. **322**(5903): p. 967-70.
34. Huebner, E.A., et al., *A multi-domain fragment of Nogo-A protein is a potent inhibitor of cortical axon regeneration via Nogo receptor 1.* J Biol Chem, 2011. **286**(20): p. 18026-36.
35. Hu, F. and S.M. Strittmatter, *The N-terminal domain of Nogo-A inhibits cell adhesion and axonal outgrowth by an integrin-specific mechanism.* J Neurosci, 2008. **28**(5): p. 1262-9.
36. Kim, J.E., et al., *Nogo-C is sufficient to delay nerve regeneration.* Mol Cell Neurosci, 2003. **23**(3): p. 451-9.
37. Fournier, A.E., T. GrandPre, and S.M. Strittmatter, *Identification of a receptor mediating Nogo-66 inhibition of axonal regeneration.* Nature, 2001. **409**(6818): p. 341-6.
38. Liu, B.P., et al., *Myelin-associated glycoprotein as a functional ligand for the Nogo-66 receptor.* Science, 2002. **297**(5584): p. 1190-3.
39. Salzer, J.L., W.P. Holmes, and D.R. Colman, *The amino acid sequences of the myelin-associated glycoproteins: homology to the immunoglobulin gene superfamily.* J Cell Biol, 1987. **104**(4): p. 957-65.
40. Schachner, M. and U. Bartsch, *Multiple functions of the myelin-associated glycoprotein MAG (siglec-4a) in formation and maintenance of myelin.* Glia, 2000. **29**(2): p. 154-65.
41. Pan, B., et al., *Myelin-associated glycoprotein and complementary axonal ligands, gangliosides, mediate axon stability in the CNS and PNS: neuropathology and behavioral deficits in single- and double-null mice.* Exp Neurol, 2005. **195**(1): p. 208-17.
42. Johnson, P.W., et al., *Recombinant myelin-associated glycoprotein confers neural adhesion and neurite outgrowth function.* Neuron, 1989. **3**(3): p. 377-85.
43. Turnley, A.M. and P.F. Bartlett, *MAG and MOG enhance neurite outgrowth of embryonic mouse spinal cord neurons.* Neuroreport, 1998. **9**(9): p. 1987-90.
44. Vourc'h, P. and C. Andres, *Oligodendrocyte myelin glycoprotein (OMgp): evolution, structure and function.* Brain Res Brain Res Rev, 2004. **45**(2): p. 115-24.
45. Wang, K.C., et al., *Oligodendrocyte-myelin glycoprotein is a Nogo receptor ligand that inhibits neurite outgrowth.* Nature, 2002. **417**(6892): p. 941-4.
46. He, X.L., et al., *Structure of the Nogo receptor ectodomain: a recognition module implicated in myelin inhibition.* Neuron, 2003. **38**(2): p. 177-85.

47. Venkatesh, K., et al., *The Nogo-66 receptor homolog NgR2 is a sialic acid-dependent receptor selective for myelin-associated glycoprotein.* J Neurosci, 2005. **25**(4): p. 808-22.
48. Dickendesher, T.L., et al., *NgR1 and NgR3 are receptors for chondroitin sulfate proteoglycans.* Nat Neurosci, 2012. **15**(5): p. 703-12.
49. Zhou, X., et al., *Interaction between amyloid precursor protein and Nogo receptors regulates amyloid deposition.* FASEB J, 2011. **25**(9): p. 3146-56.
50. Kim, J.E., et al., *Nogo-66 receptor prevents raphespinal and rubrospinal axon regeneration and limits functional recovery from spinal cord injury.* Neuron, 2004. **44**(3): p. 439-51.
51. Domeniconi, M., et al., *Myelin-associated glycoprotein interacts with the Nogo66 receptor to inhibit neurite outgrowth.* Neuron, 2002. **35**(2): p. 283-90.
52. McDonald, C.L., C. Bandtlow, and M. Reindl, *Targeting the Nogo receptor complex in diseases of the central nervous system.* Curr Med Chem, 2011. **18**(2): p. 234-44.
53. Wang, K.C., et al., *P75 interacts with the Nogo receptor as a co-receptor for Nogo, MAG and OMgp.* Nature, 2002. **420**(6911): p. 74-8.
54. Yiu, G. and Z. He, *Glial inhibition of CNS axon regeneration.* Nat Rev Neurosci, 2006. **7**(8): p. 617-27.
55. Ibanez, C.F. and A. Simi, *p75 neurotrophin receptor signaling in nervous system injury and degeneration: paradox and opportunity.* Trends Neurosci, 2012. **35**(7): p. 431-40.
56. Kraemer, B.R., S.O. Yoon, and B.D. Carter, *The biological functions and signaling mechanisms of the p75 neurotrophin receptor.* Handb Exp Pharmacol, 2014. **220**: p. 121-64.
57. Yamashita, T. and M. Tohyama, *The p75 receptor acts as a displacement factor that releases Rho from Rho-GDI.* Nat Neurosci, 2003. **6**(5): p. 461-7.
58. Fujita, Y. and T. Yamashita, *Axon growth inhibition by RhoA/ROCK in the central nervous system.* Front Neurosci, 2014. **8**: p. 338.
59. Fournier, A.E., et al., *Truncated soluble Nogo receptor binds Nogo-66 and blocks inhibition of axon growth by myelin.* J Neurosci, 2002. **22**(20): p. 8876-83.
60. Song, X.Y., et al., *Suppression of p75NTR does not promote regeneration of injured spinal cord in mice.* J Neurosci, 2004. **24**(2): p. 542-6.
61. Hui, S.P., et al., *Expression pattern of Nogo-A, MAG, and NgR in regenerating urodele spinal cord.* Dev Dyn, 2013. **242**(7): p. 847-60.
62. Hu, B., H.K. Yip, and K.F. So, *Expression of p75 neurotrophin receptor in the injured and regenerating rat retina.* Neuroreport, 1999. **10**(6): p. 1293-7.
63. Barrette, B., et al., *Expression profile of receptors for myelin-associated inhibitors of axonal regeneration in the intact and injured mouse central nervous system.* Mol Cell Neurosci, 2007. **34**(4): p. 519-38.
64. Shao, Z., et al., *TAJ/TROY, an orphan TNF receptor family member, binds Nogo-66 receptor 1 and regulates axonal regeneration.* Neuron, 2005. **45**(3): p. 353-9.
65. Park, J.B., et al., *A TNF receptor family member, TROY, is a coreceptor with Nogo receptor in mediating the inhibitory activity of myelin inhibitors.* Neuron, 2005. **45**(3): p. 345-51.
66. Kojima, T., et al., *TROY, a newly identified member of the tumor necrosis factor receptor superfamily, exhibits a homology with Edar and is expressed in embryonic skin and hair follicles.* J Biol Chem, 2000. **275**(27): p. 20742-7.
67. Mi, S., *Troy/Taj and its role in CNS axon regeneration.* Cytokine Growth Factor Rev, 2008. **19**(3-4): p. 245-51.
68. Mi, S., et al., *LINGO-1 is a component of the Nogo-66 receptor/p75 signaling complex.* Nature Neuroscience, 2004. **7**(3): p. 221-228.
69. Mosyak, L., et al., *The structure of the Lingo-1 ectodomain, a module implicated in central nervous system repair inhibition.* J Biol Chem, 2006. **281**(47): p. 36378-90.
70. Carim-Todd, L., et al., *LRRN6A/LERN1 (leucine-rich repeat neuronal protein 1), a novel gene with enriched expression in limbic system and neocortex.* European Journal of Neuroscience, 2003. **18**(12): p. 3167-3182.

71. Lehmann, M., et al., *Inactivation of Rho signaling pathway promotes CNS axon regeneration.* J Neurosci, 1999. **19**(17): p. 7537-47.
72. Mi, S., et al., *LINGO-1 negatively regulates myelination by oligodendrocytes.* Nature Neuroscience, 2005. **8**(6): p. 745-51.
73. Ji, B., et al., *LINGO-1 antagonist promotes functional recovery and axonal sprouting after spinal cord injury.* Mol Cell Neurosci, 2006. **33**(3): p. 311-20.
74. Qing-Ling Fu, B.H., Wutian Wu, R. Blake Pepinsky, Sha Mi, and Kwok-Fai So, *Blocking LINGO-1 Function Promotes Retinal Ganglion Cell Survival Following Ocular Hypertension and Optic Nerve Transection.* Investigative Ophthalmology & Visual Science, 2008. **Vol. 49**(No. 3).
75. Jepson, S., et al., *LINGO-1, a transmembrane signaling protein, inhibits oligodendrocyte differentiation and myelination through intercellular self-interactions.* J Biol Chem, 2012. **287**(26): p. 22184-95.
76. Lee, X., et al., *NGF regulates the expression of axonal LINGO-1 to inhibit oligodendrocyte differentiation and myelination.* J Neurosci, 2007. **27**(1): p. 220-5.
77. Pepinsky, R.B., et al., *Structure of the LINGO-1-anti-LINGO-1 Li81 antibody complex provides insights into the biology of LINGO-1 and the mechanism of action of the antibody therapy.* J Pharmacol Exp Ther, 2014. **350**(1): p. 110-23.
78. Pepinsky, R.B., et al., *Exposure levels of anti-LINGO-1 Li81 antibody in the central nervous system and dose-efficacy relationships in rat spinal cord remyelination models after systemic administration.* J Pharmacol Exp Ther, 2011. **339**(2): p. 519-29.
79. Cadavid, D., et al., *Safety and efficacy of opicinumab in acute optic neuritis (RENEW): a randomised, placebo-controlled, phase 2 trial.* Lancet Neurol, 2017. **16**(3): p. 189-199.
80. Tran, J.Q., et al., *Randomized phase I trials of the safety/tolerability of anti-LINGO-1 monoclonal antibody BIIB033.* Neurol Neuroimmunol Neuroinflamm, 2014. **1**(2): p. e18.
81. Lv, J., et al., *Passive immunization with LINGO-1 polyclonal antiserum afforded neuroprotection and promoted functional recovery in a rat model of spinal cord injury.* Neuroimmunomodulation, 2010. **17**(4): p. 270-8.
82. Homma, S., et al., *Expression pattern of LRR and Ig domain-containing protein (LRRIG protein) in the early mouse embryo.* Gene Expr Patterns, 2009. **9**(1): p. 1-26.
83. Ng, A. and R.J. Xavier, *Leucine-rich repeat (LRR) proteins: integrators of pattern recognition and signaling in immunity.* Autophagy, 2011. **7**(9): p. 1082-4.
84. Bourikas, D., A. Mir, and A.R. Walmsley, *LINGO-1-mediated inhibition of oligodendrocyte differentiation does not require the leucine-rich repeats and is reversed by p75(NTR) antagonists.* Molecular and Cellular Neuroscience, 2010. **45**(4): p. 363-369.
85. Matsushima, N., et al., *A nested leucine rich repeat (LRR) domain: The precursor of LRRs is a ten or eleven residue motif.* Bmc Microbiology, 2010. **10**.
86. de Wit, J., et al., *Role of leucine-rich repeat proteins in the development and function of neural circuits.* Annu Rev Cell Dev Biol, 2011. **27**: p. 697-729.
87. Takahashi, N., Y. Takahashi, and F.W. Putnam, *Periodicity of Leucine and Tandem Repetition of a 24-Amino Acid Segment in the Primary Structure of Leucine-Rich Alpha-2-Glycoprotein of Human-Serum.* Proceedings of the National Academy of Sciences of the United States of America, 1985. **82**(7): p. 1906-1910.
88. Buchanan, S.G. and N.J. Gay, *Structural and functional diversity in the leucine-rich repeat family of proteins.* Prog Biophys Mol Biol, 1996. **65**(1-2): p. 1-44.
89. Kobe, B. and J. Deisenhofer, *Proteins with Leucine-Rich Repeats.* Current Opinion in Structural Biology, 1995. **5**(3): p. 409-416.
90. Hofsteenge, J., et al., *Amino acid sequence of the ribonuclease inhibitor from porcine liver reveals the presence of leucine-rich repeats.* Biochemistry, 1988. **27**(23): p. 8537-44.
91. Kajava, A.V., *Structural diversity of leucine-rich repeat proteins.* J Mol Biol, 1998. **277**(3): p. 519-27.

92. Kobe, B. and A.V. Kajava, *The leucine-rich repeat as a protein recognition motif.* Current Opinion in Structural Biology, 2001. **11**(6): p. 725-732.
93. Kobe, B. and J. Deisenhofer, *Crystal structure of porcine ribonuclease inhibitor, a protein with leucine-rich repeats.* Nature, 1993. **366**(6457): p. 751-6.
94. Scott, P.G., et al., *Crystal structure of the dimeric protein core of decorin, the archetypal small leucine-rich repeat proteoglycan.* Proc Natl Acad Sci U S A, 2004. **101**(44): p. 15633-8.
95. Helft, L., et al., *LRR conservation mapping to predict functional sites within protein leucine-rich repeat domains.* PLoS One, 2011. **6**(7): p. e21614.
96. Chen, Y., et al., *AMIGO and friends: an emerging family of brain-enriched, neuronal growth modulating, type I transmembrane proteins with leucine-rich repeats (LRR) and cell adhesion molecule motifs.* Brain Res Rev, 2006. **51**(2): p. 265-74.
97. Kuja-Panula, J., et al., *AMIGO, a transmembrane protein implicated in axon tract development, defines a novel protein family with leucine-rich repeats.* J Cell Biol, 2003. **160**(6): p. 963-73.
98. Matz, M., et al., *Ordered differential display: a simple method for systematic comparison of gene expression profiles.* Nucleic Acids Res, 1997. **25**(12): p. 2541-2.
99. Rauvala, H. and R. Pihlaskari, *Isolation and some characteristics of an adhesive factor of brain that enhances neurite outgrowth in central neurons.* J Biol Chem, 1987. **262**(34): p. 16625-35.
100. Ono, T., et al., *Alivin 1, a novel neuronal activity-dependent gene, inhibits apoptosis and promotes survival of cerebellar granule neurons.* Journal of Neuroscience, 2003. **23**(13): p. 5887-96.
101. Rabenau, K.E., et al., *DEGA/AMIGO-2, a leucine-rich repeat family member, differentially expressed in human gastric adenocarcinoma: effects on ploidy, chromosomal stability, cell adhesion/migration and tumorigenicity.* Oncogene, 2004. **23**(29): p. 5056-67.
102. Chen, Y.A., H.H. Hor, and B.L. Tang, *AMIGO is expressed in multiple brain cell types and may regulate dendritic growth and neuronal survival.* Journal of Cellular Physiology, 2012. **227**(5): p. 2217-2229.
103. Laeremans, A., et al., *AMIGO2 mRNA expression in hippocampal CA2 and CA3a.* Brain Struct Funct, 2013. **218**(1): p. 123-30.
104. Gimelli, S., et al., *A de novo 12q13.11 microdeletion in a patient with severe mental retardation, cleft palate, and high myopia.* European Journal of Medical Genetics, 2011. **54**(1): p. 94-96.
105. Zhao, X., et al., *Amigo adhesion protein regulates development of neural circuits in zebrafish brain.* J Biol Chem, 2014. **289**(29): p. 19958-75.
106. Peltola, M.A., et al., *AMIGO-Kv2.1 Potassium Channel Complex Is Associated With Schizophrenia-Related Phenotypes.* Schizophr Bull, 2016. **42**(1): p. 191-201.
107. Ahmed, Z., et al., *AMIGO3 Is an NgR1/p75 Co-Receptor Signalling Axon Growth Inhibition in the Acute Phase of Adult Central Nervous System Injury.* PLoS One, 2013. **8**(4): p. e61878.
108. Whitford, K.L., et al., *Regulation of cortical dendrite development by Slit-Robo interactions.* Neuron, 2002. **33**(1): p. 47-61.
109. Hohenester, E., *Structural insight into Slit-Robo signalling.* Biochem Soc Trans, 2008. **36**(Pt 2): p. 251-6.
110. Hyun, J.K. and H.W. Kim, *Clinical and experimental advances in regeneration of spinal cord injury.* J Tissue Eng, 2010. **2010**: p. 650857.
111. Yu, C.Y., G. Ng, and P. Liao, *Therapeutic antibodies in stroke.* Transl Stroke Res, 2013. **4**(5): p. 477-83.
112. Wang, X., et al., *Human NgR-Fc decoy protein via lumbar intrathecal bolus administration enhances recovery from rat spinal cord contusion.* J Neurotrauma, 2014. **31**(24): p. 1955-66.
113. Li, W., et al., *A neutralizing anti-Nogo66 receptor monoclonal antibody reverses inhibition of neurite outgrowth by central nervous system myelin.* J Biol Chem, 2004. **279**(42): p. 43780-8.

114. Ledford, H., *Drug that boosts nerve signals offers hope for multiple sclerosis.* Nature, 2015. **520**(7548): p. 417.
115. Watkins, L.M., et al., *Complement is activated in progressive multiple sclerosis cortical grey matter lesions.* J Neuroinflammation, 2016. **13**(1): p. 161.
116. Kabsch, W., *Xds.* Acta Crystallogr D Biol Crystallogr, 2010. **66**(Pt 2): p. 125-32.
117. Murshudov, G.N., A.A. Vagin, and E.J. Dodson, *Refinement of macromolecular structures by the maximum-likelihood method.* Acta Crystallogr D Biol Crystallogr, 1997. **53**(Pt 3): p. 240-55.
118. J, N., *AMoRe: an automated package for molecular replacement.* Acta Crystallogr (1994). **50**: p. 157–163.
119. Brunger, A.T., et al., *Crystallography & NMR system: A new software suite for macromolecular structure determination.* Acta Crystallogr D Biol Crystallogr, 1998. **54**(Pt 5): p. 905-21.
120. Kajander, T., et al., *Crystal structure and role of glycans and dimerization in folding of neuronal leucine-rich repeat protein AMIGO-1.* J Mol Biol, 2011. **413**(5): p. 1001-15.
121. Emsley, P. and K. Cowtan, *Coot: model-building tools for molecular graphics.* Acta Crystallogr D Biol Crystallogr, 2004. **60**(Pt 12 Pt 1): p. 2126-32.
122. Wang, L., et al., *Using DelPhi capabilities to mimic protein's conformational reorganization with amino acid specific dielectric constants.* Commun Comput Phys, 2013. **13**(1): p. 13-30.
123. Winn, M.D., et al., *Overview of the CCP4 suite and current developments.* Acta Crystallogr D Biol Crystallogr, 2011. **67**(Pt 4): p. 235-42.
124. O'Callaghan C, A., et al., *BirA enzyme: production and application in the study of membrane receptor-ligand interactions by site-specific biotinylation.* Anal Biochem, 1999. **266**(1): p. 9-15.
125. Sandvig, A., et al., *Myelin-, reactive glia-, and scar-derived CNS axon growth inhibitors: expression, receptor signaling, and correlation with axon regeneration.* Glia, 2004. **46**(3): p. 225-51.
126. Meabon, J.S., et al., *LINGO-1 protein interacts with the p75 neurotrophin receptor in intracellular membrane compartments.* J Biol Chem, 2015. **290**(15): p. 9511-20.
127. Ahmed, Z., et al., *Epidermal growth factor receptor inhibitors promote CNS axon growth through off-target effects on glia.* Neurobiol Dis, 2009. **36**(1): p. 142-50.
128. Wang, X., et al., *Ligand-regulated secretion of recombinant annexin V from cultured thyroid epithelial cells.* Am J Physiol Cell Physiol, 2002. **282**(6): p. C1313-21.
129. Wang, X., et al., *Localization of Nogo-A and Nogo-66 receptor proteins at sites of axon-myelin and synaptic contact.* J Neurosci, 2002. **22**(13): p. 5505-15.
130. Choi, S.I., et al., *Effects of Red Liriope platyphylla on NGF secretion ability, NGF receptor signaling pathway and gamma-secretase components in NSE/hAPPsw transgenic mice expressing Alzheimer's Disease.* Lab Anim Res, 2012. **28**(3): p. 155-63.
131. Islam, M., et al., *The concave face of decorin mediates reversible dimerization and collagen binding.* J Biol Chem, 2013. **288**(49): p. 35526-33.
132. van Doorn, P.A. and B.C. Jacobs, *Neuronal endocytosis of anti-ganglioside antibodies: implications for Guillain-Barre syndrome.* Brain, 2016. **139**(Pt 6): p. 1622-5.
133. Maxie Rockstroh, S.M., Claudia Jende, Alexandra Kerzhner, Martin von Bergen, Janina Melanie Tomm, *Cell fractionation - an important tool for compartment proteomics.* JOURNAL OF INTEGRATED OMICS, 2011. **1**(1): p. 135-143.
134. Saxena, S., et al., *Differences in the surface binding and endocytosis of neurotrophins by p75NTR.* Mol Cell Neurosci, 2004. **26**(2): p. 292-307.
135. Pignot, V., et al., *Characterization of two novel proteins, NgRH1 and NgRH2, structurally and biochemically homologous to the Nogo-66 receptor.* J Neurochem, 2003. **85**(3): p. 717-28.
136. Klinger, M., et al., *Identification of Nogo-66 receptor (NgR) and homologous genes in fish.* Mol Biol Evol, 2004. **21**(1): p. 76-85.

137. Al Halabiah, H., et al., *Expression pattern of NOGO and NgR genes during human development.* Gene Expr Patterns, 2005. **5**(4): p. 561-8.
138. Yan, Q. and E.M. Johnson, Jr., *An immunohistochemical study of the nerve growth factor receptor in developing rats.* J Neurosci, 1988. **8**(9): p. 3481-98.
139. Shaw, G., et al., *Preferential transformation of human neuronal cells by human adenoviruses and the origin of HEK 293 cells.* FASEB J, 2002. **16**(8): p. 869-71.
140. Buntinx, M., et al., *Characterization of three human oligodendroglial cell lines as a model to study oligodendrocyte injury: morphology and oligodendrocyte-specific gene expression.* J Neurocytol, 2003. **32**(1): p. 25-38.
141. Forsyth, P.A., et al., *p75 neurotrophin receptor cleavage by alpha- and gamma-secretases is required for neurotrophin-mediated proliferation of brain tumor-initiating cells.* J Biol Chem, 2014. **289**(12): p. 8067-85.
142. Le Moan, N., et al., *Oxygen-dependent cleavage of the p75 neurotrophin receptor triggers stabilization of HIF-1alpha.* Mol Cell, 2011. **44**(3): p. 476-90.
143. Ahmed, Z., et al., *TACE-induced cleavage of NgR and p75NTR in dorsal root ganglion cultures disinhibits outgrowth and promotes branching of neurites in the presence of inhibitory CNS myelin.* FASEB J, 2006. **20**(11): p. 1939-41.
144. Satoh, J., et al., *TROY and LINGO-1 expression in astrocytes and macrophages/microglia in multiple sclerosis lesions.* Neuropathol Appl Neurobiol, 2007. **33**(1): p. 99-107.
145. Chen, Y., H.H. Hor, and B.L. Tang, *AMIGO is expressed in multiple brain cell types and may regulate dendritic growth and neuronal survival.* J Cell Physiol, 2012. **227**(5): p. 2217-29.
146. Benedetti, G., et al., *IL-17A and TNF-alpha Increase the Expression of the Antiapoptotic Adhesion Molecule Amigo-2 in Arthritis Synoviocytes.* Front Immunol, 2016. **7**: p. 254.
147. Berggard, T., S. Linse, and P. James, *Methods for the detection and analysis of protein-protein interactions.* Proteomics, 2007. **7**(16): p. 2833-42.
148. Goldoni, S., et al., *A soluble ectodomain of LRIG1 inhibits cancer cell growth by attenuating basal and ligand-dependent EGFR activity.* Oncogene, 2007. **26**(3): p. 368-81.
149. Laederich, M.B., et al., *The leucine-rich repeat protein LRIG1 is a negative regulator of ErbB family receptor tyrosine kinases.* J Biol Chem, 2004. **279**(45): p. 47050-6.
150. Bjellqvist, B., et al., *Reference points for comparisons of two-dimensional maps of proteins from different human cell types defined in a pH scale where isoelectric points correlate with polypeptide compositions.* Electrophoresis, 1994. **15**(3-4): p. 529-39.
151. Hendrickson, W.A., J.R. Horton, and D.M. LeMaster, *Selenomethionyl proteins produced for analysis by multiwavelength anomalous diffraction (MAD): a vehicle for direct determination of three-dimensional structure.* Embo Journal, 1990. **9**(5): p. 1665-72.
152. Kantardjieff, K.A. and B. Rupp, *Matthews coefficient probabilities: Improved estimates for unit cell contents of proteins, DNA, and protein-nucleic acid complex crystals.* Protein Sci, 2003. **12**(9): p. 1865-71.
153. Laskowski, R.A., et al., *AQUA and PROCHECK-NMR: programs for checking the quality of protein structures solved by NMR.* J Biomol NMR, 1996. **8**(4): p. 477-86.
154. Bella, J., et al., *The leucine-rich repeat structure.* Cell Mol Life Sci, 2008. **65**(15): p. 2307-33.
155. Seiradake, E., et al., *Structure and functional relevance of the Slit2 homodimerization domain.* EMBO Rep, 2009. **10**(7): p. 736-41.
156. Ceulemans, H., et al., *A capping domain for LRR protein interaction modules.* FEBS Lett, 1999. **456**(3): p. 349-51.
157. Kolade, O.O., et al., *In vitro characterization of the cysteine-rich capping domains in a plant leucine rich repeat protein.* Biochim Biophys Acta, 2006. **1764**(6): p. 1043-53.
158. Holm, L. and P. Rosenstrom, *Dali server: conservation mapping in 3D.* Nucleic Acids Res, 2010. **38**(Web Server issue): p. W545-9.
159. Deng, L., et al., *A structural basis for antigen recognition by the T cell-like lymphocytes of sea lamprey.* Proc Natl Acad Sci U S A, 2010. **107**(30): p. 13408-13.

160. Xu, K., et al., *Crystal structures of Lgr4 and its complex with R-spondin1.* Structure, 2013. **21**(9): p. 1683-9.
161. Scott, P.G., et al., *Crystal structure of the biglycan dimer and evidence that dimerization is essential for folding and stability of class I small leucine-rich repeat proteoglycans.* J Biol Chem, 2006. **281**(19): p. 13324-32.
162. Ohto, U., et al., *Structural basis of species-specific endotoxin sensing by innate immune receptor TLR4/MD-2.* Proc Natl Acad Sci U S A, 2012. **109**(19): p. 7421-6.
163. Fukuda, K., et al., *The snake venom protein botrocetin acts as a biological brace to promote dysfunctional platelet aggregation.* Nat Struct Mol Biol, 2005. **12**(2): p. 152-9.
164. Papageorgiou, A.C., R. Shapiro, and K.R. Acharya, *Molecular recognition of human angiogenin by placental ribonuclease inhibitor--an X-ray crystallographic study at 2.0 A resolution.* EMBO J, 1997. **16**(17): p. 5162-77.
165. Uff, S., et al., *Crystal structure of the platelet glycoprotein Ib(alpha) N-terminal domain reveals an unmasking mechanism for receptor activation.* J Biol Chem, 2002. **277**(38): p. 35657-63.
166. Morlot, C., et al., *Structural insights into the Slit-Robo complex.* Proc Natl Acad Sci U S A, 2007. **104**(38): p. 14923-8.
167. Seiradake, E., et al., *Structural basis for cell surface patterning through NetrinG-NGL interactions.* EMBO J, 2011. **30**(21): p. 4479-88.
168. Yang, J., et al., *The I-TASSER Suite: protein structure and function prediction.* Nat Methods, 2015. **12**(1): p. 7-8.
169. Huizinga, E.G., et al., *Structures of glycoprotein Ibalpha and its complex with von Willebrand factor A1 domain.* Science, 2002. **297**(5584): p. 1176-9.
170. Andrews, J.L. and F. Fernandez-Enright, *A decade from discovery to therapy: Lingo-1, the dark horse in neurological and psychiatric disorders.* Neurosci Biobehav Rev, 2015. **56**: p. 97-114.
171. Botos, I., D.M. Segal, and D.R. Davies, *The structural biology of Toll-like receptors.* Structure, 2011. **19**(4): p. 447-59.
172. Goldman, J.S. and T.E. Kennedy, *The clasp between NetrinG and NGL becomes crystal clear.* EMBO J, 2011. **30**(21): p. 4342-4.
173. Nguyen, H.H., et al., *Surface plasmon resonance: a versatile technique for biosensor applications.* Sensors (Basel), 2015. **15**(5): p. 10481-510.
174. van der Merwe, P.A., et al., *CD80 (B7-1) binds both CD28 and CTLA-4 with a low affinity and very fast kinetics.* J Exp Med, 1997. **185**(3): p. 393-403.
175. Lesk, A.M. and C. Chothia, *Evolution of proteins formed by beta-sheets. II. The core of the immunoglobulin domains.* J Mol Biol, 1982. **160**(2): p. 325-42.
176. Griffiths, K., et al., *i-bodies, Human Single Domain Antibodies That Antagonize Chemokine Receptor CXCR4.* J Biol Chem, 2016. **291**(24): p. 12641-57.
177. Schroeder, H.W., Jr. and L. Cavacini, *Structure and function of immunoglobulins.* J Allergy Clin Immunol, 2010. **125**(2 Suppl 2): p. S41-52.
178. Saha, N., et al., *Ganglioside mediate the interaction between Nogo receptor 1 and LINGO-1.* Biochem Biophys Res Commun, 2011. **413**(1): p. 92-7.

Appendix

Primer sequences used for PCR

Restriction sites that were incorporated into the primers are highlighted in red, start codons are boxed and stop codons are underlined.

	Primer Sequence	Restriction site	Length of product
Amigo1 forward	5'GATCGAATTC|ATG|CA CCCCCACCGTGACCCG 3'	EcoR1	1476bp
Amigo1 reverse	3'AGACTATGCGGGTAA CACCACGAGCTCCTAG 5'	Xho1	1476bp
Amigo2 forward	5'GATCGGATCC|ATG|TC GTTACGTGTACACACT 3'	BamH1	1569bp
Amigo2 reverse	3' TGTGGAAAACACCGC AGGTGAGAGCTCCTAG 5'	Xho1	1569bp
Amigo3 forward	5'GATCGGATCC|ATG|AC CTGGTTGGTGCTGCTG 3'	BamH1	1509bp
Amigo3 reverse	3'AGGCTCCCAGGGTAC TGTTGGGAGCTCCTAG 5'	Xho1	1509bp
Lingo1 forward	5'GATCGGATCC|ATG|CA GGTGAGCAAGAGGATG 3'	BamH1	
Lingo1 reverse	3' TTCAAGTTGTACTTC TACTATGAGCTCCTAG 5'	Xho1	
NgR forward	5'GATCGAATTC|ATG|AA GAGGGCGTCCGCTGGA 3'	EcoR1	1461bp
NgR reverse	3'TGTCACGAACCCGGG ACGACTGAGCTCCTAG 5'	Xho1	1461bp
p75 forward	5'GATCGAATTC|ATG|GGG GCAGGTGCCACCGGC 3'	EcoR1	1323bp
p75 reverse	3'TGACGGTGTAGGGGCC ACACTGAGCTCCTAG 5'	Xho1	1323bp

Internal primer sequences used for DNA sequencing

Name	Primer sequence
hAmigo1 int 1	5′ATGGCCCAGCTGCAGAAA 3′
hAmigo1 int 2	5′AACGGGTGCTAGATGAGG 3′
hAmigo2 int 1	5′TATGTTGGAAGGTTCAAG 3′
hAmigo2 int 2	5′GAAAGCCCTCGTTTTGAG 3′
hAmigo2 int 1-2	5′ TATGTTGGAAGGTTCAAG 3′
hAmigo3 int 1	5′ACGAGCATGCCTTCCACG 3′
hAmigo3 int 2	5′ATAGGCAACGTACAGGAG 3′
hNgR int 1	5′ATGACACCTTCCGCGACC 3′
hNgR int 2	5′TTACCATCCCATCTGGAC 3′
hp75 int 1	5′TGTGCGAGGACACCGAGC 3′
hp75 int 2	5′AGAAAAACTCCACAGCGA 3′

Primer sequences used for overlap extension PCR

hAM1HA OLF	5′ GATGTTCCAGATTATGCTGGCCGAGCCGTGGTTAGC 3′

hAM1HA OLR	5′ GCTAACCACGGCTCGGCCAGCATAATCTGGAAC ATC 3′
hAM1 rev	5′ GATCCTCGAGTCACACCACAATGGGCGTATCAGA 3′
hAM2HA OLF	5′ GATGTTCCAGATTATGCTGTGTGCCCCACCGCT TGC 3′
hAM2HA OLR	5′ GCAAGCGGTGGGGCACACAGCATAATCTGGAAC ATC 3′
hAM2 rev	5′ GATCCTCGAGTTAAGTGGACGCCACAAAAGGTGT 3′
hAM3HA OLF	5′ GATGTTCCAGATTATGCTACCCCGGACTCCGAG GGT 3′
hAM3HA OLR	5′ ACCCTCGGAGTCCGGGGTAGCATAATCTGGAAC ATC 3′
hAM2 rev	5′ GATCCTCGAGCTAGGTTGTCATGGGACCCTCGGA 3′
hNgRHA OLF	5′ GATGTTCCAGATTATGCTTGCCCAGGTGCCTGCGTA 3′
hNgRHA OLR	5′ TACGCAGGCACCTGGGCAAGCATAATCTGGAAC ATC 3′
hp75HA OLF	5′ GATGTTCCAGATTATGCTAAGGAGGCATGCCCCACA 3′
hp75HA OLR	5′ TGTGGGGCATGCCTCCTTAGCATAATCTGGAAC ATC 3′
HAEco FOR	5′ GATCGAATTCATGTCTGCACTTCTGATCCTA 3′
HABamHI FOR	5′ GATCGGATCCATGTCTGCACTTCTGATCCTA 3′